COASTAL HAZARD ANALYSIS AT SAN ONOFRE NUCLEAR GENERATING STATION

Part 1: Coastal Hazards



for

SOUTHERN CALIFORNIA EDISON
P.O. Box 128, MS D3D
5000 Pacific Coast Highway
San Clemente, CA 92672

Coastal Environments, Inc.
2166 Avenida de la Playa, Suite E
La Jolla, CA 92037

CE Reference No. 22-02
31 March 2022

TABLE OF CONTENTS

EXECUTIVE SUMMARY vii

1.0 INTRODUCTION 1
1.1 SONGS UNITS 1, 2, AND 3 DESCRIPTION 2
1.2 HISTORICAL CONTEXT 3
1.3 GEOLOGIC SETTING AND CLIFF COMPOSITION 4
1.4 HISTORICAL CLIFF RETREAT 4

2.0 MEAN SEA LEVEL RISE IMPACT ASSESSMENT 11
2.1 SONGS SEA LEVEL INFORMATION 11
2.2 MEAN SEA LEVEL RISE GUIDANCE 12
2.2.1 California OPC (2018) MSLR Projections 12
2.2.2 IPCC (2021) MSLR Projections 14
2.3 SONGS SEA LEVEL EXTREMES 17

3.0 BEACH AND CLIFF RETREAT MODEL 25
3.1 MODEL SCENARIO 26
3.2 MODEL INPUTS AND PARAMETERS 27
3.3 MODEL RESULTS 28

4.0 SONGS REVETMENT 36
4.1 DESCRIPTION OF THE SONGS REVETMENT 36
4.1.1 Revetment and Walkway Maintenance 2018-2019 36
4.2 SITE VISIT 36
4.2.1 Rock Measurement Discussion 37
4.2.2 Revetment Laser Scanner Survey 37
4.3 RIPRAP ROCK UNIT WEIGHT 38
4.4 DESIGN WATER LEVEL 38
4.5 DESIGN WAVE ESTIMATION 39
4.6 SONGS REVETMENT STABILITY ESTIMATION 39
4.7 ASSESSMENT OF SAN ONOFRE BEACH 40
4.8 EVALUATION CRITERIA 41
4.9 REVETMENT STABILITY FROM FEBRUARY 2020 TO FEBRUARY 2021 41
4.10 MAINTENANCE AND ADAPTIVE CAPACITY 42
4.11 GROUNDWATER 43

5.0 RUN-UP AND OVERTOPPING ANALYSIS 76
5.1 RANDOM WAVE METHOD 76
5.2 OVERTOPPING 77
5.3 RESULTS 78
5.4 PROBABILITY ANALYSIS 78
5.5 SUMMARY 79

6.0 SUMMARY AND CONCLUSIONS 86

7.0 REFERENCES 88

LIST OF APPENDICES

Appendix A. Modeled Beach and Cliff Profile Changes by 2050 due to MSLR A-1
Appendix B. Digital Elevation Models (DEM) from 2020 and 2021 Revetment Surveys.....B-1
Appendix C. Cross Section Elevations of SONGS Revetment.....C-1
Appendix D. Aerial Photographs North and South SONGS, 2003-2020..... D-1

LIST OF FIGURES

Figure 1-1. Location of SONGS.....5
Figure 1-2. Location of Cristianitos Fault with respect to SONGS, at the south end of the fault line.....6
Figure 1-3. Unit 1 (left dome), and Units 2 and 3 (right domes), prior to dismantlement of Unit 1.....7
Figure 1-4. Locations of the Independent Spent Fuel Storage Installations (ISFSIs) at the North Industrial Area (NIA) where Unit 1 was previously located.....7
Figure 1-5. Maps of the study area showing 1889 topography, 1934 topography and cliff edge, and 2009 topography and cliff edge lines.....8
Figure 1-6. Long-term cliff retreat rates and spatial distribution for Oceanside littoral cell.....9
Figure 1-7. Geological description of cliffs north of SONGS and south of SONGS.....10
Figure 2-1. Annual and monthly average water level relative to NAVD88 at La Jolla, 1925-2021, and annual global MSL reconstruction.....21
Figure 2-2. La Jolla average MSL data, 1925-2021, annual, monthly. Same for 2000-2021. Both with OPC (2018) La Jolla MSLR projections, 2000-2050.....22
Figure 2-3. La Jolla average MSL data, 1925-2021, annual, monthly, with IPCC (2021) LA MSLR projections, 2004.5-2050.....23
Figure 2-4. Monthly maximum sea level at La Jolla relative to NAVD88 datum, 1925-2021. Maximum observed 7.62 ft height on 25 November 2015 during 2015-16 El Niño.....24
Figure 3-1. Model profile adjustments and erosion from MSLR.....29
Figure 3-2. Map showing model transects and contours displayed over aerial photograph and the 2009 bare earth digital elevation model.....30
Figure 3-3. Modeled beach retreat on all 27 modeled profiles at SONGS for each scenario.....32
Figure 3-4. Modeled cliff retreat for profiles south of SONGS, intersecting SONGS, and north of SONGS for each scenario.....33
Figure 3-5. Modeled H++ extreme-scenario cliff retreat for Scenarios A and B at transect 227 located north of SONGS.....34
Figure 3-6. Modeled extreme-scenario cliff retreat for Scenarios A and B at transect 217 located south of SONGS.....35
Figure 4-1. Photo of SONGS revetment, 20 August 2018.....44
Figure 4-2. Photo of southern end of SONGS revetment.....45

Figure 4-3. Photo of riprap revetment toward south, 20 March 2018 before placement of additional rock. Photo on 17 December 2019 after placement of rock in gaps and settled areas 46
Figure 4-4. Photo of south end of riprap and access walkway on 15 October 2019 before repairs. Photo on 17 December 2019 after repairs 47
Figure 4-5. Measurement of long axis (length) of riprap rock 48
Figure 4-6. Histograms of rock length, width, and height 49
Figure 4-7. Cumulative distributions of rock length, width, and height 50
Figure 4-8. Photo of Trimble SX10 scanning total station used by Coastal Environments for SONGS topographic surveys 51
Figure 4-9. Location of 21 transects along the revetment, spaced 100 ft apart 52
Figure 4-10. Elevation model of SONGS revetment from laser scanner, Transects 1-7 53
Figure 4-11. Elevation model of SONGS revetment from laser scanner, Transects 8-15 54
Figure 4-12. Elevation model of SONGS revetment from laser scanner, Transects 16-21 55
Figure 4-13. Typical revetment cross sections showing slope "β" 56
Figure 4-14. Elevation of the top of revetment for the 21 transects 58
Figure 4-15. Weight distribution of existing SONGS revetment rocks 61
Figure 4-16. Design wave heights for various return periods at San Onofre 62
Figure 4-17. Measured wave spectral density for various storms 63
Figure 4-18. Historical beach width adjacent to Unit 1, 1928-2000 67
Figure 4-19. Beach width fronting SONGS, 1991-1993 and 2016-2020 68
Figure 4-20. Wave height and wave period at SONGS, 1 January 2020 to 28 February 2021 70
Figure 4-21. Wave height and wave period at SONGS, 6-11 November 2020 71
Figure 4-22. Wave height and wave period at SONGS, 1 January to 28 February 2021 72
Figure 4-23. Wave height and wave period at SONGS, 25-29 January 2021 73
Figure 4-24. Photos of north portion of SONGS revetment covered by beach sand, spring 2020, but covered with cobble, winter 2021 74
Figure 4-25. Groundwater elevations in 2020, and for OPC (2018) 0.5% and H++ MSLR projections by 2050 75
Figure 5-1. Wave run-up on a slope 80
Figure 5-2. Exposed area in the walkway wall 83
Figure 5-3. Probability of 10-, 25-, 50-, and 100-year waves return period to occur in the next 100 years 84
Figure 5-4. Joint Probability distribution between significant wave height and tide level 85

LIST OF TABLES

Table 2-1. OPC (2018) MSLR Projections, La Jolla 19
Table 2-2. IPCC (2021) Mid-Range MSLR Projections, Los Angeles 19
Table 2-3. IPCC (2021) Low-High Range MSLR Projections, Los Angeles 19
Table 2-4. Highest Maximum Observed Total Water Levels, La Jolla 20
Table 2-5. NOAA La Jolla Extreme Water Level Statistics 20
Table 3-1. Beach and cliff retreat 2010-2050 31
Table 4-1. Riprap and walkway wall heights and revetment slope β 57

Table 4-2. Length, width, height, and estimated weight of the measured rocks 59
Table 4-3. Mean and standard deviation for rock parameters 60
Table 4-4. Design wave characteristics at San Onofre 64
Table 4-5. Largest 20 waves at San Onofre ranked in descending order (1976-1994) 65
Table 4-6. Rock weights (W50) needed for revetment stability, 2020 and 2050 66
Table 4-7. Mean beach widths (ft) at San Onofre, 1990-1993 vs 2017-2020 69
Table 5-1. Run-up and overtopping summary for 0.5 % (1:200) scenario 81
Table 5-2. Run-up and overtopping summary for OPC (2018) H++ scenario 82

APPENDIX FIGURES

Figure A-1. Observed 2010 and modeled 2050 Profile 210 ..... A-2
Figure A-2. Observed 2010 and modeled 2050 Profile 211 ..... A-3
Figure A-3. Observed 2010 and modeled 2050 Profile 212 ..... A-4
Figure A-4. Observed 2010 and modeled 2050 Profile 213 ..... A-5
Figure A-5. Observed 2010 and modeled 2050 Profile 214 ..... A-6
Figure A-6. Observed 2010 and modeled 2050 Profile 215 ..... A-7
Figure A-7. Observed 2010 and modeled 2050 Profile 216 ..... A-8
Figure A-8. Observed 2010 and modeled 2050 Profile 217 ..... A-9
Figure A-9. Observed 2010 and modeled 2050 Profile 218 ..... A-10
Figure A-10. Observed 2010 and modeled 2050 Profile 219 ..... A-11
Figure A-11. Observed 2010 and modeled 2050 Profile 220 ..... A-12
Figure A-12. Observed 2010 and modeled 2050 Profile 221 ..... A-13
Figure A-13. Observed 2010 and modeled 2050 Profile 222 ..... A-14
Figure A-14. Observed 2010 and modeled 2050 Profile 223 ..... A-15
Figure A-15. Observed 2010 and modeled 2050 Profile 224 ..... A-16
Figure A-16. Observed 2010 and modeled 2050 Profile 225 ..... A-17
Figure A-17. Observed 2010 and modeled 2050 Profile 226 ..... A-18
Figure A-18. Observed 2010 and modeled 2050 Profile 227 ..... A-19
Figure A-19. Observed 2010 and modeled 2050 Profile 228 ..... A-20
Figure A-20. Observed 2010 and modeled 2050 Profile 229 ..... A-21
Figure A-21. Observed 2010 and modeled 2050 Profile 230 ..... A-22
Figure A-22. Observed 2010 and modeled 2050 Profile 231 ..... A-23
Figure A-23. Observed 2010 and modeled 2050 Profile 232 ..... A-24
Figure A-24. Observed 2010 and modeled 2050 Profile 233 ..... A-25
Figure A-25. Observed 2010 and modeled 2050 Profile 234 ..... A-26
Figure A-26. Observed 2010 and modeled 2050 Profile 235 ..... A-27
Figure A-27. Observed 2010 and modeled 2050 Profile 236 ..... A-28

Figure B-1. Location of 21 transects along the revetment, spaced 100 ft apart....B-2
Figure B-2. DEM comparison between 2021 and 2020 showing Transect 1....B-3
Figure B-3. DEM comparison between 2021 and 2020 showing Transect 2....B-4
Figure B-4. DEM comparison between 2021 and 2020 showing Transect 3....B-5
Figure B-5. DEM comparison between 2021 and 2020 showing Transect 4....B-6
Figure B-6. DEM comparison between 2021 and 2020 showing Transect 5....B-7
Figure B-7. DEM comparison between 2021 and 2020 showing Transect 6....B-8
Figure B-8. DEM comparison between 2021 and 2020 showing Transect 7....B-9
Figure B-9. DEM comparison between 2021 and 2020 showing Transect 8....B-10
Figure B-10. DEM comparison between 2021 and 2020 showing Transect 9....B-11
Figure B-11. DEM comparison between 2021 and 2020 showing Transect 10....B-12
Figure B-12. DEM comparison between 2021 and 2020 showing Transect 11....B-13
Figure B-13. DEM comparison between 2021 and 2020 showing Transect 12....B-14
Figure B-14. DEM comparison between 2021 and 2020 showing Transect 13....B-15
Figure B-15. DEM comparison between 2021 and 2020 showing Transect 14....B-16
Figure B-16. DEM comparison between 2021 and 2020 showing Transect 15....B-17
Figure B-17. DEM comparison between 2021 and 2020 showing Transect 16....B-18
Figure B-18. DEM comparison between 2021 and 2020 showing Transect 17....B-19
Figure B-19. DEM comparison between 2021 and 2020 showing Transect 18....B-20
Figure B-20. DEM comparison between 2021 and 2020 showing Transect 19....B-21
Figure B-21. DEM comparison between 2021 and 2020 showing Transect 20....B-22
Figure B-22. DEM comparison between 2021 and 2020 showing Transect 21....B-23

Figure C-1. Cross sections of SONGS revetment along transects 1-3....C-2
Figure C-2. Cross sections of SONGS revetment along transects 4-6....C-3
Figure C-3. Cross sections of SONGS revetment along transects 7-9....C-4
Figure C-4. Cross sections of SONGS revetment along transects 10-12....C-5
Figure C-5. Cross sections of SONGS revetment along transects 13-15....C-6
Figure C-6. Cross sections of SONGS revetment along transects 16-18....C-7
Figure C-7. Cross sections of SONGS revetment along transects 19-21....C-8

LIST OF PHOTOGRAPHS

Photo D-1. Photograph showing revetment covered by sand and fronted by a wide beach at the northern end of SONGS (10 March 2003).... D-2
Photo D-2. Photograph showing waves from north swell attacking SONGS revetment at the southern end of SONGS (10 March 2003).... D-2
Photo D-3. Photograph showing waves attacking the revetment and the presence of a sand beach at the northern end of SONGS (26 November 2003).... D-3
Photo D-4. Photograph showing waves attacking SONGS revetment at the southern end of SONGS (26 November 2003).... D-3
Photo D-5. Photograph showing revetment covered by sand and fronted by a wide beach at the northern end of SONGS (2 August 2006) D-4
Photo D-6. Photograph showing waves from north swell attacking SONGS revetment at the southern end of SONGS (2 August 2006).... D-4

Photo D-7. Photograph showing revetment covered by sand and fronted by a wide beach at the northern end of SONGS (31 January 2006)..... D-5
Photo D-8. Photograph showing waves from north swell attacking SONGS revetment and refracting towards south at the southern end of SONGS (31 January 2006) D-5
Photo D-9. Photograph showing revetment covered by sand and fronted by a wide beach at the northern end of SONGS (31 January 2008)..... D-6
Photo D-10. Photograph showing waves attacking SONGS revetment at the southern end of SONGS (31 January 2008) D-6
Photo D-11. Photograph showing revetment covered by sand and fronted by a wide beach at the northern end of SONGS (12 November 2013) D-7
Photo D-12. Photograph showing waves attacking SONGS revetment and refracting towards south at the southern end of SONGS (12 November 2013)..... D-7
Photo D-13. Photograph showing revetment exposed and fronted by a wide beach at the northern end of SONGS (27 April 2014)..... D-8
Photo D-14. Photograph showing waves attacking SONGS revetment and refracting towards south at the southern end of SONGS (27 April 2014) D-8
Photo D-15. Photograph showing revetment exposed and fronted by a sand beach at the northern end of SONGS (19 February 2018)..... D-9
Photo D-16. Photograph showing waves from north swell attacking SONGS revetment and refracting towards south at the southern end of SONGS (19 February 2018) D-9
Photo D-17. Photograph showing revetment exposed and fronted by a wide beach at the northern end of SONGS (24 August 2018)..... D-10
Photo D-18. Photograph showing waves from north swell attacking SONGS revetment and refracting towards south at the southern end of SONGS (24 August 2018) D-10
Photo D-19. Photograph showing revetment exposed and fronted by a wide beach at the northern end of SONGS (15 October 2020) D-11
Photo D-20. Photograph showing waves attacking SONGS revetment and refracting towards south at the southern end of SONGS (15 October 2020)..... D-11

EXECUTIVE SUMMARY

The objective of this study is to discuss coastal hazards at San Onofre Nuclear Generating Station (SONGS) in order to evaluate impacts of sea level rise, waves, and wave run-up on the beach, nearshore zone, and SONGS facilities, specifically the SONGS NUHOMS Independent Spent Fuel Storage Installation (ISFSI). The present report describes the possible future effects of sea level rise on the ongoing and long-term influences of waves on the beach, cliffs, protective structures, and wave run-up and overtopping under extreme conditions.

Projections of future Mean Sea Level Rise (MSLR) are evolving rapidly and continuously as the understanding of key climate change processes improves. MSLR projections through 2050 that could impact SONGS are presented in Chapter 2. Discussion and summaries of the currently applicable MSLR guidance, unchanged since OPC (2018), and the newly issued IPCC (2021, 2022) findings are presented in Sections 2.2.1 and 2.2.2, respectively. Maximum high-water level applicable to SONGS is discussed in Section 2.3. Overall, the new IPCC (2021, 2022) projections are lower than existing guidance.

The Young *et al*. (2014) beach and cliff erosion model presented in Chapter 3 is used to compute coastal retreat from MSLR to 2050. The model is tested by simulating historical cliff retreat at Marine Corps Base Camp Pendleton from 1934 to 1998 reported by Hapke and Reid (2007) and using the associated historical MSLR rate and sand budgets from Inman and Masters (1991). Minimum, mean, and maximum modeled retreat rates were generally similar to the observations, suggesting the model is valid for use at San Onofre.

An assessment of the SONGS revetment is given in Chapter 4, including a review of routine maintenance and repair in 2018 and 2019. Section 4.2 gauges the current revetment condition, describes its characteristics, including dimension and weight distributions, from a 2021 inspection. Sections 4.3-4.6 discuss factors influencing revetment stability. Threats in the future remain wave storms exacerbated by MSLR. During winter 2020-2021, the revetment was subject to large waves higher than the previously estimated wave height for the 100-year-return period. Despite these conditions, damage to the revetment and walkway was minimal. This study concludes that with routine maintenance, the revetment can continue to function as intended until at least 2050.

Impacts of groundwater on the ISFSI based on quarterly measurements of the groundwater from nine coastal wells located near the ISFSI are also presented in Chapter 4. The OPC (2018) “medium high-risk aversion” 1:200 (0.5%) and extreme H++ MSLR scenarios for groundwater elevation by 2050 are discussed.

Revetment wave run-up and overtopping analysis is presented in Chapter 5. This work considers the same projection scenarios as in Chapter 4, in combination with ranges of extreme wave return periods, and future high-water elevations. Study conclusions are stated in Chapter 6.

As part of this analysis, Coastal Environments has reviewed the 2001 and 2015 SONGS ISFSI Coastal Development Permit (CDP) and staff report materials and found that the Coastal Commission’s conclusions in those reports remain correct.

COASTAL HAZARD ANALYSIS AT SAN ONOFRE NUCLEAR GENERATING STATION

Part 1: Coastal Hazards

1.0 INTRODUCTION

Southern California Edison (SCE) is undertaking the decommissioning and dismantlement of the San Onofre Nuclear Generating Station (SONGS) (Figure 1-1). Ultimately, the site will be returned to the U.S. Marine Corps Base, Camp Pendleton (MCBCP), under the authority of the Department of the Navy. The present study seeks to determine future coastal hazards impacts at SONGS with respect to climate change, focused on mean sea level rise (MSLR) and waves.

This report discusses the results of our efforts to project future beach, cliff, and nearshore evolution, as well as impact on protected structures, and to assess the probability of flooding at the site with and without the existing seawalls up to 2050.

Following this introduction, the report is organized as follows: Chapter 2 discusses MSLR projections from 2000-2050. The long-term beach and cliff retreat coastal analysis model is described in Chapter 3. Results for revetment stability and beach erosion and accretion due to waves, as well as estimated extreme wave statistics and water surface levels, are discussed in Chapter 4. Estimation of wave run-up and overtopping due to MSLR are presented in Chapter 5. A summary of the study with its conclusions is presented in Chapter 6, followed by a list of references in Chapter 7. Lastly, there are four appendices, A-D.

The best approach to determining future cliff and beach changes is to apply existing peer-reviewed coastal retreat and shoreline fluctuation models, and wave shoaling, run-up, and overtopping methods, with the latest available MSLR guidance.

Power generation at SONGS involved three units, called Units 1, 2, and 3 (Figure 1-3). Construction of SONGS Unit 1 took place from 1964-1966. Unit 1 began operation in 1968. SONGS Units 2 and 3 were built on a prominent natural point of land south of Unit 1, from 1974-1984. Temporary adjacent sheet-pile laydown pads existed for the construction on the beach adjacent to Unit 1 and Units 2 and 3 for each period, respectively. Sand from cliff excavations was placed in each laydown pad. The Units 2 and 3 pads extended about 300 ft across the beach from the seawall. The sand used for both pads dispersed naturally along the beach after each pad was removed, and moved both northward and southward (Flick *et al.*, 2010).

Shoreline change modeling covers about 0.6 mi to the north and south of SONGS, encompassing about 4 mi of coastline from San Mateo Creek in the north to the Cristianitos Fault in the south (Figure 1-2). This coastline consists of an uplifted marine terrace backed by coastal slopes. Erosion of the terrace by marine and subaerial processes has resulted in coastal cliffs and

gullies dissecting the terrace. The sea cliffs extend along the seaward edge of the terrace and are typically 80-125 ft high.

Waves and sand supply from offshore areas, rivers, and cliffs are the major factors controlling the cyclic erosion and accretion of the beach. Waves, rainfall, and drainage from inland areas are primarily responsible for cliff erosion and landslides. The coast is oriented northwest-southeast and is exposed to waves generated by local winds and distant storms in both hemispheres (Flick, 1994). During the winter, swells from the North Pacific and Gulf of Alaska are most energetic, whereas during the summer, swell from the South Pacific dominates (Shepard, 1950). Waves reaching the southern California coast undergo a complex transformation, and wave shadowing from the Channel Islands creates strong alongshore variations in wave height (Pawka, 1983).

Wave erosion of the cliff base and talus occurs when the total water level, defined as the sum of tides and the vertical height of wave run-up (Shih *et al.*, 1994; Kirk *et al.*, 2000; Ruggiero *et al.*, 2001), exceeds the beach elevation at the cliff base. Total water levels are tidally modulated, and tidal fluctuations are more than 6-7 ft during spring tides. However, even large swells arriving during relatively low tides may not reach the cliff base.

Unit 1 was permanently shut down on 30 November 1992. Deconstruction of SONGS Unit 1 began in 1999, and all of the above-ground major structures associated with it below 20 ft MLLW[1] (Mean Lower Low Water, 1941-1960 Epoch), have been demolished and removed. The Unit 1 conduits have been plugged and the intake and discharge risers have also been removed. The Unit 1 site is currently being used as an Independent Spent Fuel Storage Installation (ISFSI) for storing spent nuclear fuel. Units 2 and 3 began commercial operation in 1983 and 1984, and were shut down on 9 January and 31 January 2012, respectively. Small volumes of water intake by the Units 2 and 3 conduits for waste water dilution continues, but heat production no longer occurs. A brief description of Units 1, 2, and 3 may be found in Section 1.1. Sections 1.2 through 1.4 describe changes in the grading of the study area associated with SONGS construction from 1964-1984, the geological composition of the cliffs, and the historical cliff retreat.

1.1 SONGS UNITS 1, 2, AND 3 DESCRIPTION

SONGS Unit 1 was constructed on 12 acres of land facing San Onofre State Beach. The area where Unit 1 was located is now known as the North Industrial Area (NIA). The construction of Unit 1 began with cliff excavation and site grading in March 1964. Unit 1 was positioned along a low straight cliff area next to somewhat higher cliffs, immediately to the northwest and southeast. The cliffs were excavated and some of the sand from the cliffs was placed on the beach to fill a temporary sheet-pile laydown pad seaward of the site that was used for construction activities. The beach to the north of the laydown pad widened due to the construction and remained wide through the end of 1965, at which time the sheet piles were

[1] MLLW (mean lower low water) is a tidal datum calculated as the average value of the lowest observed water level elevations each day over the National Tidal Datum Epoch, a fixed 19-yr period, currently 1983-2001. Tidal datum relationships among each other and relative to geodetic datums, like NAVD88, change with MSL.

removed. The sand in the pad was allowed to redistribute naturally along the beach, resulting in rapid decrease of beach width adjacent to the plant and more gradual adjustment over several years on beaches to the north (Flick *et al.,* 2010). The surface grade of the NIA is about 20 ft MLLW. The top of the permanent tsunami and wave protection seawall fronting the plant at Unit 1 is at an elevation of 28.2 ft MLLW.

SONGS Units 2 and 3 each had an operational capacity of about 1,200 megawatts (MW). The once-through cooling water system for each unit had a flow rate of 830,000 gallons per minute (GPM) and a normal operating temperature increase across the condensers of about 19°F. The single-port intakes of Units 2 and 3 are located about 3,300 ft offshore in 32-ft water depth. The Units 2 and 3 intakes are fitted with velocity caps to minimize entrainment of marine organisms. Large organism exclusion devices have been installed around the intake structures beneath the velocity caps to prevent marine mammals or sea turtles from entering the conduits.

Units 2 and 3 have diffuser-type discharges consisting of 63 ports, spread over a distance of approximately 2,500 ft and extending above the seafloor. The Unit 2 diffuser ports begin 5,900 ft offshore and end 8,400 ft seaward measured from the seawall, and range in water depth from 39 ft to 49 ft MLLW. The Unit 3 diffuser begins 3,600 ft offshore, extends to 6,100 ft at its terminus, and ranges in water depth from 32 ft to 38 ft MLLW (Koh *et al*., 1974).

The top of the permanent tsunami and wave protection seawall fronting the plant at Units 2 and 3 is at an elevation of 30.0 ft MLLW. The bottom of the seawall is at 0.5 ft MLLW. The surface grade east of the seawall is about 30 ft MLLW. A walkway protected by a second lower retaining wall was constructed seaward of the main plant seawall to provide lateral beach access and transit up and downcoast of SONGS. The public beach-access walkway retaining wall is also fronted by rock riprap (revetment) to prevent scour and undermining from the ocean.

NIA was selected as the best location for storing spent fuel from Units 1, 2, and 3 in casks. There are two storage sites at the NIA (Figure 1-4). The eastern location, which was completed in 2003, is the NUHOMS ISFSI, while the western location, which was completed in 2017, is the Holtec ISFSI.

1.2 HISTORICAL CONTEXT

Grading associated with SONGS construction from 1964-1985 significantly changed the pre-existing topography, including major gully infilling north of SONGS (see existing gullies mapped on 1889 and 1934 T-Sheets, Figure 1-5) and cliff excavation at SONGS. The site contains a large seawall fronted by riprap and a lateral beach access walkway, while the cliffs to the north and south are unprotected. A narrow, sandy, and sometimes cobble beach fronts the sea cliffs. Local roads, Interstate 5, and a coastal railroad are immediately inland of SONGS. Construction of these roads and highways has altered natural drainage patterns by concentrating flow in culverts under the roads and railroad.

1.3 GEOLOGIC SETTING AND CLIFF COMPOSITION

The sea cliffs at SONGS are composed of two geologic units with an unconformable contact. The lower portion of the cliff is comprised of the 1- to 3-million-year-old San Mateo Formation, which is composed of massive, poorly cemented, dense sandstone forming a near-vertical face (Hunt, 1975). The upper unit consists of poorly to well-consolidated terrace deposits containing marine and non-marine mixtures and layers of cobbles and fine silty sand 80,000 to 120,000 years old. Both layers are subject to sub-aerial erosion, mainly from rain and associated runoff that produce cliff-face retreat, as well as deep gullies locally known as "barrancas." The lower layer is generally more erosion resistant but is also exposed to wave action.

The Cristianitos Fault (currently inactive) intersects the coastline at the southern end of the study site, causing a change in the lower unit from the sandy San Mateo Formation in the north to landslide deposits underlain by the Monterey Formation in the south (Tan, 2001; Kennedy and Tan, 2007; Young *et al.*, 2010a, 2010b). Cliff samples of the San Mateo Formation and the terrace deposits taken in or near the study area by Young *et al.* (2010a, 2010b) consisted of about 94% sand size particles or larger.

1.4 HISTORICAL CLIFF RETREAT

Hapke and Reid (2007) present the only historical cliff retreat data for MCBCP (Marine Corps Base Camp Pendleton) using the digitized cliff-top positions from a 1934 T-Sheet and 1998 airborne LiDAR data (Figure 1-5). In total, 81 transects from Hapke and Reid (2007) are located in the present study area. For these transects, the cliff retreat from 1934-1998 ranged from 0.0-4.4 ft/yr with an average of about 1 ft/yr (Figure 1-6). The composition of the cliffs north and south of SONGS is shown in Figure 1-7.

Other cliff studies near MCBCP include USACE (1988, 1990), Everts (1991), Runyan and Griggs (2003), Young and Ashford (2006), Hapke *et al.* (2009). These studies estimate mean cliff retreat and gully erosion rates ranging from about 0.5-0.7 ft/yr, respectively. It is difficult to directly compare these studies because they use different quality data sources, time periods, coastline extents, and methods. However, most historical studies agree that over the last century, cliff retreat has generally decreased toward the south in MCBCP.

All historical studies that assess cliff and gully erosion, erosion due to land sliding, and damage to infrastructure from erosion at MCBCP have attributed this erosion to heavy rainfall. To date, no studies document the historical infrastructure damage from marine processes, such as wave action-induced failure. Complete understanding of cliff and gully erosion processes and rates is limited by the fact that spatially and/or temporally averaged histories miss the episodic nature of rapid and extreme short-term erosion events. For example, Kuhn and Shepard (1984) describe several rapid retreat events in excess of 100 ft, including 230 ft of retreat during a single storm. Additionally, retreat rates can vary widely alongshore, and local retreat rates are often several times larger than mean rates. In the MCBCP cliff section, Hapke and Reid (2007) measured a maximum local retreat rate of 5.7 ft/yr.

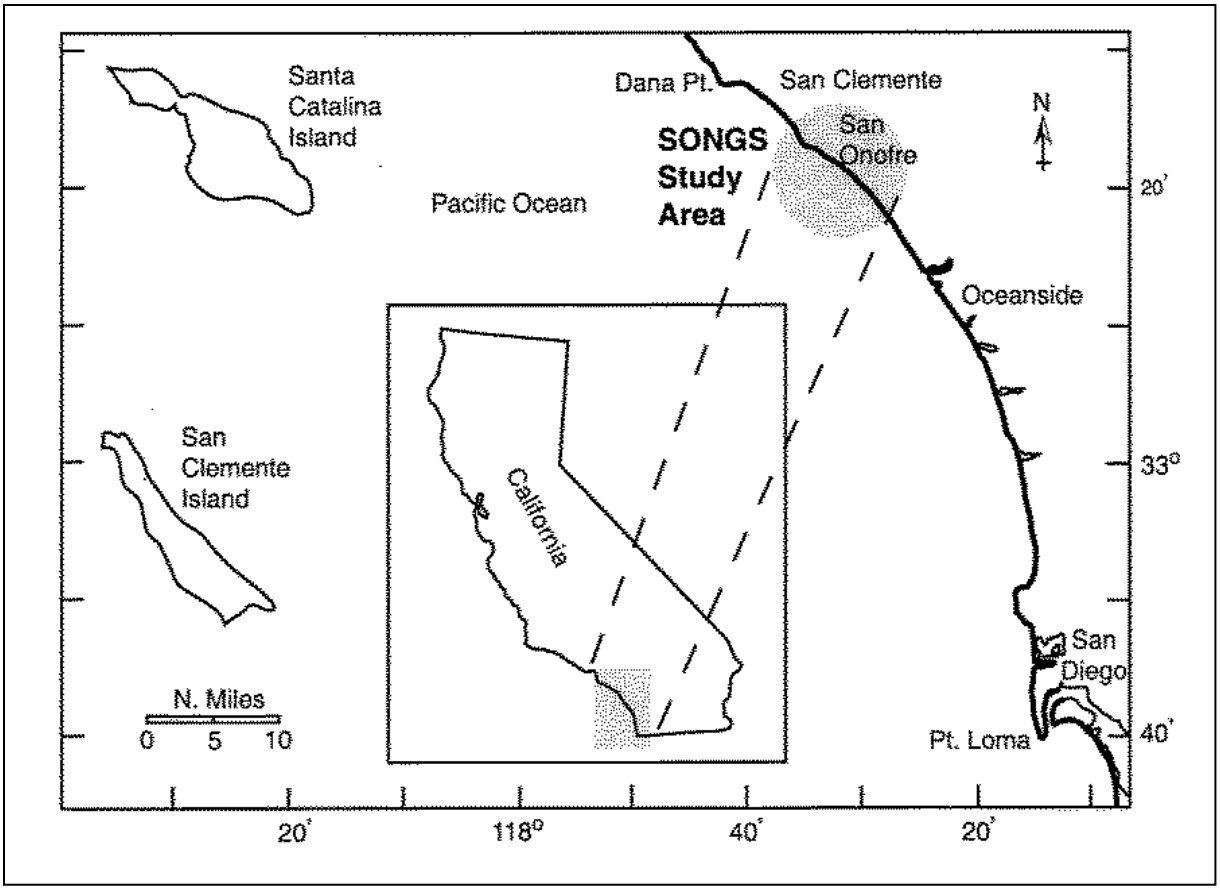


Figure 1-1. Location of SONGS. On the map scale, "N. Miles" stands for nautical miles.

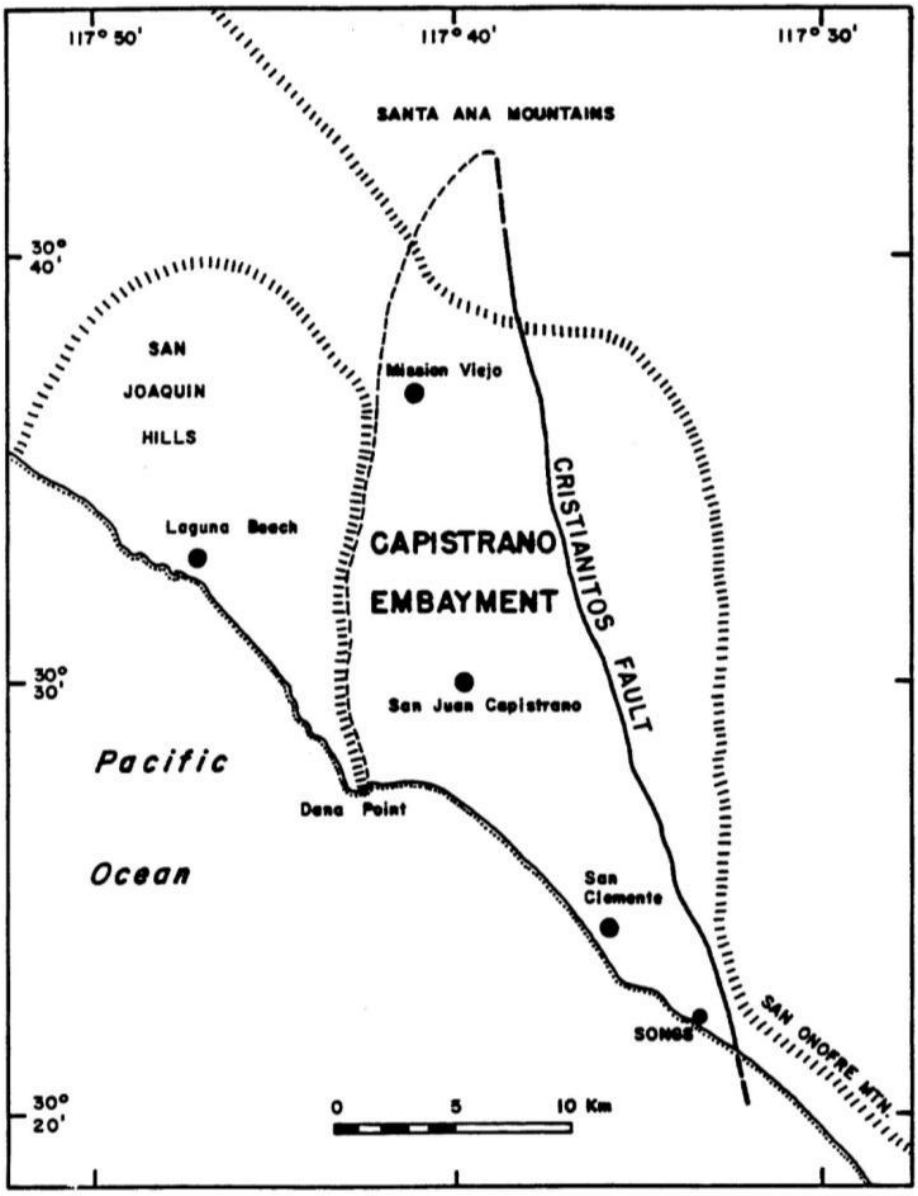


Figure 1-2. Location of Cristianitos Fault with respect to SONGS, located at the south end of the fault line.



Figure 1-3. Unit 1 (left dome), and Units 2 and 3 (right domes), prior to dismantlement of Unit 1.



Figure 1-4. Locations of the Independent Spent Fuel Storage Installations (ISFSIs) at the North Industrial Area (NIA) where Unit 1 was previously located.

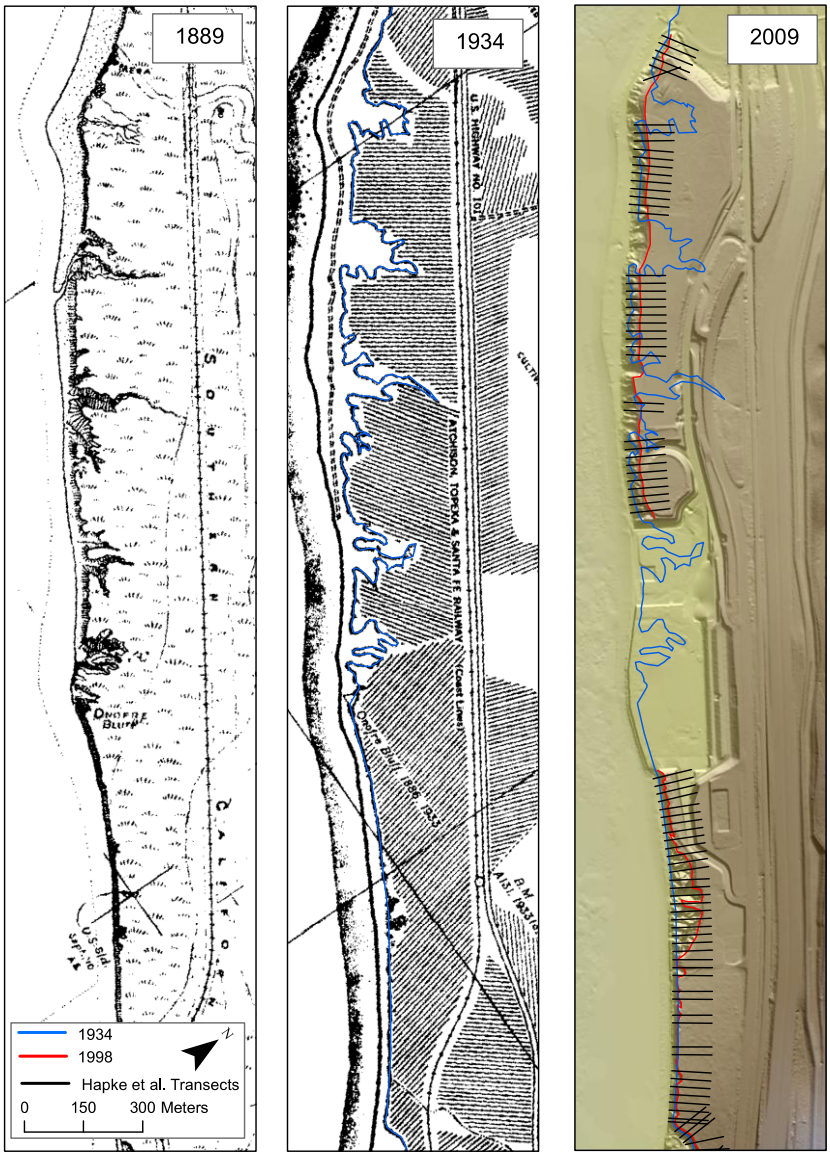


Figure 1-5. Maps of the study area showing 1889 topography (left), 1934 topography and cliff edge (center), and 2009 topography and cliff edge lines (1934 blue, 1998 red) with transects used by Hapke and Reid (2007) (right). A blue line showing the location of the previously-existing undeveloped bluffs from 1934 and a red line showing the developed site as of 1998 are included for reference in the 2009 image.

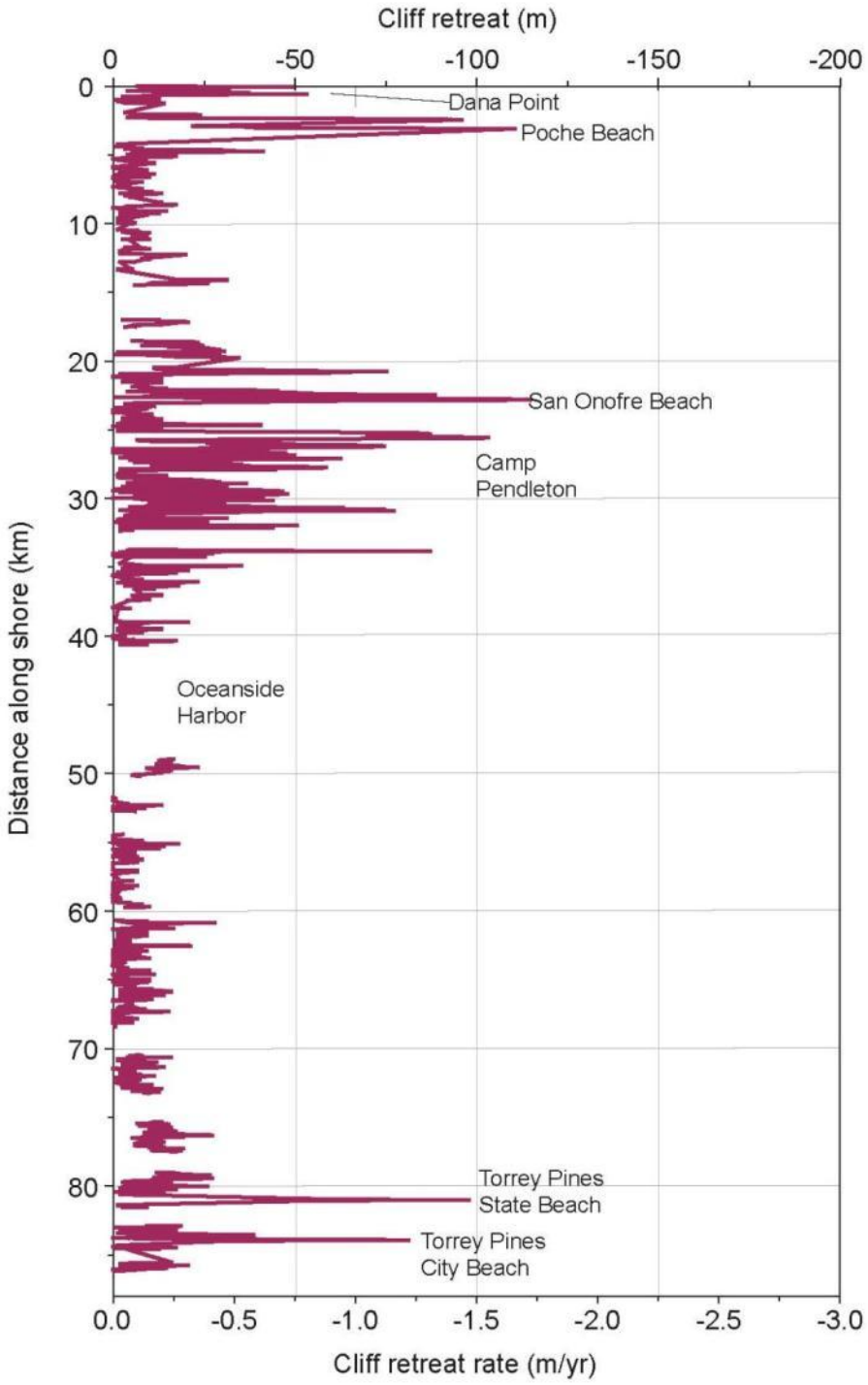


Figure 1-6. Long-term cliff retreat rates and spatial distribution for Oceanside littoral cell (Hapke and Reid, 2007).

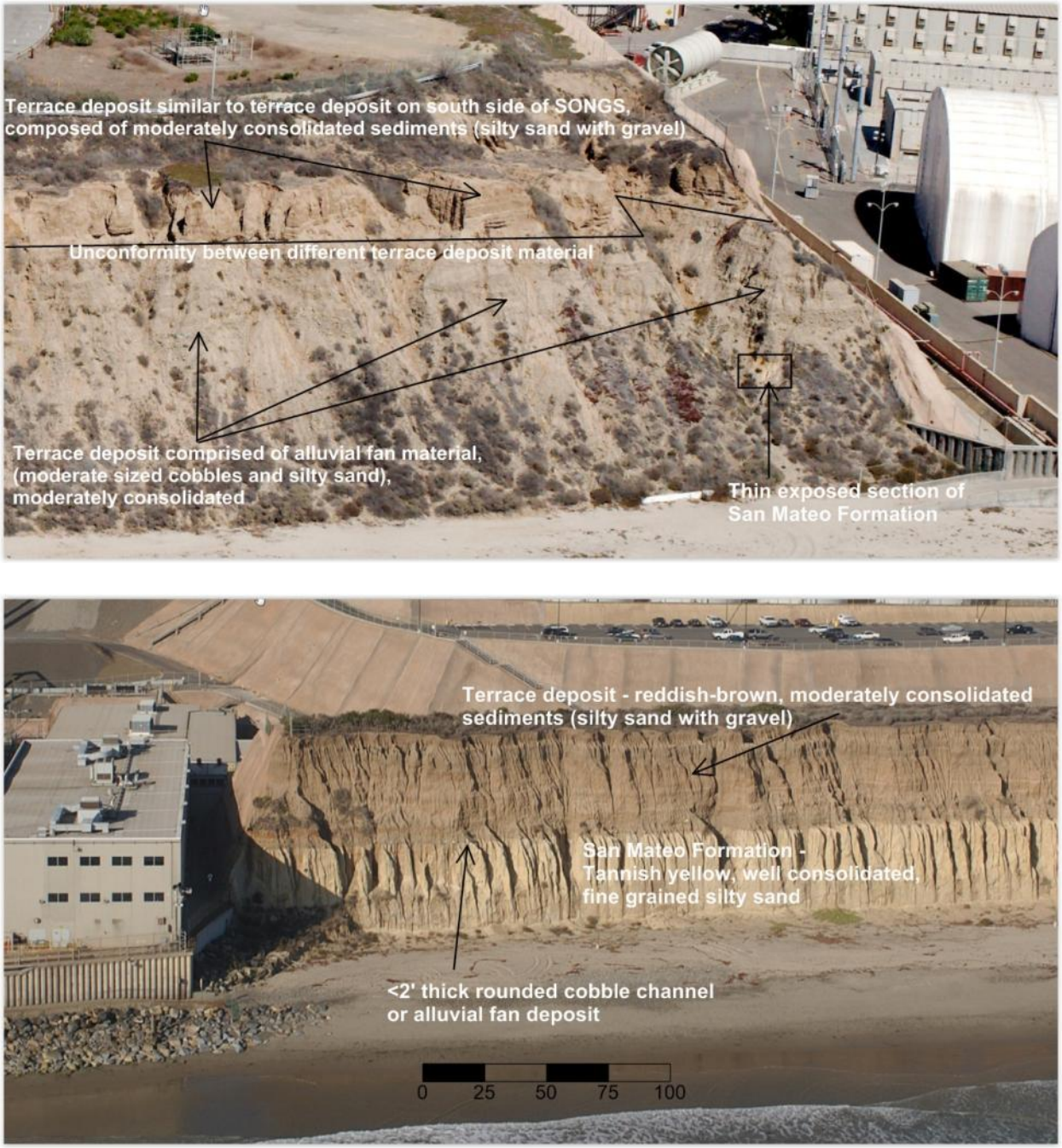


Figure 1-7. Geological description of cliffs north of SONGS (upper) and south of SONGS (lower).

2.0 MEAN SEA LEVEL RISE IMPACT ASSESSMENT

This chapter describes future MSLR scenarios that are used in the SONGS beach and cliff retreat modeling discussion in Chapter 3, and to quantify likely future extreme high-water levels, including tsunamis, to determine facility flooding and structural integrity risks. This chapter also summarizes future MSLR projections developed by the California Ocean Protection Council (OPC 2018) and adopted by the California Coastal Commission (CCC 2015, updated 2018) as official stage guidance for coastal development. The latest MSLR projections from the Intergovernmental Panel on Climate Change (IPCC), Sixth Assessment reports (AR6, IPCC 2021, 2022) are also discussed.

Sea level in this context refers to past measured and future projected mean and extreme (high) water levels, both globally and regionally. Coastal water levels in the San Diego area, including San Onofre, are well represented by data from the La Jolla tide gauge (NOAA Station 941-0230) located at the end of the UCSD/Scripps Institution of Oceanography pier. SONGS area tide and other water level fluctuations are also well represented by data from the Los Angeles (LA) tide gauge (NOAA Station 941-0660) located in Los Angeles Harbor, although the overall historical MSL upward trend is lower at LA than La Jolla.

Figure 2-1 shows the annual and monthly average water levels measured at the La Jolla tide gauge from 1925 to 2021 (black line/symbols, and grey dots, respectively), compared with the global trend (red line) reconstructed by Church and White (2011) from 1880-2009, and extended to 2021 using NASA data (Beckley *et al.*, 2010). Note that the trend of 0.67 ft/century at La Jolla is about 30% greater than the overall global trend of 0.51 ft/century. The acceleration of MSLR about 1970 is also evident, as recognized in the AR6 reports (IPCC 2021, 2022), further considered below.

Regional month-to-month, year-to-year, and decadal water level fluctuations are much larger than corresponding variations in global sea level. This is mainly due to seasonal fluctuations mainly driven by weather changes for the monthly data, as well as El Niño and large-scale oscillations in North Pacific Ocean circulation (e.g., Bromirski *et al*., 2011, 2012; Flick, 1998, 2016) for monthly, year-to-year, and decadal variability that varies from region to region. Note for example that 2016-2021 annual levels at La Jolla show a small and likely short-term downward trend associated with large scale cooling in the North Pacific.

2.1 SONGS SEA LEVEL INFORMATION

Elwany, *et al.* (2020) introduced new California state agency documents that provide updated MSLR policy, plans, or other information potentially affecting SONGS activities. State agency advances include four reports that essentially laid out the guidance provisions still in effect as of this writing in early 2022. These reports were: Griggs *et al.* (2017) from the California Ocean Protection Council and Ocean Science Trust; Bedsworth *et al.* (2018) titled, "*California's Fourth Climate Change Assessment, Statewide Summary Report"* from the California Governor's Office of Planning and Research, Scripps Institution of Oceanography, California Energy Commission, and California Public Utilities Commission; OPC (2018) with update sea level rise guidance; and CCC (2015, updated 2018), which adopted the OPC (2018)

framework as its official policy. Elwany, *et al.* (2021) discusses MSLR vulnerability of the revetment fronting SONGS and an update of the sea level information presented in Elwany *et al*. (2020). This included a summary of existing State of California guidance; 2020 mean sea level (MSL) data, and California state agency documents included CCC (2020a), CCC (2020b), OPC (2020), and CNRA-CEPA (2020). Elwany *et al*. (2022) summarizes the currently existing guidelines applicable MSLR guidance and the newly issued Intergovernmental Panel on Climate Change (IPCC 2021, 2022) findings. These reports are being written to comply with California State Lands Commission Provision 14 in Lease No. PRC 6785.1

2.2 MEAN SEA LEVEL RISE GUIDANCE

Current CCC MSLR guidance (CCC 2015, updated 2018) for coastal development is based on findings from OPC. OPC (2018) developed a set of probability-of-occurrence future MSLR scenarios through 2150, relative to 2000. This study considers the extreme H++ projection scenario from this guidance, and in combination with the 1-, 2-, 10-, and 100-year return period high-water events, which include so-called "King Tides" through 2050. We compare the OPC (2018) guideline scenarios with newly published future MSLR trajectories (also made to 2150), from the latest IPCC reports (AR6, IPCC 2021, 2022). In summary, the IPCC projections are lower than those from OPC.

OPC (2018) contains MSLR projections specific to numerous California coastal areas, including La Jolla. This was part of a statewide effort to improve upon projections from IPCC AR5 (IPCC 2013, 2014) in three respects: First, to produce a low-probability but large-impact extreme high scenario (i.e., H++) that AR5 was missing because consensus could not be reached on future rates of Greenland and Antarctic ice contributions; Second, to assign likelihood probabilities for an array of future MSLR scenarios based on the IPCC AR5 "Representative Concentration Pathway" (RCP) future global socio-economic ranges considered; And finally, to make available regional projections for different parts of the California coast. The OPC (2018) scenarios were adopted by the CCC for their Sea Level Rise Policy Guidance policy document (CCC 2015, updated 2018), which must be considered when applying for a coastal development permit.

MSLR projections are continuously evolving in response to rapid data acquisition and improved scientific understanding of key climate change processes (e.g., IPCC 2021, 2022 for a full discussion). Of special concern are the possible ongoing and future ranges and rates of glacial ice loss in Greenland and Antarctica (e.g., DeConto and Pollard, 2016). Future MSLR is highly uncertain, especially after about 2050, for several reasons. The largest unknown is what mitigation strategies humans will employ to decrease the rates and amounts of greenhouse gas (GHG) emitted and ultimately resident in the atmosphere. Second, the climate sensitivity, or amount and rate of warming for a given increase in GHGs, is not precisely known. In particular, polar ice response to existing and future warming is not yet reliably predictable.

2.2.1 California OPC (2018) MSLR Projections

With one caveat concerning a potential increase in the maximum State of California MSLR guidance target value from 2.8-3.5 ft by 2050 (please see Elwany *et al.*, 2021 for details),

the currently existing guidance, so far unchanged, is summarized herein. OPC (2018) and CCC (2015, updated 2018) MSLR projections for La Jolla from 2000-2050 are listed in Table 2-1. These projections have probability ranges associated with them that originated from IPCC AR5 (2013) by calculating probabilities of each RCP scenario, as mentioned above. Each RCP has a numerical designation condensing a host of projected socio-economic factors into a final average global radiation imbalance in Watts/m^2 by 2100. The full range is RCP2.6 to RCP8.5, respectively from "Low" to "High." Thus, for example, "RCP4.2" represents a "Moderate" total GHG trajectory that results in a net radiative Earth heating imbalance 4.2 Watts/m^2 by 2100. The probability estimates use the framework of Kopp *et al.* (2014).

From 2000-2050, only the "High" MSLR set of trajectories are considered in OPC (2018). This is based on two factors: First, there are no ambitious global GHG emissions reduction plans presently apparent, and second, even if emissions immediately dropped to net-zero, warming and MSLR would continue for at least many more decades owing to ocean warming and ice-melt inertia. In effect, both High and Low trajectories produce near-identical projections between 2000 and 2050, and only begin to differ after mid-century.

Table 2-1 shows five columns (Columns 2-6) headed with percentage probability numbers, and one (Column 7) indicated as H++. Column 2 titled "50%" indicates the median projected MSLR each year (Column 1) relative to 2000. That means, for example, there is a 50:50, or "even" chance that MSLR will be less than or greater than 0.9 ft by 2050, that is from 2.5-3.4 ft, NAVD88[2] relative to 2000. Columns 3-4 titled "Lo > 67% < Hi" bracket the 2/3 probability that MSLR will fall outside these numbers. In other words, it is 2/3 likely that MSLR will be above the 67% Lo trajectory (Column 3), and 2/3 likely that it will be below the 67% Hi projection (Column 4). Equivalently, it is 1/3 likely that MSL will reach between 3.2-3.7 ft by 2050, and 1/3 likely each that it will remain either below 3.2 ft, or rise above 3.7 ft. Columns 5 and 6, respectively, provide the MSLR path that has a 5%, or "1 in 20," and a 0.5% or "1 in 200" chance of being exceeded. This means there is only a 1 in 200 chance that MSL will reach or exceed 4.5 ft by 2050. The H++ scenario (Column 7) is included in OPC (2018) to account for the for now still remote possibility that *"…rapid ice sheet loss on Antarctica could drive rates of sea level rise in California above 50 mm/year (2 inches/year) by the end of the century, leading to potential sea level rise exceeding 10 feet. This rate of sea level rise would be about 30-40 times faster than the sea level rise experienced over the last century."* This suggests there is an unquantifiable, but small, probability that MSL will reach 5.3 ft or higher by 2050 Table 2-1, Column 7).

Figure 2-2 (upper and lower) illustrate the OPC (2018) trajectories described above along with the actual average annual and monthly MSL data measured at the La Jolla tide gauge also shown in Figure 2-1. The projections in Figure 2-2 were adjusted so their average over the 19-year epoch 1991--2009 (centered on year 2000) was 2.5 ft NAVD88 to match the corresponding

[2] NAVD88 – North American Vertical Datum of 1988 – A fixed geodetic reference for elevations determined by geodetic leveling of the United States, Canada, and Mexico. NAVD88 is currently the official national reference used by engineers and surveyors and supported by NOAA-National Geodetic Service. Geodetic refence elevations do not change with MSL, as opposed to tidal datums, which do.

average value of the observations over the same epoch.[3] Figure 2-2 (upper) shows the entire measured water level record from 1925-2021, along with the projections from 2000-2050. Figure 2-2 (lower) is the same information but focused from 2000-2050 to facilitate comparison between data and projections. This shows that all annual average except 2015 so far fall close to or below the 50-50 trajectory (blue broken line). This could be interpreted to mean that the OPC (2018) projections since 2000 overestimate actual MSLR. However, as Figure 2-1 indicates, the natural inter-annual variability range is about 0.5 ft, while the seasonal and other variations in monthly means ranges about 1.2 ft, which is larger than the current difference between the highest and lowest scenarios (~0.4 ft). Which trajectory MSLR is actually on should become more apparent approaching mid-century (2035-2050), when projected values increase significantly and their range broadens to 1-2 ft.

2.2.2 IPCC (2021) MSLR Projections

Following the IPCC (2013, 2014) AR5 reports, and in accord with its approximately -seven-year cycle, the IPCC has prepared the Sixth Assessment Report (AR6, IPCC 2022) scheduled for release in September 2022. Three specialized working groups have contributed to this undertaking, including Working Group I (WGI), which published its findings concerning the *"Physical Science Basis"* in IPCC (2021). The topics assessed by WGI cover: atmospheric GHGs and aerosols; air, land, and ocean temperature changes; climate sensitivity; extreme weather; and hydrological, glacier, ice sheet, ocean, sea level, carbon cycle, and biogeochemical processes. WGI combined modern observations, paleoclimate data, and extensive, international, inter-comparison data-adaptive modeling to build a more robust picture of Earth's climate and its rapid changes.

The primary conclusion of the WGI (IPCC 2021) report is:

A.1 It is unequivocal that human influence has warmed the atmosphere, ocean and land. Widespread and rapid changes in the atmosphere, ocean, cryosphere and biosphere have occurred.

Specific to sea level rise, key findings include:[4]

A.1.7 Global mean sea level increased by 0.20 m between 1901 and 2018. The average rate of sea level rise was 1.3 mm yr^{-1} between 1901 and 1971, increasing to 1.9 mm yr^{-1} between 1971 and 2006, and further increasing to 3.7 mm yr^{-1} between 2006 and 2018. Human influence was very likely the main driver of these increases since at least 1971.

A.2.4 Global mean sea level has risen faster since 1900 than over any preceding century in at least the last 3,000 years. The global ocean has warmed faster over the past century than since the end of the last deglacial transition (around 11,000 years ago).

[3] For details concerning datum adjustments for these purposes please see Flick *et al*. (2013).
[4] Some conclusions edited or shortened for clarity and brevity. Original report heading numbers retained.

B.5 Many changes due to past and future greenhouse gas emissions are irreversible for centuries to millennia, especially changes in the ocean, ice sheets and global sea level.

B.5.4 Sea level is committed to rise for centuries to millennia due to continuing deep ocean warming and ice-sheet melt and will remain elevated for thousands of years. Over the next 2,000 years, global mean sea level will rise by about 2-3 m if warming is limited to 1.5°C, 2-6 m if limited to 2°C and 19-22 m with 5°C of warming, and it will continue to rise over subsequent millennia (low confidence). Projections of multi-millennial global mean sea level rise are consistent with reconstructed levels during past warm climate periods: likely 5-10 m higher than today around 125,000 years ago, when global temperatures were very likely 0.5°C-1.5°C higher than 1850-1900; and very likely 5-25 m higher roughly 3 million years ago, when global temperatures were 2.5°C-4°C higher.

A vital part of the massive 3,949-page WGI *"The Physical Science Basis"* document (IPCC 2021) is the development of new MSLR projections, both for the global mean trajectory, and for regional trajectories at hundreds of coastal and island locations around the world. Projection data are publicly available, through a creative commons international license, from NASA[5] (Fox-Kemper *et al*., 2021, Garner *et al.*, 2021). Inexplicably, only projections from San Diego Bay Quarantine Station and LA are available nearest San Onofre, while La Jolla is absent. While the LA tide regime closely matches that at La Jolla, the overall historical upward MSLR trend at LA (1 mm/yr) is half that at La Jolla (2 mm/yr), over the period of 1925--2020. However, the trends are much more similar from 1975-2021, with 1.6 mm/yr at LA and 1.8 mm/yr at La Jolla. In addition, IPPC (2021) projection trends at other southern California locations and Ensenada, Mexico available on the NASA website suggest that these are at least similar or nearly identical to LA. It is therefore assumed that projections at La Jolla, if they had been made, would be the same as those at LA, so these are utilized in this report.

IPCC uses two conditional descriptors, *"likelihood,"* and *"confidence"* to characterize their conclusions and projections, including, MSLR. "*Likelihood*" gauges the probability spread that a projection will fall in a specified numerical range. Likelihood is quantifiable, and spans high to low (probability) from, *"virtually certain"* (99-100%); *"very likely"* (90-100%); *"likely"* (66-100%); *"about as likely as not"* (33-66%); *"unlikely"* (0-33%); *"very unlikely"* (0-10%); to *"exceptionally unlikely"* (0-1%). "*Confidence*," on the other hand, is not quantitative or statistical, but a more subjective assessment of how reliable a particular result may be. Confidence levels range from "*very low," "low," "medium," "high,"* to *"very high.*" These terms are based on IPPC "*author teams' judgments about the validity of findings as determined through evaluation of evidence and agreement*" (Mastrandrea *et al.*, 2010).

Like OPC (2018), the IPCC (2021) MSLR projections are based on an intricate analysis of a wide range of possible future Earth warming scenarios and the processes that contribute to

[5] https://sealevel.nasa.gov/ipcc-ar6-sea-level-projection-tool

MSLR. These include ocean warming and resulting expansion, addition of water from land-based ice melt, changes in freshwater runoff due to global groundwater pumping and dam construction, changes in ocean circulation that affect the dynamical water height at coasts, and land movement such as uplift from glacial unweighting, among others.

AR6 (IPCC 2021) produced future MSLR projections that could be made with at least "*medium confidence,*" or somewhere near the middle of the "confidence" range. The projections were based on five possible future climate evolutions termed "*Shared Socioeconomic Pathway*" (SSP) scenarios that are analogous to, but broader than, the "Representative Concentration Pathway" (RCP) trajectories used in AR5 (IPCC 2013). The MSLR projections are assessed based on the combination of uncertainty in temperature change associated with emissions scenarios, and uncertainty in the relationships between global temperature and processes responsible for projected MSLR. In this context, *"likely"* means a probability of occurrence at least 66%. Each scenario has a low, median, and high MSLR amount associated with it for 2030, 2050, and additional years through 2150 relative to 2004-2005 (adjusted to 2000).

The five IPCC (2021) scenarios are described as follows and involving *"very likely"* (i.e., at least 90% probable) global temperature increases by 2100 above the 1850-1900 median:

- **SSP1-1.9** – Low emissions scenario with net-zero CO_2 by mid-century (~2050). Temperature warming projected as 1.0°-1.8°C by 2100, after a slight overshoot.
- **SSP1-2.6** – Low to moderate pathway with net zero emissions in second half of century (2050-2100). Warming 1.3°-2.4°C.
- **SSP2-4.5** – Moderate scenario in line with upper end of aggregate "Nationally Determined Contribution" emission by 2030. Warming 2.1-3.5°C.
- **SSP3-7.0** – Medium to high "reference" scenario with no additional climate policy (i.e., "business as usual"), resulting in particularly high non-CO_2 emissions, including high aerosols. Warming 2.8°-4.6°C.
- **SSP5-8.5** – High "reference" scenario with no additional climate policy. Emission levels from fossil fueled SSP5 socioeconomic development pathway. Warming 3.3-5.7°C.

A sixth "*low confidence*" but high potential impact scenario projection ("**SSP5-8.5Lo**" herein, where "Lo" stands for "Low Confidence") added for the first time by IPCC in AR6 indicates the possible, but as yet unlikely, effects of deeply uncertain ice sheet processes supported by limited evidence and little current agreement among experts. The projection uses Greenland and Antarctic findings from a "Structured Expert Judgement" study by Bamber *et al.* (2019), and results from Antarctic marine ice cliff instability simulations by DeConto *et al.* (2021). This scenario is roughly comparable to the OPC (2018) H++ trajectory, albeit with a considerably lower upper range of MSLR.

The IPCC (2021) projections use the 20-yr period 1995-2014 (center years 2004-2005) as their base with MSLR reckoned from there. This is slightly different from the OPC projections, which used a 19-yr base of 1991-2009 (center year 2000). However, the adjustment for the LA

MSLR projections to make their start year 2000 is small, about 0.014 ft, which has been applied in what follows.

This report concerns projected MSLR through 2050. The relevant IPCC (2021) values are summarized in Tables 2-2 and 2-3 and plotted in Figure 2-3. Table 2-2 shows the median MSLR value for each SSP scenario for 2000, 2030, and 2050 in ft, NAVD88. Table 2-3 shows the range low to high for each scenario. Comparison with the OPC (2018) scenarios (Table 2-1, Column 7) shows that the IPCC (2021) SP5-8.5Lo values in 2030 and 2050 (Column 7) are 0.7 ft and 1.9 ft lower, respectively, than the OPC (2018) H++ numbers. Furthermore, Tables 2-2 and 2-3 (Columns 7) suggest that the range from 2000-2050 of the SSP5-8.5Lo scenario is fairly small, with the median value rising 0.8 ft (2.5-3.3 ft), and a low to high range change of 0.6-1.4 ft (2.5-3.1 ft and 2.5-3.9 ft, respectively). Except for the H++ and SSP5-8.5Lo scenarios, the (respective) OPC (2018) and IPCC (2021) trajectories in Tables 2-1 to 2-3 are not directly comparable, since the IPCC SSP scenarios do not have associated probabilities of occurrence, only that they are "*very likely*." However, the overall results suggest that all IPCC scenarios produce mostly lower, or at most equal, projected MSLR by 2050 than all OPC trajectories, including H++.

Figure 2-3 illustrates the narrow range of likely MSLR from IPCC (2021) between now and 2050. The high, median, and low SSP5-8.5Lo MSLR scenarios are shown with solid red lines. The spread between high and low in 2050 is 0.8 ft (i.e., 3.1-3.9 ft, Column 7). The remaining SSP scenario median value trajectories (broken lines) are labelled only with their numerical value range, and "Conf" indicating "*medium confidence,"* and "Mid" meaning "*median*" values (Table 2-2), as opposed to the "low" to "high" range (Table 2-3). All median values of the lowest five SSP trajectories (Table 2-2, Columns 2-6) fall between the median and low SSP5-8.5Lo projections. Finally, it is apparent that the IPCC (2021) projections more closely fit the actual MSLR data from 2000-2021 compared to the OPC (2018) scenarios.

2.3 SONGS SEA LEVEL EXTREMES

It is important to recognize that water elevation at or around MSL generally does not cause flooding, erosion, or infrastructure damage. Damages almost always occur during times of extreme high water levels that, on the California coast, are driven mainly by coincidence of peak high tides and large storm waves. Elevated water levels due to El Niño and other large-scale oceanographic phenomenon also raise maximum water levels for months to several years. Of course, a continued and likely accelerated MSLR will continuously worsen these effects causing them to become more severe and last longer. For further details, see Elwany *et al.* (2020).

Observed maximum monthly water levels (in ft, NAVD88) published by NOAA for the La Jolla tide gauge are plotted in Figure 2-4, which is updated from Elwany *et al.* (2020). It is apparent that monthly maxima are increasing as sea level rises, which is expected to continue in the future. Table 2-4 lists the six highest maximum monthly water levels observed at La Jolla relative to NAVD88 and NGVD.[6] The legacy NGVD was useful since it regionally lay close to

[6] NGVD – National Geodetic Vertical Datum - A fixed geodetic reference for elevations determined by leveling in the United States and Canada. Also known as "NGVD29" or "MSL29." This is a legacy datum no longer supported

MSL in the past. While NGVD is no longer supported by NGS or routinely employed by surveyors and engineers, it is still beneficial because of its extensive and long use for coastal measurements and studies, including many at SONGS. NGVD lies 0.43 ft below current MSL (as defined by the 1983-2001 epoch), and 2.11 ft below NAVD88.).

The all-time maximum reading occurred on 25 November 2015 during the 2015-16 El Niño warming event, which also produced the highest-ever annual average level observed at La Jolla. Note that the four highest events exceeding the previous record elevation of 1983 occurred in only 18 years, from 1997-2015.

NOAA-NOS also provides statistics of extreme sea levels based on the observations discussed. Their current estimates of "return period," or the probability of exceeding a given value in any year, are summarized in Table 2-5 relative to NAVD88 and NGVD. Note the relatively small spread of less than 1 ft between the 1% (100-yr) and 99% (1-yr) extreme high water level events. This illustrates the dominant influence of the astronomical tide on extreme water levels along the California coast. The highest tide is about 7 ft above NAVD88, less than about 0.5 ft below the 100-yr return event. It also illustrates the exceedingly rare coincidence of peak high tides with extraordinary storm surges or other water level enhancing processes, such as El Niño, which can raise MSL up to about 1.5 ft over time scales of days to a year (Flick, 2016).

by NOAA-National Geodetic Survey.

Table 2-1. OPC (2018) MSLR Projections, La Jolla (ft NAVD88).

1	2	3	4	5	6	7
Year	**50%**	**Lo > 67% < Hi**		**5%**	**0.5%**	**H++**
2000	2.5	2.5	2.5	2.5	2.5	2.5
2030	3.0	2.9	3.1	3.2	3.4	3.6
2040	3.2	3.0	3.4	3.5	3.8	4.3
2050	3.4	3.2	3.7	3.9	4.5	5.3

Table 2-2. IPCC (2021) Mid-Range MSLR Projections, Los Angeles (ft NAVD88).

1	2	3	4	5	6	7
Year[7]	**SSP1-1.9**	**SSP1-2.6**	**SSP2-4.5**	**SSP3-7.0**	**SSP5-8.5**	**SSP5-8.5[8]**
2000	2.5	2.5	2.5	2.5	2.5	2.5
2030	2.8	2.9	2.9	2.9	2.9	2.9
2050	3.1	3.2	3.2	3.2	3.3	3.3

Table 2-3. IPCC (2021) Low-High Range MSLR Projections, Los Angeles (ft NAVD88).

1	2	3	4	5	6	7
Year[8]	**SSP1-1.9**	**SSP1-2.6**	**SSP2-4.5**	**SSP3-7.0**	**SSP5-8.5**	**SSP5-8.5[9]**
2000	2.5	2.5	2.5	2.5	2.5	2.5
2030	2.7-3.0	2.7-3.0	2.7-3.0	2.7-3.0	2.8-3.0	2.8-3.1
2050	2.9-3.4	3.0-3.5	3.0-3.5	3.0-3.5	3.1-3.6	3.1-3.9

[7] IPCC (2021) 2004-2005 base year projections adjusted to base year 2000 (see text).
[8] SSP5-8.5 "low confidence" projection conceptually equivalent to OPC (2018) H++ scenario (see text).

Table 2-4. Highest Maximum Observed Total Water Levels, La Jolla (ft).

Year Month	NAVD88	NGVD
2015 Nov	7.62	5.51
2005 Jan	7.47	5.36
1997 Nov	7.46	5.35
2012 Dec	7.42	5.31
1983 Aug	7.36	5.25
1983 Jan	7.26	5.15

Table 2-5. NOAA La Jolla Extreme Water Level Statistics (ft).

Percent/Yr	Return (Yrs)	NAVD88	NGVD
1%	100	7.43	5.32
10%	10	7.20	5.09
50%	2	6.94	4.82
99%	1	6.51	4.40

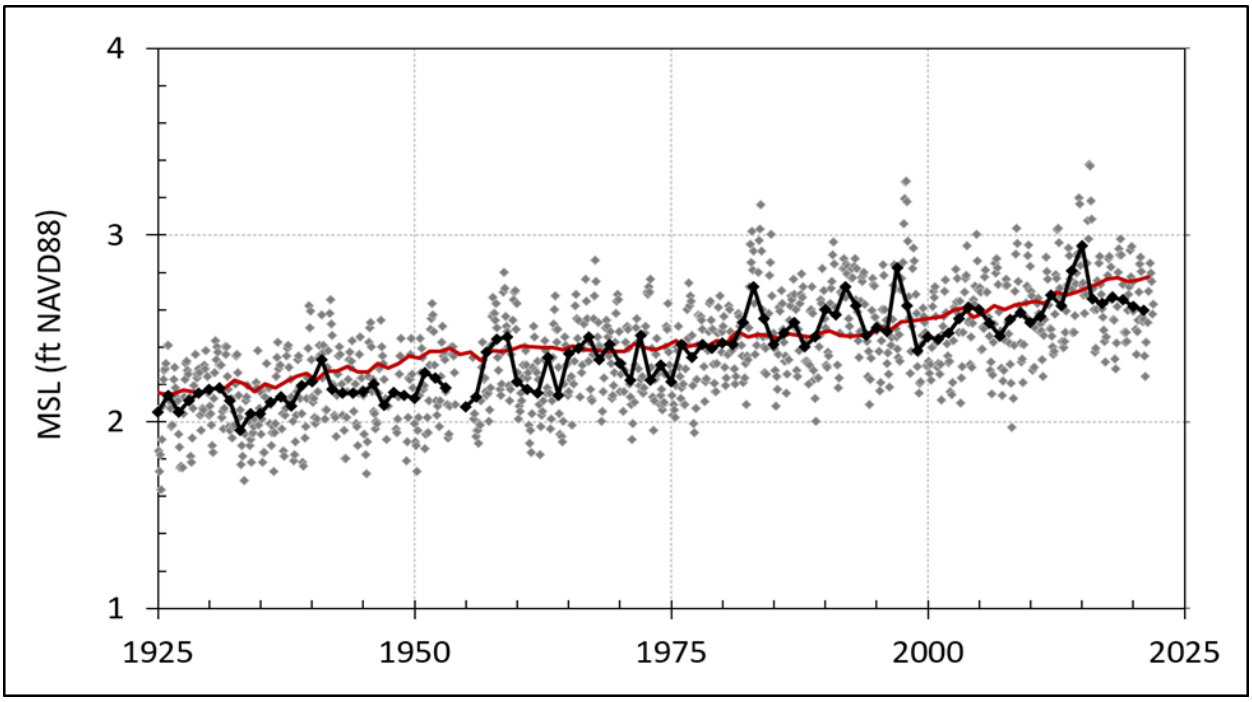


Figure 2-1. Annual and monthly average water level relative to NAVD88 at La Jolla, 1925-2021 (black line/symbols, grey symbols, respectively), and annual global MSL reconstruction (red line).

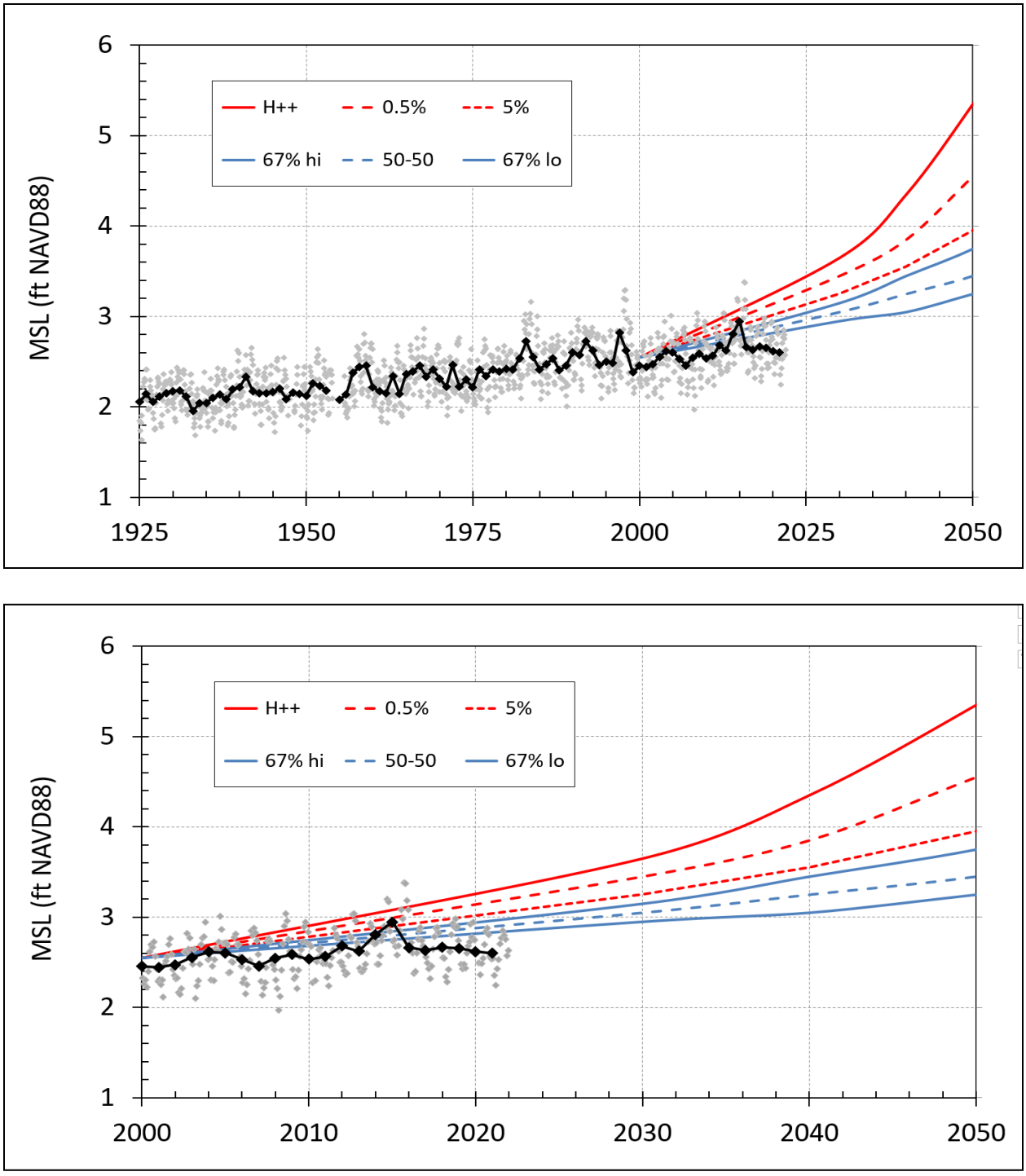


Figure 2-2. La Jolla average MSL data, 1925-2021, annual (black), monthly (grey) (upper). Same for 2000-2021 (lower). Both with OPC (2018) La Jolla MSLR projections, 2000-2050 (see legend and text).

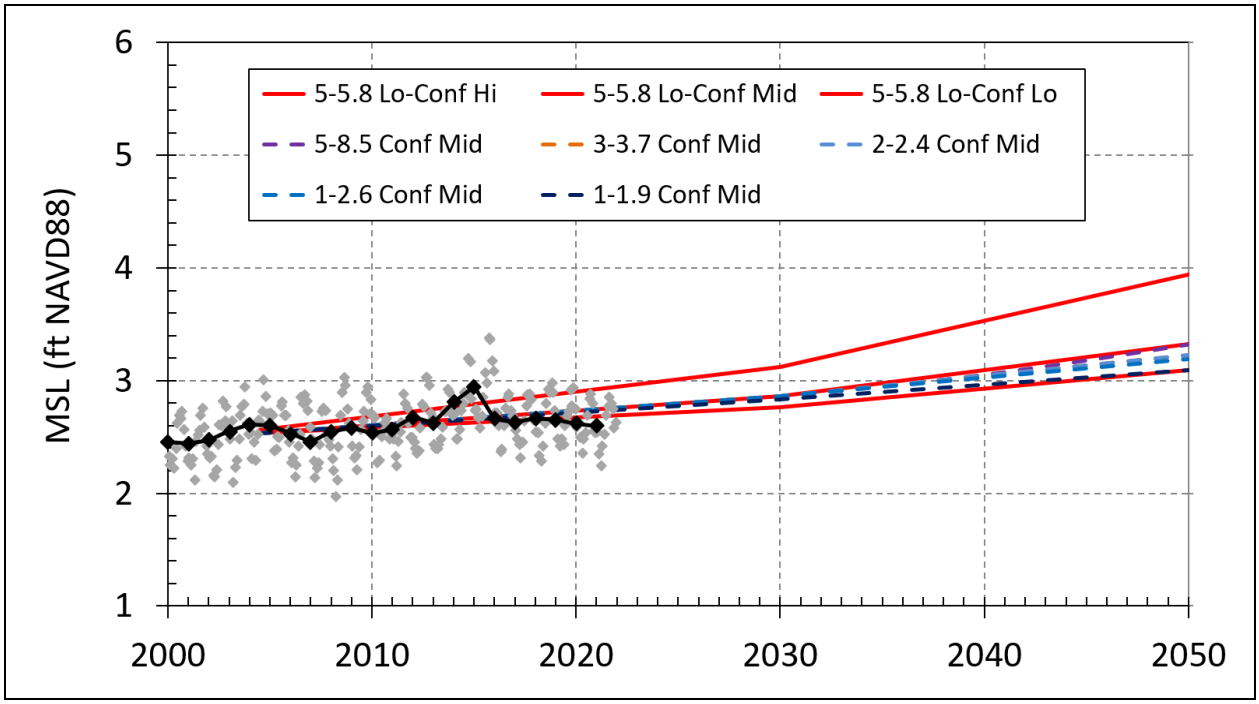


Figure 2-3. La Jolla average MSL data, 1925-2021, annual (black), monthly (grey), with IPCC (2021) LA MSLR projections, 2004.5-2050 (see legend and text).

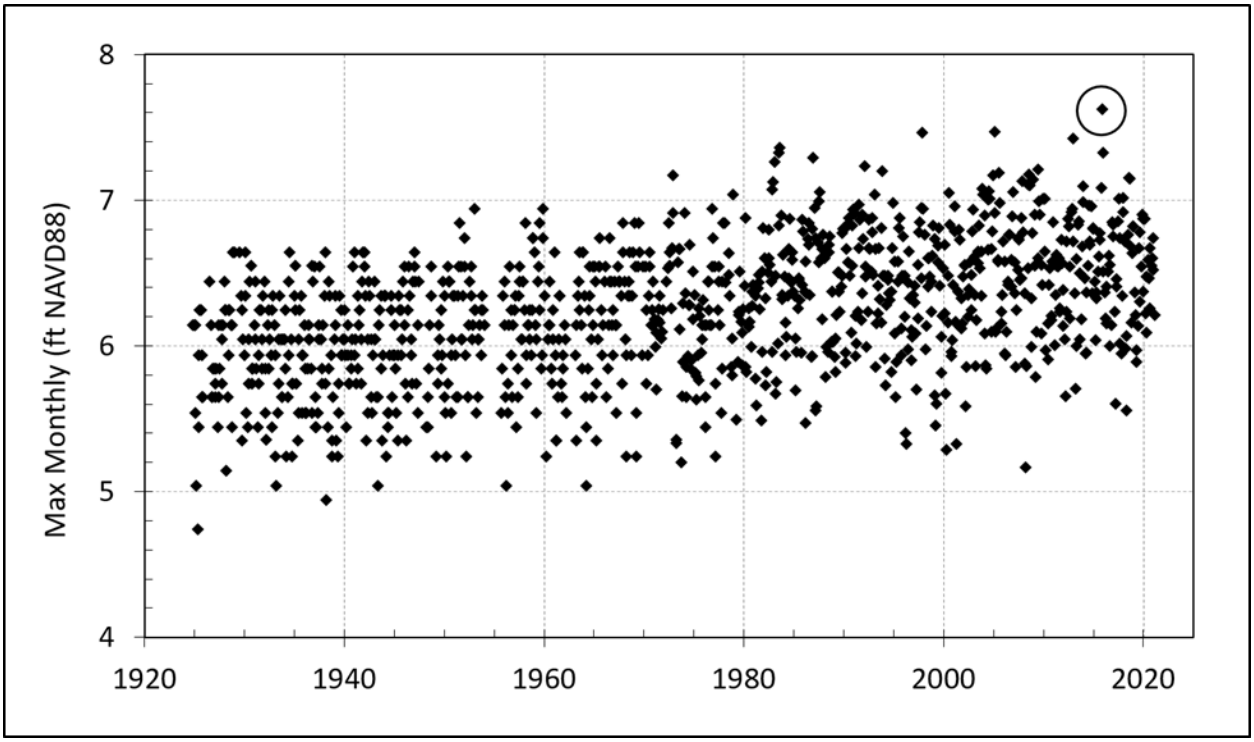


Figure 2-4. Monthly maximum sea level at La Jolla relative to NAVD88 datum, 1925-2021 (black symbols). Maximum observed 7.62 ft height (circled) on 25 November 2015 during 2015-16 El Niño. Note 2020-2021 well below historical maxima (1983-2015).

3.0 BEACH AND CLIFF RETREAT MODEL

We employed the "conditionally decoupled profile model" of Young *et al.* (2014) to project the long-term (2010-2050) sea level rise-driven coastal retreat. The model draws on aspects of complex and sand equilibrium modeling (Wolinsky and Murray, 2009; Ashton *et al*., 2011) and incorporates these results into a sand balance model specifically adapted for coastal cliffs fronted by beaches subjected to marine and subaerial erosional processes. The model was originally developed with Space and Naval Warfare (SPAWAR) Systems Center Pacific to estimate cliff retreat at MCBCP. Subsequently, the model was also selected and applied to Naval Base Coronado (Chadwick *et al.*, 2014) and along the Los Angeles coast as part of regional efforts to quantify future land loss (USC, 2013).[9]

Coastal recession associated with MSLR is often estimated using "Bruun rule" concepts of equilibrium profile and volume conservation (e.g., Bruun, 1962). The original Bruun rule, designed for low-lying sandy coasts, assumes a fixed, active beach profile during coastal recession, homogeneous coastal material, and no external sand sources or sinks. Although commonly applied (e.g., Zhang *et al.*, 2004), the Bruun rule assumptions are often ignored or not satisfied, prompting criticism (e.g., Cooper and Pilkey, 2004; Pilkey and Cooper, 2004; Woodroffe and Murray-Wallace, 2012). Cliffed coasts rarely (if ever) satisfy the original Bruun rule assumptions, leading to the use of modifications, including heterogeneous coastal material, external sand sources and sinks, and variable inland topography (Dean and Maurmeyer, 1983; Hands, 1983; Dean, 1991; Bray and Hooke, 1997; Wolinsky and Murray, 2009).

Young *et al.* (2014) built upon these Bruun rule modifications, recent equilibrium profile cliff modeling (Wolinsky and Murray, 2009; Ashton *et al.*, 2011), and established rock coast concepts to estimate cliff retreat based on coastal system sand balance, process-based relationships, and conditionally decoupled active beach and cliff profiles. The model is specifically adapted for cliffed coasts fronted by beaches, but applicable to other coasts where sand balance is important. A primary assumption of sand balance models is attainable sand balance. For cliffs resistant to erosion, these models may force retreat rate results potentially exceeding the maximum physically possible. For cliffs that contain little or no coarse sand, the model is forced to produce unrealistically large or even infinite coastal retreat in the effort to produce adequate sand.

The crucial assumption underlying the Bruun model is that as sea level rises, the geometric relationship between the beach profile and sea level remains constant, all other variables (i.e., wave climate, sand grain size and availability) being equal. In other words, as sea level goes up, the beach cross-section moves upward at the same rate, but also migrates landward, eroding the upland at a rate sufficient to provide just enough sand to maintain the upward shifting profile. The idea is that beaches look essentially the same relative to sea level no matter what the actual sea level. Over long time scales, centuries to millennia, this is a reasonable assumption. Over shorter timescales such as years to decades, the model also assumes that the upland can erode fast enough and contains sufficient sand to maintain the profile. This criterion is readily met in the case of wide beaches where sand from the upper profile moves

[9] http://dornsife.usc.edu/uscseagrant/adaptla/

offshore to raise the active profile, as sea level rises. For narrow beaches backed by sea cliffs, the model also considers the percentage of beach-size sand in the cliffs, and their erodibility.

For each model time step, the active beach profile (defined as extending from the upper active beach limit to the offshore closure depth where no change in profile occurs) shifts vertically by the amount of projected sea level rise, and the sand needed to accommodate the shift is calculated (Figure 3-1). As long as the upper beach is sufficiently wide to provide the needed sand, the beach is "decoupled" from the upland, i.e., the cliff, and marine erosion does not affect it. Marine-driven cliff erosion occurs when the beach retreats landward sufficiently for the active profile to reach the cliff.

Decoupling the active beach and cliff profiles in the Young *et al.* (2014) model allows the beach and cliff to conditionally retreat at different rates. Typical profile adjustments show that initial beach landward shifts can obtain sand balance without marine-driven cliff erosion. When the beach buffer width vanishes, waves begin to erode the cliff base and (ignoring possible lag time) the active beach and cliff profile become coupled, thereafter retreating at the same rate.

Young *et al.* (2014) tested the model by simulating measured historical cliff retreat at Marine Corps Base Camp Pendleton from 1934 to 1998 (Hapke and Reid, 2007) using the associated historical MSLR of (2.5 mm/yr) from the La Jolla tide gauge, and historical sand budgets (Inman and Masters, 1991). Minimum, mean, and maximum historical modeled retreat rates of 0.3, 0.9, and 4.3 ft/yr, respectively, were closely similar to the observed corresponding values of 0.0, 0.7, and 4.4 ft/yr from Hapke and Reid (2007), and well within the observed data error range of ±0.7 ft/yr. These results suggest that the model and its assumptions are valid for use at San Onofre.

The Young *et al.* (2014) model and other sand-balance-based models predict that cliff retreat increases with decreasing cliff height because taller cliffs provide more beach sand per unit of retreat (holding other variables equal), therefore reducing the amount of retreat needed to reach the modeled sand balance. Highly variable retreat is also an artifact of the modeling approach, which does not include local beach-width smoothing from alongshore sand transport (equilibrium shoreline straightening). A key modification used in this study was to allow sand exchange between profiles to maintain the initial plan-view shoreline configuration, except where seawalls are fixing the shoreline position. Other modifications for this study include enforcing no cliff retreat behind seawalls and allowing the beach profile to shorten (from the landward end) when encountering a seawall, thus deviating from the initial equilibrium profile and causing beach profile submergence in front of seawalls. After the seawalls are removed, the initial active beach equilibrium profile reemerges, presumably very quickly.

3.1 MODEL SCENARIO

The model was run for H++ OPC (2018) MSLR projection, and two seawall scenarios, A and B. Each model run used the same 27 starting profiles. In scenario A, the revetment and seawall remain through 2050. In Scenario B, for theoretical modeling and for purposes of a conservative analysis, the revetment and seawall are assumed to be removed in 2030, and the area behind the walls backfilled. Backfilling is specified to elevation 20 ft NAVD88 for Unit 1

(Transects 223-224), and 30 ft NAVD88 for Units 2 and 3 (Transects 219-222). Seawalls are assumed non-erodible while in place. In Scenario A, beach erosion occurs in front of SONGS, but cliff erosion is limited to adjacent areas north and south, since the revetment and main seawall are assumed to remain unchanged. Scenario B is the same as Scenario A until 2030, when the revetment and seawall are theoretically removed in this hypothetical conservative analysis.

3.2 MODEL INPUTS AND PARAMETERS

The following list contains the key model inputs and parameters applied in our approach:

- 2009 topo-bathy bare earth digital elevation model
- Twenty-seven transect profiles spaced 328 ft (100 m) apart
- One sea level rise curve
- Estimated closure depth of -23 ft NAVD88
- Back shore/cliff sand content 80% based on samples from Young *et al.* (2010)
- Estimated upper active beach elevation of MHHW[10] plus 1.6 ft
- Model shoreline retreat step of 1 ft
- Long-term shoreline retreat projected annually
- Output in (x,y,z) UTM, NAVD88 meters (reported here in feet)
- Enforcement of equal plan shape shoreline retreat across profiles
- Backshore erosion is initiated when waves reach backshore
- Armoring considered 100% effective when in place
- Material behind the seawall is of similar sand content and erodibility as adjacent cliffs
- Back shore sand content does not change as cliff retreat occurs

The model was used to project shoreline and cliff change annually from 2010-2050 on transects spaced 328 ft (100 m) alongshore perpendicular to the shoreline (Figure 3-2). Topographic and bathymetric profiles were obtained at each transect using 6.6-ft (2-m) resolution bare earth digital topo/bathy elevation model from NOAA's Ocean Service (NOS) Office for Coastal Management (OCM, 2013). The primary data source for this elevation at SONGS was topo/bathy airborne LiDAR collected in 2009. The vertical and horizontal accuracy of the elevation is estimated at 0.5 ft and 0.33 ft, respectively.

The initial 2009 topography was assumed to represent an equilibrium shoreline and cliff configuration. Future net alongshore and cross-shore sand movement into and out of the study area was assumed negligible. Future blockage of alongshore sand transport, natural or anthropogenic, will negate this assumption. Future beach replenishment in the study area was not considered. The San Onofre State Beach dirt parking lot to the north of SONGS was assumed erodible and unprotected in future conditions.

[10] MHHW (mean higher high water) is a tidal datum calculated as the average value of the highest observed water level elevations each day over the National Tidal Datum Epoch, a fixed 19-yr period, currently 1983-2001. Tidal datum relationships among each other and relative to geodetic datums, like NAVD88, change with MSL.

Cliff base and cliff top locations at each transect were identified and defined manually. The upper active beach profile elevation subject to regular wave action was assumed to be 7 ft, NAVD88, which includes 1.6 ft of run-up above MHHW. The lower active beach profile offshore extent (closure depth) subject to regular wave action was assumed to be -23 ft NAVD88 (Hallermeier, 1978). The model was run permitting sand exchange between profiles to enforce uniform beach shoreline retreat across all transects within the study area. This constraint preserves the overall shoreline plan shape after the seawalls are removed. This assumption is consistent with the SONGS setting and experience.

A key model assumption is that the areas behind seawalls are assumed backfilled with material similar in beach sand content (80%; Young *et al*., 2010) and erodibility compared to the *in-situ* cliff material to the north and south of the seawalls, consisting of the San Mateo Formation. The model also assumes removal of all surface and subsurface concrete and other infrastructure. Any deviation from these assumptions could cause notably different model results.

3.3 MODEL RESULTS

Modeled beach profile retreat was 102 ft and 100 ft, while mean cliff retreat was 30.6 ft and 38.2 ft by 2050, for Scenarios A and B, respectively (Table 3-1, Figure 3-3). In Scenario A, where seawalls remain in place, beach retreat at profiles crossing SONGS (Transects 219-221) caused beach submergence. Modeled cliff retreat ranged from 0-84 ft. Modeled cliff retreat varied widely because of differences in initial beach width between transects, and cliff topography (Figure 3-4). Modeled cliff retreat north of SONGS was generally smaller than to the south because of a mostly larger initial beach width. Figures 3-5 and 3-6 show the modeled H++ extreme-scenario cliff retreat for Scenarios A and B at two transects that are representative of the natural formations around the SONGS site: transect 227 located north of SONGS (Figure 3-5) and transect 217 located south of SONGS (Figure 3-6).

Modeled cliff retreat rates near the SONGS site under the H++ extreme-scenario ranged from 0-3 ft/yr from 2010-2050, for both Scenario A and Scenario B. This maximum retreat rate is less than the maximum historical cliff erosion rates of 4.3 ft/yr +/-0.7 ft/yr from Hapke and Reid (2007). In addition, rapid and considerable cliff erosion at MCBCP was documented by Kuhn and Shepard (1984). Taken together, this suggests the modeled maximum rates are locally attainable. Appendix A shows the modeled H++ extreme scenario cliff retreat profiles for Scenario A and Scenario B, respectively. No bluff retreat occurs fronting SONGS while the seawall remains in place, and the two scenarios are remarkably similar, suggesting little difference in erosion between 2030 and 2050.

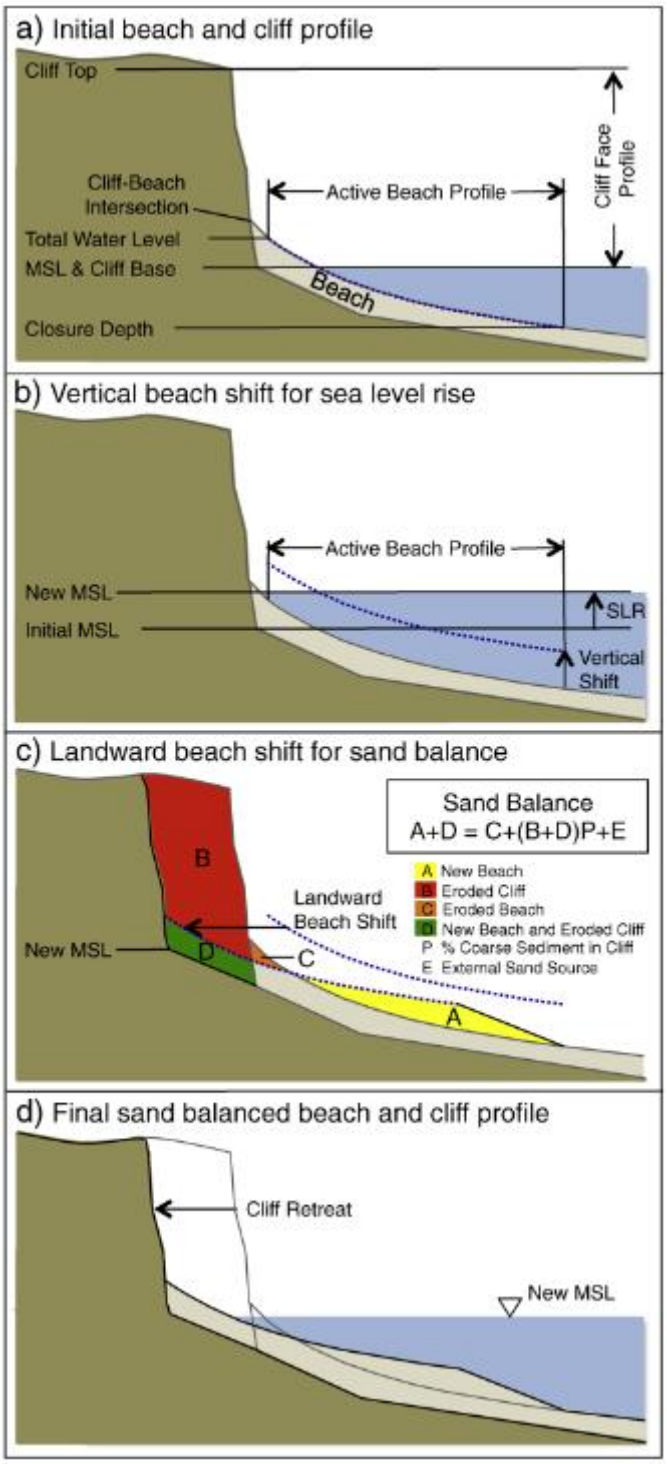


Figure 3-1. Model profile adjustments and erosion from MSLR. (a) Initial profile and active beach bounded by total water level and closure depth. (b) Active beach profile shifts vertically equal to the amount of sea level rise, and (c) landward by maintaining sand balance (d). Figure from Young *et al.* (2014).

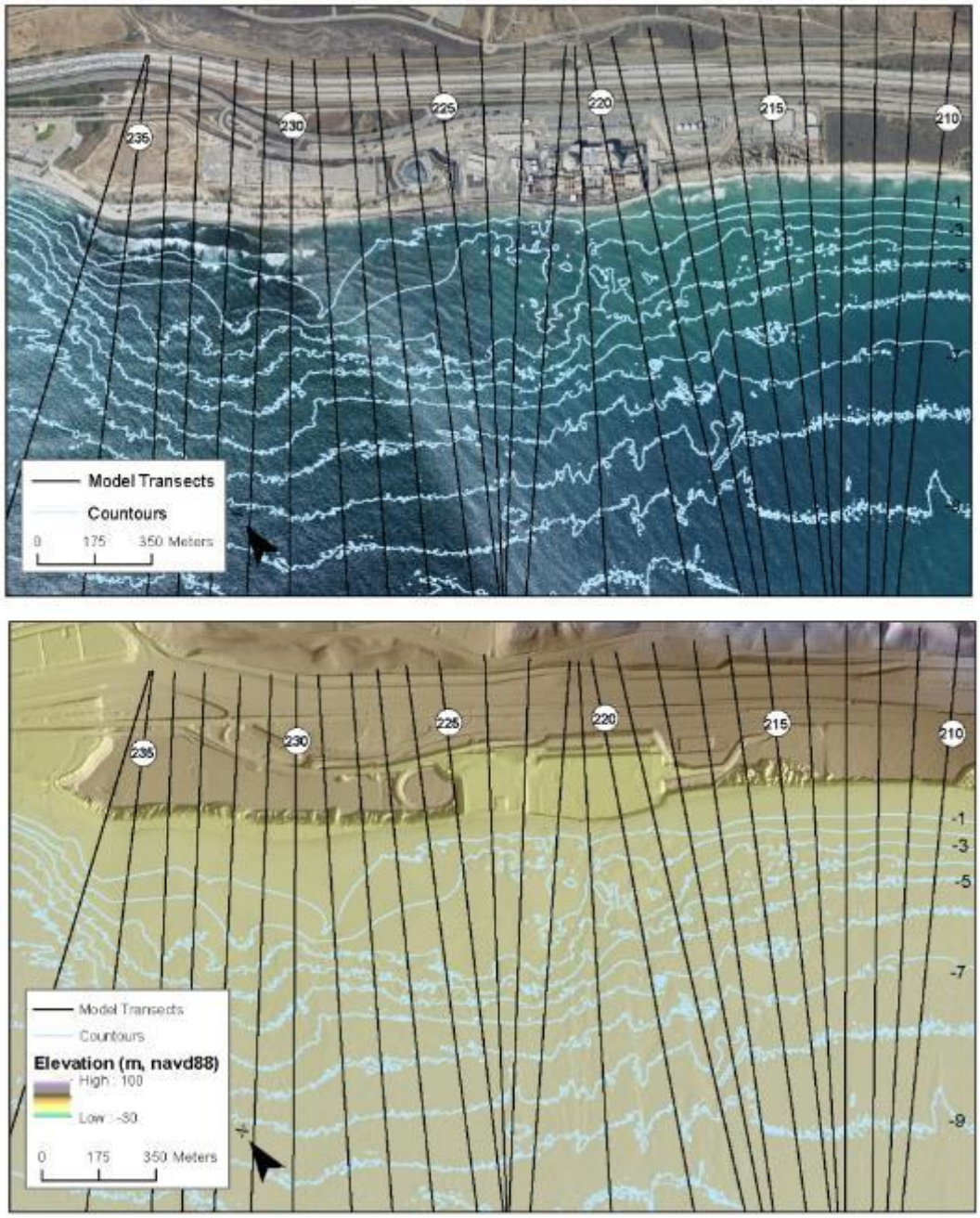


Figure 3-2. Map showing model transects and contours displayed over aerial photograph (top) and the 2009 bare earth digital elevation model (bottom).

Table 3-1. Beach and cliff retreat 2010-2050 (ft).

Beach/Cliff Retreat (ft)	Scenario A Seawalls Remain	Scenario B Seawalls Removed 2030
Beach Profile Retreat	102	100
Cliff Retreat Min[a]	0.0	0.0
Cliff Retreat Mean[b]	30.6	38.2
Cliff Retreat Max[c]	83.6	81.6

[a] Minimum cliff retreat, 2010-2050 at 27 modeled profiles.
[b] Mean cliff retreat, 2010-2050 at 27 modeled profiles.
[c] Maximum cliff retreat, 2010-2050 at the 27 modeled profiles.

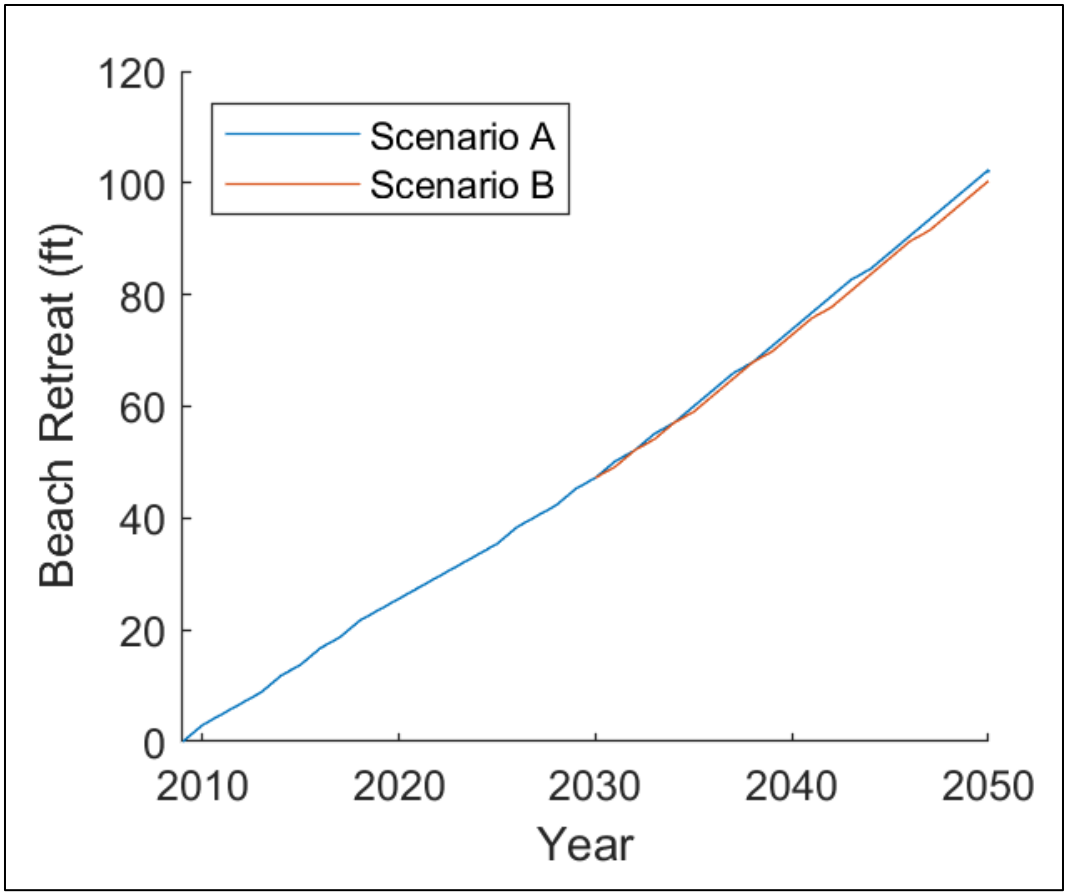


Figure 3-3. Modeled beach retreat on all 27 modeled profiles at SONGS for each scenario.

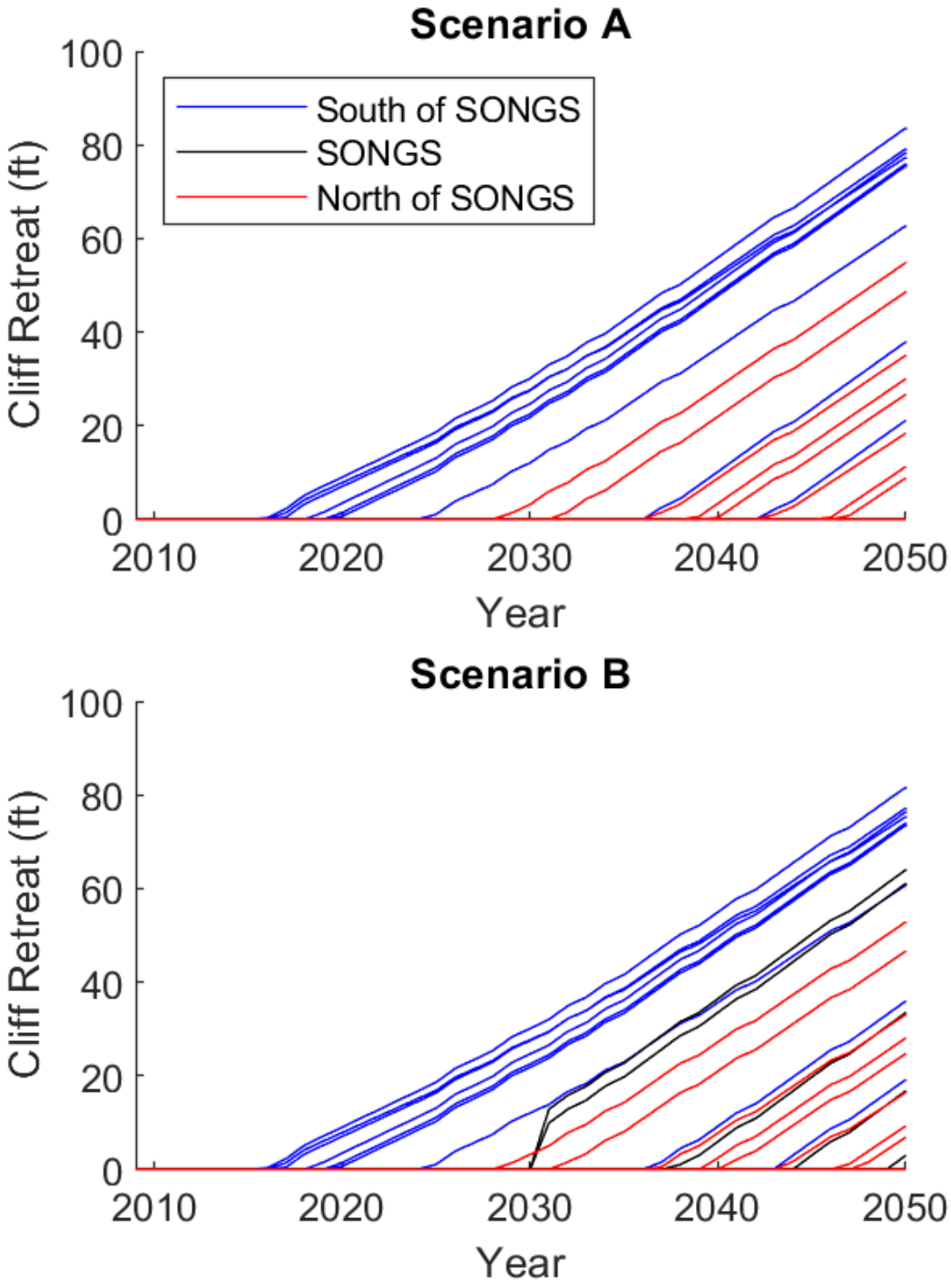


Figure 3-4. Modeled cliff retreat for profiles south of SONGS (blue lines), intersecting SONGS (black lines), and north of SONGS (red lines) for each scenario.

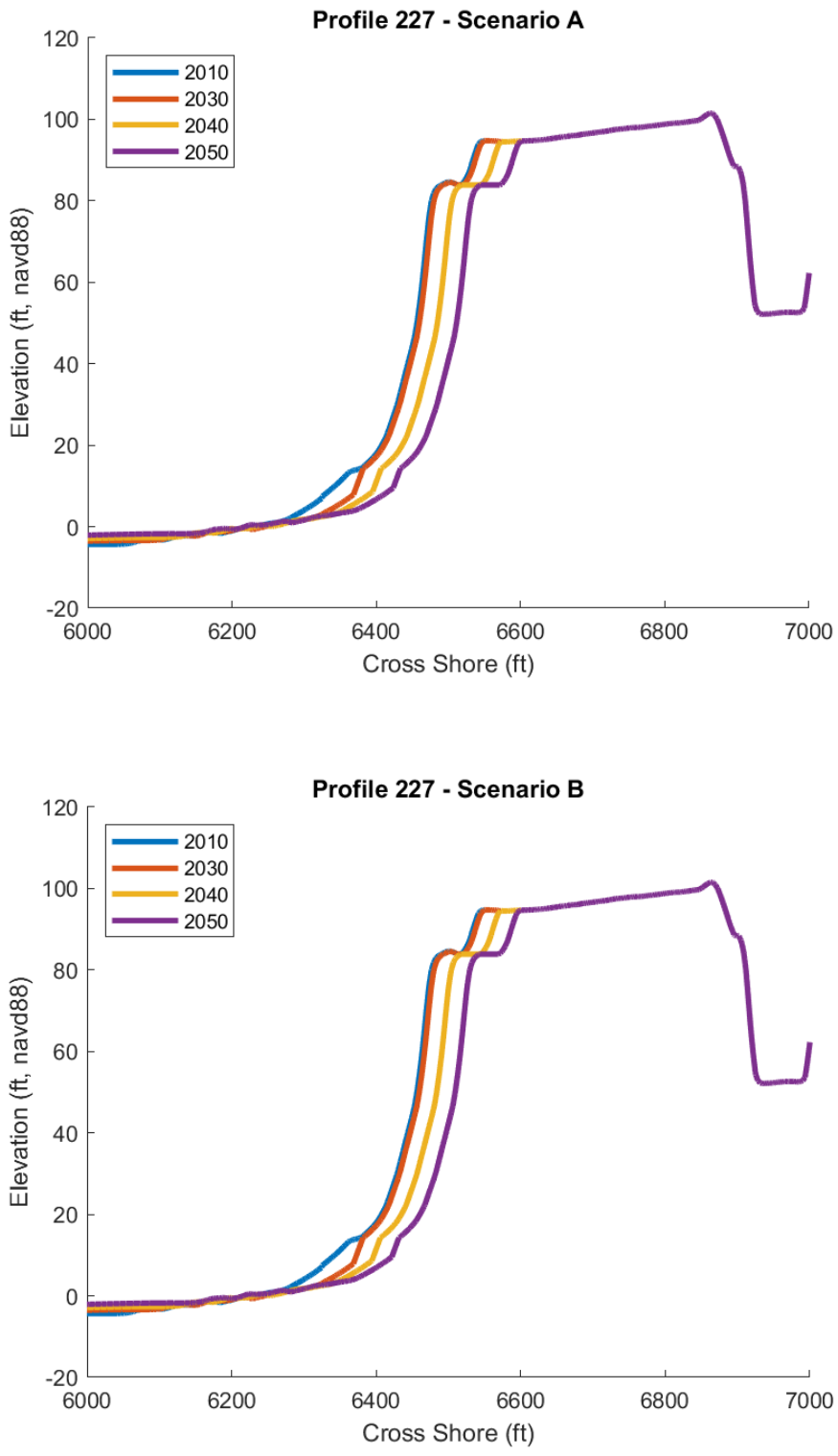


Figure 3-5. Modeled H++ extreme-scenario cliff retreat for Scenarios A and B at transect 227 located north of SONGS. Transect location is shown in Figure 3-2.

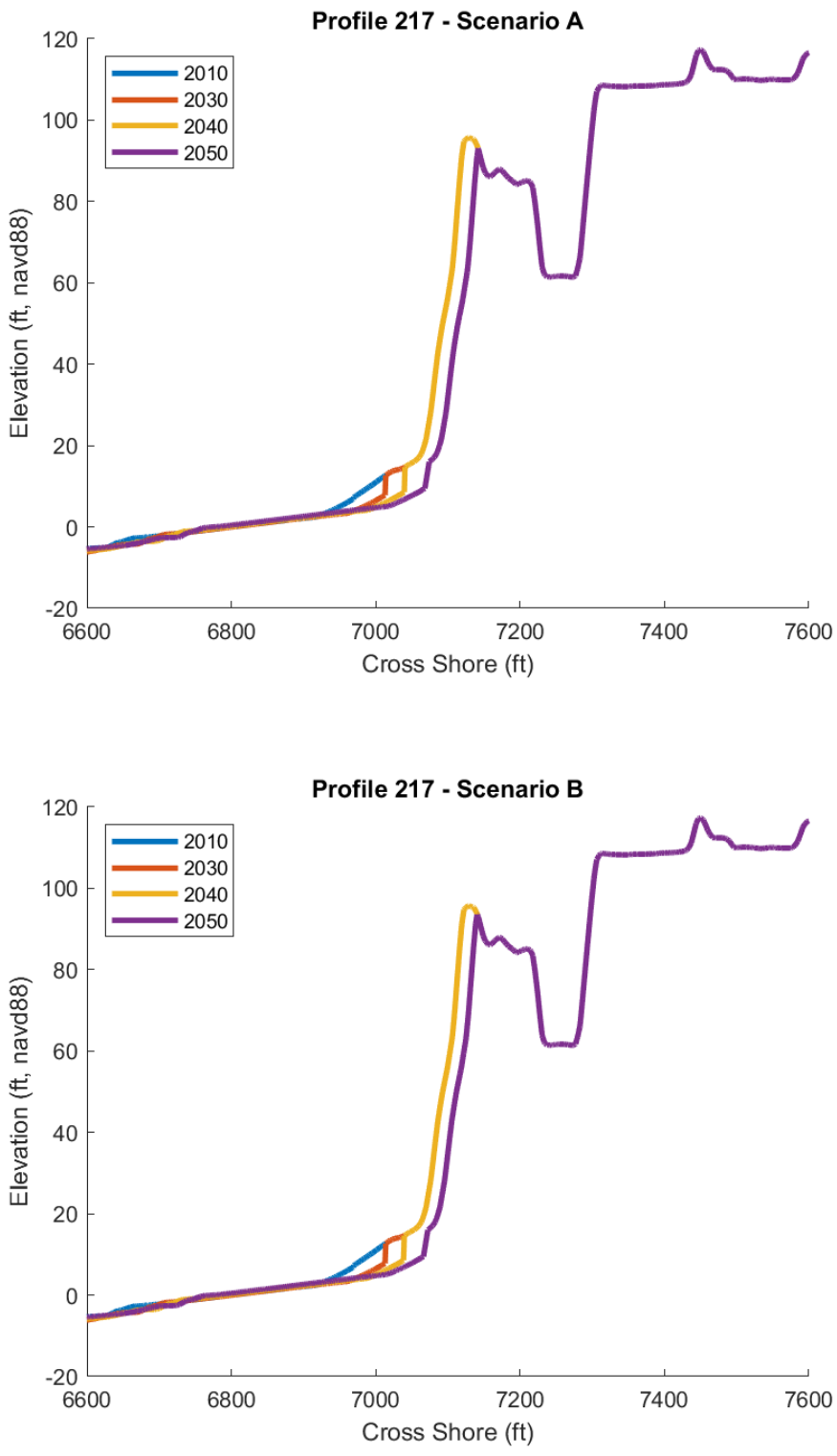


Figure 3-6. Modeled H++ extreme-scenario cliff retreat for Scenarios A and B at transect 217 located south of SONGS. Transect location is shown in Figure 3-2.

4.0 SONGS REVETMENT

4.1 DESCRIPTION OF THE SONGS REVETMENT

The SONGS revetment provides partial front-line protection for the SONGS seawall. It is also essential to maintaining the walkway that enables safe lateral access for beach users. The revetment shelters the walkway from most wave run-up and overtopping, thus preventing or reducing negative impact to lateral beach access due to flooding and other hazards from high water levels and waves, as well preventing direct wave attack on the seawall.

Figure 4-1 is an aerial photograph showing the revetment, which extends about 2,200 ft along the entire length of SONGS, on the beach fronting the walkway. Figure 4-2 is a close-up of the revetment at its southern end. The revetment is constructed of multiple layers of placed riprap of quarry rock "rubble." A well-known and desirable characteristic of placed rubble structures is their ability to adjust and resettle under wave attack. The advantage of using rock riprap is that it is highly durable and readily available in southern California. Furthermore, due to their rough surface, rock revetments produce less wave run-up and overtopping as opposed to smoothed-faced structures.

4.1.1 Revetment and Walkway Maintenance 2018-2019

Maintenance repairs of the SONGS revetment were done in two phases, with Phase 1 extending from 7 May to 10 October 2018, and Phase 2 from 15 October to 16 December 2019. No substantial maintenance was conducted in 2020 or 2021. During the Phase 1 repairs, SCE first placed additional riprap along 500 linear feet at the southern portion of the public access walkway (Figure 4-3), and then elevated the access ramp to this walkway using imported cobbles and sand. Elevating the south access ramp compensated for sand losses due to wave action that had resulted in an approximately 10-ft lowering of the beach at that location, as well as scouring of the revetment.

During Phase 2 repairs, SCE placed an additional 150 linear feet of imported riprap north of the riprap placed in Phase 1, for a total of 650 linear ft of revetment repair. SCE also added 70 linear feet of riprap in front of the sheet pile seawall closure section at the south end of the public walkway and reinstalled the Vehicle Barrier System at the south end of the walkway. Figure 4-4 shows the south end of the walkway before and after the repair.

4.2 SITE VISIT

Inspection of the SONGS revetment was made by CE on 25-26 February 2021. During this visit, we took photos fronting the revetment at the 21 transects shown in Figure 4-9, and a laser scan survey to construct a digital elevation model (DEM) of the revetment shown in Figures 4-10, 4-11, and 4-12.

4.2.1 Rock Measurement Discussion

Rock revetments, including the one at SONGS, are constructed of rubble of varying sizes that in southern California is generally quarried from the southern end of Catalina Island. The size of individual rocks is expressed by the dimensions of their three axes. The long axis, 'a', is the maximum length of the stone (Figure 4-5); the intermediate axis, 'b', is the maximum width perpendicular to the long axis; and the short axis, 'c', is the height of the stone perpendicular to the plane of the a-axis and b-axis. The size of an individual rock is usually expressed as its b-axis dimension, or alternatively by its calculated or actual weight. Rock weight estimates, which are needed to evaluate riprap stability, are discussed in Section 4.3 below. Histograms of the lengths, widths, and heights of the 80 sample rocks measured at SONGS are presented in Figure 4-6, and their cumulative distributions in percentage are shown in Figure 4-7.

4.2.2 Revetment Laser Scanner Survey

A laser scanner survey was carried out using a Trimble SX10 scanning total station (Figure 4-8) for the purpose of creating a digital elevation model (DEM) to visualize the spatial characteristics of the revetment. Control points were established to aid in subsequent station setups. The revetment was scanned from the beach and the scanner location was determined from the control points. The system scanned in a vertical direction and slowly rotated horizontally to cover the areas of the revetment at a high resolution. A total of 14 scans were carried out to capture the entire SONGS revetment.

The survey on 25-26 February 2021 acquired over 47 million data points, assembled in a "point cloud." The data set was pre-processed using "Global Mapper" software, which enables the outlier points, and those points likely reflected from the walkway wall, to be removed. The pre-processed data were then graphically presented to show the revetment and adjacent beach. The model results at each of the transects are presented in Appendix B. High water levels from the tide was a limiting factor in obtaining complete coverage from the beach at the southern portion of the revetment. Therefore, some scans were carried out from the top of the revetment near the walkway to fill data gaps.

An advantage of creating a DEM is that the model can be "sampled" to show cross sections and contour maps that would otherwise be difficult or impossible to derive in a reliable way. Twenty-one cross section transects were generated from the DEM at locations shown in Figure 4-9. Results of the revetment laser scanner survey are shown in Figures 4-10 through 4-12 for the 21 transects. For clarity, Appendix B shows the DEM comparison between 2021 and 2020 for each transect. Representative cross sections are shown in Figure 4-13; all 21 transect cross sections are presented in Appendix C. Table 4-1 provides riprap height, walkway wall height, and the revetment slope β for each transect.

The DEM was also used to determine the height of the revetment along its upper edge adjacent to the walkway retaining wall (Figure 4-14). The height of this upper edge varies from about 8 ft to 12 ft (NGVD), a few feet lower than the upper edge of the retaining wall, which lies at about 14 ft. The laser scanner survey clearly described the rock shapes and sizes while the

photographs highlighted the sand and cobble areas on the beach. Aerial photographs of the revetment for the period from 2003 to 2020 are presented in Appendix D.

4.3 RIPRAP ROCK UNIT WEIGHT

Riprap rock unit weights and their variations are essential to estimating the stability of a revetment. Individual rock weight is proportional to volume and specific weight (density) of the stone. The estimation of weight is complicated by the fact that each rock unit is not a simple geometric form, such as a sphere or rectangular shape, like a brick.

Individual rock weight, W(x), was estimated from Equation 4-1, which assumes each rock (x) is equivalent to a sphere with diameter D(x) = b(x), the maximum width perpendicular to the long axis, as described in Section 4.1 above. Dimension 'b' is often referred to as rock "diameter." Then:

$$W\ x\ =\ \frac{\pi\gamma_S\ D(x)^{\ 3}}{6}, \tag{4-1}$$

where γ_s = Specific weight of revetment rock.

Table 4-2 gives the dimensions and weights of each sampled rock. The mean and standard deviations for the length, width, and weight of the rocks are presented in Table 4-3. Percent distribution of rock weights and the cumulative distribution of estimated rock weights are shown in Figure 4-15.

A key design parameter for any revetment is the median rock weight, designated W_{50}. Half of the rocks are heavier, and the other half are lighter than W_{50}. We estimated W_{50} in two different ways using standard coastal engineering practice from the U.S. Army Corps of Engineers (USACE 1994a, 1994b). First, we determined the individual rock weight estimates from each rock diameter, D(x), as described in Equation 4-1. The result was W_{50} = 600 kg. Second, we calculated the median diameter of the 80 sampled rocks, which was D_{50} = 2.5 ft. We then used this number in place of D(x) in Equation 3-1, which resulted in W_{50} = 580 kg, a nearly identical result.

4.4 DESIGN WATER LEVEL

Water surface elevation is dependent on tides, storm surge, and other factors described in Chapter 2. Future water levels also depend on MSLR. These factors are discussed in Section 2.3, and the values of current extreme water levels are given in Table 2-5. Table 2-5 gives the NOAA estimates for the extreme water level for various return estimates. The 100-year return period for surface water elevation at La Jolla is 7.43 ft NAVD88 (5.32 ft, NGVD), while the maximum observed water surface elevation of 7.62 ft NAVD88 (5.51 ft NGVD) occurred on 25 November 2015 during the 2015-16 El Niño warming event.

These estimations include astronomical tide, storm surge, and sea level fluctuations due to normal seasonal heating and cooling, as well as El Niño condition enhancements. They do not include wave setup caused by breaking waves, since tide gauges are located offshore of the surf

zone, and their water level sampling system filters out relatively high-frequency fluctuations such as wave surges. The design water level used for this study is the extreme thus far observed: 5.5 ft (1.7 m) NGVD, or 7.6 ft (2.3 m) NAVD88 (rounded to one significant figure).

4.5 DESIGN WAVE ESTIMATION

Wave run-up can be the dominant contribution to high water levels on beaches, depending on the state of the tide, and the height, direction, and period of the waves, especially during storms. A typical wave storm on the southern California coast has a wave height of about 6.9 ft. The wave record for San Onofre, estimated from measurements at SONGS and a comparison with the Oceanside wave array data between 1978 through 1994, were used to calculate wave height return periods for San Onofre.

The Seasonal Maxima Distribution Model (SMDM), developed by Borgmann (USACE 1988), was selected as the appropriate analysis method to estimate the design wave height at a range of return periods. Monthly wave maxima were extracted from the wave data and split into seasonal sets. The seasonal maximum wave-height distribution functions were calculated for each season and then multiplied together to produce the annual maximum distribution. This distribution function was used to estimate extreme wave-height return periods.

The design wave analysis shown in Figure 4-16 was used to identify the significant wave heights associated with a range of return periods at San Onofre. Wave spectra matching those wave heights were extracted from the UCSD Scripps Institution of Oceanography Coastal Data Information Program (CDIP) database.[11] The wave spectra from the selected storms (Figure 4-17) were used to estimate the peak period associated with wave-heights for 5-, 10-, 25-, 50-, and 100-year return periods. The extreme wave height and period information is summarized in Table 4-4.

The largest storm on record between 1980 and 2016 occurred on 18 January 1988. The deepwater wave height was 16 ft with a period of 17 sec (as measured at the CDIP Oceanside buoy). The corresponding wave height at San Onofre was about 12.5 ft approaching the shore from the west. Table 4-5 represents the highest significant wave heights at San Onofre in descending order estimated from the Oceanside buoy wave measurements for summer, winter, and all data.

4.6 SONGS REVETMENT STABILITY ESTIMATION

As outlined above, the median rock weight W_{50} is a key parameter in assessing the stability of a revetment. Hudson's formula (Ahrens, 1981a, Ahrens 1981b; USACE 1984, 1994a,b; BCMELP, 2000) is the standard practice method used to estimate W_{50} necessary for revetment stability:

[11] https://cdip.ucsd.edu

$$W_{50} = \frac{\gamma_r H^3}{K_D \left(\frac{\gamma_r}{\gamma_w} - 1\right)^3 \cot\alpha} \quad (4\text{-}2)$$

Where:

W_{50} = required median armor unit weight,
γ_r = specific weight of the rock unit, Kg/m^3,
H = wave height at the toe of the revetment,
K_D = stability coefficient,
γ_w = specific weight of water at the site,
α = revetment slope angle from horizontal.

K_D values vary primarily with the shape of the rocks, surface roughness, sharpness of edges, and degree of interlocking. Typically, K_D = 2.1. Wave height H at the structure is estimated by shoaling the design waves to the breaking point (H_b). If H_b is less than the wave height at the toe, H_{toe}, of the revetment, we use H_b; otherwise, H_{toe} is used.

The height of the wave at the toe of the revetment is depth limited. The highest estimated water depth at the toe of the SONGS revetment (Ds) is 5.5 ft + 2.29 ft = 7.79 ft, MLLW, where 5.5 ft, NGVD is extreme water level (Section 4.4) and 2.29 is the difference in elevation between datums NGVD and MLLW.

The water depth at the toe of the structure (Ds) varies as the sea level rises. In 2050, the water depth at the toe of the structure is projected to be 9.79 ft, MLLW (OPC, 2018, Medium-High Scenario) and 10.59 ft, MLLW (OPC, 2018 H++ Scenario). A calculation of the wave height (H) was made from the equation H = 0.56 x Ds (Thornton and Guza, 1982 and 1983).

Equation 4-2 is used to compute the W_{50} for stable revetment. Table 4-6 gives the values of W_{50} for the MSLR projections (medium-high and H++ at 2020 and 2050).

4.7 ASSESSMENT OF SAN ONOFRE BEACH

The condition of the beach fronting SONGS is significant since it prevents or buffers wave attack of the revetment and retaining wall, which in turn protect the walkway required for lateral beach access. The stability of the SONGS revetment depends on the condition of the beach. Presence of a healthy beach causes waves to break farther seaward of the revetment, thus reducing wave run-up, splashing, and overtopping. The beach also prevents toe scouring that can undermine the revetment and cause rock units to settle. When the beach is narrow, or water level unusually high, or both, waves breaking on the revetment can cause dislocation of individual rocks, which contributes to revetment instability.

Recent beach conditions are defined by the 2017-2020 quarterly profile measurements, which characterize the beach configuration in autumn, winter, spring, and summer seasons. Comparisons with earlier beach profiles dating back as early as 1964 show long-term erosion or accretion tendencies. The main factors controlling erosion or accretion are waves and sand supply. Other contributing factors are the nearshore and offshore bathymetry of the region, particularly any wide, flat shelf areas, and the presence of reefs, all of which limit wave height.

Structures, particularly the SONGS temporary laydown pads used for Units 1, 2, and 3 construction, also influence beach width and stability. In the future, MSLR will cause beaches worldwide to migrate landward and upward. Depending on the state of the backshore, especially its erodibility, beaches may or may not continue to exist. The study documents the complex changes of beach conditions at SONGS and puts these into their Southern California context.

Four beach profile surveys were carried out each year from 2017 through 2021 at SONGS. The results of each survey have been presented in reports by Elwany *et al.* (2021a). Longer-term beach change patterns are characterized by comparing beach widths from these recent surveys to comparable measurements from 1985-1993 sponsored by SCE. The earliest directly comparable data were taken in May 1985, just after the sand release of the SONGS Units 2 and 3 laydown pad (Flick and Wanetick, 1989), and from 1990-1993 (Elwany *et al.*, 1994), 2000 (Elwany *et al.*, 2000), and 2017-2020 (Elwany *et al*., 2021a). Figures 4-18 and 4-19, and Table 4-7 show the long-term changes of beach width.

The beach profile surveys, and photography programs sponsored by SCE since 1964 have provided valuable information and understanding of the response at San Onofre to beach filling and the construction of stabilizing structures (Flick and Wanetick, 1989; Flick *et al.*, 2010). This insight will be valuable as MSLR accelerates in the future.

4.8 EVALUATION CRITERIA

A "stable" rock revetment must perform satisfactorily in the sense that it functions as designed even though individual rocks may move such that portions or the entire revetment settles or changes slope. Such changes are expected in rock revetments, and as previously noted, and are accounted for in the original design. In short, a revetment is functioning properly if it provides protection as designed and is considered stable if no damage exceeds ordinary maintenance needs. At a minimum, the design must withstand conditions that have a 50% probability of being exceeded during the revetment's economic life.

Revetment failure can be caused by large dislocation of individual rocks such that they become sufficiently separated to no longer function as a unit to dampen wave attack; or extreme settlement where the height is no longer sufficient to prevent excessive overtopping. In addition, failure of a protective revetment during maximum design conditions, should not result in loss of life or unreasonable repair expenses.

4.9 REVETMENT STABILITY FROM FEBRUARY 2020 TO FEBRUARY 2021

Wave data (wave height, period, and direction) from wave buoy number 46224, located offshore of the City of Oceanside in 238 m water depth, were used to estimate the wave heights and periods in front of the SONGS revetment in 10 m water depth for the period from 1 January 2020 through 28 February 2021. These computed wave heights and periods are shown in Figure 4-20. The wave heights during this period were generally calm except for the periods from 7-9 November 2020 and from 25 January-21 February 2021 (Figure 4-20).

During November 2020 and between 25 January and 21 February 2021, the revetment was subject to large waves with heights varying between 6.6 ft and 14 ft, and with short periods of about 8 seconds. The observed 14-ft waves were higher than the previously estimated wave height for the 100-year-return period of 12.5 ft. Despite the height and duration of these waves, the damage to the revetment and walkway was minimal.

The November 2020 wave event lasted three days and had an average wave height of about 11.3 ft (Figure 4-21). The period from 1 January-28 February 2021 (Figure 4-22) was characterized by a series of large wave storms having an average wave height of about 6.6 ft with maximum wave height of 14.2 ft observed between 25-26 January 2021 as shown in Figure 4-23. The wave period during the wave storms varied between 8 and 12 secs. These wave events offered a good opportunity to examine the stability of the revetment using actual wave storm events.

The damage to the revetment was minor, occurring at two locations, Transects 1 and 10. The revetment damage at Transect 1 occurred at the drainage structure. These wave events impacted the beach fronting SONGS by removing the thin layer of sand covering the cobbles. Some of the cobbles were pushed inshore to the toe of the revetment and between the rocks at even higher elevations. Cobble was thrown onto the walkway in few locations near Transect 10 by waves splashing over the revetment. No damages were observed in the walkway, indicating that the revetment protected the walkway from wave run-up and overtopping.

It is notable from the DEM (Appendix B) that most of the storm-caused rock movement in the revetment occurred at the toe. These changes included movement of a limited number of small rocks by a few feet, exposure of some rocks previously under the sand, and pushing cobbles inshore towards and over the revetment. The changes of large rock locations that constitute the main revetment were insignificant and did not negatively impact revetment stability.

In February 2020, the north portion of the revetment was covered by beach sand. Large waves in early 2021 removed this sand, exposing cobble and more of the revetment rocks that were under the sand (Figure 4-24). The beach changes at San Onofre caused by the January and February 2021 large wave storms were normal and expected. They were typical of what has been observed at other southern California beaches, such as Camp Pendleton, Oceanside, and the City of Del Mar.

4.10 MAINTENANCE AND ADAPTIVE CAPACITY

As described in Section 4.9, the SONGS revetment is currently in good condition and can likely provide wave protection to the retaining wall and walkway through at least 2050. The major threats to revetment stability in the future include wave storms, or clusters of wave storms. As described above, revetment damages depend on the height of waves and the duration of wave attack. Large waves can cause dramatic narrowing and lowering of the beach fronting the revetment, leading to rock settlement and displacement, wave run-up, and overtopping.

Section 4.9 of this study showed that the revetment was capable of withstanding both a single large wave event of 2-4 days and a series of large wave storms. It should be pointed out that the revetment is expected to occasionally sustain future damages larger than were observed during January and February 2021, and therefore the revetment will require occasional maintenance in the future. It is not expected to collapse or fail in a way that would prevent its function if properly maintained. Such damages are expected in rock revetments, as previously noted, and accounted for in the original design such that no damage exceeds ordinary maintenance needs. In this respect, the revetment's adaptive capacity to MSLR is high in the sense that it is currently in a stable condition and has recently been tested by the January-February 2021 wave storms.

For these reasons, it is important to continue monitoring the cross-sections of the revetment at various locations by surveys and photographs (Sections 4.2.1 and 4.2.2), especially before and after large wave storms. It is also important to monitor the beach fronting the revetment and at the north and south of it as described in Section 4.7. In addition to crucial public lateral beach access, the revetment, retaining wall, and walkway also provide additional protection to the main SONGS seawall. It is crucial that these structures remain in place at least until the deconstruction efforts of Units 2 and 3 are completed.

4.11 GROUNDWATER

Groundwater elevation under the ISFSI in 2020 based on quarterly data from nine coastal wells located near the ISFSI, was 2.43 ft NGVD (Elwany *et al*., 2021). Projections of future groundwater elevations estimated from OPC (2018) medium-high 0.5% (1:200) and extreme H++ MSLR scenarios through 2050, are 4.43 ft and 5.23 ft NGVD, respectively. These elevations are respectively 1.54 ft and 0.74 ft lower, than the bottom of the ISFSI support foundation, which is 3 ft thick, as illustrated in Figure 4-25.



Figure 4-1. Photo of SONGS revetment, 20 August 2018. Northern part of revetment (left) is covered by beach sand.



Figure 4-2. Photo of southern end of SONGS revetment.

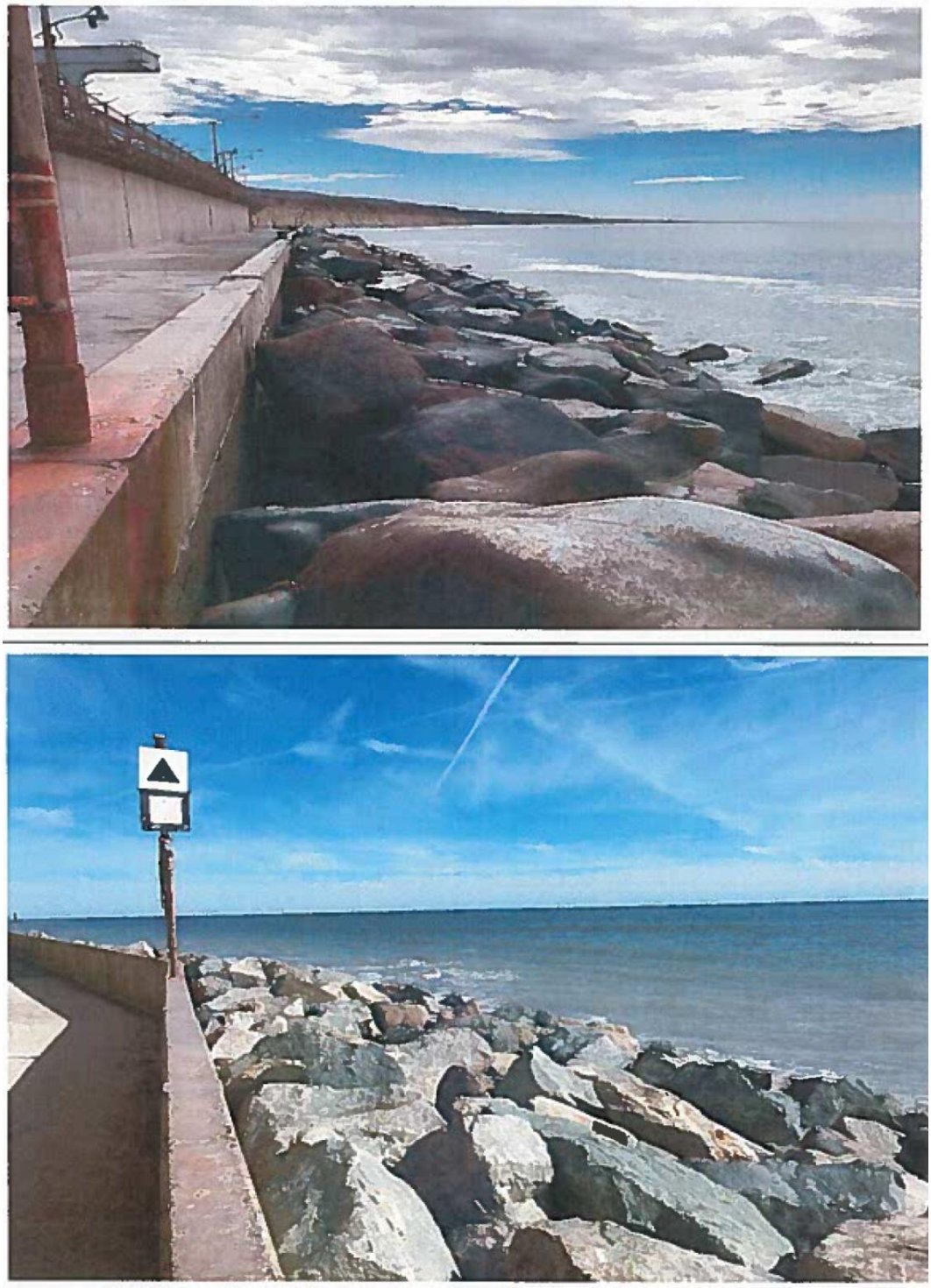


Figure 4-3. Photo of riprap revetment toward south on 20 March 2018 before placement of additional rock (upper). Photo on 17 December 2019 after placement of rock in gaps and settled areas.

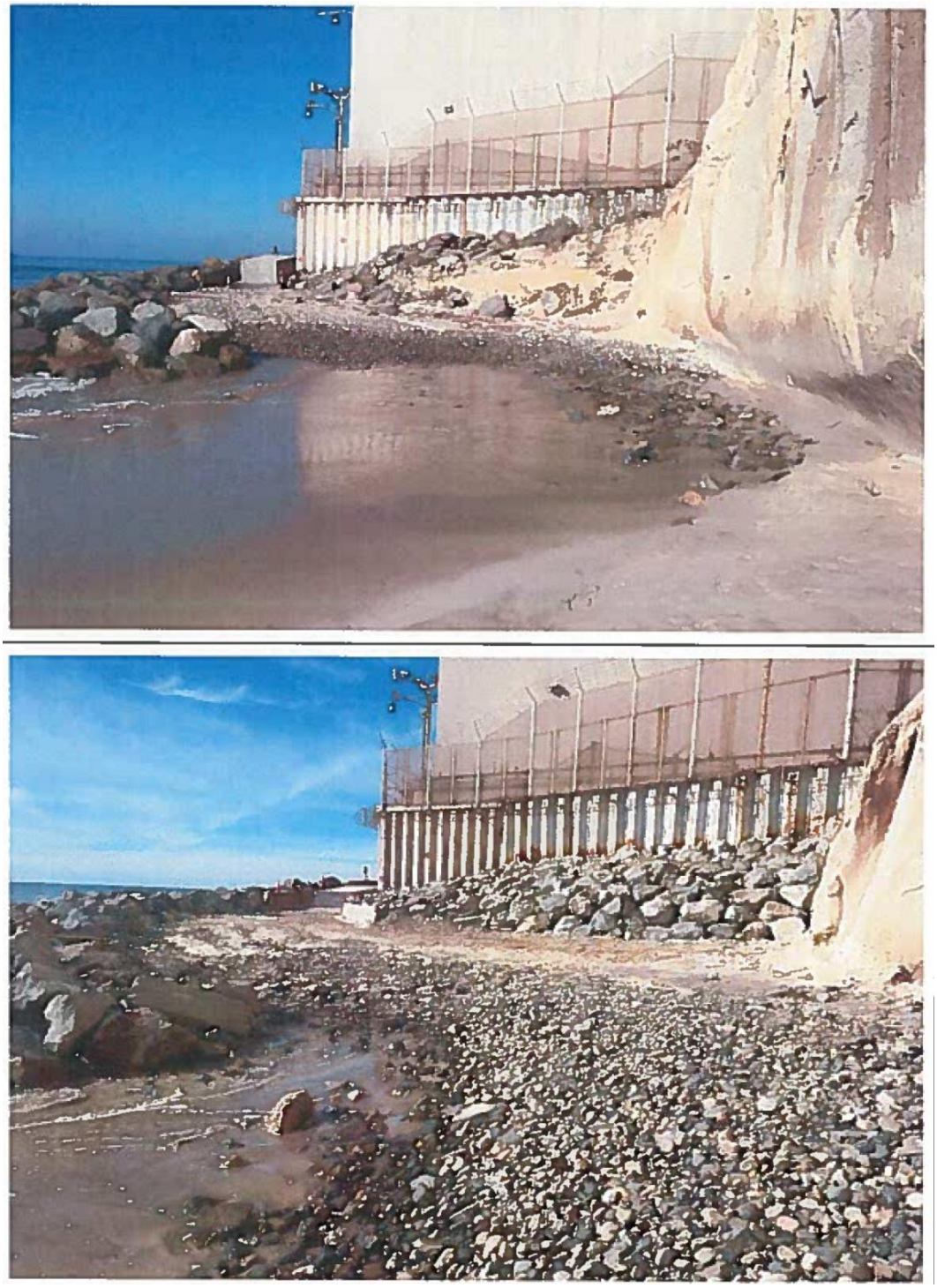


Figure 4-4. Photo of south end of riprap and access walkway on 15 October 2019 before repairs (upper). Photo on 17 December 2019 after repairs (lower).



Figure 4-5. Measurement of long axis (length) of riprap rock.

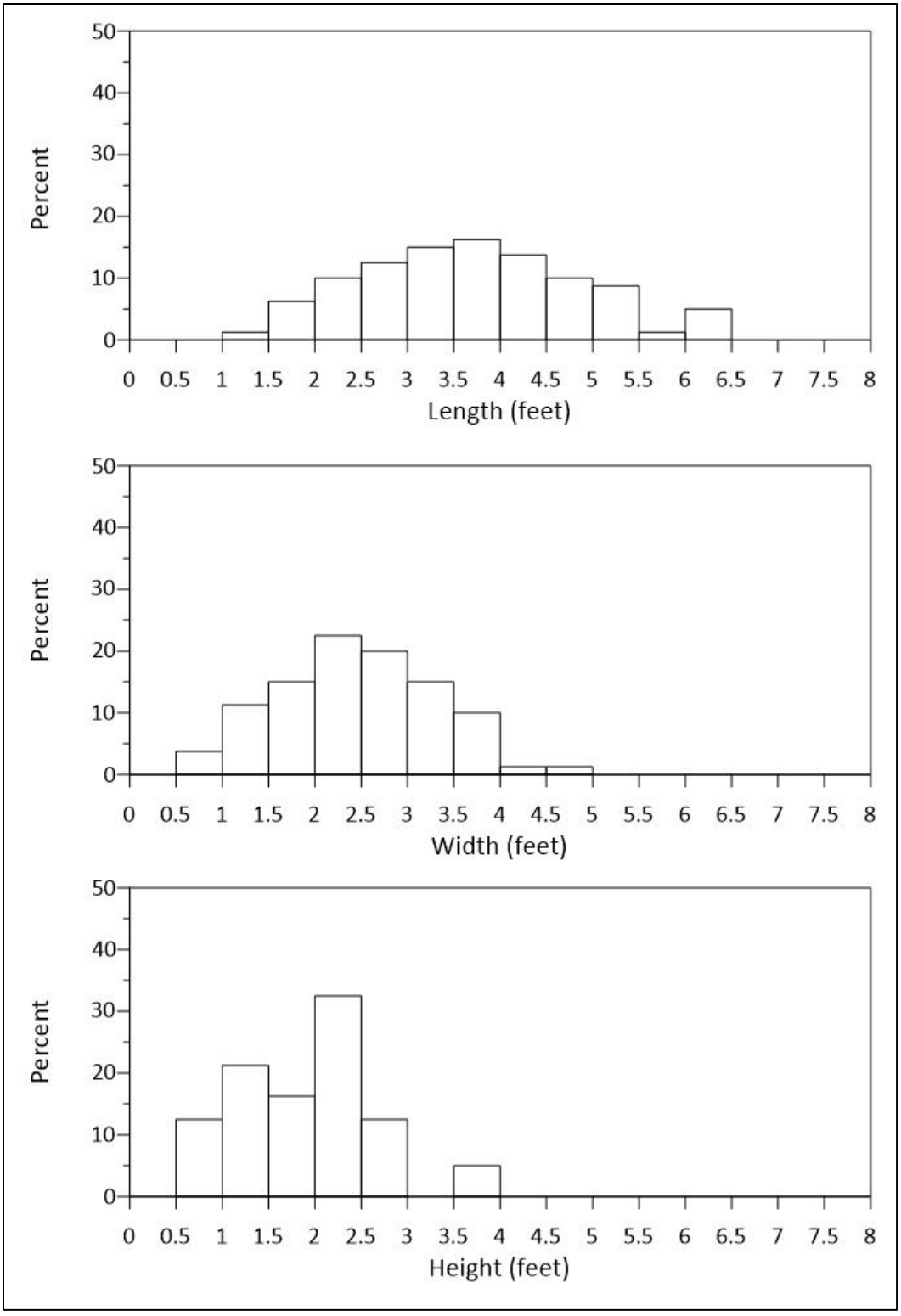


Figure 4-6. Histograms of rock length, width, and height.

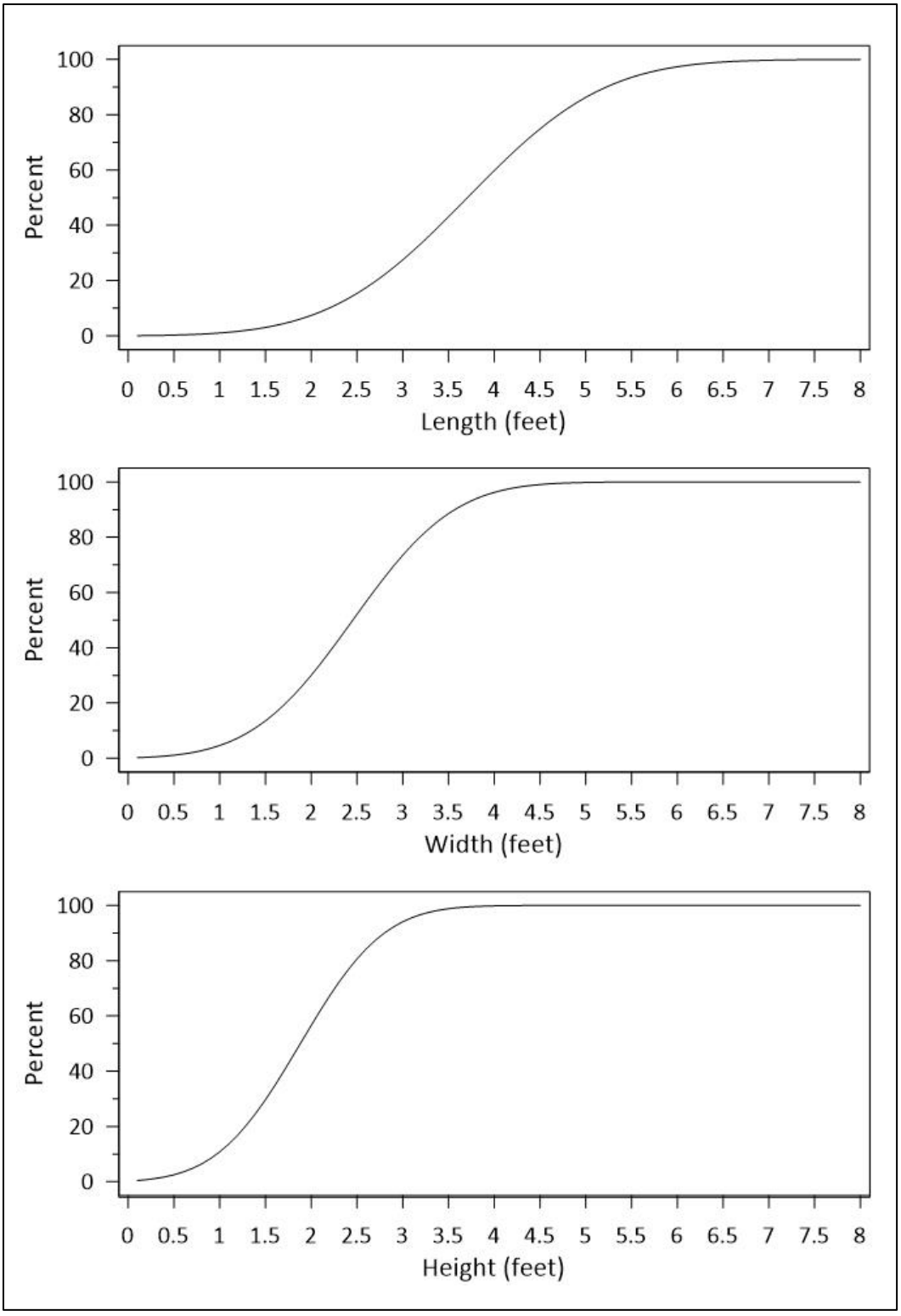


Figure 4-7. Cumulative distributions of rock length, width, and height.



Figure 4-8. Photo of Trimble SX10 scanning total station used by Coastal Environments for SONGS topographic surveys.



Figure 4-9. Location of 21 transects along the revetment, spaced 100 ft apart.

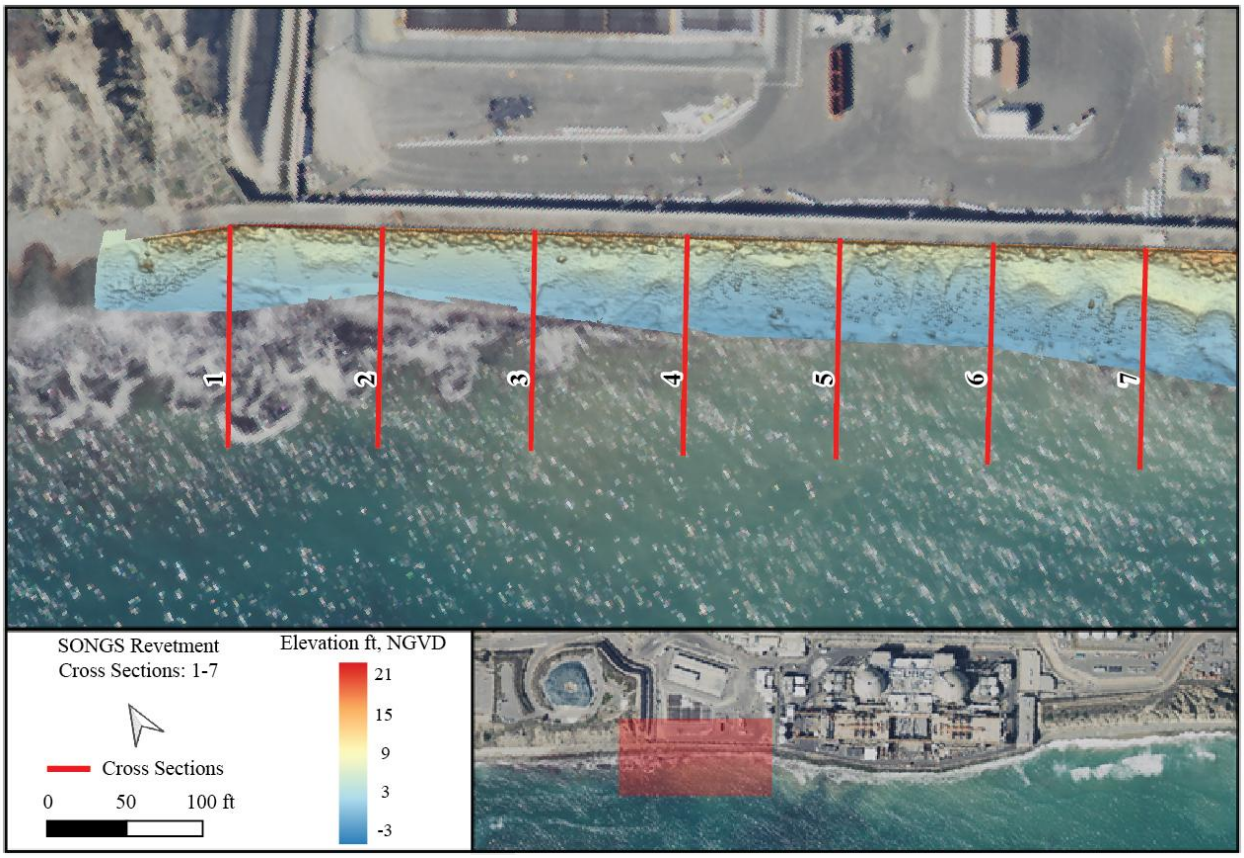


Figure 4-10. Elevation model of SONGS revetment from laser scanner, Transects 1-7.

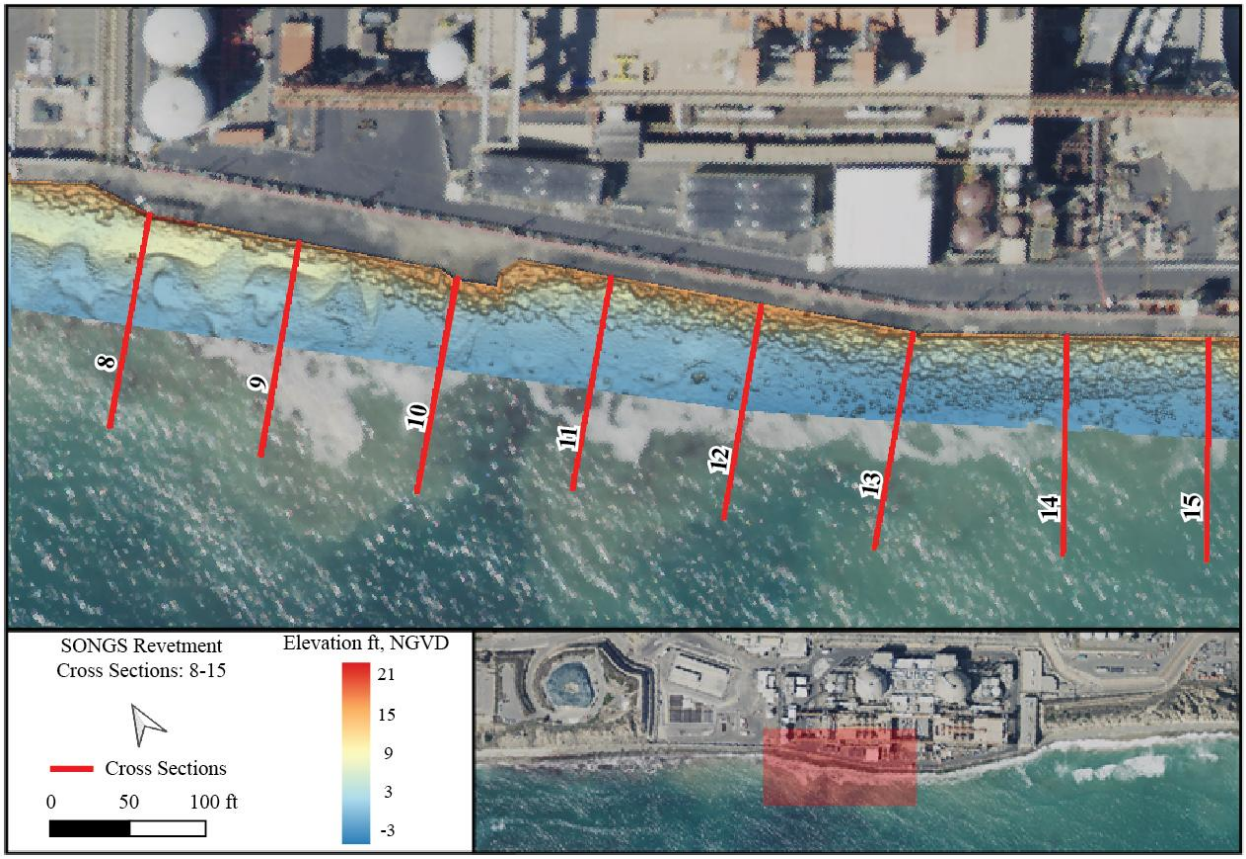


Figure 4-11. Elevation model of SONGS revetment from laser scanner, Transects 8-15.

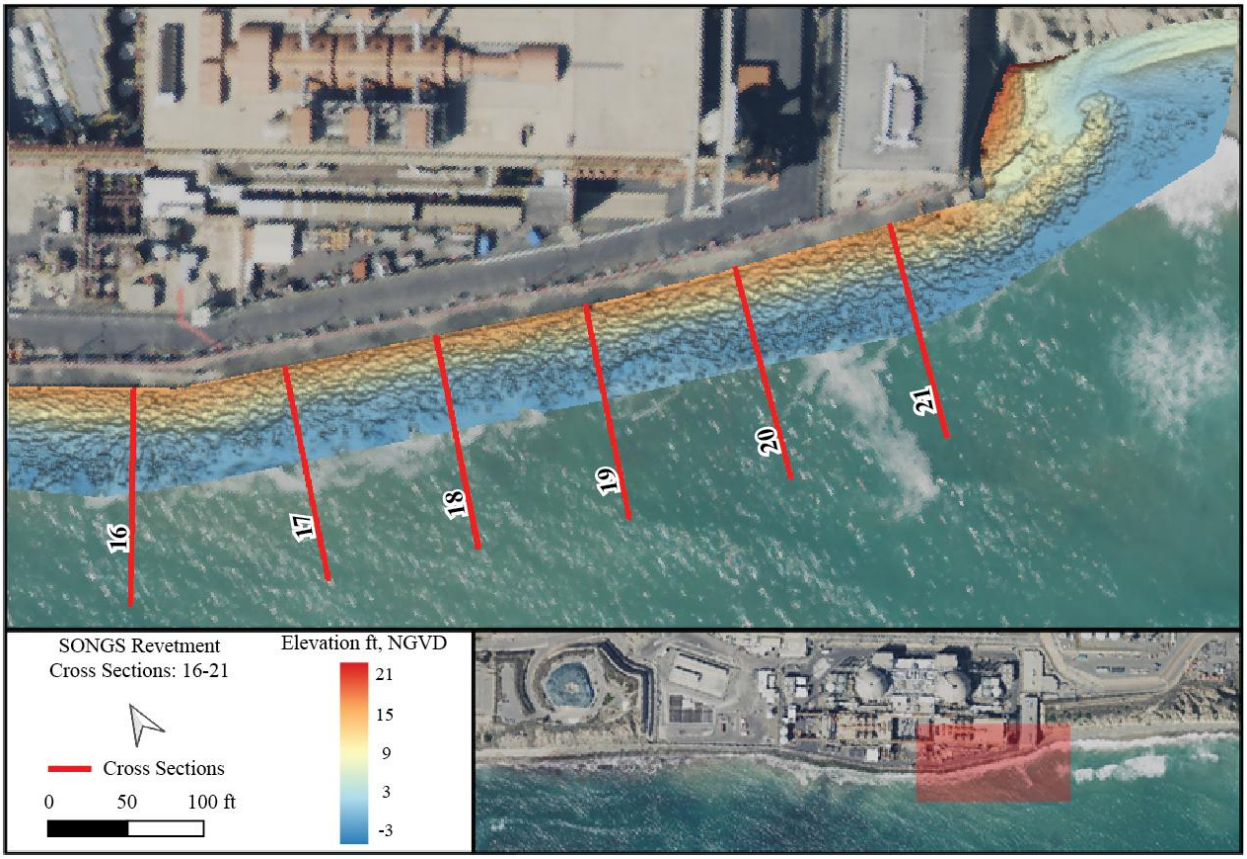


Figure 4-12. Elevation model of SONGS revetment from laser scanner, Transects 16-21.

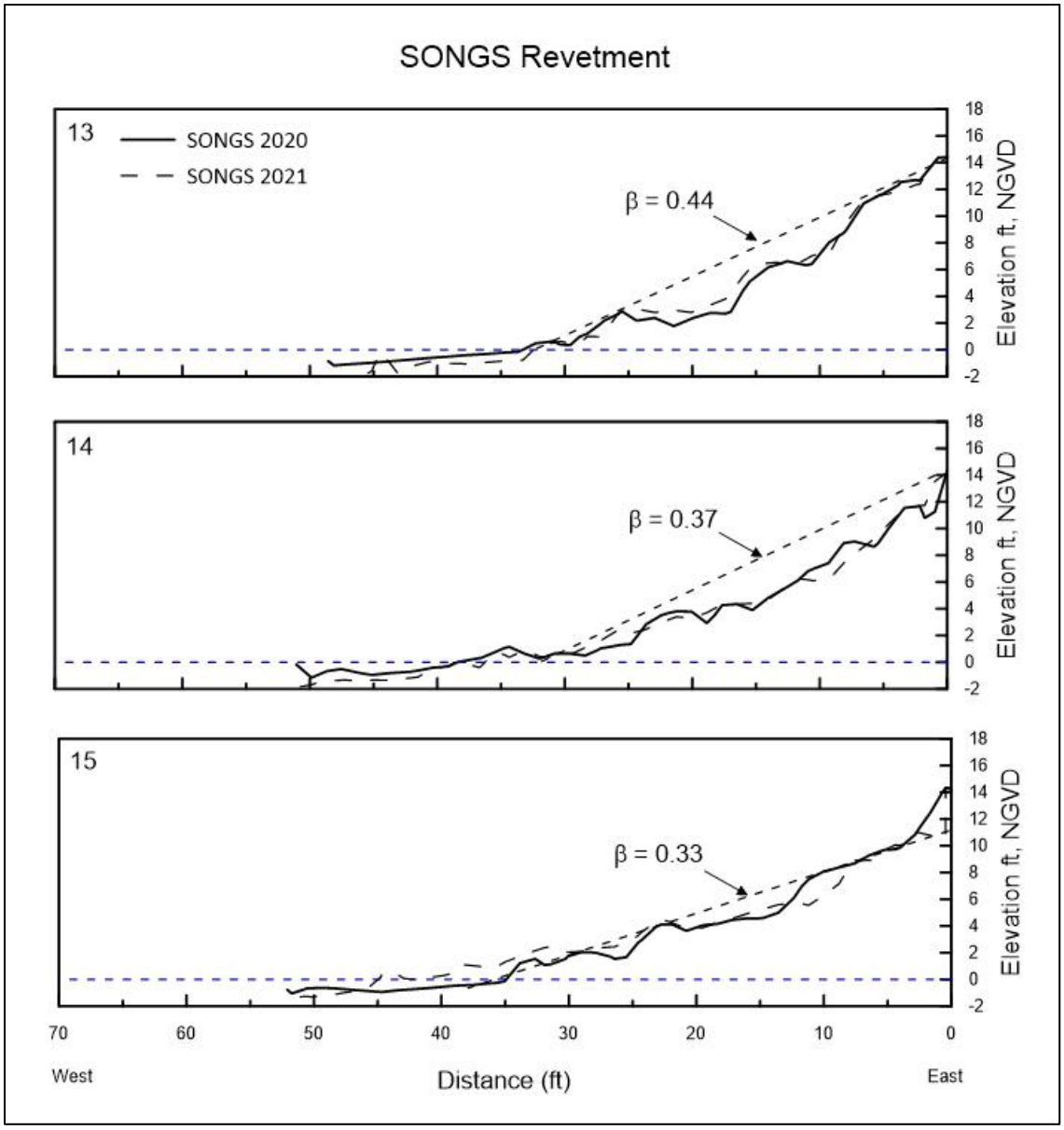


Figure 4-13. Typical revetment cross sections showing slope β at the indicated section.

Table 4-1. Riprap and walkway wall elevations and revetment slope β.

Transect #	Riprap Elevation (ft NGVD)	Wall Elevation (ft NGVD)	Slope (β)
1	12.89	16.79	0.90
2	12.27	14.27	0.66
3	12.15	14.27	1.52
4	9.22	14.32	1.13
5	9.44	14.27	0.35
6	10.13	14.2	0.43
7	12.48	14.34	0.67
8	9.55	14.39	0.20
9	10.59	14.29	0.38
10	15.12	14.39	0.46
11	13.69	14.34	0.40
12	13.63	14.39	0.54
13	12.37	14.39	0.44
14	12.34	14.37	0.37
15	10.34	14.34	0.33
16	14.24	14.21	0.42
17	12.98	14.27	0.38
18	13.58	14.22	0.39
19	14	14.31	0.40
20	13.49	14.32	0.37
21	14.4	14.32	0.35

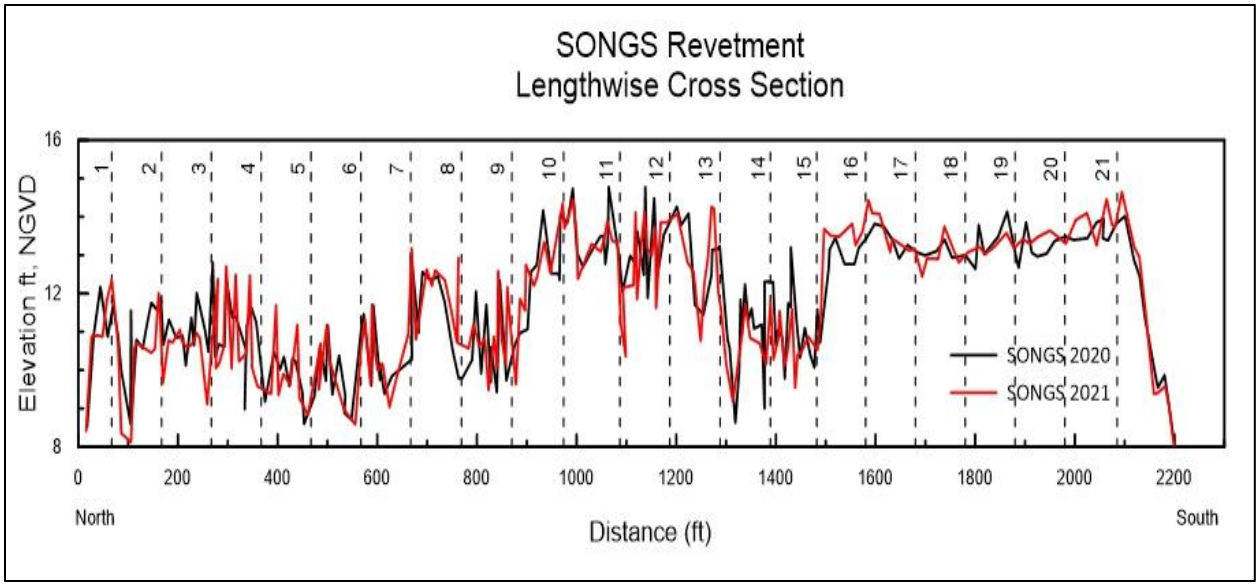


Figure 4-14. Elevation of revetment top at the 21 transects in Figure 4-9.

Table 4-2. Length, width, height, and estimated weight of the measured rocks.

Rock #	Length (ft)	Width (ft)	Height (ft)	Weight (kg)
1	2.6	2.1	2.0	369
2	3.3	2.4	2.7	551
3	3.3	2.9	2.1	973
4	2.0	1.8	1.4	233
5	4.8	3.9	1.8	2,366
6	3.5	1.7	1.2	196
7	3.2	2.6	2.5	701
8	2.8	1.6	1.0	163
9	3.2	2.4	1.7	551
10	1.9	1.0	1.0	40
11	3.5	1.9	2.0	274
12	2.0	1.5	0.9	135
13	2.6	2.3	1.1	485
14	4.3	3.5	2.5	1,710
15	3.8	2.6	1.3	701
16	2.3	1.7	1.0	196
17	5.2	3.0	1.4	1,077
18	4.3	3.9	1.2	2,366
19	5.3	3.6	3.0	1,861
20	4.4	3.2	2.1	1,307
21	4.3	3.5	2.7	1,710
22	4.7	3.0	2.6	1,077
23	2.6	1.4	1.5	109
24	4.8	3.2	1.8	1,307
25	5.2	2.9	2.3	973
26	3.7	2.5	2.5	623
27	3.4	1.9	1.6	274
28	4.6	2.2	2.1	425
29	4.0	3.4	2.1	1,568
30	3.4	1.9	1.3	274
31	3.8	2.7	2.1	785
32	4.6	3.9	0.9	2,366
33	4.3	3.2	2.3	1,307
34	4.9	2.4	2.3	551
35	3.5	2.7	2.2	785
36	2.8	2.8	1.5	876
37	3.0	2.2	1.6	425
38	3.6	1.8	0.9	233
39	4.5	3.8	3.7	2,189
40	3.8	2.2	2.0	425
41	4.9	4.6	2.4	3,883
42	2.9	2.7	2.4	785
43	3.6	2.1	2.1	369
44	4.0	2.4	2.6	551
45	4.3	2.7	3.6	785
46	3.8	2.2	3.6	425
47	4.1	3.3	2.1	1,433
48	3.6	2.5	1.5	623
49	3.9	2.4	1.2	551
50	6.3	3.4	2.3	1,568
51	5.1	2.9	2.2	973
52	2.2	1.5	1.1	135
53	2.0	1.2	0.9	69
54	2.3	1.6	1.6	163
55	4.4	2.7	2.1	785
56	3.3	2.6	1.2	701
57	2.4	2.1	1.1	369
58	2.5	2.1	2.1	369
59	5.5	3.7	2.7	2,020
60	3.4	1.9	2.2	274
61	4.2	1.7	1.9	196
62	2.9	1.4	2.1	109
63	5.4	4.2	2.8	2,955
64	2.9	1.9	2.3	274
65	5.0	3.2	1.6	1,307
66	5.8	3.3	2.0	1,433
67	6.1	3.4	3.7	1,568
68	6.4	4.0	2.8	2,553
69	4.2	3.7	2.9	2,020
70	6.3	3.2	2.2	1,307
71	3.0	1.1	2.2	53
72	3.4	2.2	1.3	425
73	2.2	1.1	1.3	53
74	1.3	1.1	0.6	53
75	1.6	1.0	0.8	40
76	3.8	2.7	2.7	785
77	5.4	2.4	2.1	551
78	2.3	1.2	0.7	69
79	2.1	0.7	1.4	14
80	3.8	2.9	2.0	973

Table 4-3. Mean and standard deviation for rock parameters.

Rock Parameters	Length (ft)	Width (ft)	Height (ft)	Calculated weight (kg)
Mean	3.8	2.5	1.9	849
Minimum	1.3	0.7	0.6	14
Maximum	6.4	4.6	3.7	3,882
Std Dev	1.2	0.9	0.7	779

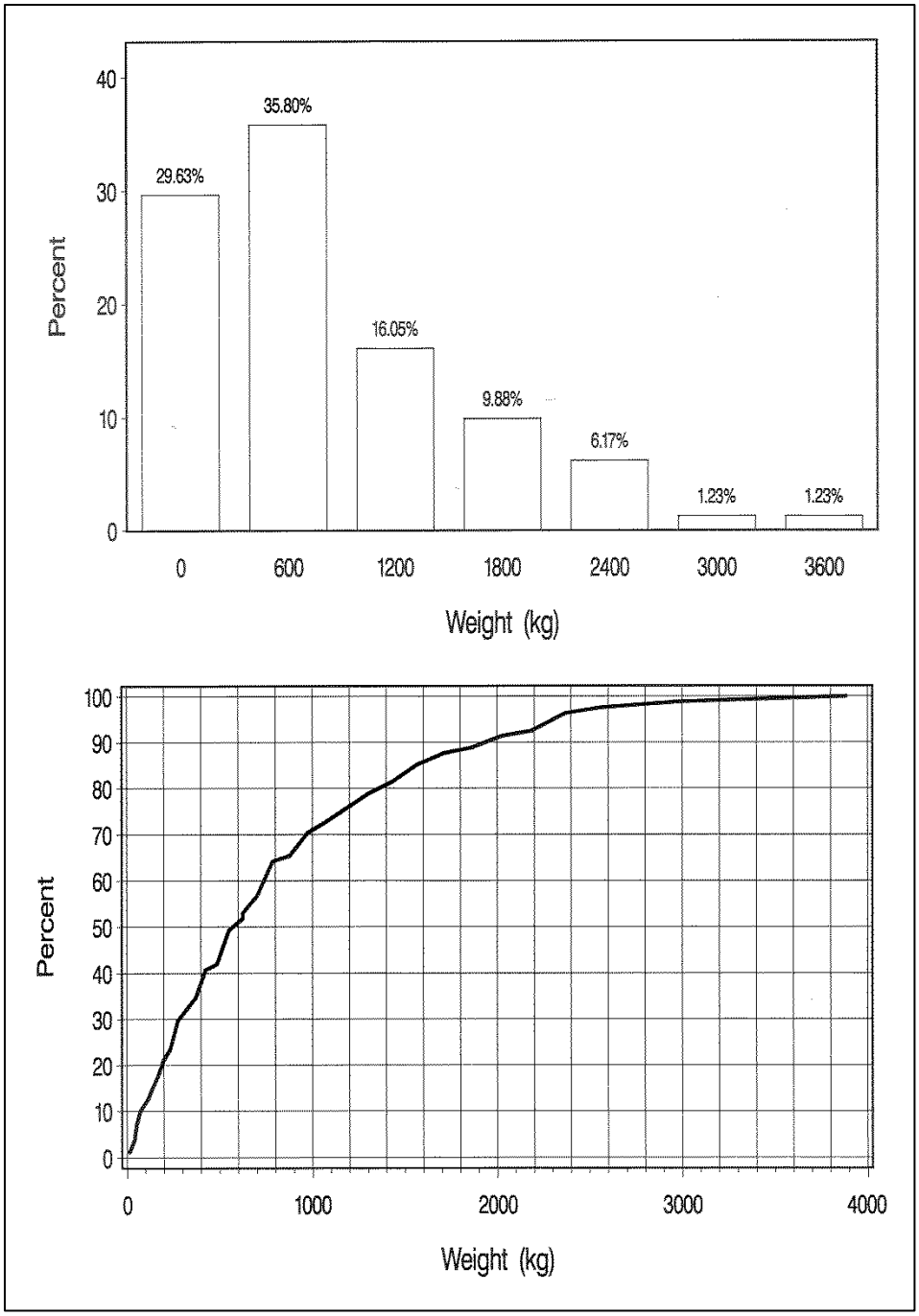


Figure 4-15. Weight distribution of existing SONGS revetment rocks.

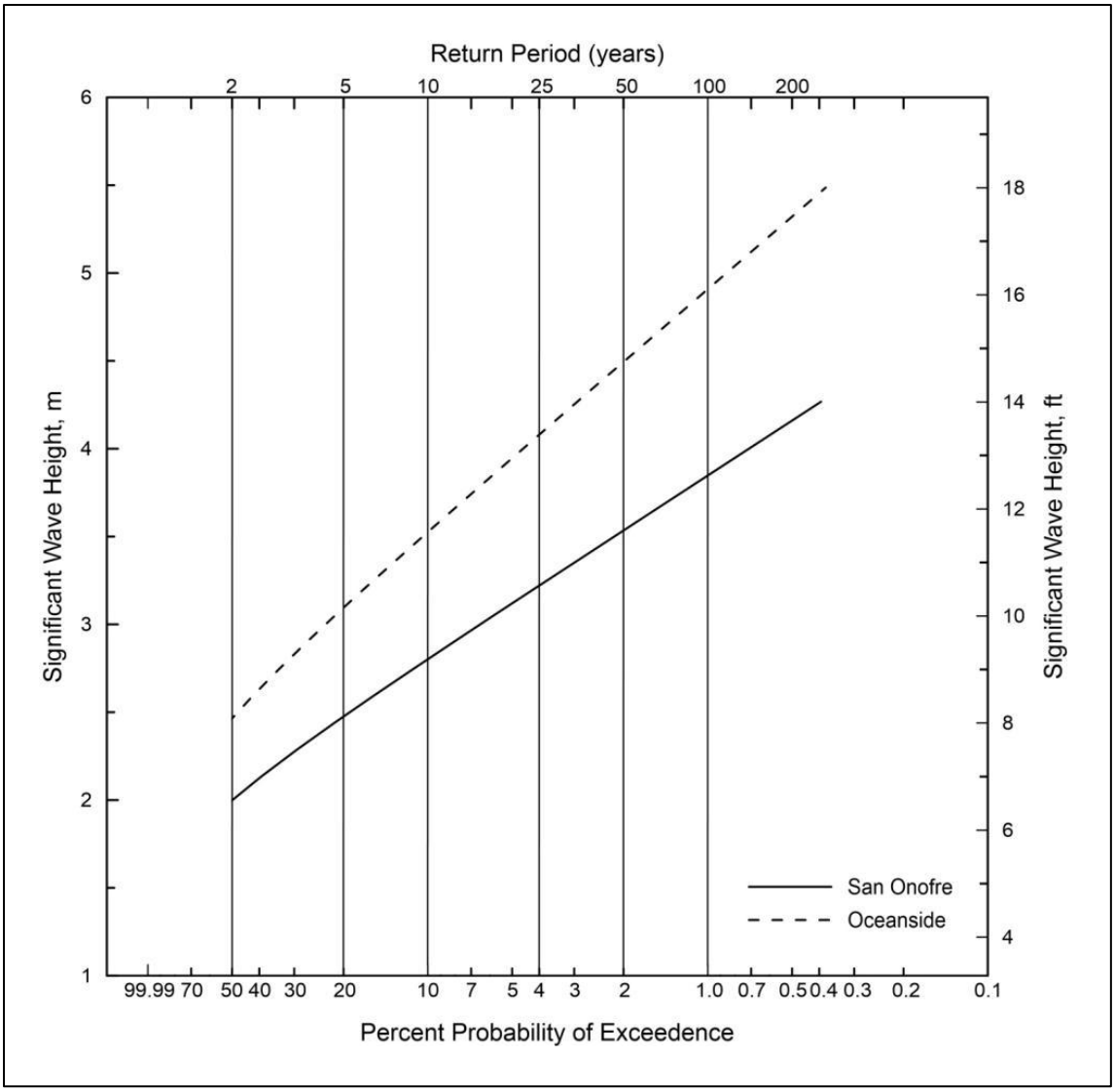


Figure 4-16. Design wave heights for various return periods at San Onofre.

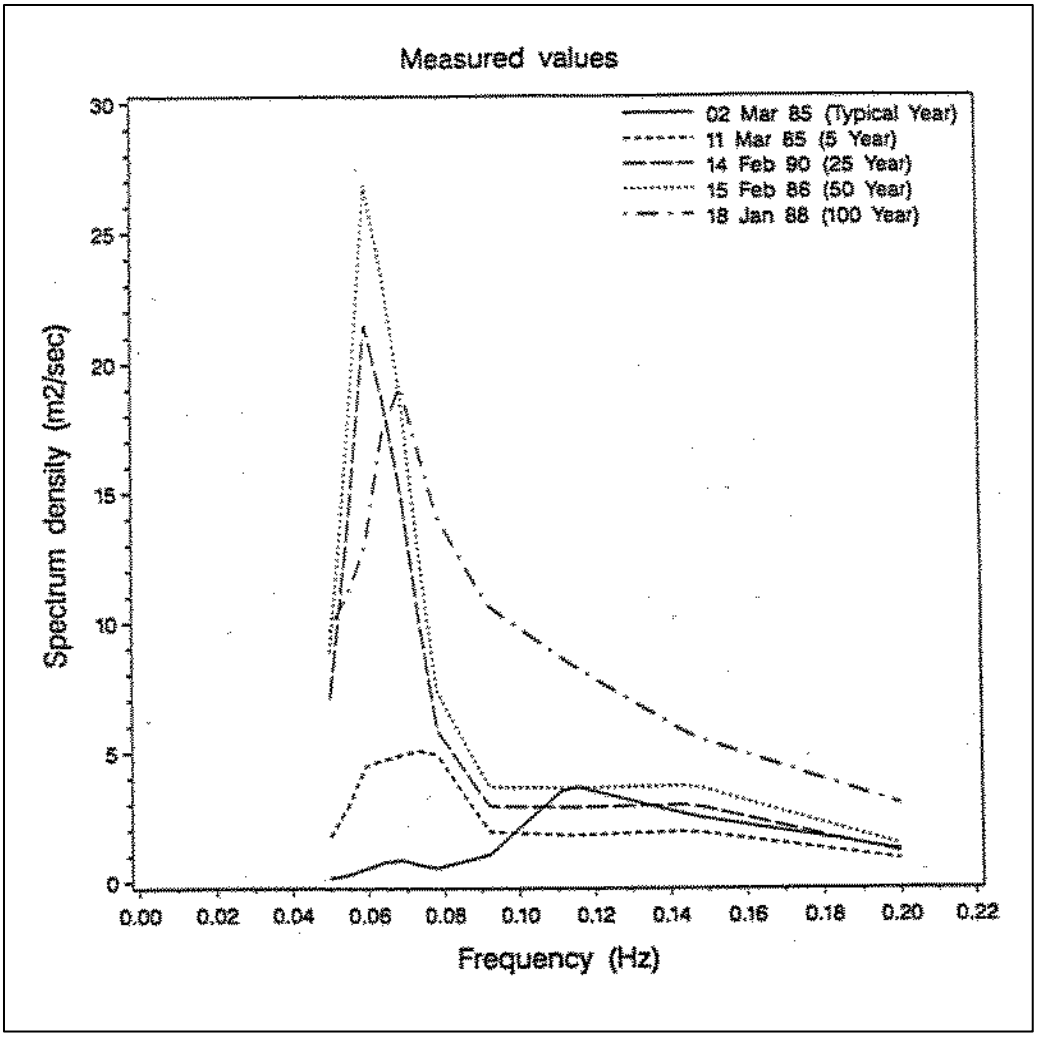


Figure 4-17. Measured wave spectral density for various storms.

Table 4-4. Design wave characteristics at San Onofre.

Storm Return Period (yrs)	Significant Wave Height Hs (ft)	Peak Period Tp (sec)
2	6.6	9
5	7.9	12
10	9.2	12
25	10.5	17
50	11.5	17
100	12.5	16

Table 4-5. Largest 20 waves at San Onofre ranked in descending order (1976-1994).

Rank	Winter		Summer		All	
	Hs (ft)	Tp (secs)	Hs (ft)	Tp (secs)	Hs (ft)	Tp (secs)
1	12.63	14.2	6.59	8.0	12.63	14.2
2	10.76	12.8	5.77	8.5	10.76	12.8
3	9.45	14.2	5.68	7.1	9.45	14.2
4	9.45	8.5	5.58	8.5	9.45	8.5
5	8.27	12.8	5.38	16.0	8.27	12.8
6	7.91	8.5	5.38	8.3	7.91	8.5
7	7.74	8.5	5.25	7.5	7.74	8.5
8	7.58	7.5	5.22	7.1	7.58	7.5
9	7.42	6.7	4.99	8.5	7.42	6.7
10	7.38	12.8	4.92	7.5	7.38	12.8
11	7.38	12.8	4.82	8.0	7.38	12.8
12	6.96	12.8	4.82	9.5	6.96	12.8
13	6.76	7.5	4.72	14.2	6.76	7.5
14	6.76	14.2	4.72	7.5	6.76	14.2
15	6.76	12.8	4.66	7.5	6.76	12.8
16	6.73	14.2	4.66	7.5	6.73	14.2
17	6.69	7.5	4.66	16.0	6.69	7.5
18	6.66	9.1	4.63	6.7	6.66	9.1
19	6.66	7.5	4.63	9.8	6.66	7.5
20	6.66	14.2	4.63	16.0	6.66	14.2

Table 4-6. Rock weights (W_{50}) needed for revetment stability, 2020 and 2050.

Year	MSLR Scenario	Water Depth (ft)	Design Wave Height (ft)	Rock Weight W_{50} (kg)
2020	--	7.8	4.4	276
2050	1:200 (0.5%)	9.8	5.5	548
2050	H++	10.6	5.9	685

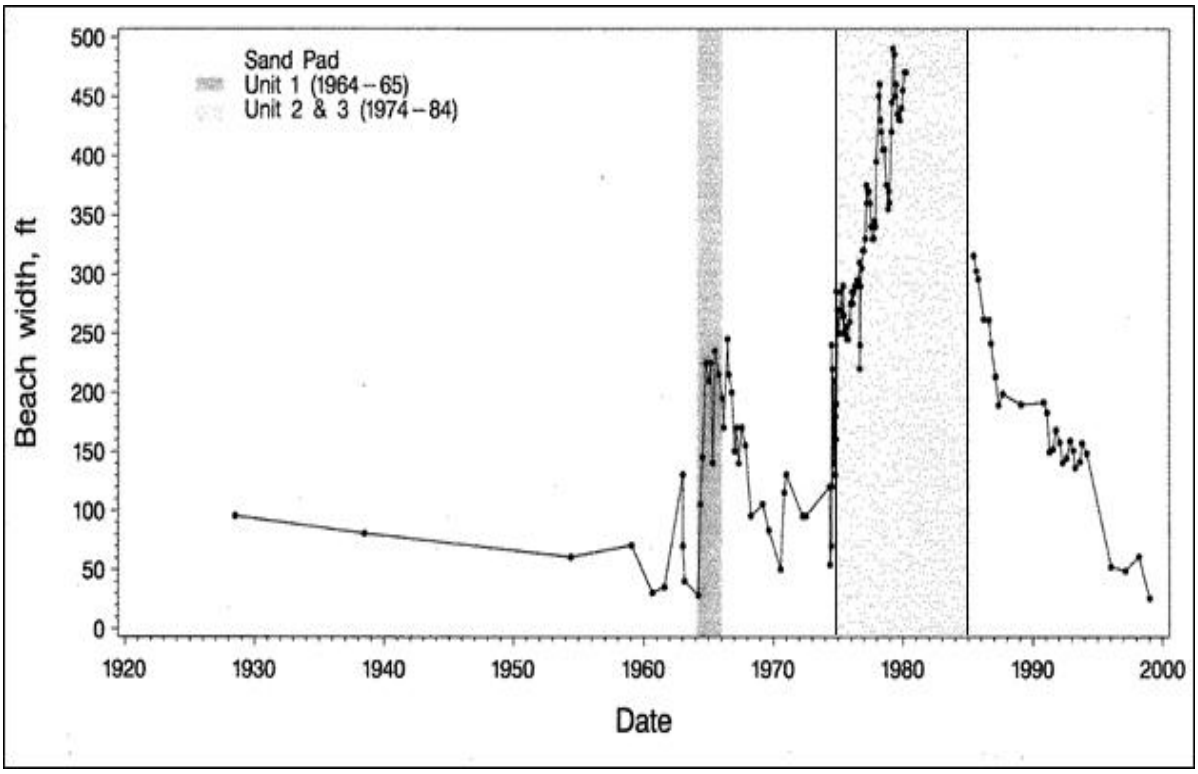


Figure 4-18. Historical beach width adjacent to Unit 1, 1928-2000. Vertical columns show periods when laydown pads were in place.

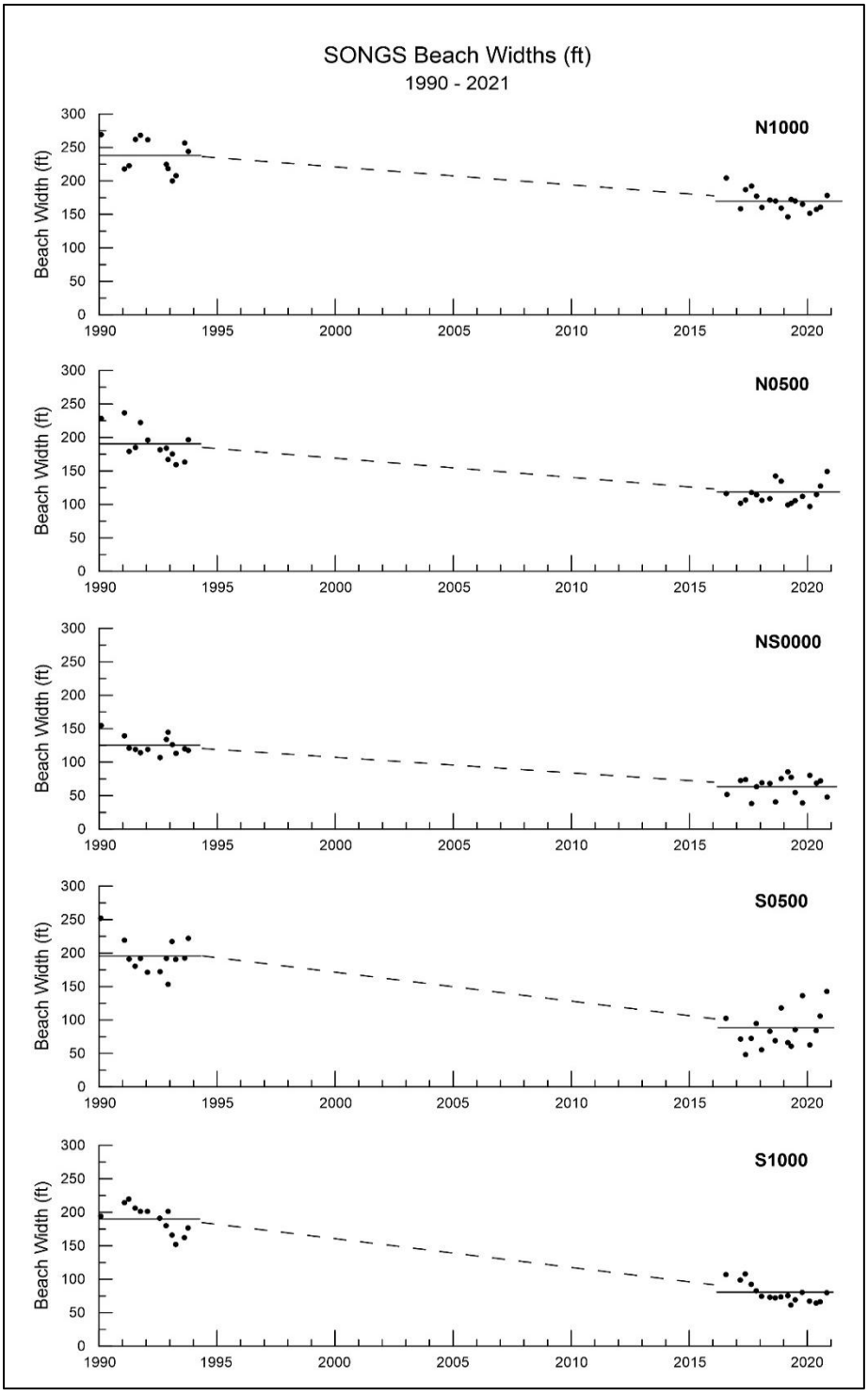


Figure 4-19. Beach width fronting SONGS, 1991-1993 and 2016-2020. Solid lines are mean beach width for each period. Dotted lines suggest long-term narrowing over years with no data.

Table 4-7. Mean beach widths (ft) at San Onofre, 1990-1993 vs 2017-2020.

Profile	1990-1993		2017-2020		Difference in mean	p-value
	Mean	Std. Dev	Mean	Std. Dev		
N1000	237.9	25.1	167.4	12.4	70.5	2.09E-07
N0500	190.4	25.0	114.9	15.6	75.5	1.19E-08
NS0000	125.4	13.9	64.3	15.3	61.1	1.02E-11
S0500	195.8	26.0	84.9	28.0	110.9	2.64E-11
S1000	189.8	20.9	77.5	12.8	112.3	6.05E-13

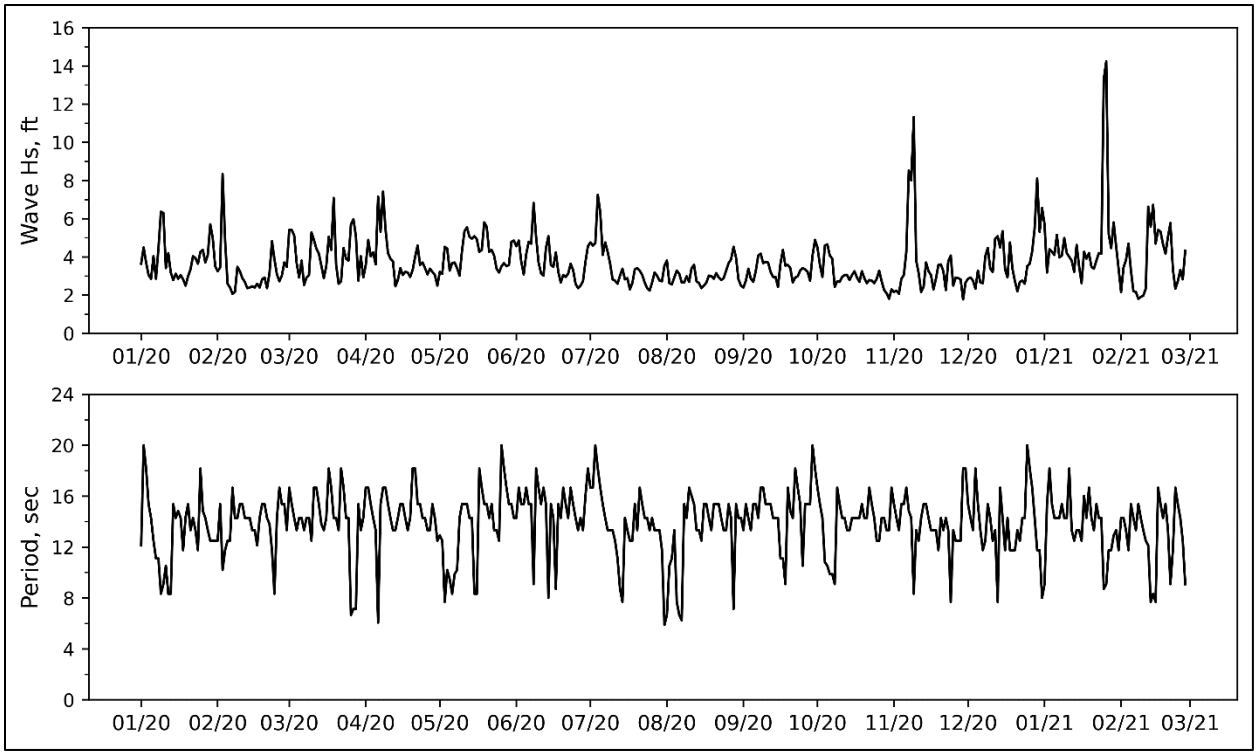


Figure 4-20. Wave height and period at SONGS, 1 January 2020 to 28 February 2021.

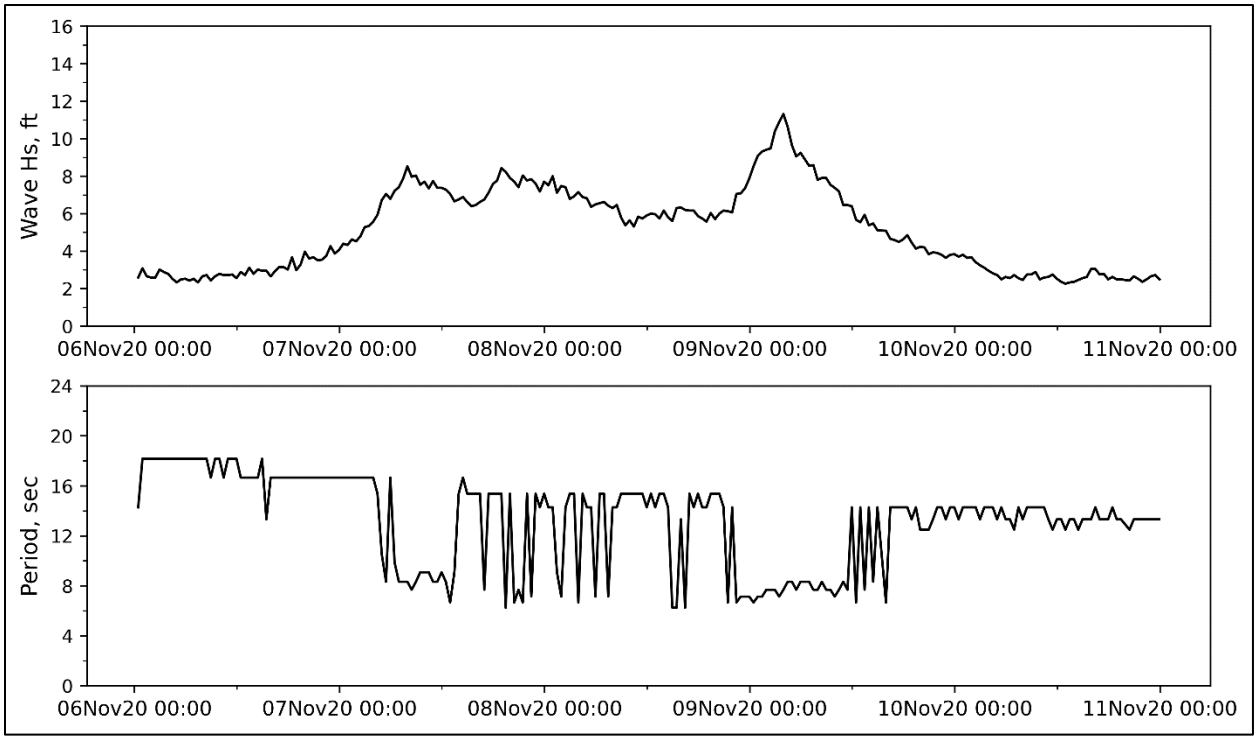


Figure 4-21. Wave height and period at SONGS, 6-11 November 2020.

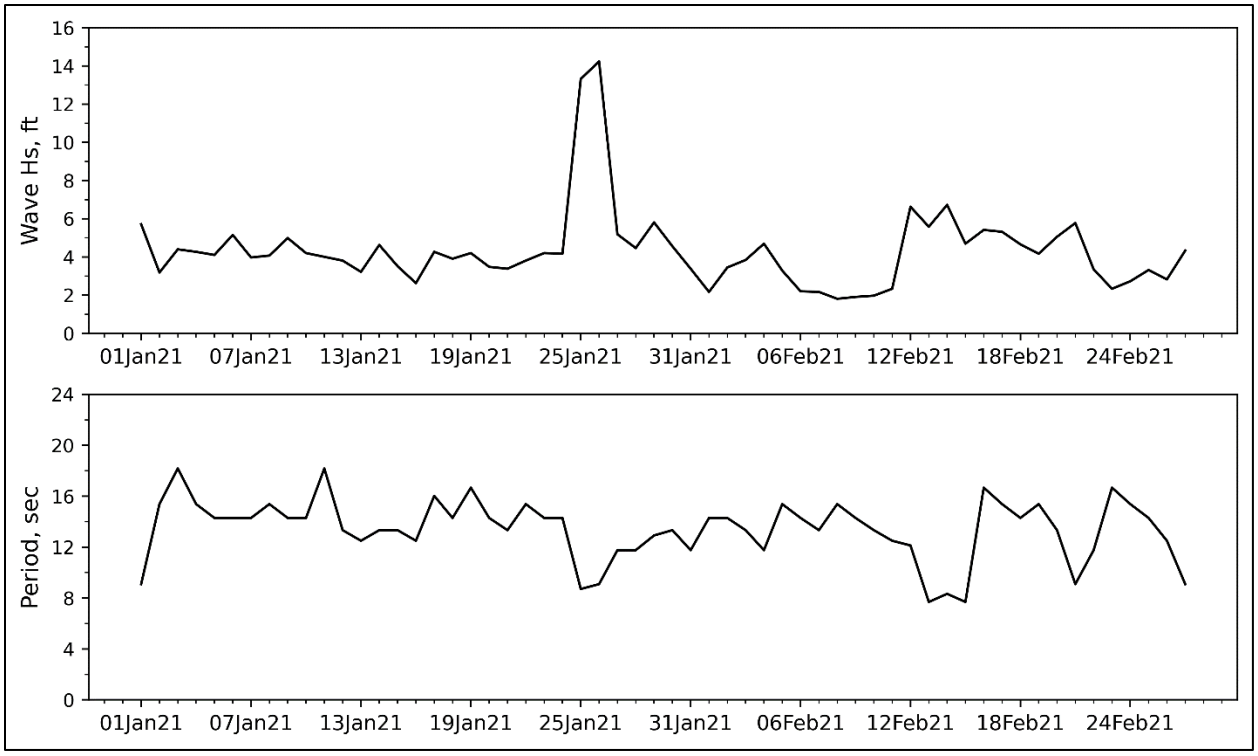


Figure 4-22. Wave height and period at SONGS, 1 January to 28 February 2021.

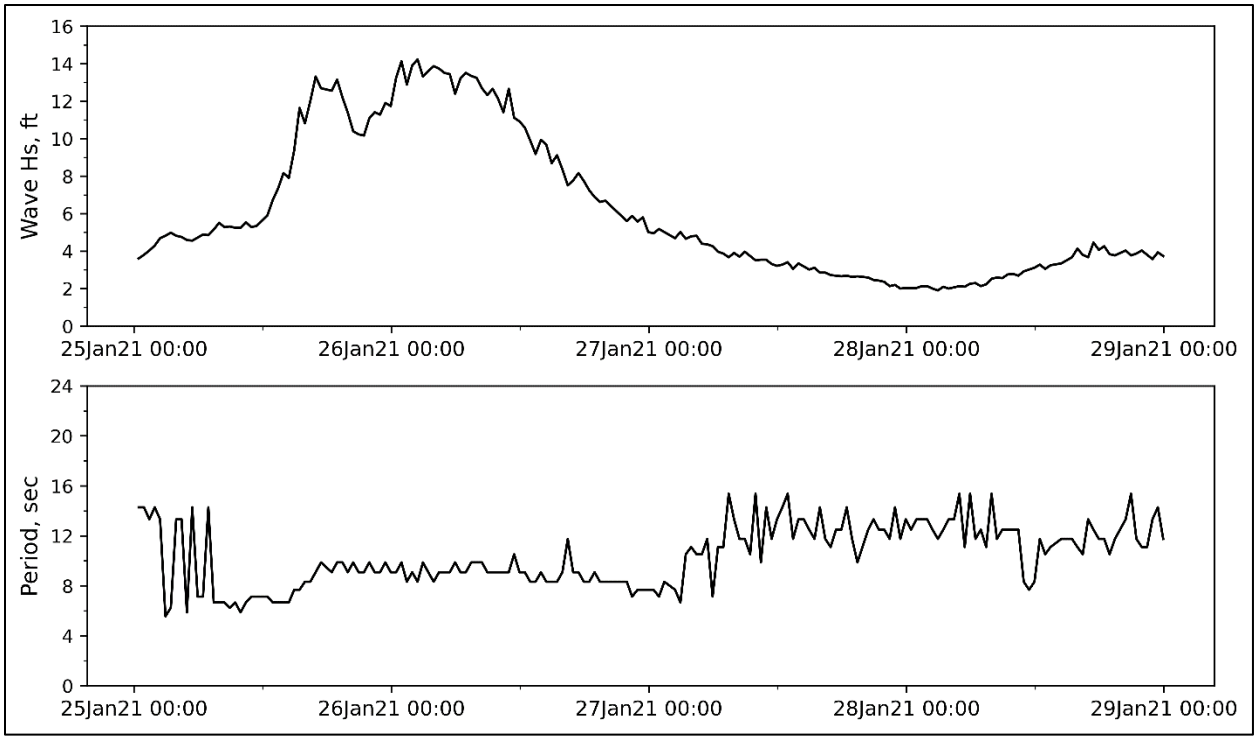


Figure 4-23. Wave height and period at SONGS, 25-29 January 2021.



Figure 4-24. Photos of north portion of SONGS revetment covered by beach sand, spring 2020 (upper), but covered with cobble, winter 2021 (lower).

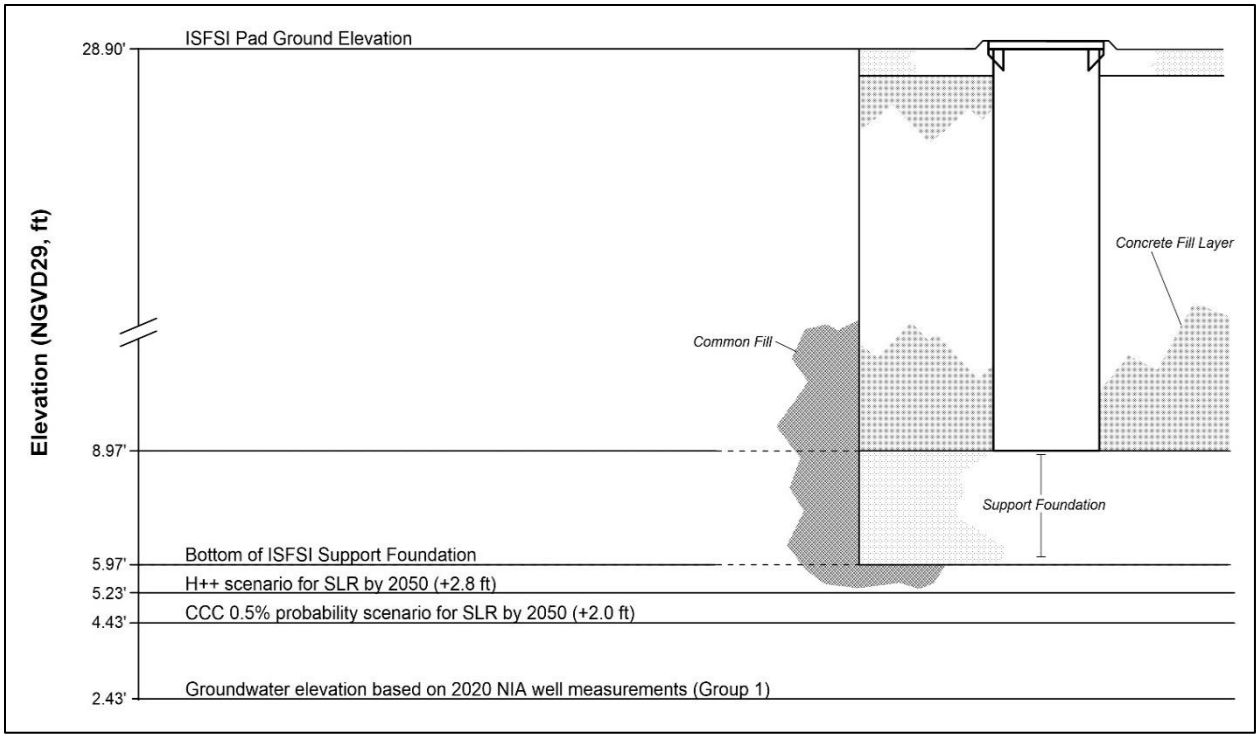


Figure 4-25. Groundwater elevations in 2020, and for OPC (2018) 0.5% and H++ MSLR projections by 2050. From Coastal Environments (2021).

5.0 RUN-UP AND OVERTOPPING ANALYSIS

Wave run-up is defined as the rush of water up a beach or coastal structure caused by, or associated with, wave-breaking. The run-up elevation, designated R (Figure 5-1), is the maximum vertical height above still water level that the run-up will reach. If the run-up elevation is higher than the back of the beach berm, the excess constitutes overtopping. Run-up elevation is dependent on the incident wave characteristics, beach slope and porosity, and if a structure is present, on that structure's shape, slope, roughness, permeability, and water depth at the toe. Run-up analysis is important to assess possible flooding and damage to the SONGS revetment, walkway, and seawall. The amount and type of possible damage depends on run-up elevation and amount of overtopping, as well as on storm wave duration. The SONGS revetment reduces wave run-up by a factor varying from 0.5-0.6 (USACE 1994b, Table 7-2) due to rock roughness and interstitial permeability.

5.1 RANDOM WAVE METHOD

Wave run-up (R) is composed of wave setup and swash run-up. The swash run-up is defined as a super elevation of the mean water level and fluctuation about that mean (S). *R* is given by the equation:

$$R = \acute{\eta} + S/2 \tag{5-1}$$

where $\acute{\eta}$ is the setup and *S* is swash run-up.

Many small- and large-scale laboratory studies have been conducted to measure run-up on model beaches, sloped dikes, and seawalls (e.g., Hunt, 1959; Van der Meer and Jenssen, 1995; Hedges and Reis, 1998). Based on laboratory experiments, Hunt (1959) proposed various formulas for estimating wave run-up on a smooth slope as a function of offshore wave height, H, and the Iribarren number, ζ, such that:

$$R = k\, H\, \zeta, \tag{5-2}$$

where k is a constant and ζ is the Iribarren number defined as:

$$\zeta = \frac{\tan\beta}{Ho/Lo} \tag{5-3}$$

where tanβ is beach slope, Ho is deepwater wave height, and Lo is deepwater wavelength.

Fewer studies have centered on run-up on beaches (Holland and Holman 1993; Raubenheimer *et al.*, 1995; Ruggiero *et al.*, 2004; Stockdon *et al.*, 2006). Stockdon *et al.* (2006) considered the contribution from both incident and infra gravity waves, using data from 10 field experiments with varying bathymetries and wave heights. They empirically estimated the highest 2% run-up exceedance elevation, $R_{2\%}$ with,

$$R_2 = A \quad 0.35\,\beta_f \; H_0 L_0 \;^{1/2} + \frac{H_0 L_0 \quad 0.563\beta_r^2 + 0.004 \quad ^{1/2}}{2} \;, \tag{5-4}$$

where β_f is the foreshore beach slope, H_o is the deepwater significant wave height, A is a coefficient equal to 1.1, as estimated by Stockdon *et al.* (2006), and the units are in meters.

5.2 OVERTOPPING

The overtopping rate, Q is defined as the volume of water that overtops a coastal structure or beach berm per unit time and unit length. Resulting units of Q are volume per second per unit length, or ft^3/sec-ft. Overtopping empirical models are based on laboratory studies of structure overtopping. These models are used to test design specifications intended to limit the overtopping of levees and dikes, and they therefore give conservative values. A beach berm can act in the same manner as these structures to protect backshore development from wave attack and flooding.

Wave overtopping depends on the difference of freeboard height and wave run-up height. Freeboard, Rc, is defined as the height of the berm crest above mean water level. In order for waves to overtop a berm, the run-up heights must be greater than the freeboard height. Overtopping is dependent on run-up height and, therefore, dependent on incident wave height and period, and beach slope.

Hedges and Reis (1998) introduced a semi-empirical model (H&R model) based on an overtopping theory for regular waves developed by Kikkawa *et al.* (1968), which assumed that a seawall or beach berm acted as a weir whenever the incident water level exceeded the seawall level and the described instantaneous discharge by the weir formula. The H&R model extended the concept to random waves and had good agreement with data.

The H&R model can be written as:

$$\frac{Q}{\sqrt{gRmax}} = A \quad 1 - \frac{Rc}{\gamma r Rmax} \quad B \qquad \text{for } 0 \leq \frac{Rc}{\gamma r Rmax} < 1 \tag{5-5}$$

and

$$\frac{Q}{\sqrt{gR3max}} = 0 \qquad\qquad for \qquad \frac{Rc}{\gamma r Rmax} \geq 1, \tag{5-6}$$

where *g* is gravitational acceleration, R_{max} is the maximum run-up on smooth slope, and γr is a reduction factor to account for rough slope. R_{max} is estimated by Equation 9 in Reis *et al.* (2008). Additionally, the coefficients of the HR model were given by Reis *et al.* (2008) as:

$$A = \begin{cases} 0.0033 + 0.0025 \;^{1}/_{\beta} & \text{for } 0.08 \leq \beta \leq 1 \\ 0.0333 & \text{for } 0.05 \leq \beta < 0.083 \end{cases} \tag{5-7}$$

$$B = \begin{cases} 2.8 + 0.65\ \frac{1}{\beta} & \text{for } 0.13 \leq \beta \leq 1 \\ 10.2 - 0.275\ \frac{1}{\beta} & \text{for } 0.05 \leq \beta < 0.13 \end{cases} \quad (5\text{-}8)$$

where β is the beach slope.

Reis *et al.* (2008) compared the H&R model with three other methods used to estimate the overtopping rate for various structures subject to random wave action. The slopes of these structures varied from 1:1 to 1:20, and wave steepness varied from 0.01 to 0.3. The models were: (1) Owen (1980); (2) Van der Meer Janssen (1995); and (3) the AMAZON Numerical Model (Hu, 2000). There was general agreement between the H&R and AMAZON models, while Owen (1980) systematically over-predicted the discharges. Van der Meer and Janssen (1995) gave similar results to the H&R model, except that they over-predicted discharges for some conditions that are outside the ranges of applicability.

5.3 RESULTS

Figure 4-13 shows typical cross sections of the SONGS revetment. The locations of these profiles are shown in Figure 4-9. The slope, β, of the revetment varies from 0.33-0.44. The height of the walkway is about 14 ft (NGVD). The design water level is estimated as 5.5 ft (NGVD). Table 5-1 provides run-up and overtopping results for all design wave and water level conditions, including MSLR under the medium-high scenario for 2020, 2030, 2040, and 2050. Table 5-2 shows these results for the extreme H++ MSLR projection. Tables 5-1 and 5-2 suggest that wave overtopping of the revetment already occurs for storm wave conditions meeting or exceeding a 10-year return period (i.e., 10% probability of occurrence in a given year), which is consistent with observations (e.g., 2020).

As MSLR progresses, overtopping rates are expected to increase. For large storms, rates are projected to reach 0.5 ft^3/sec-ft by 2030 and 1-1.6 ft^3/sec-ft by 2050. There is a short segment in the walkway where the concrete wall has been replaced by rails to provide a flow path for the saltwater cooling system during plant operations. This opening in the wall will increase overtopping on the walkway (Figure 5-2). However, it does not represent a significant hazard to pedestrians since the walkway will be closed during storms and there are no more discharges from the system.

5.4 PROBABILITY ANALYSIS

The probability associated with run-up and overtopping is considered in quantitative terms. This risk is defined as the probability that a "T-year" return-period event will occur at least once during a given "n-year" long time period. The run-up results in Tables 5-1 and 5-2 can be used to estimate the risk for any selected "n-year" long time period. The results can also be used to estimate the probability of run-up of a given size during a specified time period. The probability of a T-year run-up in any one year is $P = 1/T$.

In other words, there is a one-percent chance that the 100-year run-up will occur during a given year. The probability is equal to the sum of the probabilities of having one run-up, two

run-ups, or *n* run-up events occurring during *n* years of interest, or to 1 minus the probability of having no run-ups. The risk can be calculated from Equation 5-9:

$$P = 1 - (1- 1/T)^n \quad (5\text{-}9)$$

Equation 5-9 indicates that there is a 63% chance that the 100-year magnitude run-up will occur at least once during any 100-year time interval. Similarly, Equation 5-9 can be used to calculate the risk associated with any T-year run-up during any time period. Figure 5-3 gives the probability of occurrence of T = 25-year, 50-year and 100-year run-ups in an n-year period based on Equation 5-9.

5.5 SUMMARY

Observations suggest that over the last decade or longer, the SONGS revetment has adjusted to reach an equilibrium configuration. Under its current condition, the revetment is expected to withstand projected wave forces with acceptable minimum rock displacement and settling that will not impact the integrity of the revetment as a whole.

The walkway elevation at 14 ft (NGVD) is relatively low and will continue to flood under large wave conditions that overtop the revetment. However, it should be noted that the results of run-up and overtopping presented in this study are conservative for the following reasons:

1. The results are based on an extreme high water level of 5.3 ft (NGVD) that includes king tides, El Niño enhancements, and 1-ft storm surges. Observations suggest that it is exceedingly unlikely for large storm waves to occur precisely at the time of peak high (King) tides (e.g., Elwany and Flick, 1999; Flick, 1998, 2016; Young *et al.*, 2018).

2. Figure 5-4 illustrates the joint probability distribution between significant wave height and water level between 1976-1994, a period characterized by large wave events occurring between 1981 and 1984. Figure 5-3 shows that the probability of 50-year and 100-year waves occurring in the next 30 years is 0.45 and 0.28, respectively. Multiplying these probabilities by the probability of larger waves occurring at high tides will lead to an extremely low probability of co-occurrence.

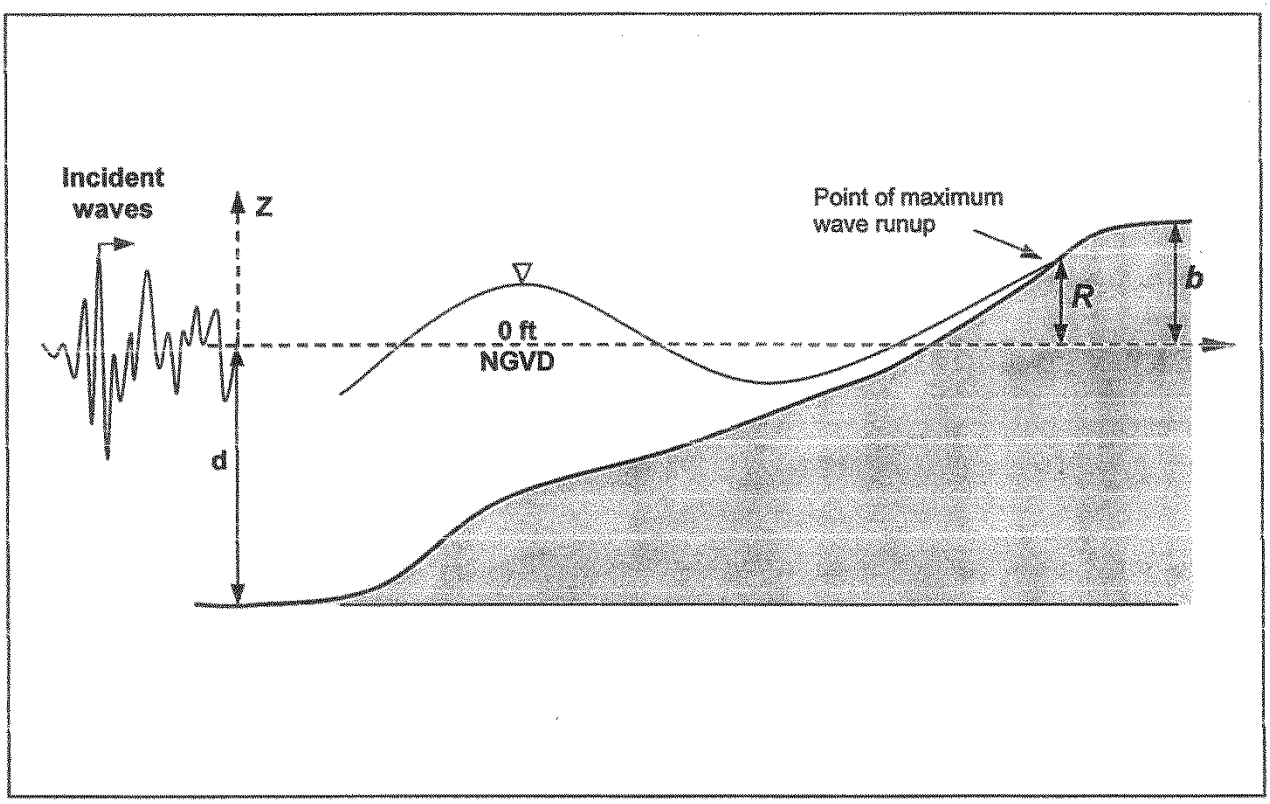


Figure 5-1. Wave run-up on a slope. R is the run-up elevation; b is the height of the beach berm. If R > b, then overtopping will occur.

Table 5-1. Run-up and overtopping summary for 0.5 % (1:200) scenario.

Year	Return Period (yr)	Hs (ft)	Tp (sec)	MSLR (ft)	Run-up (ft)	Run-up Elevation (ft NGVD)	Overtopping Rate (ft^3/sec-ft)
2020	2	2.0	9	0.0	5.27	10.77	0.00
	5	2.4	12	0.0	7.23	12.73	0.00
	10	2.8	12	0.0	7.81	13.31	0.01
	25	3.2	17	0.0	10.58	16.08	0.18
	50	3.5	17	0.0	11.06	16.56	0.28
	100	3.8	16	0.0	11.09	16.59	0.32
2030	2	2.0	9	0.9	5.27	11.67	0.00
	5	2.4	12	0.9	7.23	13.63	0.01
	10	2.8	12	0.9	7.81	14.21	0.04
	25	3.2	17	0.9	10.58	16.98	0.34
	50	3.5	17	0.9	11.06	17.46	0.49
	100	3.8	16	0.9	11.09	17.49	0.56
2040	2	2.0	9	1.3	5.27	12.07	0.00
	5	2.4	12	1.3	7.23	14.03	0.02
	10	2.8	12	1.3	7.81	14.61	0.06
	25	3.2	17	1.3	10.58	17.38	0.44
	50	3.5	17	1.3	11.06	17.86	0.62
	100	3.8	16	1.3	11.09	17.89	0.71
2050	2	2.0	9	2.0	5.27	12.77	0.00
	5	2.4	12	2.0	7.23	14.73	0.05
	10	2.8	12	2.0	7.81	15.31	0.12
	25	3.2	17	2.0	10.58	18.08	0.69
	50	3.5	17	2.0	11.06	18.56	0.94
	100	3.8	16	2.0	11.09	18.59	1.05

Table 5-2. Run-up and overtopping summary for OPC (2018) H++ scenario.

Year	Return Period (yr)	Hs (ft)	Tp (Sec)	MSLR (ft)	Run-up (ft)	Run-up Elevation (ft NGVD)	Overtopping Rate (ft^3/sec-ft)
2020	2	2.0	9	0.0	5.27	10.77	0.00
	5	2.4	12	0.0	7.23	12.73	0.00
	10	2.8	12	0.0	7.81	13.31	0.01
	25	3.2	17	0.0	10.58	16.08	0.18
	50	3.5	17	0.0	11.06	16.56	0.28
	100	3.8	16	0.0	11.09	16.59	0.32
2030	2	2.0	9	1.1	5.27	11.87	0.00
	5	2.4	12	1.1	7.23	13.83	0.02
	10	2.8	12	1.1	7.81	14.41	0.05
	25	3.2	17	1.1	10.58	17.18	0.39
	50	3.5	17	1.1	11.06	17.66	0.55
	100	3.8	16	1.1	11.09	17.69	0.63
2040	2	2.0	9	1.8	5.27	12.57	0.00
	5	2.4	12	1.8	7.23	14.53	0.04
	10	2.8	12	1.8	7.81	15.11	0.10
	25	3.2	17	1.8	10.58	17.88	0.61
	50	3.5	17	1.8	11.06	18.36	0.84
	100	3.8	16	1.8	11.09	18.39	0.94
2050	2	2.0	9	2.8	5.27	13.57	0.01
	5	2.4	12	2.8	7.23	15.53	0.12
	10	2.8	12	2.8	7.81	16.11	0.24
	25	3.2	17	2.8	10.58	18.88	1.12
	50	3.5	17	2.8	11.06	19.36	1.47
	100	3.8	16	2.8	11.09	19.39	1.62



Figure 5-2. Exposed area in the walkway wall.

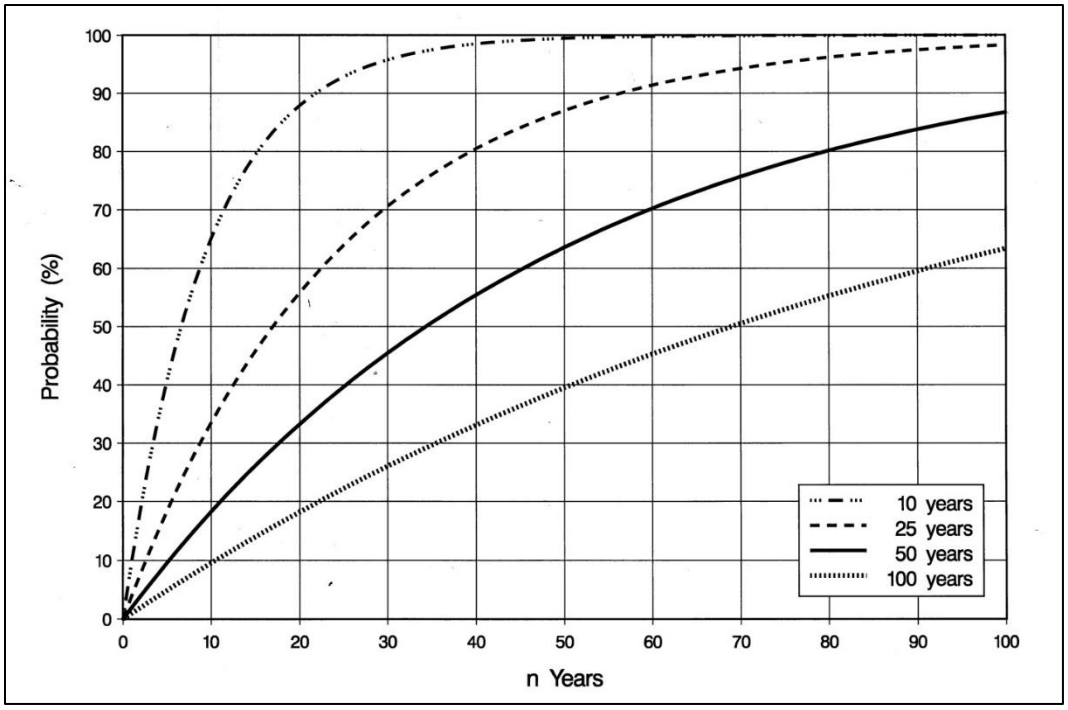


Figure 5-3. Probability of 10-, 25-, 50-, and 100-year waves return period to occur in the next 100 years.

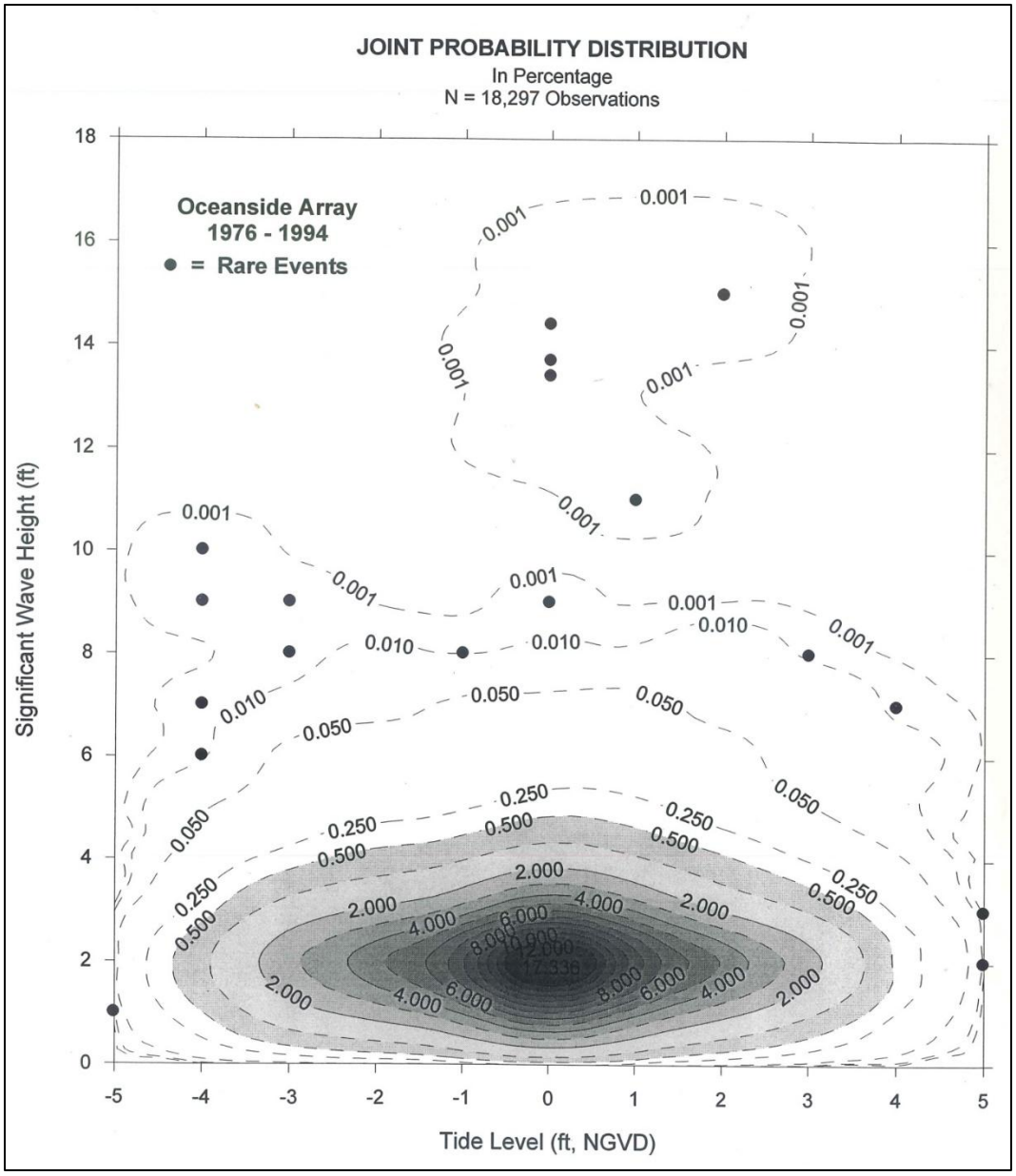


Figure 5-4. Joint Probability distribution between significant wave height and tide level. From Elwany and Flick (1999).

6.0 SUMMARY AND CONCLUSIONS

The objective of this study is to describe coastal hazards at SONGS in order to evaluate impacts of sea level rise for H++ sea level rise scenario up to 2050, waves, and wave run-up on the beach, nearshore zone, and SONGS facilities, including protective and coastal structures, particularly the revetment, access walkway and seawall. The report considers the possible future effects of sea level rise on the ongoing and long-term influences of waves on the beach, cliffs, protective structures, and wave run-up and overtopping under extreme conditions.

The findings and conclusions of our investigation are summarized as follows:

1. Waves and sand supply from offshore areas, rivers, and cliffs are the major factors controlling the cyclic erosion and accretion of the beach at SONGS. These factors together with MSLR determine long-term beach retreat. When the beaches become narrow enough for waves to impact the sea cliffs, these erode from wave action at the base, as well as from rainfall and inland drainage.
2. SONGS is fronted by a riprap rock revetment on the ocean front backed by a low retaining wall and a walkway that provides public lateral beach access. The main seawall, 28-30 ft, MLLW in elevation, backs the walkway and provides plant security and protection from erosion, and wave and tsunami overtopping.
3. Projections of future sea level rise are evolving as the understanding of key climate change processes improves. Currently applicable OPC (2018) and CCC (2015, updated 2018) State of California MSLR guidance projections through 2050 that could impact SONGS are reviewed. New IPCC (2021, 2022) projections are also discussed. Overall, the IPCC (2021, 2022) MSLR trajectories through 2050 are lower than existing guidance.
4. The relatively narrow beaches fronting and adjacent to SONGS are subject to normal seasonal fluctuations, as well as longer-term erosion and accretion. Measurements since 1991 suggest slow erosion to the present. Cliffs north and south of SONGS are exposed to marine erosion when beaches are sufficiently narrow. Beaches and cliffs are vulnerable to long-term retreat from MSLR. Beach retreat of up to 100 ft, and widely varying cliff retreat up to 84 ft by 2050 with mean value about 30 ft, is projected to occur for the highest extreme H++ MSLR scenario. (Table 3-1).
5. During winter 2020-2021, SONGS was subjected to a series of large wave events with heights up to 14 ft, which were higher than the previously estimated 100-year wave event. Despite the height and duration of these waves, damage to the revetment was minimal, being limited to normal rock settling and displacement, with expected water overtopping.
6. The integrity of the revetment as a whole was unaffected by the 2020-2021 storm waves. Stability and adaptive capacity analyses suggest that the revetment and adjacent walkway should withstand wave forces over the next 30 years, assuming regular monitoring of revetment condition, and with normal maintenance, repair, and small adjustment that may be required as MSLR proceeds.

7. Projections of future groundwater elevations estimated from the OPC (2018) 0.5% (1:200) and H++ MSLR scenarios through 2050, suggest that these will be (respectively) 1.54 ft and 0.74 ft lower than the bottom of the ISFSI support foundation, which is 3 ft thick.

7.0 REFERENCES

Ahrens, J. P., 1981a. Irregular Wave Runup on Smooth Slopes. Coastal Engineering Technical Aid No. 81-17, USACE, 26 pp.

Ahrens, J. P., 1981b. Design of Riprap Revetments for Protection Against Wave Attack. Technical Paper No. 81-5, USACE, 31 pp.

Ashton, A.D., M.J.A. Walkden, and M.E. Dickson, 2011. Equilibrium responses of cliffed coasts to changes in the rate of sea level rise. Mar. Geol., 284 (1-4), 217-229.

Bamber, J.L., M. Oppenheimer, R.E. Kopp, W.P. Aspinall, and R.M. Cooke, 2019. Ice sheet contributions to future sea-level rise from structured expert judgment. Proc. Nat. Acad. Sci., 116 (23), 11195-11200.

Bedsworth, L., D. Cayan, G. Franco, L. Fisher, and S. Ziaja, 2018. Statewide Summary Report, California's Fourth Climate Change Assessment. California Governor's Office of Planning and Research, Scripps Institution of Oceanography, California Energy Commission, and California Public Utilities Commission. Publication Number SUM-CCCA4-2018-013, 133 pp.

Beckley, B.D., N.P. Zelensky, S.A. Holmes, F.G. Lemoine, R.D. Ray, G.T. Mitchum, S.D. Desai, and S.T. Brown, 2010. Assessment of the Jason-2 Extension to the TOPEX/Poseidon, Jason-1 Sea-Surface Height Time Series for Global Mean Sea Level Monitoring. Marine Geodesy, 33(1).

Bray, M.J., and J.M. Hooke, 1997. Prediction of soft-cliff retreat with accelerating sea level rise. J. Coast. Res., 13, 453-467.

British Columbia Ministry of Environment, Lands and Parks (BCMELP), 2000. Riprap Design and Construction Guide. Public Safety Section, Water Management Branch, 12 pp.

Bromirski, P.D., A.J. Miller, R.E. Flick, and G. Auad, 2011. Dynamical Suppression of Sea Level Rise Along the Pacific Coast of North America: Indications for Imminent Acceleration. J. Geophys. Res., 116(C7).

Bromirski, P.D., A.J. Miller, and R.E. Flick, 2012. North Pacific Sea Level Trends. Eos Trans. AGU, 93(27), 249-256.

Bruun, P., 1962. Sea level rise as cause of shore erosion. J. Waterways Harbors Div., Amer. Soc. Civil Eng., 88, 117-130.

California Coastal Commission (CCC), 2001. Construction of San Onofre Nuclear Generating Station (SONGS) Units 2 and 3 Temporary Spent Nuclear Fuel Storage Facility. Southern California Edison Company, San Diego Gas and Electric Company, City of

Anaheim, and City of Riverside. Staff Report, Regular Calendar, Application File No. E-00-014, 114 pp.

California Coastal Commission (CCC), 2015. California Coastal Commission Sea Level Rise Policy Guidance: Interpretive Guidelines for Addressing Sea Level Rise in Local Coastal Programs and Coastal Development Permits, 293 pp. http://www.coastal.ca.gov/climate/slrguidance.html

California Coastal Commission (CCC), 2015 (updated 2018). California Coastal Commission Sea Level Rise Policy Guidance, Interpretive Guidelines for Addressing Sea Level Rise in Local Coastal Programs and Coastal Development Permits. San Francisco, CA, 307 pp.

California Coastal Commission (CCC), 2020a. Protecting California's Coast for Present and Future Generations, 2021-2025. San Francisco, CA, 56 pp. https://www.coastal.ca.gov/strategicplan/spindex.html.

California Coastal Commission (CCC), 2020b. Sea Level Rise in California: Planning for the Future. San Francisco, CA, 17 pp. https://storymaps.arcgis.com/stories/d0c1df224a97418bb4dad129ea4c6d17.

California Natural Resources Agency (CNRA) and California Environmental Protection Agency (CEPA), 2020. Making California's Coast Resilient to Sea Level Rise: Principles for Aligned State Action. Sacramento, CA, 29 April 2020, 6 pp. https://www.adaptationclearinghouse.org/resources/making-california-eys-coast-resilient-to-sea-level-rise-principles-for-aligned-state-action.html.

Cayan, D.R., J. Kalinsky, S. Iacobellis, and D. Pierce (with R. Kopp), 2016. Creating Probabilistic Sea Level Rise Projections. Unpublished White Paper, Division of Climate, Atmospheric Sciences, and Physical Oceanography, Scripps Institution of Oceanography, La Jolla, CA, 16 pp.

Chadwick, D.B., P.F. Wang, M. Brand, R.E. Flick, A.P. Young, W.C. O'Reilly, P.D. Bromirski, W.A. Crampton, R.T. Guza, J.J. Helly, T. Nishikawa, S. Boyce, M. Landon, M. Martinez, I. Canner, and B. Leslie, 2014. A Methodology for Assessing the Impact of Sea Level Rise on Representative Military Installations in the Southwestern United States (RC-1703). Final report submitted to The Strategic Environmental Research and Development Program, Alexandria, VA, 688 pp. http://www.serdp.org/Program-Areas/Resource-Conservation-and-Climate-Change/Climate-Change/Vulnerability-and-Impact-Assessment/RC-1703

Coastal Environments, 2000. SONGS Unit 1 Deconstruction Marine Impacts Study, Phase I. Unpublished report submitted to Southern California Edison Company, 24 January 2000, CE Ref. No. 2000-03, 44 pp. and 2 appendices.

Coastal Environments, Inc., 2021. 2020 Groundwater Levels at San Onofre Nuclear Generating Station, San Onofre, CA. Report submitted to Southern California Edison, Rosemead, CA 91770, 8 March 2021, CE Ref No. 21-05, 14 pp. and 1 appendix.

Cooper, J.A.G. and O.H. Pilkey, 2004. Sea level rise and shoreline retreat: Time to abandon the Bruun Rule. Global and Planetary Change, 43, 157-171.

Church, J.A. and N.J. White, 2011. Sea-Level Rise from the Late 19th to the Early 21st Century. Surv. Geophys., 32, 585–602.

Dean, R.G., 1991. Equilibrium beach profiles: Characteristics and applications. J. Coast. Res. 7 (1), 53-84.

Dean, R.G. and E.M. Maurmeyer, 1983. Models for beach profile response. In CRC Handbook of Coastal Processes and Erosion, CRC Press, Boca Raton, FL.

DeConto, R., and D. Pollard, 2016. Contribution of Antarctica to past and future sea level rise. Nature 531, 591-597.

DeConto, R.M., D. Pollard, R.B. Alley, I. Velicogna, E. Gasson, N. Gomez, S. Sadai, A. Condron, D.M. Gilford, E.L. Ashe, R.E. Kopp, D. Li, and A. Dutton, 2021. The Paris Climate Agreement and future sea-level rise from Antarctica. Nature 593, 83-89.

Elwany, H., R. Flick and S. Aijaz, 1994. 1993 Beach Profile Surveys at San Onofre, Final Report. Submitted to Southern California Edison, Rosemead, CA 91770, CE Ref. No. 94-07, 32 pp. and 2 appendices.

Elwany, H., and R. E. Flick, 1999. Coastal and Oceanographic Conditions in the Vicinity of the Proposed Manchester Resort Development Oceanside, California. Coastal Environments Reference No. 99 03, prepared for Manchester Resort, 1 Market Place, San Diego, CA, 61 pp. and 4 appendices.

Elwany, H., R.E. Flick, and F. Scarelli, 2020. SONGS Mean Sea Level Impact Assessment, Provision 14 In Lease NO. Prc 6785.1. Report prepared for Southern California Edison, Rosemead CA 91770, 30 March 2020, CE Ref No. 20-08, 64 pp. and 6 appendices.

Elwany, H., R.E. Flick, and F. Scarelli, 2021. SONGS Mean Sea Level Impact Assessment, Provision 14 In Lease NO. Prc 6785.1. Report prepared for Southern California Edison, Rosemead CA 91770, 25 March 2021, CE Ref No. 21-07, 76 pp. and 6 appendices.

Elwany, H., R.E. Flick, and F. Scarelli, 2022 SONGS Mean Sea Level Impact Assessment, Provision 14 In Lease NO. Prc 6785.1. Report prepared for Southern California Edison, Rosemead CA 91770, 30 March 2020, CE Ref No. 22-07, 77 pp. and 6 appendices.

Elwany, H., R.E. Flick, and F. Scarelli, 2021a. Beach Profile Surveys at San Onofre Nuclear Generating Station (SONGS), Units 2 and 3 Decommissioning Project. Report prepared for Southern California Edison, Rosemead CA 91770, 20 December 2021, CE Ref No. 21-22, 49 pp. and 2 appendices.

Everts, C.H., 1991. Seacliff retreat and coarse sediment yields in southern California. In Proceedings of Coastal Sediments '91, Vol. 2, pp. 1586–1598, American Society of Civil Engineers, Seattle, WA.

Flick, R.E. (ed.), 1994. Shoreline Erosion Assessment and Atlas of the San Diego Region (2 volumes). Sacramento, CA: California Department of Boating and Waterways and San Diego Association of Governments.

Flick, R. E., 1998. Comparison of California Tides, Storm Surges, and Sea Level During the El Niño Winters of 1982-83 and 1997-98. Shore & Beach, 66(3), 7-11.

Flick, R. E., 2016. California tides, sea level, and waves. Shore & Beach, Winter 2015-2016, 84(2), 25-30.

Flick, R.E., and J.R. Wanetick, 1989. San Onofre Beach Study. Unpublished report submitted to Southern California Edison Co., Rosemead, CA, October 1989, SIO Ref. No 89-20, 26 pp. and 25 figures.

Flick, R.E., J.R. Wanetick, M.H. Elwany, R.S. Grove, and B.W. Waldorf, 2010. Beach changes from construction of San Onofre Nuclear Generating Station, 1964-1989. Shore & Beach, 78(4), 12-25.

Fox-Kemper, B., H.T. Hewitt, C. Xiao, G. Aðalgeirsdóttir, S.S. Drijfhout, T.L. Edwards, N.R. Golledge, M. Hemer, R.E. Kopp, G. Krinner, A. Mix, D. Notz, S. Nowicki, I.S. Nurhati, L. Ruiz, J-B. Sallée, A.B.A. Slangen, and Y. Yu, 2021. Ocean, Cryosphere and Sea Level Change. In Climate Change 2021: The Physical Science Basis. Contribution of Working Group I to the Sixth Assessment Report of the Intergovernmental Panel on Climate Change. Masson-Delmotte, V., P. Zhai, A. Pirani, S.L. Connors, C. Péan, S. Berger, N. Caud, Y. Chen, L. Goldfarb, M.I. Gomis, M. Huang, K. Leitzell, E. Lonnoy, J.B.R. Matthews, T.K. Maycock, T. Waterfield, O. Yelekçi, R. Yu, and B. Zhou (eds.), Cambridge University Press.

Garner, G.G., T. Hermans, R.E. Kopp, A.B.A. Slangen, T. L. Edwards, A. Levermann, S. Nowikci, M.D. Palmer, C. Smith, B. Fox-Kemper, H.T. Hewitt, C. Xiao, G. Aðalgeirsdóttir, S.S. Drijfhout, T.L. Edwards, N.R. Golledge, M. Hemer, R.E. Kopp, G. Krinner, A. Mix, D. Notz, S. Nowicki, I.S. Nurhati, L. Ruiz, J-B. Sallée, Y. Yu, L. Hua, T. Palmer, B. Pearson, 2021. IPCC AR6 Sea-Level Rise Projections, Version 20210809. PO.DAAC, CA, USA.

Griggs, G., J. Arvai, D. Cayan, R. DeConto, J. Fox, H.A. Fricker, R.E. Kopp, C. Tebaldi, and E.A. Whiteman, 2017. Rising Seas in California: An Update on Sea Level Rise Science. California Ocean Protection Council Science Advisory Team Working Group, California Ocean Science Trust, 71 pp.

Hallermeier, R.J., 1978. Uses for a calculated limit depth to beach erosion. Proceedings, 16th Coastal Engineering Conference, American Society of Civil Engineers, 1493-1512.

Hands, E.B., 1983. The Great Lakes as a test model for profile responses to sea level changes. In Komar, P.D. (ed.), Handbook of Coastal Processes and Erosion. CRC Press, Boca Raton, Florida, pp. 176-189.

Hapke, C.J. and D. Reid, 2007. National Assessment of Shoreline Change, Part 4: Historical Coastal Cliff Retreat Along the CA Coast. USGS Report 2007-1133.

Hapke, C.J., D. Reid, and B. Richmond, 2009. Rates and trends of coastal change in California and the regional behavior of the beach and cliff system. J. Coast. Res., 25(3), 603-615.

Hedges, T.S., and M.T., Reis, 1998. Random wave overtopping of simple sea walls: A new regression model. Proc. Inst. Civ. Eng., Water Maritime Energy, 130(1), 1-10.

Holland, K.T. and R.A. Holman, 1993. Statistical distribution of swash maxima on natural beaches. J. Geophys. Res., v. 98, no. C6, 10271-10278.

Hu, K., C.G. Mingham, and D.M. Causon, 2000. Numerical simulation of wave overtopping of coastal structures using the non-linear shallow water equations. Coastal Engineering, 41(4), 433-465.

Hunt, G.S., 1975. Geology of the San Onofre area and parts of the Cristianitos Fault. In Studies on the Geology of Camp Pendleton and Western San Diego County, California, S. Ross and R.J. Dowlen (ed). San Diego, CA: San Diego Association of Geologists, 90 pp.

Hunt, I.A., 1959. Design of seawalls and breakwaters. J. Waterways and Harbors Div., ASCE, Vol. 85, No. WW3.

Inman, D.L., and P.M. Masters, 1991. Budget of sediment and prediction of the future state of the coast. In California Storm and Tidal Waves Study, State of the Coast Report, Chapter 9. U.S. Army Corps of Engineers, Los Angeles District, 111 pp.

Intergovernmental Panel on Climate Change (IPCC), 2013. Climate Change 2013: The Physical Science Basis, Contribution of Working Group I to the Fifth Assessment Report of the Intergovernmental Panel on Climate Change. Cambridge University Press, Cambridge, United Kingdom and New York, NY, 1535 pp.

Intergovernmental Panel on Climate Change (IPCC), 2014. Climate Change 2014: Synthesis Report, Contribution of Working Groups I, II and III to the Fifth Assessment Report of the Intergovernmental Panel on Climate Change. Geneva, Switzerland, 151 pp.

Intergovernmental Panel on Climate Change (IPCC), 2021. Climate Change 2021: The Physical Science Basis, Contribution of Working Group I to the Sixth Assessment Report of the Intergovernmental Panel on Climate Change. Cambridge University Press, 3949 pp.

Intergovernmental Panel on Climate Change (IPCC), 2022. AR6 Synthesis Report: Climate Change 2022, Sixth Assessment Report of the Intergovernmental Panel on Climate Change. Cambridge University Press, in press.

Kennedy, M.P., and S.S. Tan, 2007. Geologic map of the Oceanside 30'×60'quadrangle, California, California Department of Conservation, Division of Mines and Geology, scale 1:100,000, 1 plate.

Kikkawa, H., H. Shiigaki, and T. Kono, 1968. Fundamental study of wave over-topping on levees. Coastal Eng. Japan, 11, 107-115.

Kirk, R.M., P.D. Komar, J.C. Allen, and W.J. Stephenson, 2000. Shoreline erosion on 473 Lake Hawea, New Zealand, caused by high lake levels and storm-wave runup. J. Coastal Res., 16 (2): 346-356.

Koh, R.C.Y., N.H. Brooks, and E.J. List, 1974. Hydraulic Modeling of Thermal Outfall Diffusers for the San Onofre Nuclear Power Plant. Unpublished report, California Institute of Technology, Pasadena, CA. http://resolver.caltech.edu/CaltechKHR:KH-R-30

Kopp, R.E., R.M. Horton, C.M. Little, J.X. Mitrovica, M. Oppenheimer, D.J. Rasmussen, B.H. Strauss, and C. Tebaldi, 2014. Probabilistic 21st and 22nd century sea-level projections at a global network of tide-gauge sites. Earth's Future, 2, 383-406.

Kuhn, G.G., and F.P. Shepard, 1984. Seacliffs, Beaches, and Coastal Valleys of San Diego County. Berkeley, California: University of California Press.

NOAA's Ocean Service (NOS), Office for Coastal Management (OCM), 2013. 2013 NOAA Coastal California TopoBathy Merge Project. https://coast.noaa.gov

Mastrandrea, M.D., C.B. Field, T.F. Stocker, O. Edenhofer, K.L. Ebi, D.J. Frame, H. Held, E. Kriegler, K.J. Mach, P.R. Matschoss, G.-K. Plattner, G.W. Yohe, and F.W. Zwiers, 2010. Guidance Note for Lead Authors of the IPCC Fifth Assessment Report on Consistent Treatment of Uncertainties. Intergovernmental Panel on Climate Change (IPCC), 6 pp. http://www.ipcc.ch.

National Research Council (NRC), 2012. Sea-Level Rise for the Coasts of California, Oregon, and Washington: Past, Present, and Future. National Academy Press, Washington, D.C., 201 pp.

Ocean Protection Council (OPC), 2018. State of California Sea Level Rise Guidance, 2018 Update (California Natural Resources Agency Ocean Protection Council), 84 pp.

Ocean Protection Council (OPC), 2020. Strategic Plan to Protect California's Coast and Ocean 2020–2025. California Natural Resources Agency Ocean Protection Council, 64 pp. https://www.opc.ca.gov/webmaster/ftp/pdf/2020-2025-strategic-plan/OPC-2020-2025-Strategic-Plan-FINAL-20200228.pdf.

Owen, M.W., 1980. Design of Seawalls Allowing for Wave Overtopping. Report EX924, Hydraulics Research Station, Wallingford, U.K.

Pawka, S.S, 1983. Island shadows in wave directional spectra. Jour. Geophys. Res., 88(C4), 2579 2591.

Pilkey, O.H., and J.A.G. Cooper, 2004. Society and sea level rise. Science, 303 (5665), 1781-1782.

Raubenheimer, B., R.T. Guza, S. Elgar, and N. Kobayashi, 1995. Swash on a gently sloping beach. J. Geophys. Res., 100, 8751-8760.

Raubenheimer, B., and R.T. Guza, 1996. Observations and predictions of run-up. J. Geophys. Res. 101 (C10), 25575-25587.

Reis, M.T., K. Hu, T.S. Hedges, and H. Mase, 2008. A comparison of empirical, empirical, and numerical wave overtopping models. J. Coastal Res., 24(2A), 250-262.

Ruggiero, P., P.D. Komar, J.J. Marra, W.G. McDougal, and R.A. Beach, 2001. Wave runup, extreme water levels, and the erosion of properties backing beaches. J. Coastal Res., 17, 407-419.

Ruggiero, P., R.A. Holman, and R.A. Beach, 2004. Wave run-up on a high-energy dissipative beach. J. Geophys. Res., 109, no. C6, 12 pp.

Runyan, K., and G.B. Griggs, 2003. The effects of armoring seacliffs on the natural sand supply to the beaches of California. J. Coast. Res. 19 (2), 336-347.

Shepard, F.P., 1950. Beach cycles in southern California. U.S. Army Corps of Engineers, Beach Erosion Board, Tech. Memo. No. 20, 26 pp.

Shih, S.M., P.D. Komar, K.J. Tillotson, W.G. McDougal, and P. Ruggiero, 1994. Wave 517 run up and sea-cliff erosion. In Coastal Engineering 1994 Proceedings, 24th International 518 Conference, American Society of Civil Engineers, 2170-2184.

Stockdon, H. F., Holman, R. A., Howd, P. A., and Sallenger, A. H., 2006. Empirical parameterization of setup, swash, and runup. Coastal Engineering, 53, 573-588.

Tan, S.S., 2001. Geologic map of the San Onofre Bluff 7.5'quadrangle, San Diego County, California: A digital database, version 1.0. California Department of Conservation, Division of Mines and Geology, scale 1:24000, 1 plate.

Thornton, E. B. and Guza, R. T., 1982. Energy Saturation and Phase Speeds Measured on a Natural Beach. Journal of Geophysical Research, 87(C12), 9499-9508.

Thornton, E. B. and Guza, R. T., 1983. Transformation of Wave Height Distribution. Journal of Geophysical Research, 88 (C10), 5925-5938.

United States Army Corps of Engineers (USACOE), 1984. Shore Protection Manual. Waterways Experiment Station, Coastal Engineering Research Center, Vicksburg, MS, 2 vols.

United States Army Corps of Engineers (USACOE), 1988. Historic Wave and Sea Level Data Report: San Diego Region. Coast of California Storm and Tidal Wave Study, Reference No. 88-6.

United States Army Corps of Engineers (USACOE), 1994a. Hydraulic Design of Flood Control Channels. Department of the Army. CECW-EH-D, Engineer Manual 1110-2-1601.

United States Army Corps of Engineers (USACOE), 1994b. Shore Protection Manual, Volume II. Department of the Army. Coastal Engineering Research Center.

United States Army Corps of Engineers (USACOE), 1990. Sediment Budget Report, Oceanside Littoral Cell, Coast of California Storm and Tidal Wave Study. Reference No. 90-2.

University of Southern California (USC) Sea Grant Program, 2013. Sea Level Rise Vulnerability Study for the City of Los Angeles. Report prepared for the Mayor of Los Angeles, 85 pp.

Van der Meer, J.W. and J.P.F.M. Janssen, 1995. Wave runup and wave overtopping at dikes. In Wave Forces on Inclined and Vertical Wall Structures. Ed. N. Kobayashi and Z. Demirbilek, ASCE, Ch. 1, pp. 1-27.

Wolinsky, M.A., and A.B. Murray, 2009. A unifying framework for shoreline migration: Application to wave-dominated coasts. J. Geophys. Res., 114 (F1), F01009.

Woodroffe, C.D., and C.V. Murray-Wallace, 2012. Sea level rise and coastal change: The past as a guide to the future. Quaternary Science Reviews, 54, 4-11.

Yates, M.L., R.T. Guza, and W.C. O'Reilly, 2009. Equilibrium shoreline response: Observations and modeling. J. Geophys. Res. C, 114, C0910.

Yates, M.L., R.T. Guza, W.C. O'Reilly, J.E. Hansen, and P.L. Barnard, 2011. Equilibrium shoreline response of a high wave energy beach. J. Geophys. Res., 116, C04014, 13 pp.

Young, A.P., and S.A. Ashford, 2006. Application of airborne LiDAR for seacliff volumetric change and beach sediment budget contributions. J. Coast. Res., 22, 307-318.

Young, A.P., J.H. Raymond, J. Sorenson, E.A. Johnstone, N.W. Driscoll, R.E. Flick, and R.T. Guza, 2010a. Coarse sediment yields from seacliff erosion in the Oceanside Littoral Cell. J. Coast. Res., 26, 580-585.

Young, A.P., M.J. Olsen, N. Driscoll, R.E. Flick, R. Gutierrez, R.T. Guza, E. Johnstone, and F. Kuester, 2010b. Comparison of airborne and terrestrial LiDAR estimates of seacliff erosion in southern California. Photogrammetric Engineering and Remote Sensing 76, 421-427.

Young, A.P., R.E. Flick, W.C. O'Reilly, D.B. Chadwick, R.T. Guza, W.C. Crampton, and J.J. Helly, 2014. Estimating cliff retreat in southern California considering sea level rise using a sand balance approach. Mar. Geology, 348, 15-2.

Young, A.P., R. E. Flick, T.W. Gallien, S. N. Giddings, R.T. Guza, M. Harvey, L. Lenain, B.C. Ludka, W. K. Melville, and W. C. O'Reilly, 2018. Southern California coastal response to the 2015-2016 El Niño, J. Geophys. Res: Earth Surface, 123.

Zhang, K., Douglas, B.C., and S.P. Leatherman, 2004. Global warming and coastal erosion. Climatic Change, 64 (1), 41-58.

APPENDIX A

MODELED BEACH AND CLIFF PROFILE CHANGES BY 2050 DUE TO MSLR

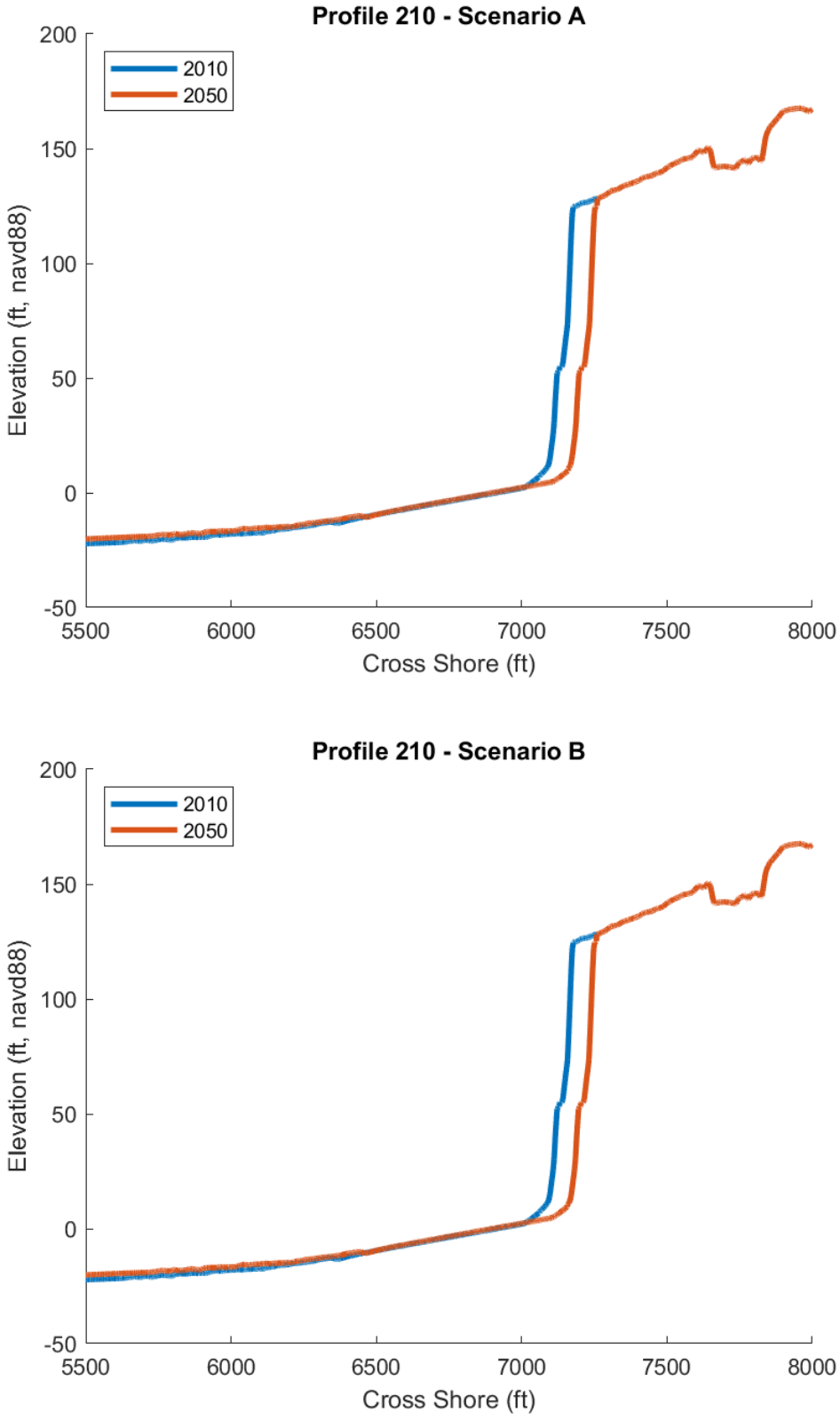


Figure A-1. Observed 2010 and modeled 2050 Profile 210.

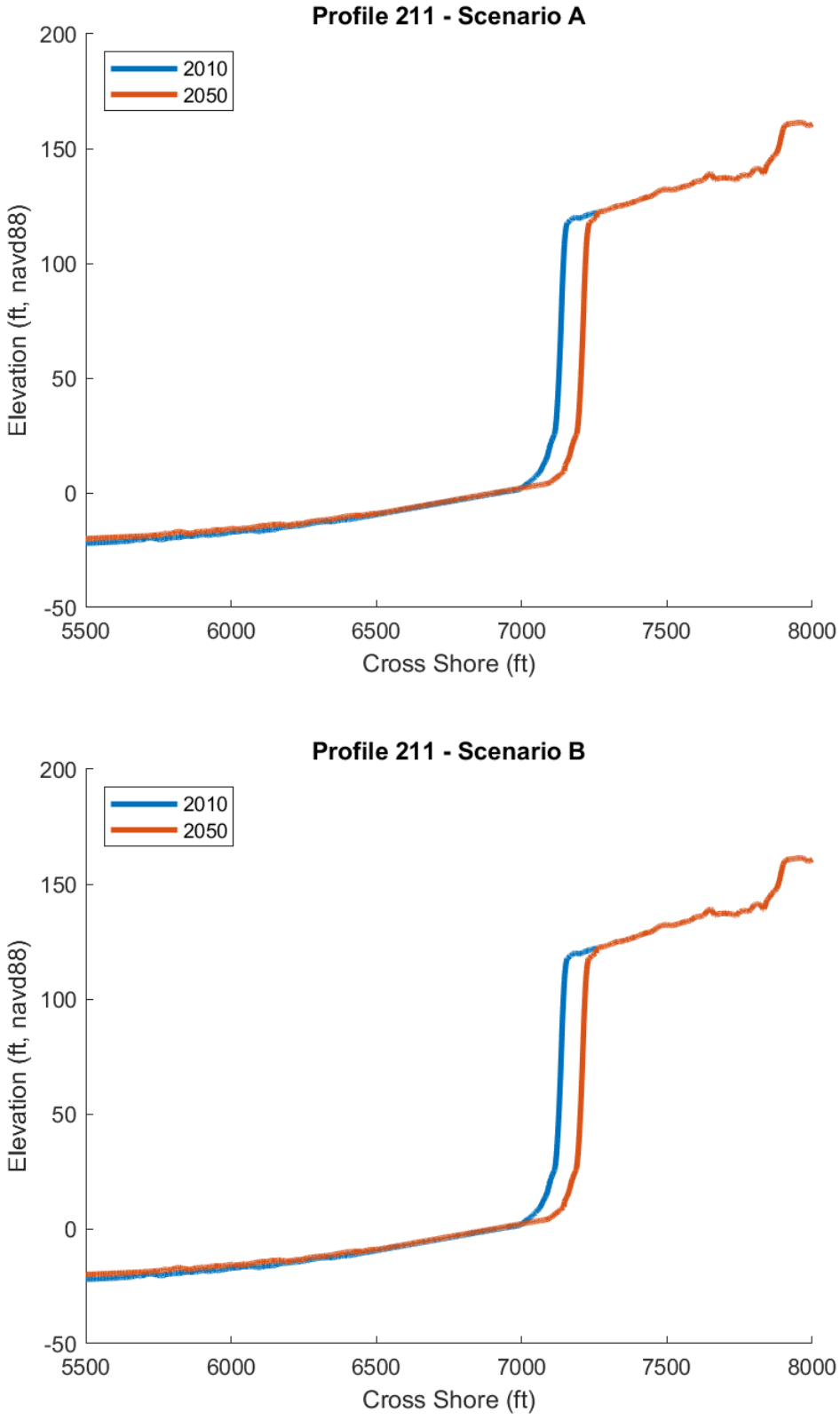


Figure A-2. Observed 2010 and modeled 2050 Profile 211.

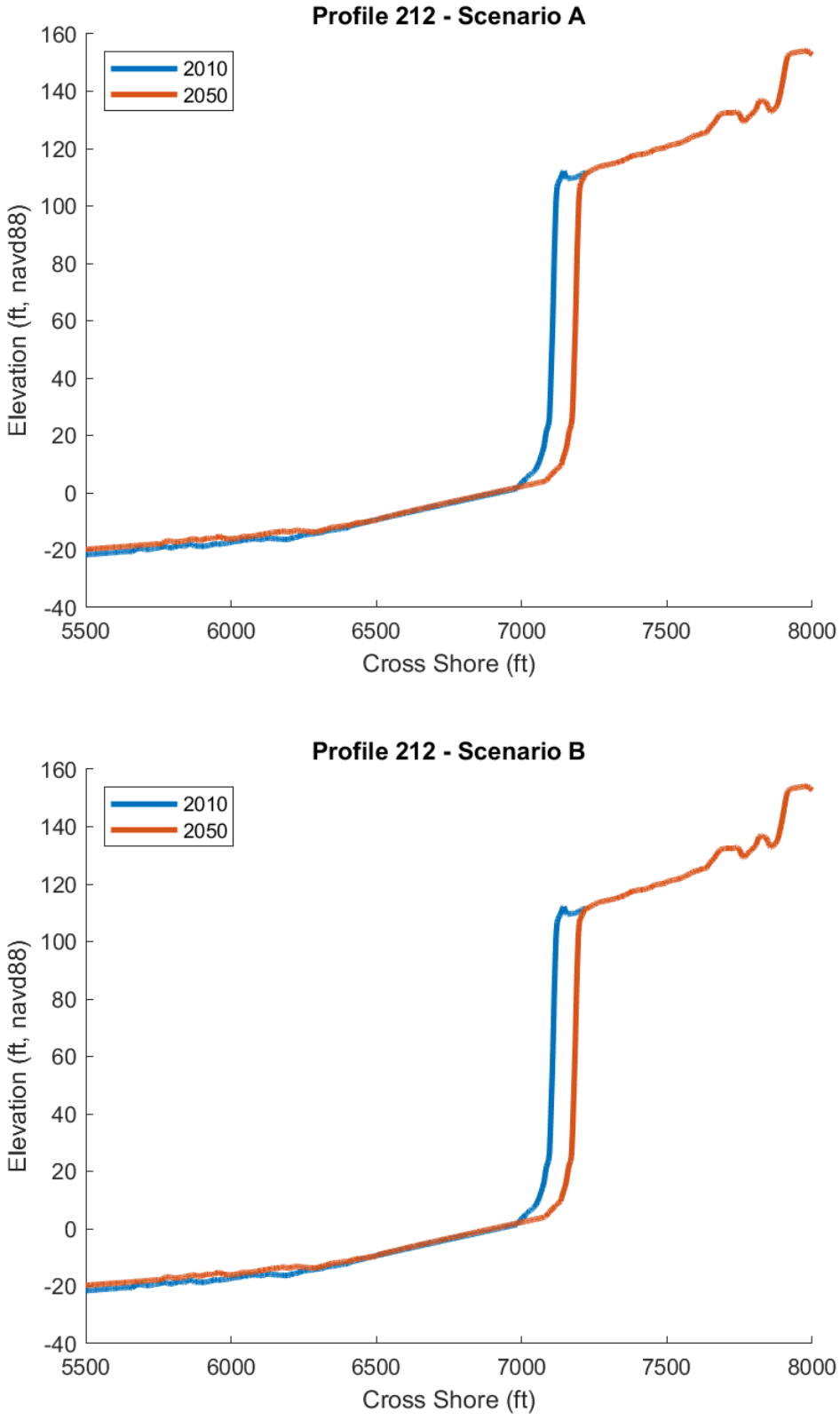


Figure A-3. Observed 2010 and modeled 2050 Profile 212.

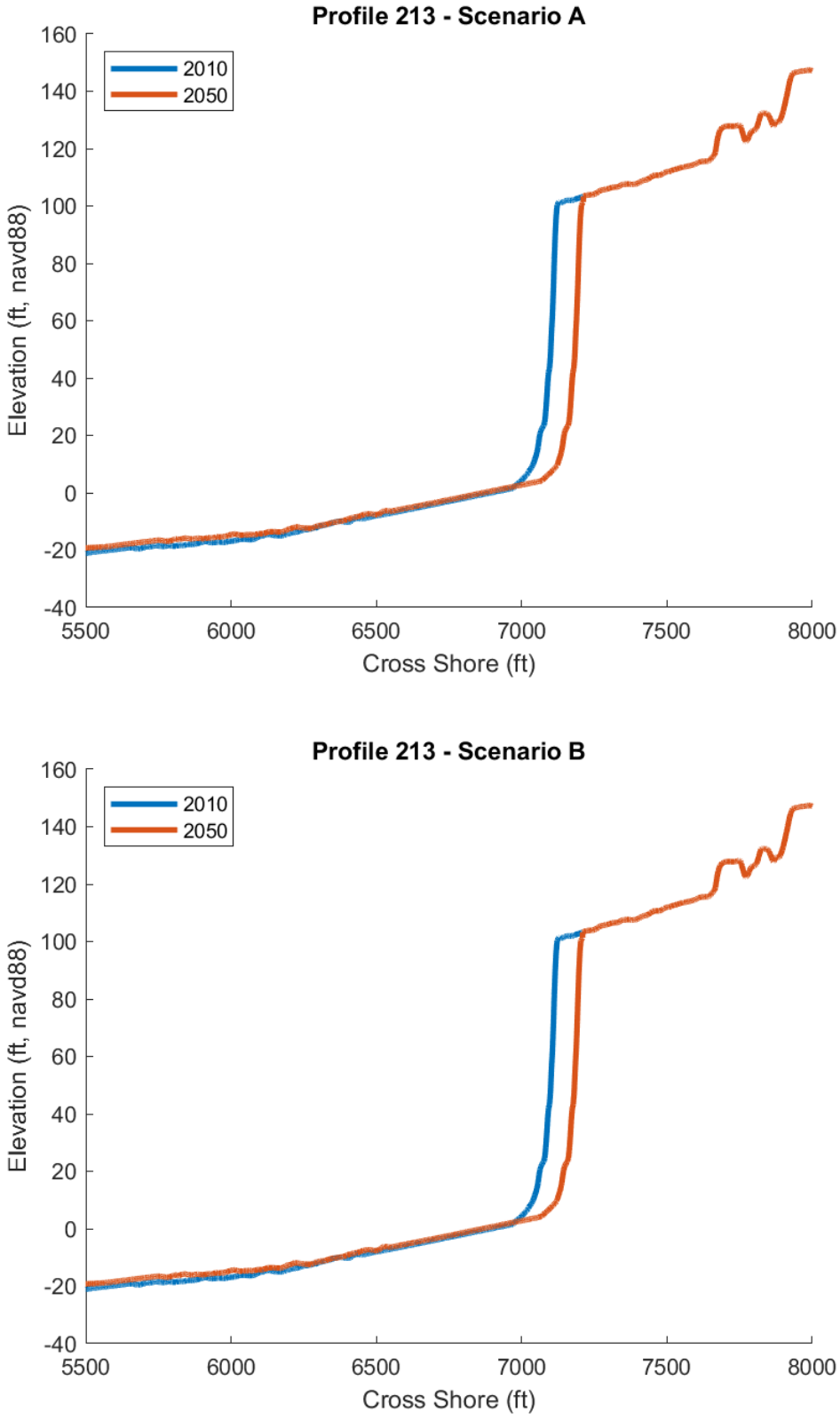


Figure A-4. Observed 2010 and modeled 2050 Profile 213.

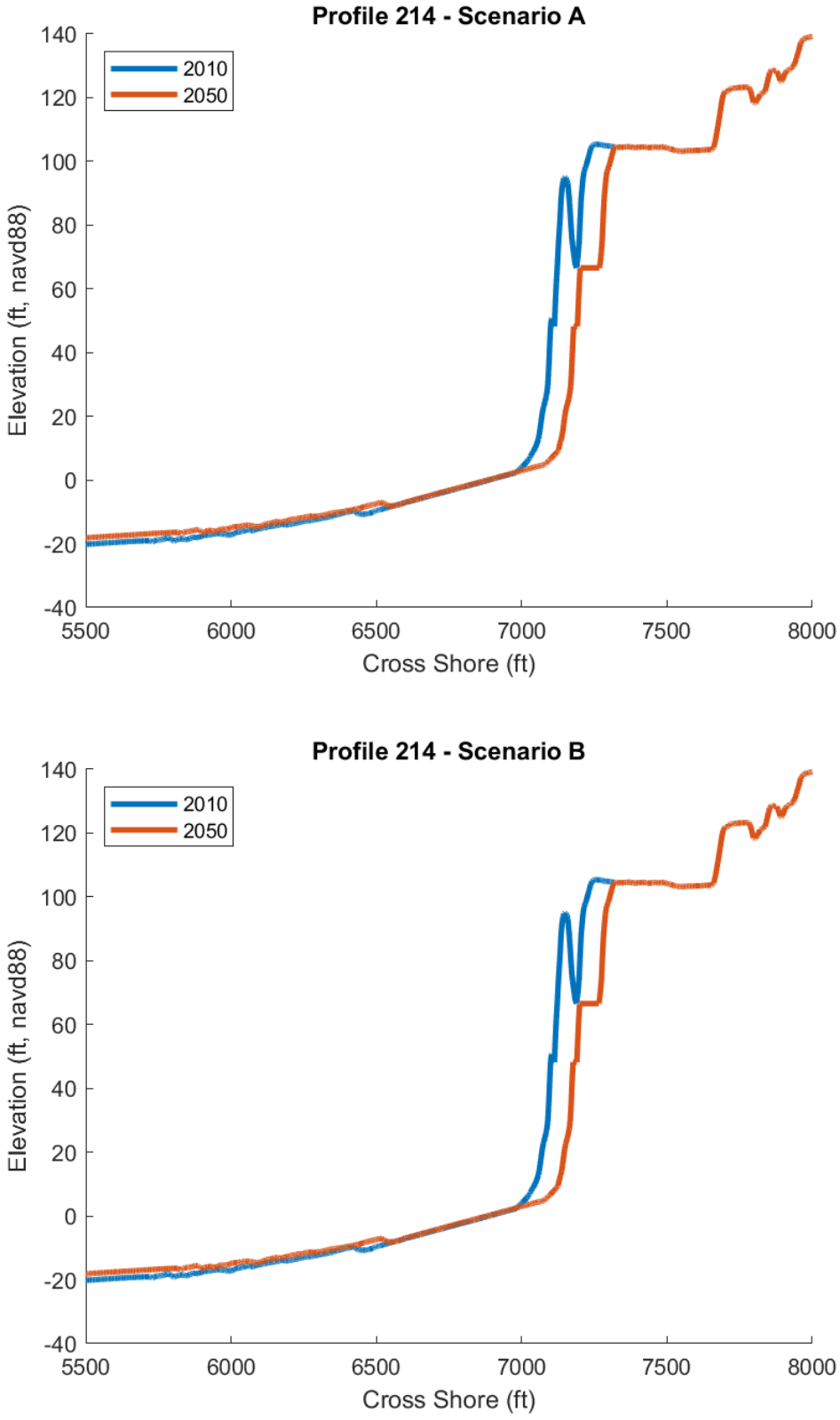


Figure A-5. Observed 2010 and modeled 2050 Profile 214.

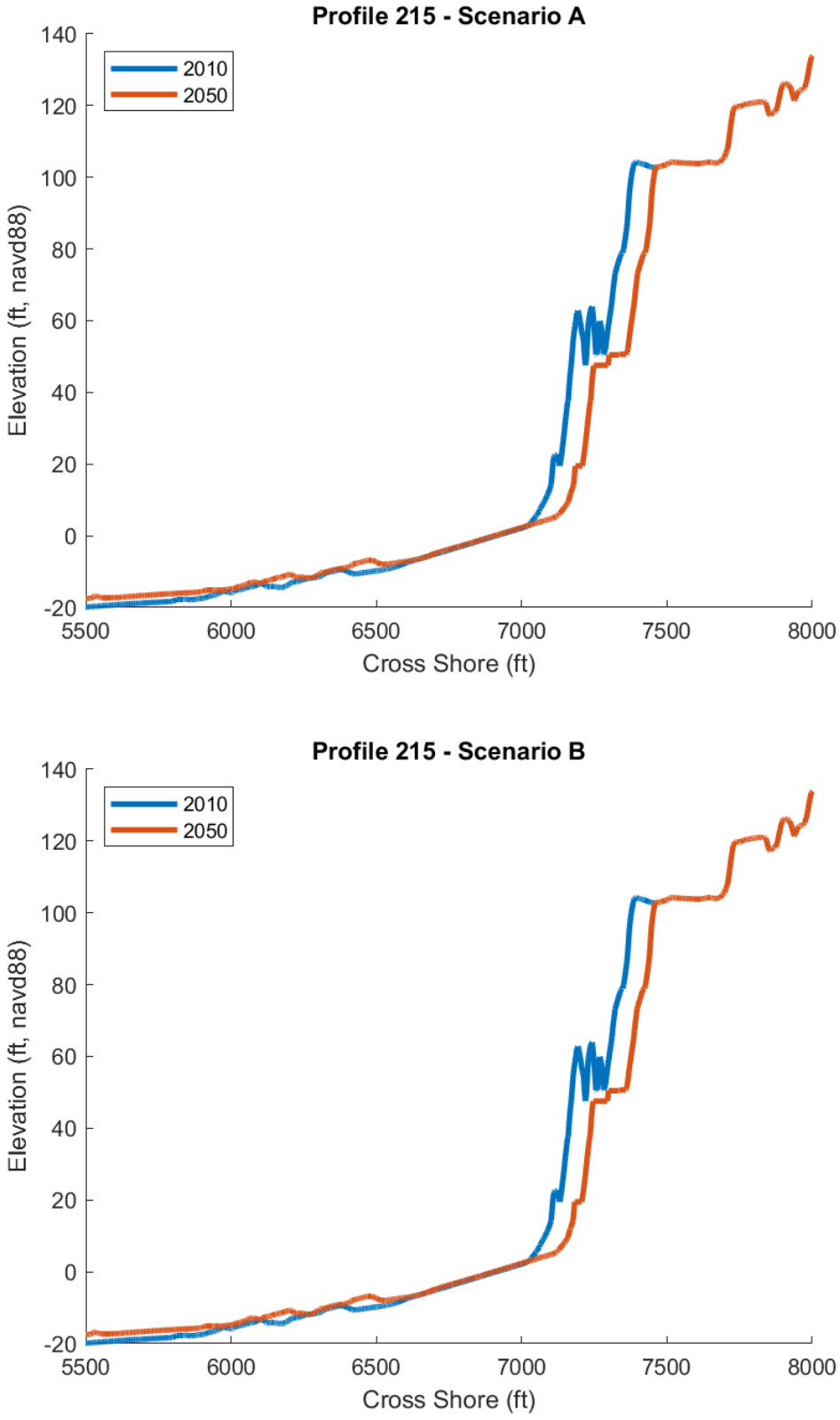


Figure A-6. Observed 2010 and modeled 2050 Profile 215.

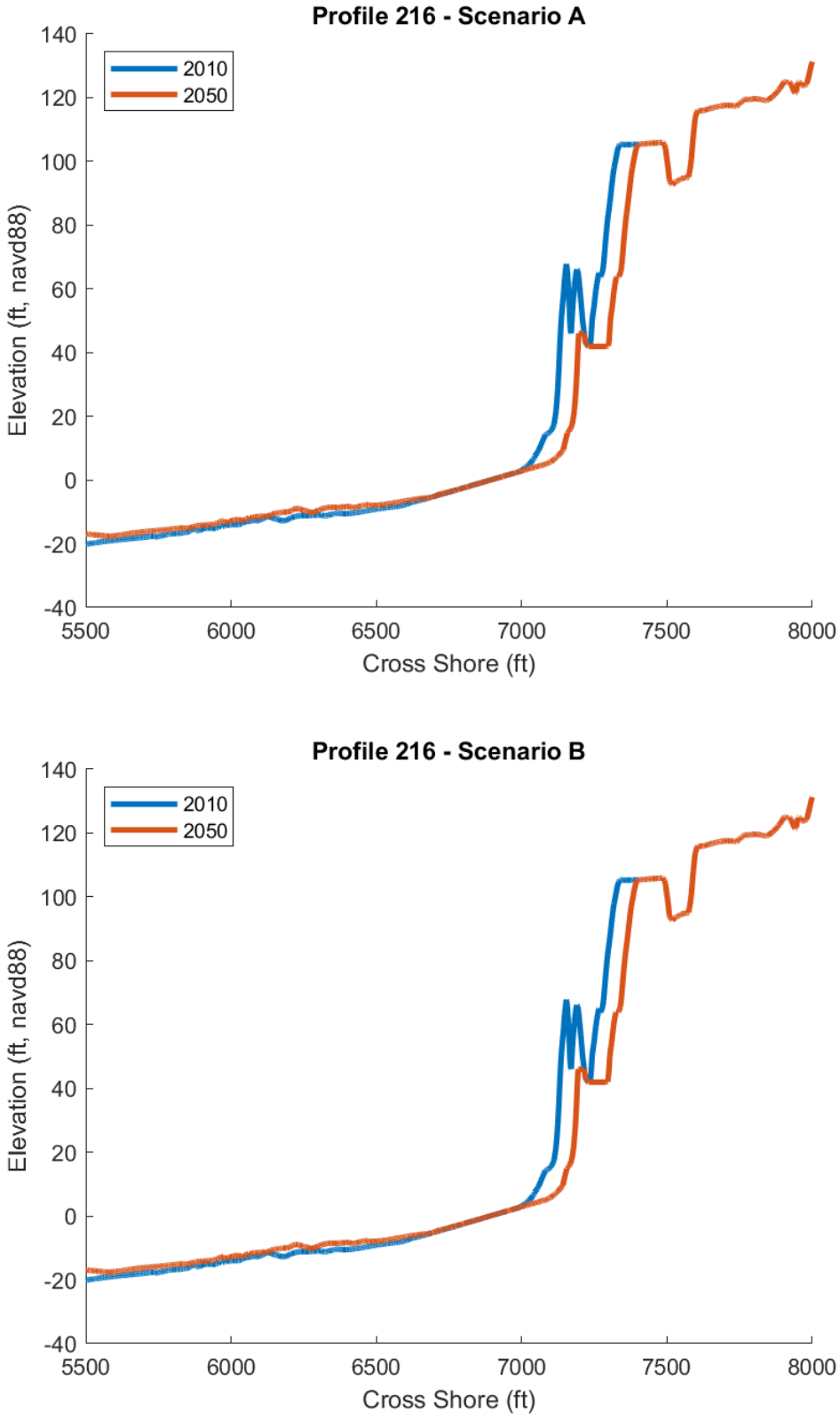


Figure A-7. Observed 2010 and modeled 2050 Profile 216.

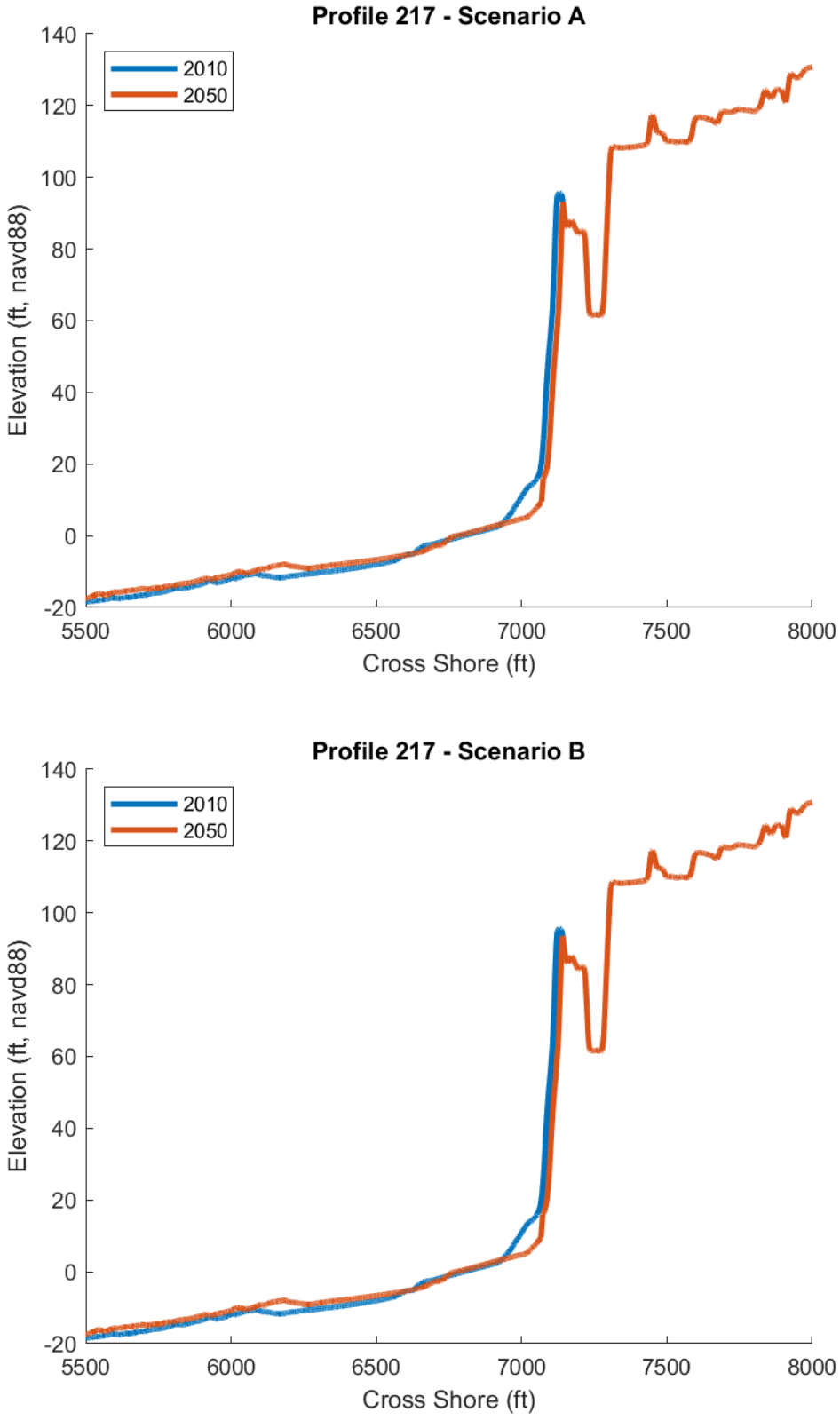


Figure A-8. Observed 2010 and modeled 2050 Profile 217.

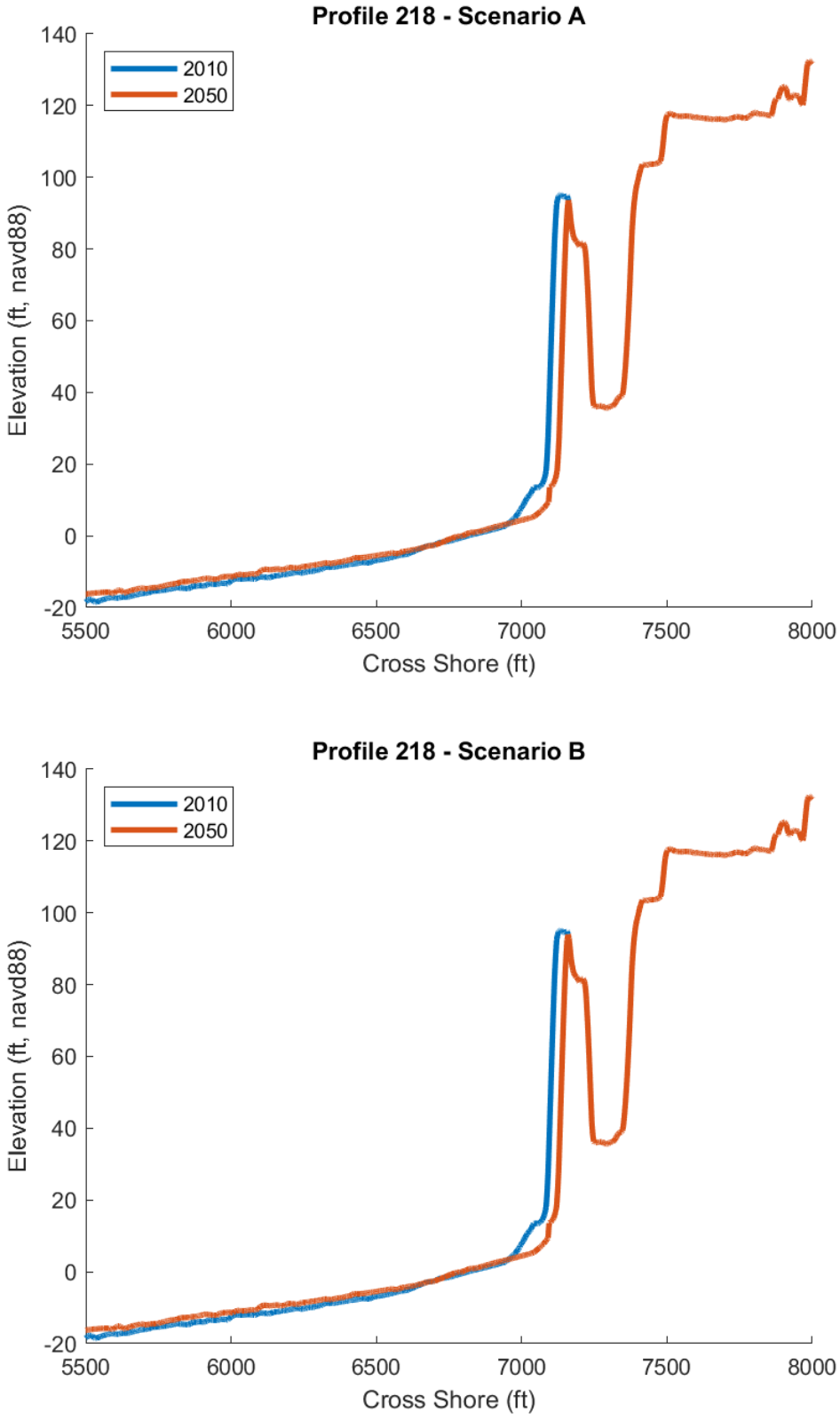


Figure A-9. Observed 2010 and modeled 2050 Profile 218.

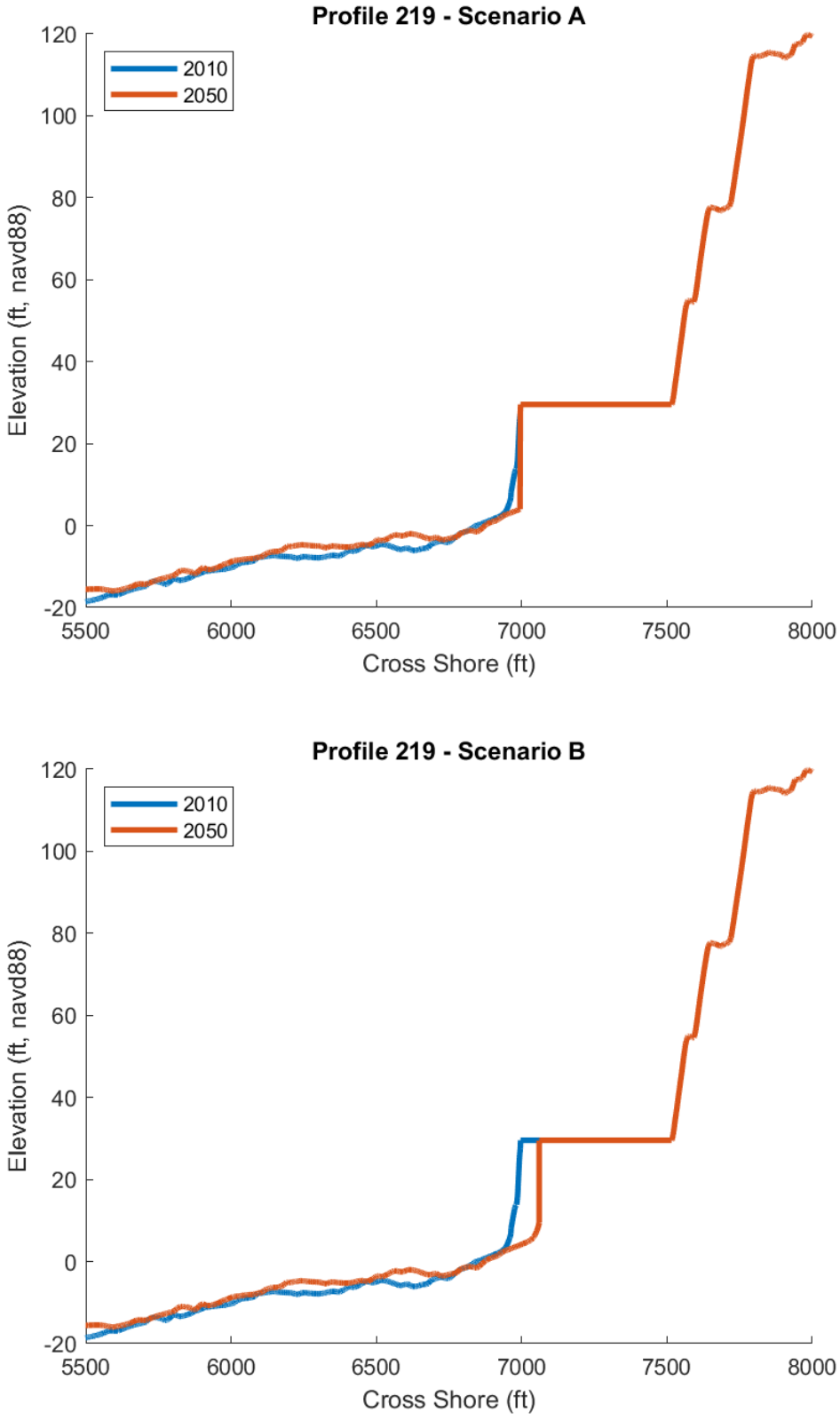


Figure A-10. Observed 2010 and modeled 2050 Profile 219.

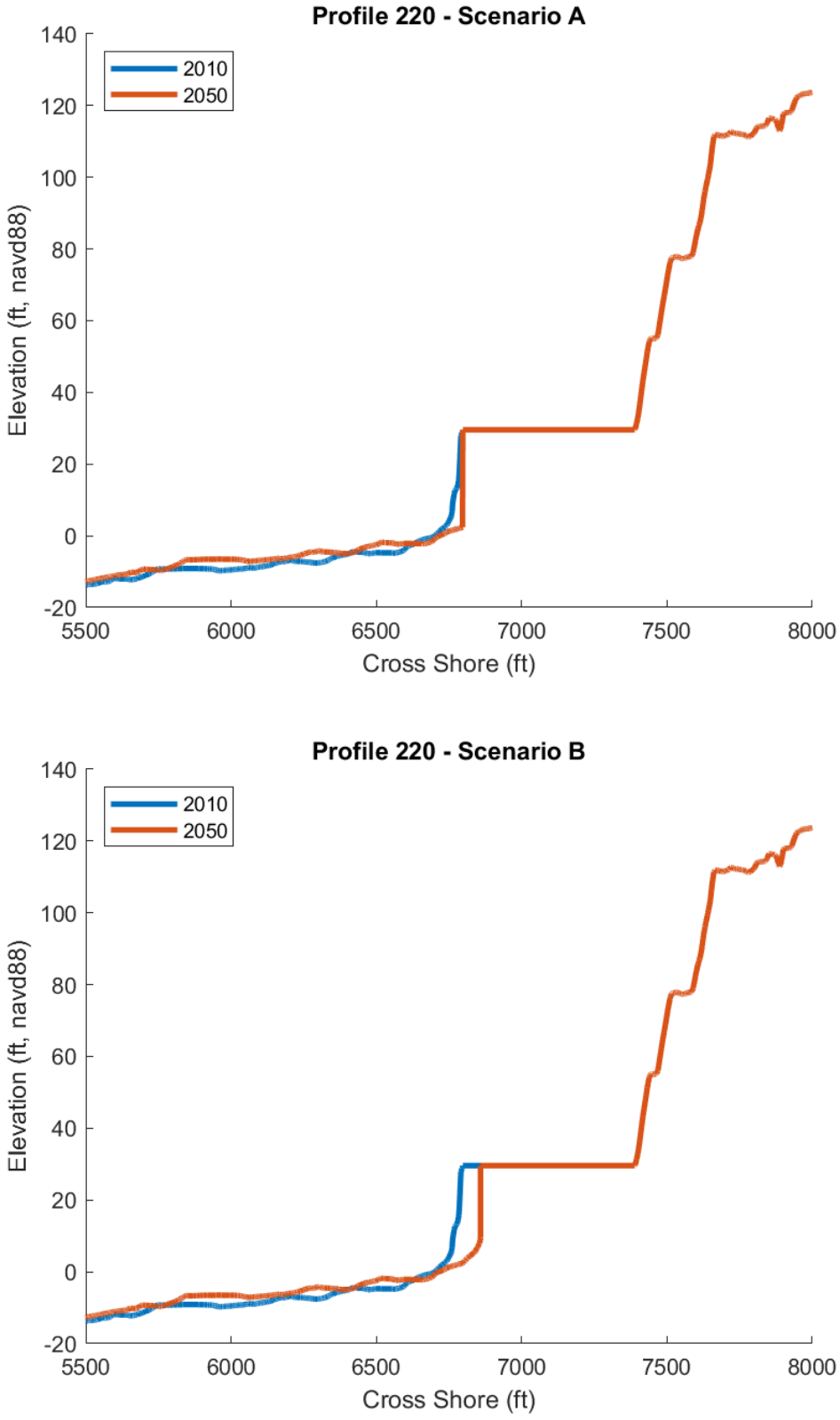


Figure A-11. Observed 2010 and modeled 2050 Profile 220.

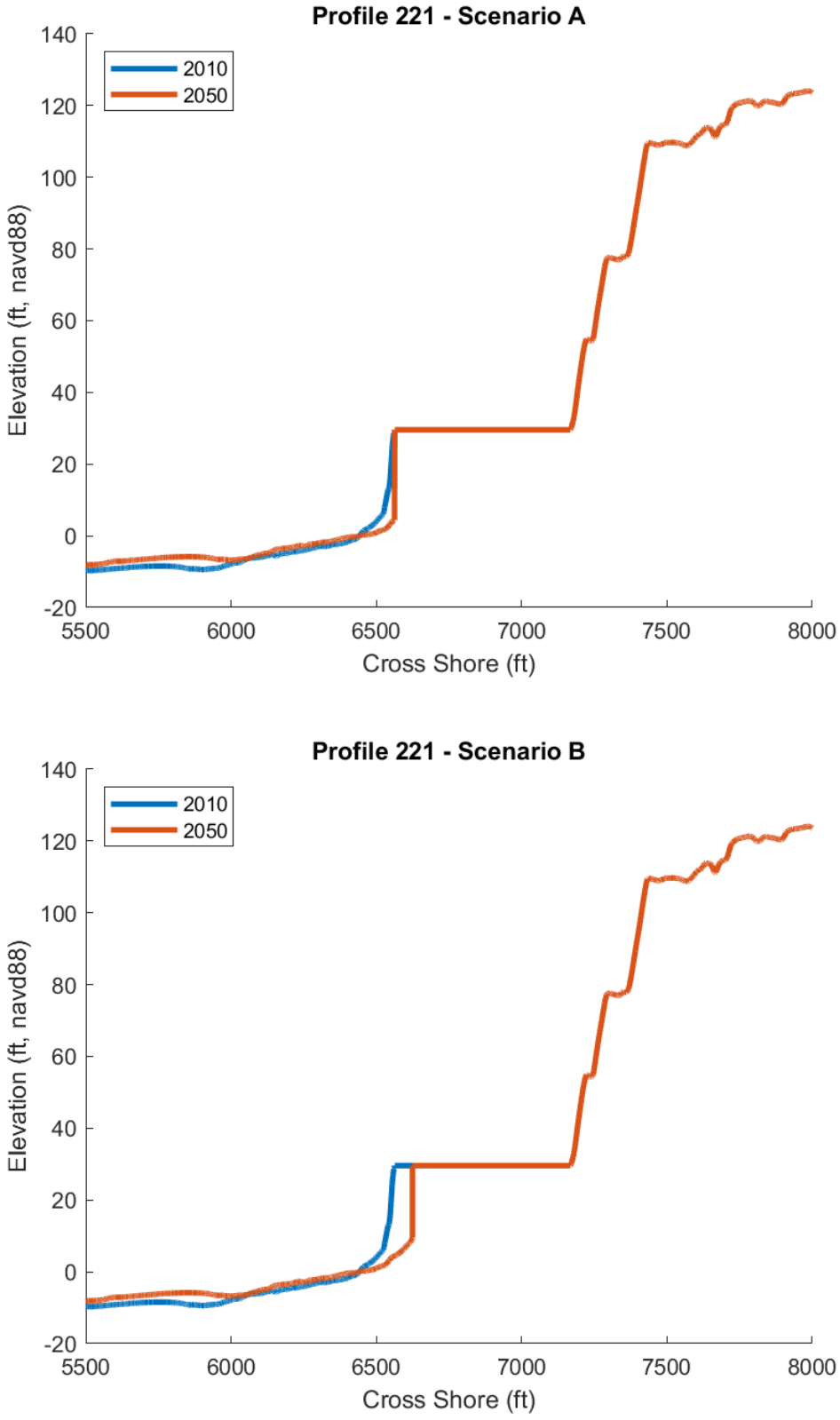


Figure A-12. Observed 2010 and modeled 2050 Profile 221.

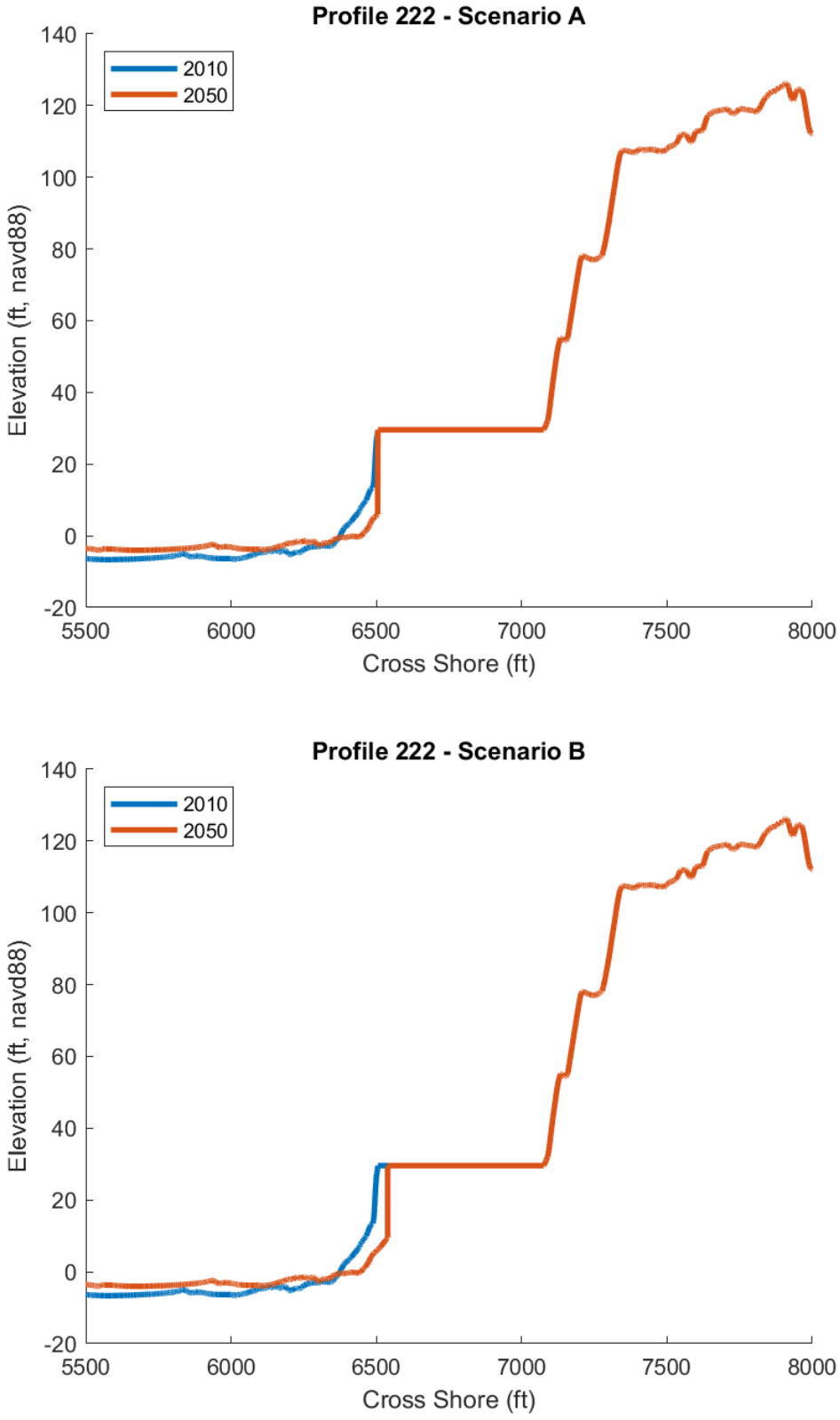


Figure A-13. Observed 2010 and modeled 2050 Profile 222.

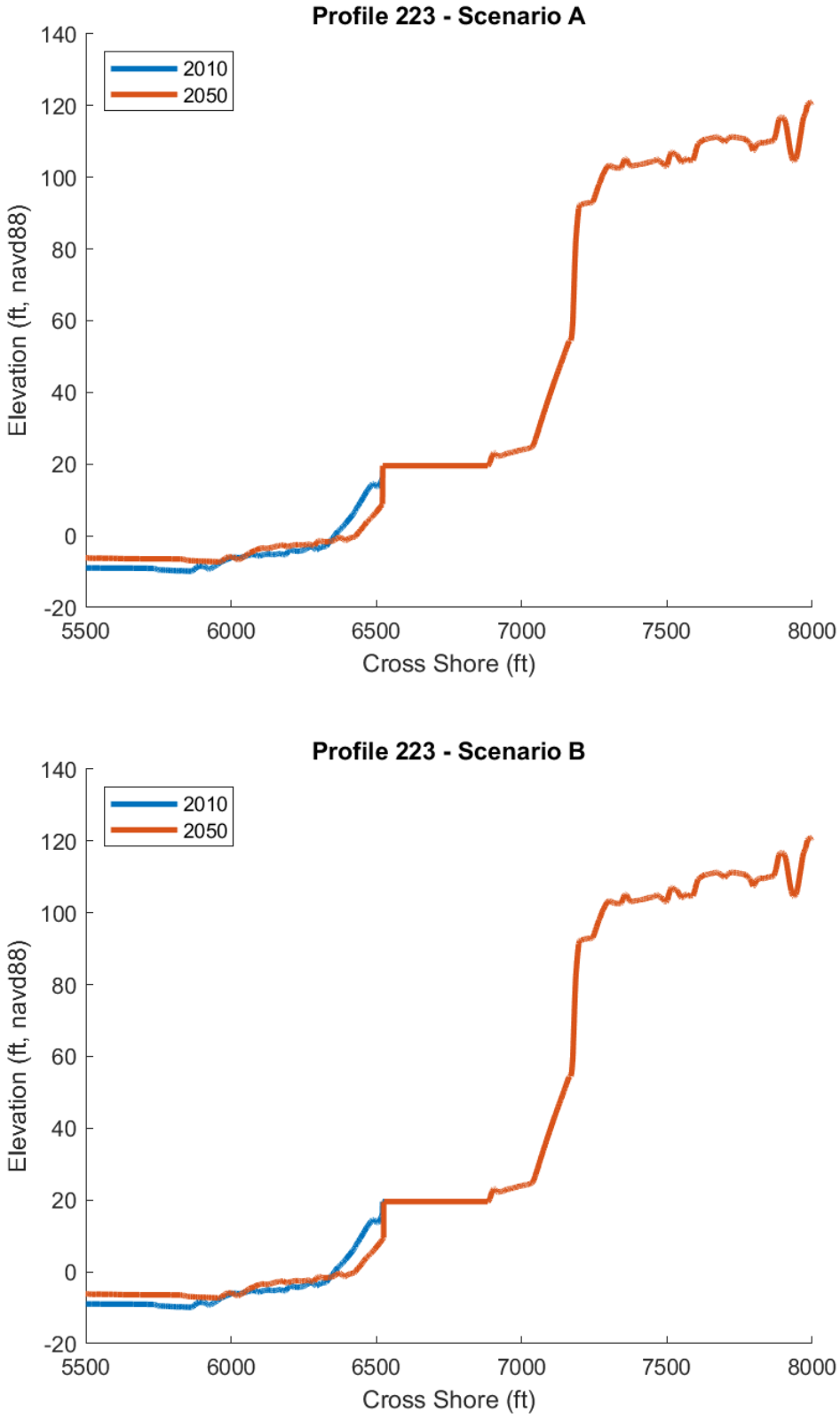


Figure A-14. Observed 2010 and modeled 2050 Profile 223.

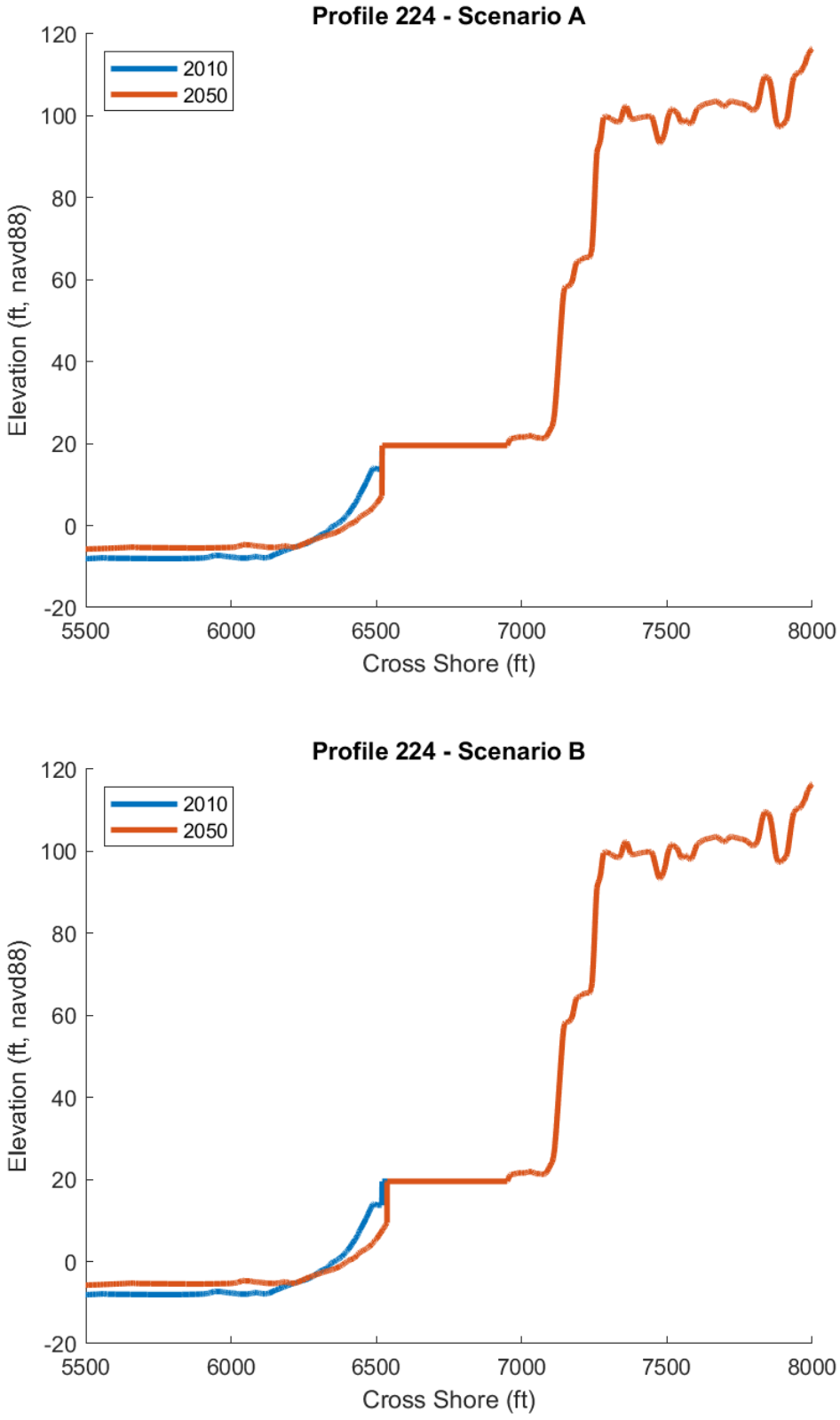


Figure A-15. Observed 2010 and modeled 2050 Profile 224.

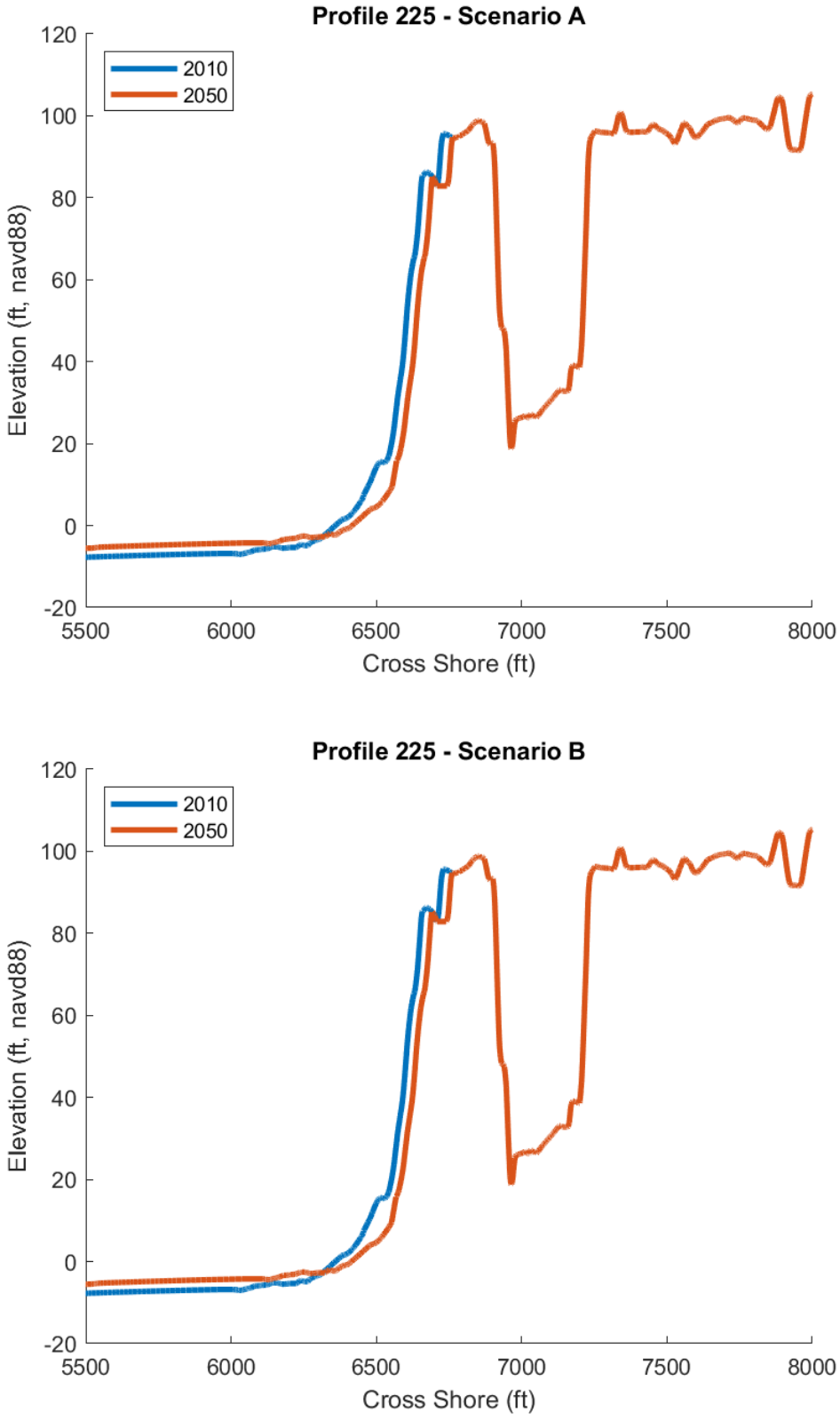


Figure A-16. Observed 2010 and modeled 2050 Profile 225.

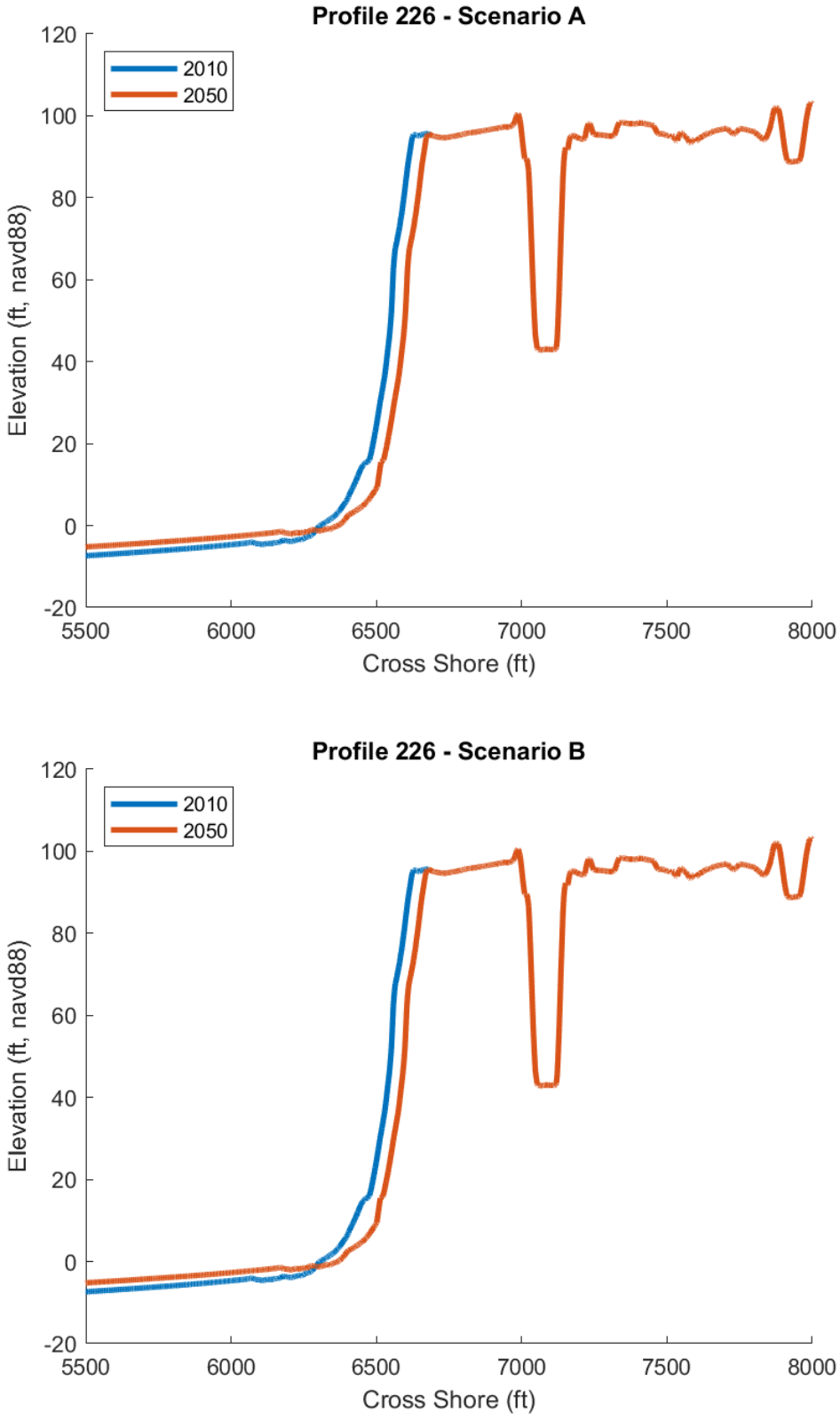


Figure A-17. Observed 2010 and modeled 2050 Profile 226.

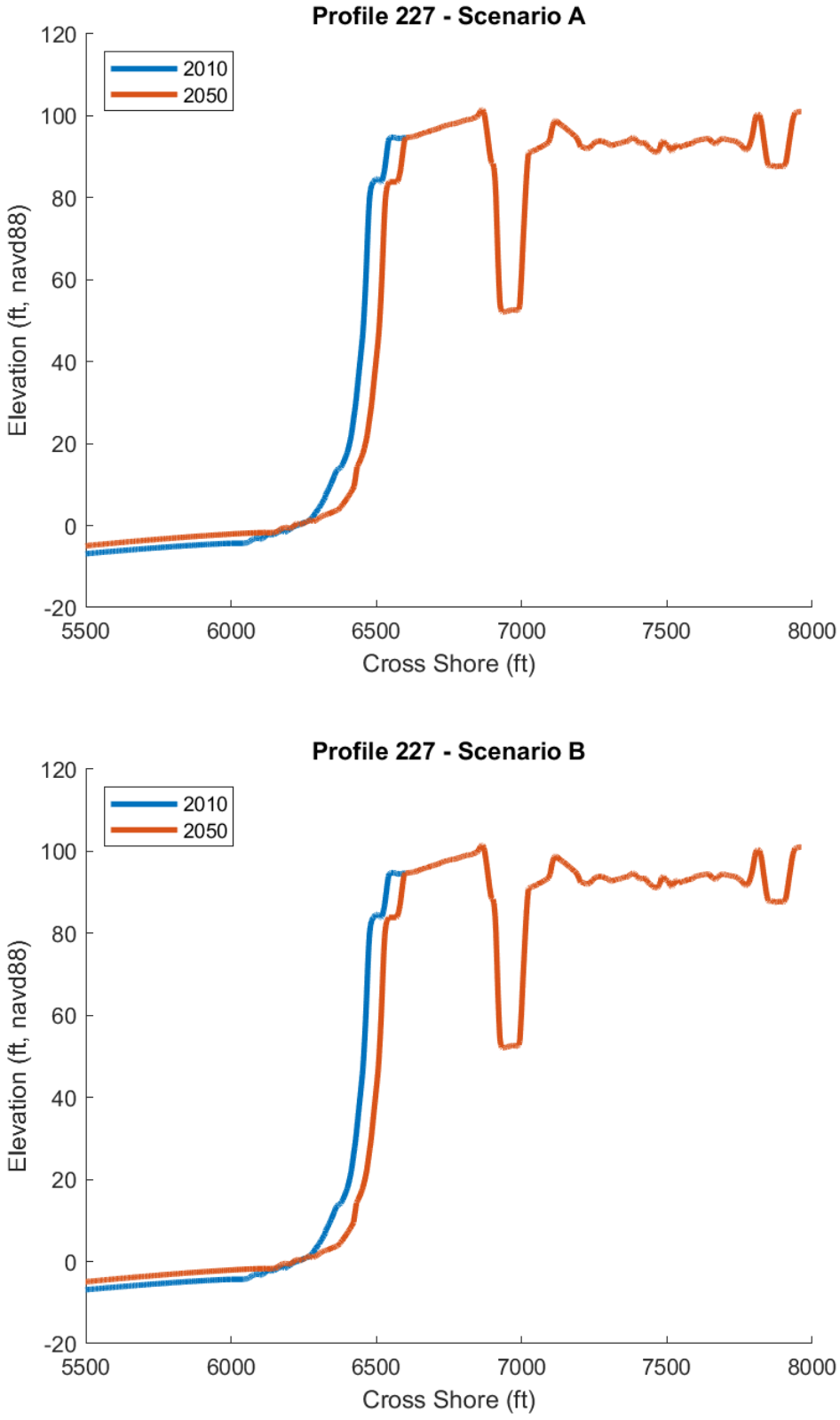


Figure A-18. Observed 2010 and modeled 2050 Profile 227.

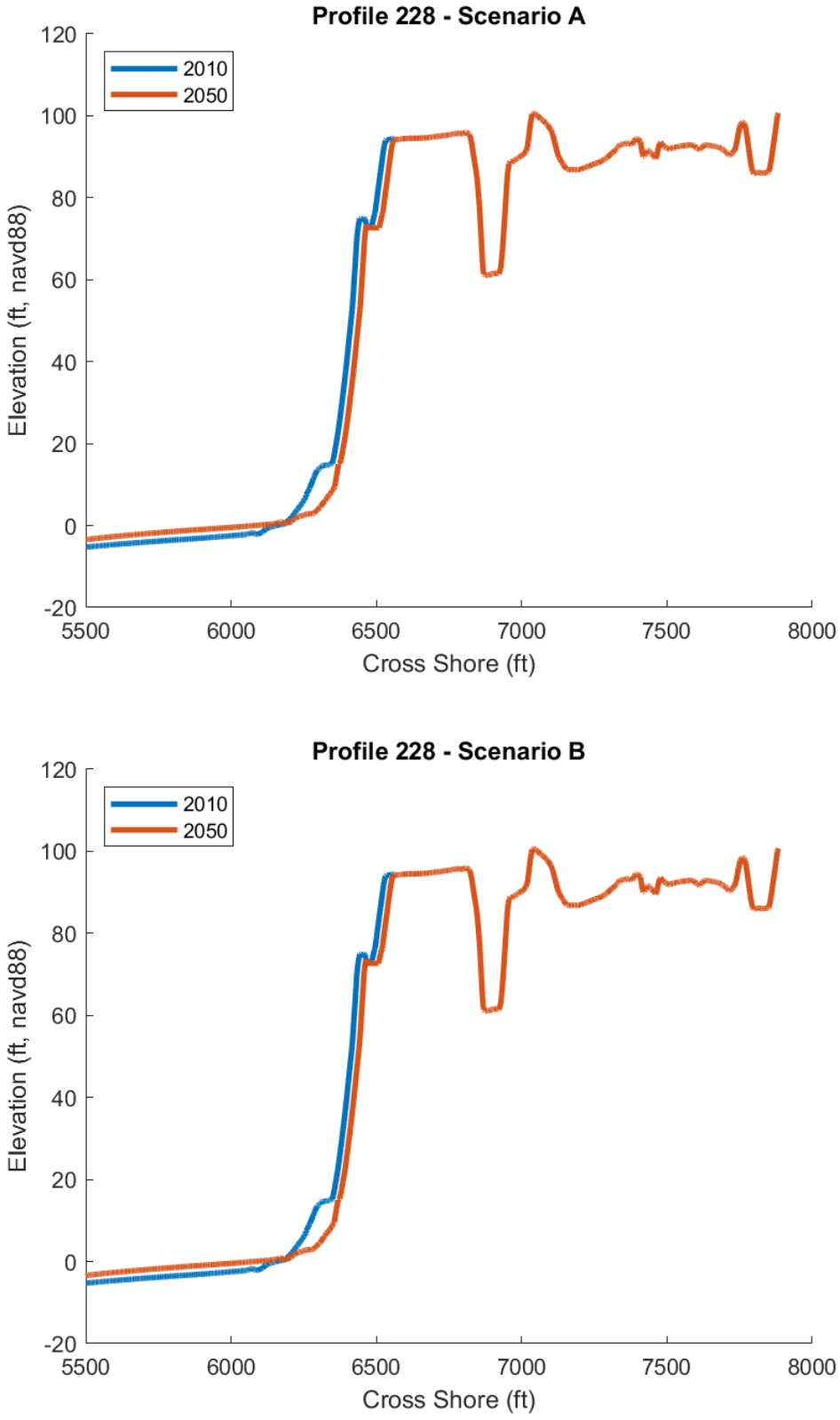


Figure A-19. Observed 2010 and modeled 2050 Profile 228.

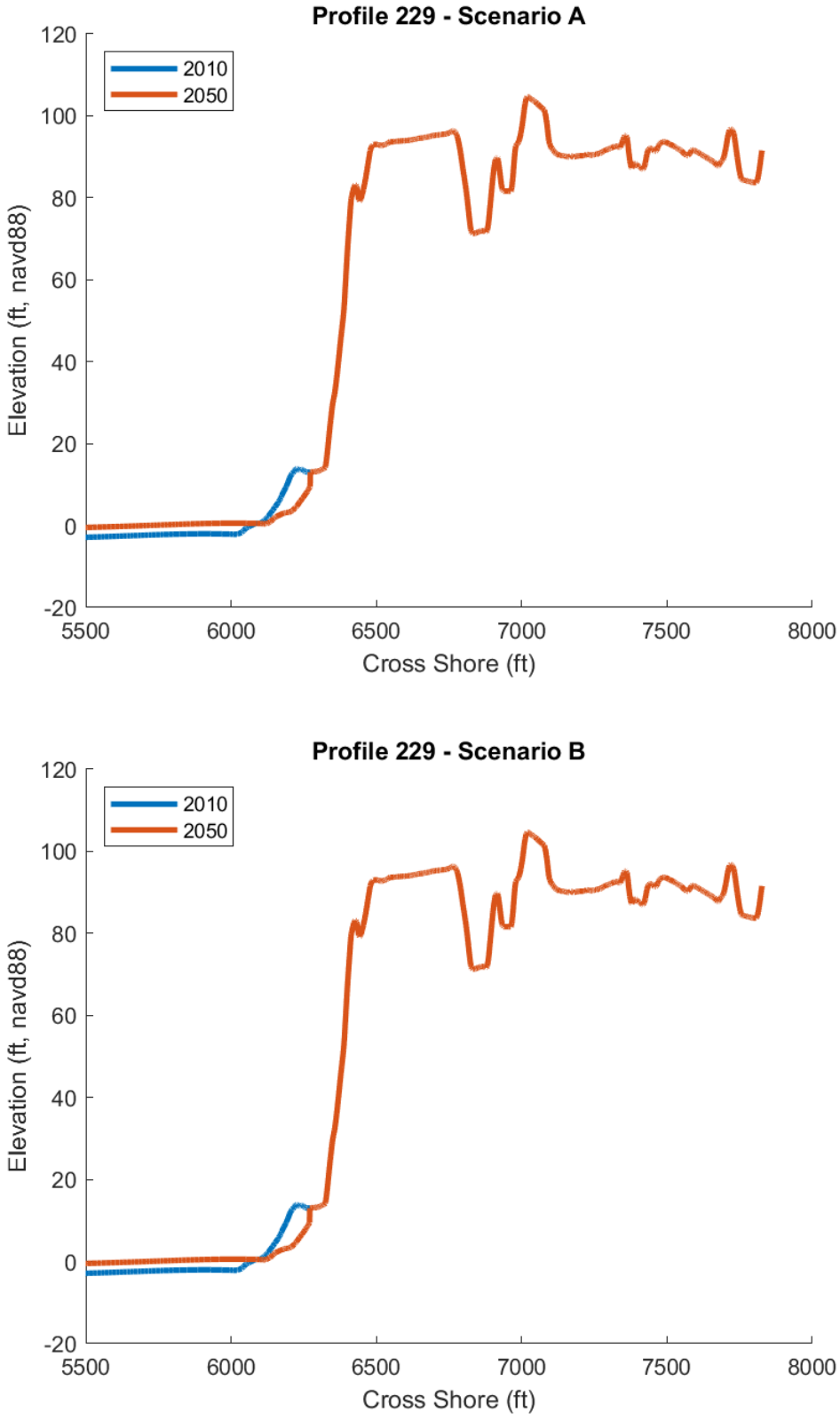


Figure A-20. Observed 2010 and modeled 2050 Profile 229.

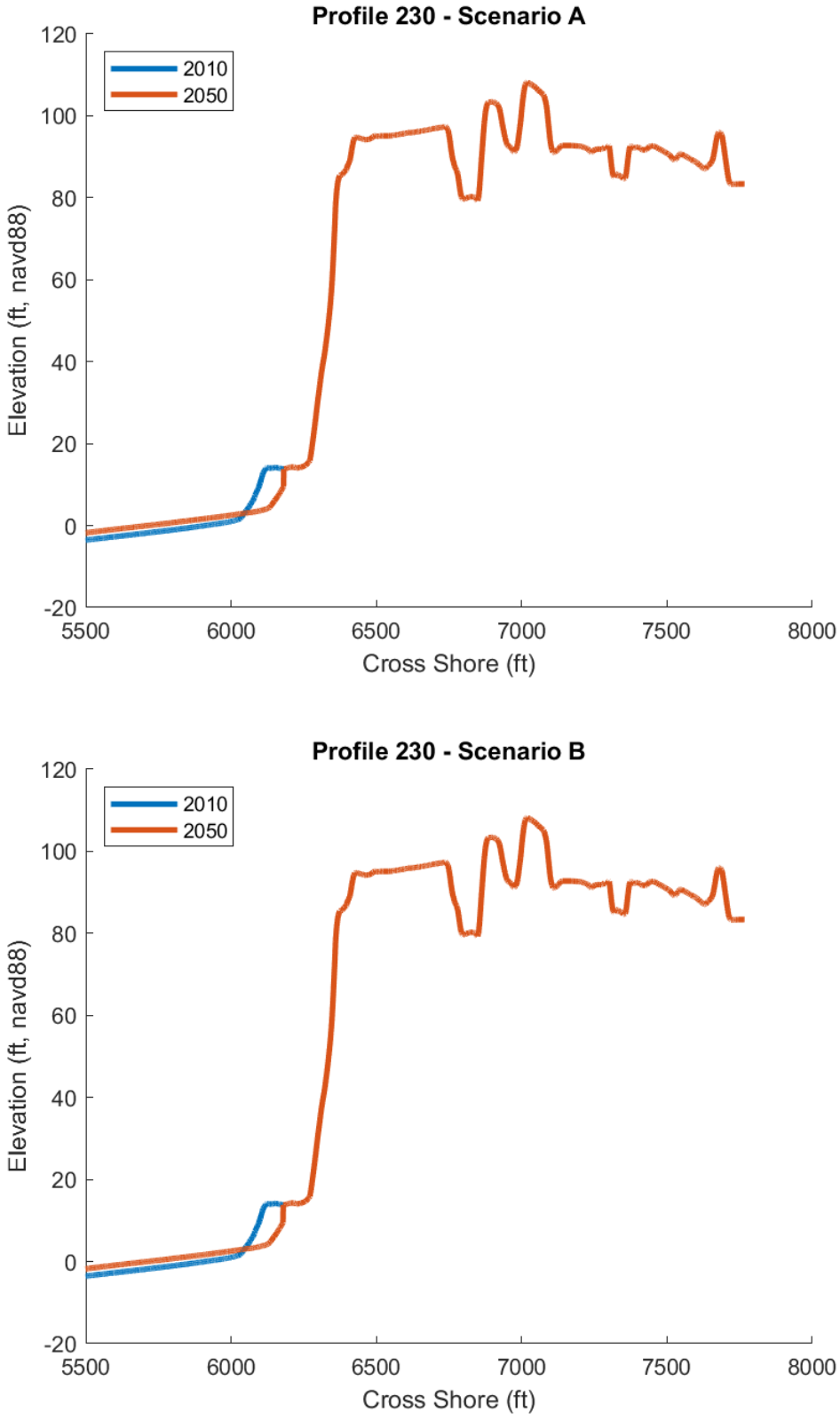


Figure A-21. Observed 2010 and modeled 2050 Profile 230.

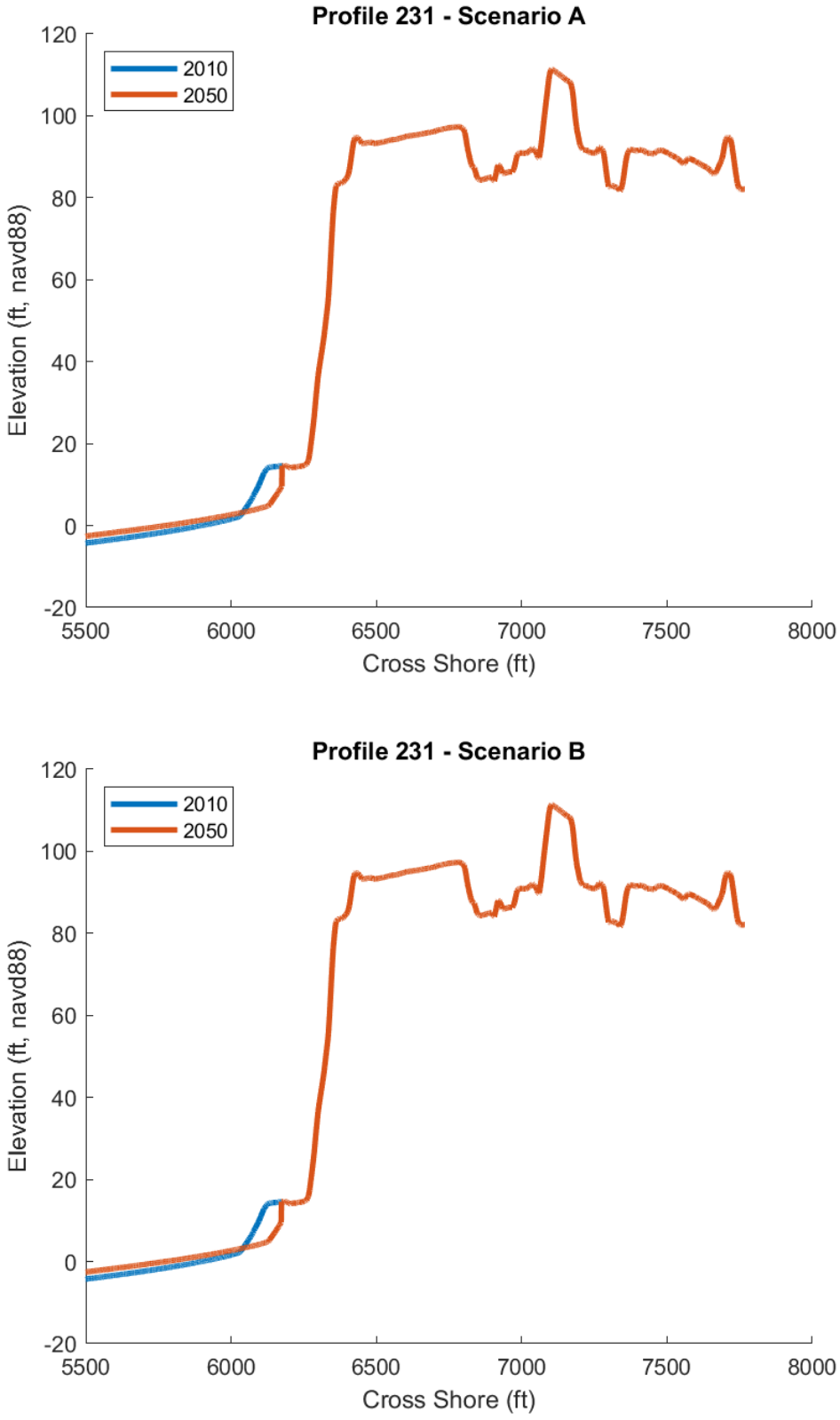


Figure A-22. Observed 2010 and modeled 2050 Profile 231.

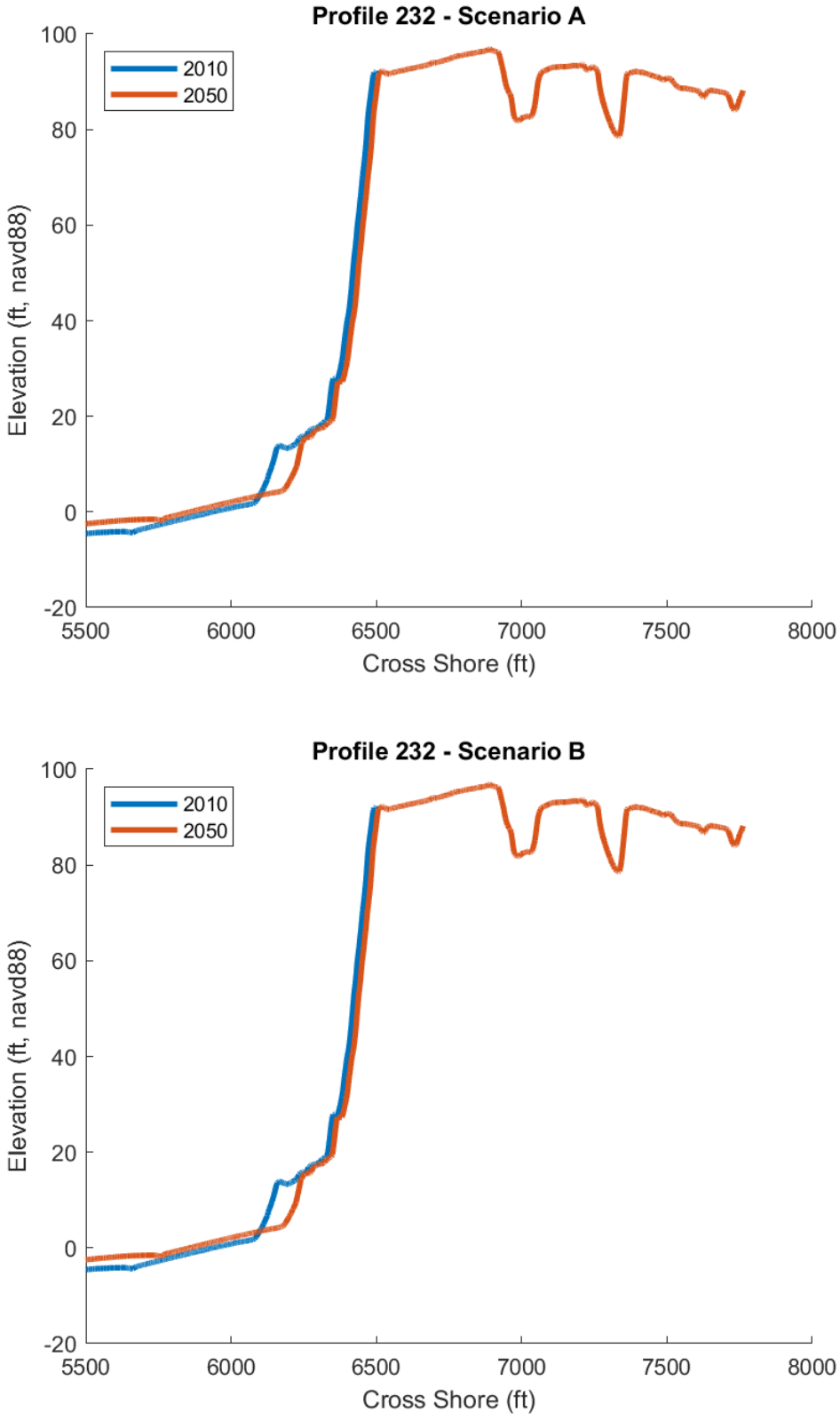


Figure A-23. Observed 2010 and modeled 2050 Profile 232.

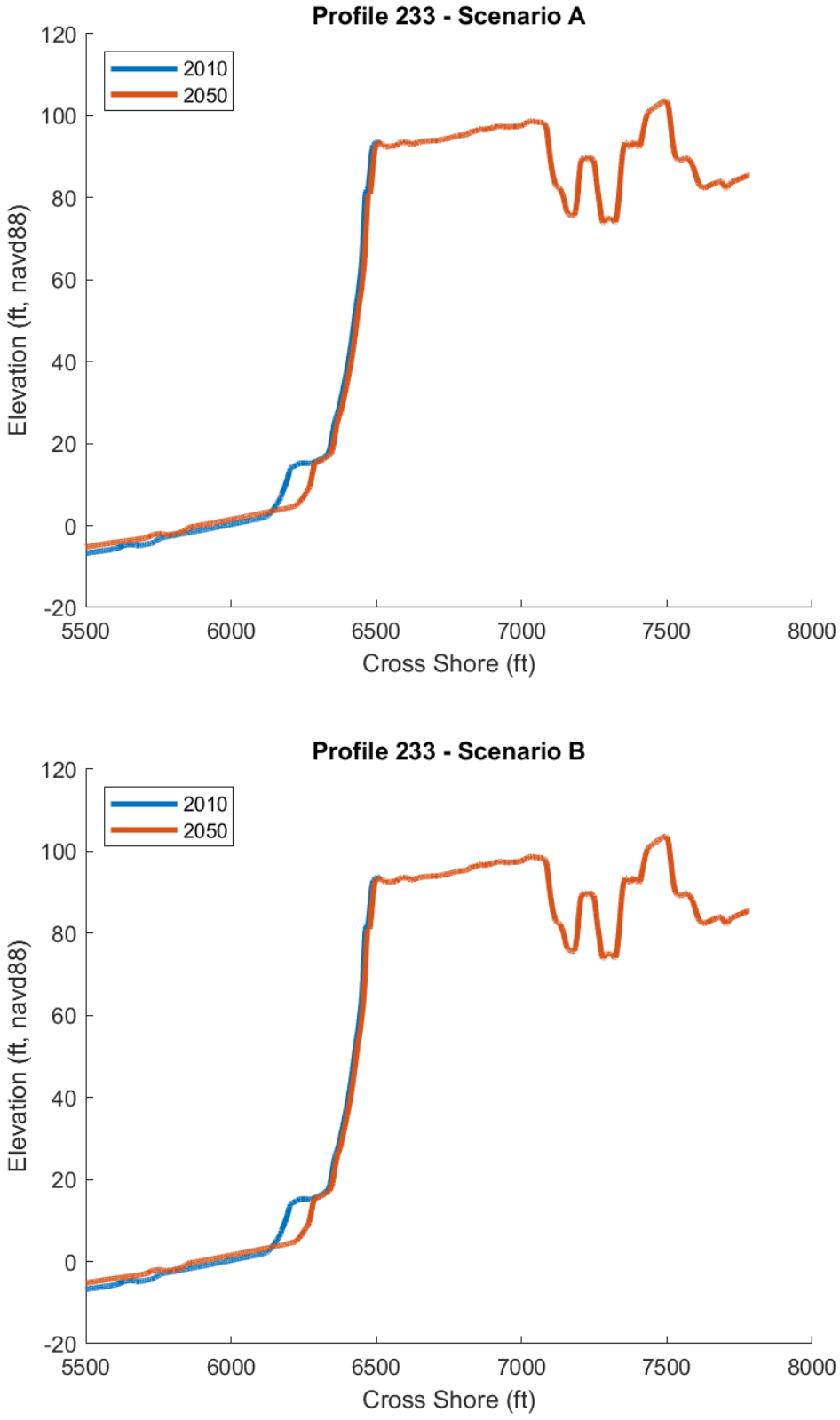


Figure A-24. Observed 2010 and modeled 2050 Profile 233.

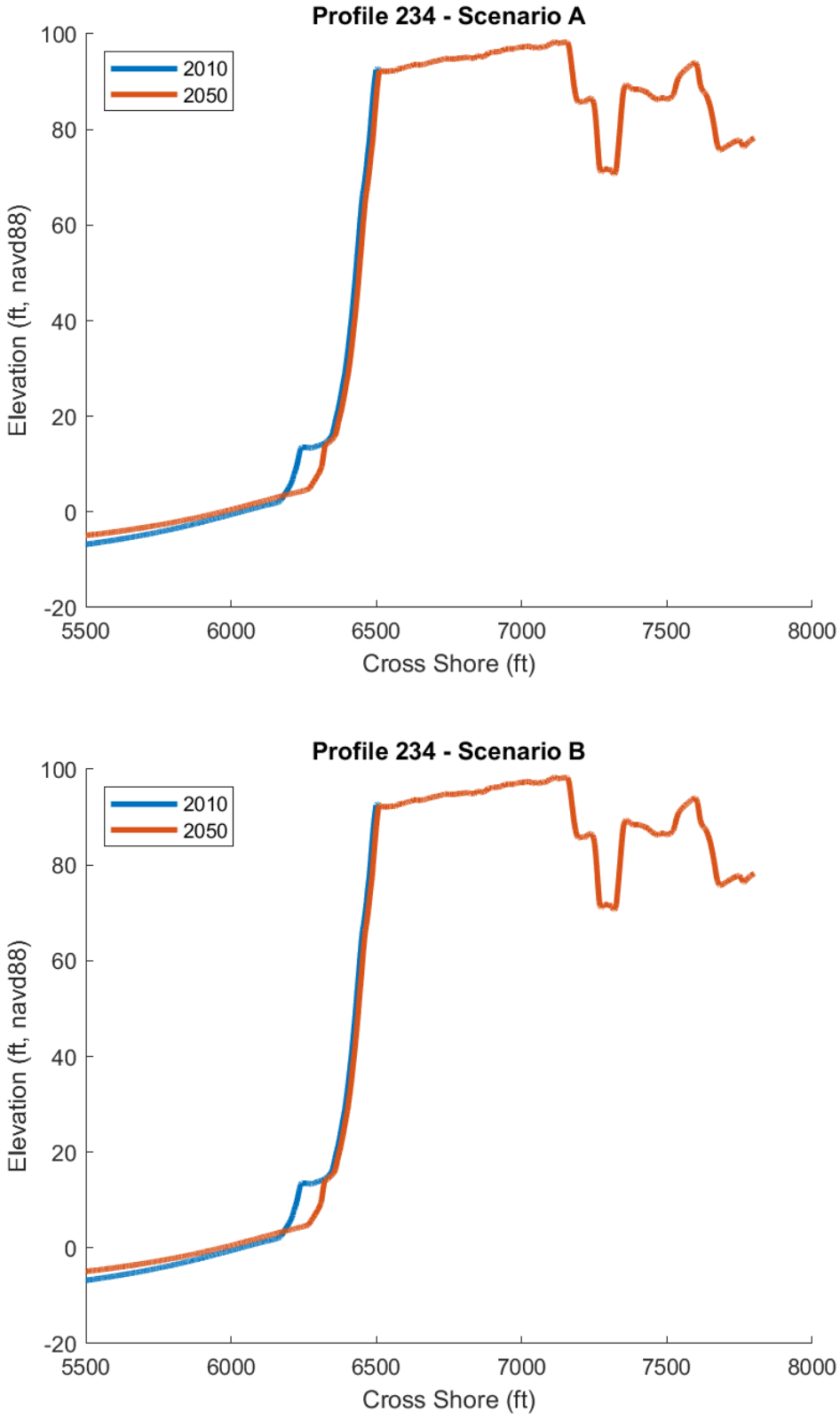


Figure A-25. Observed 2010 and modeled 2050 Profile 234.

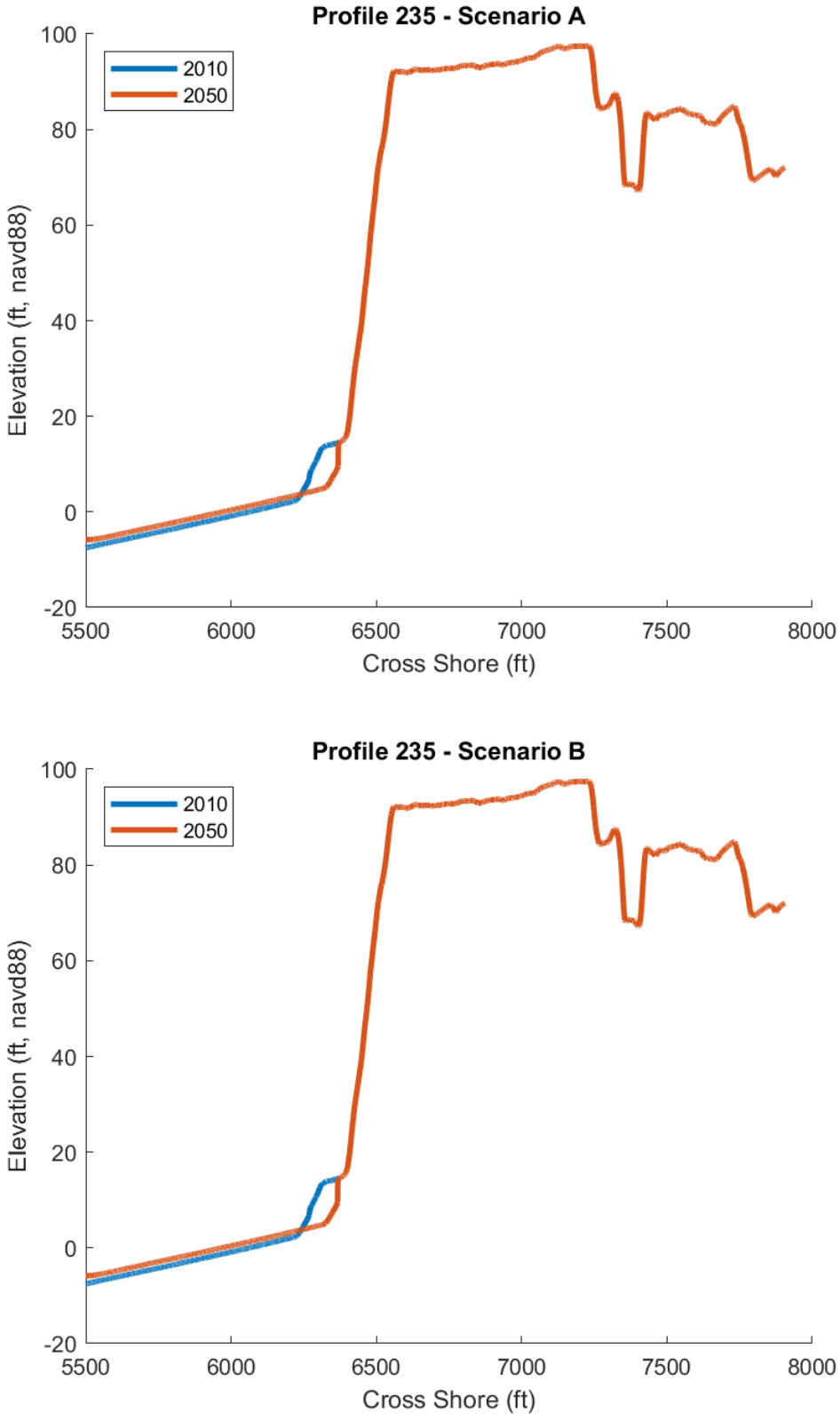


Figure A-26. Observed 2010 and modeled 2050 Profile 235.

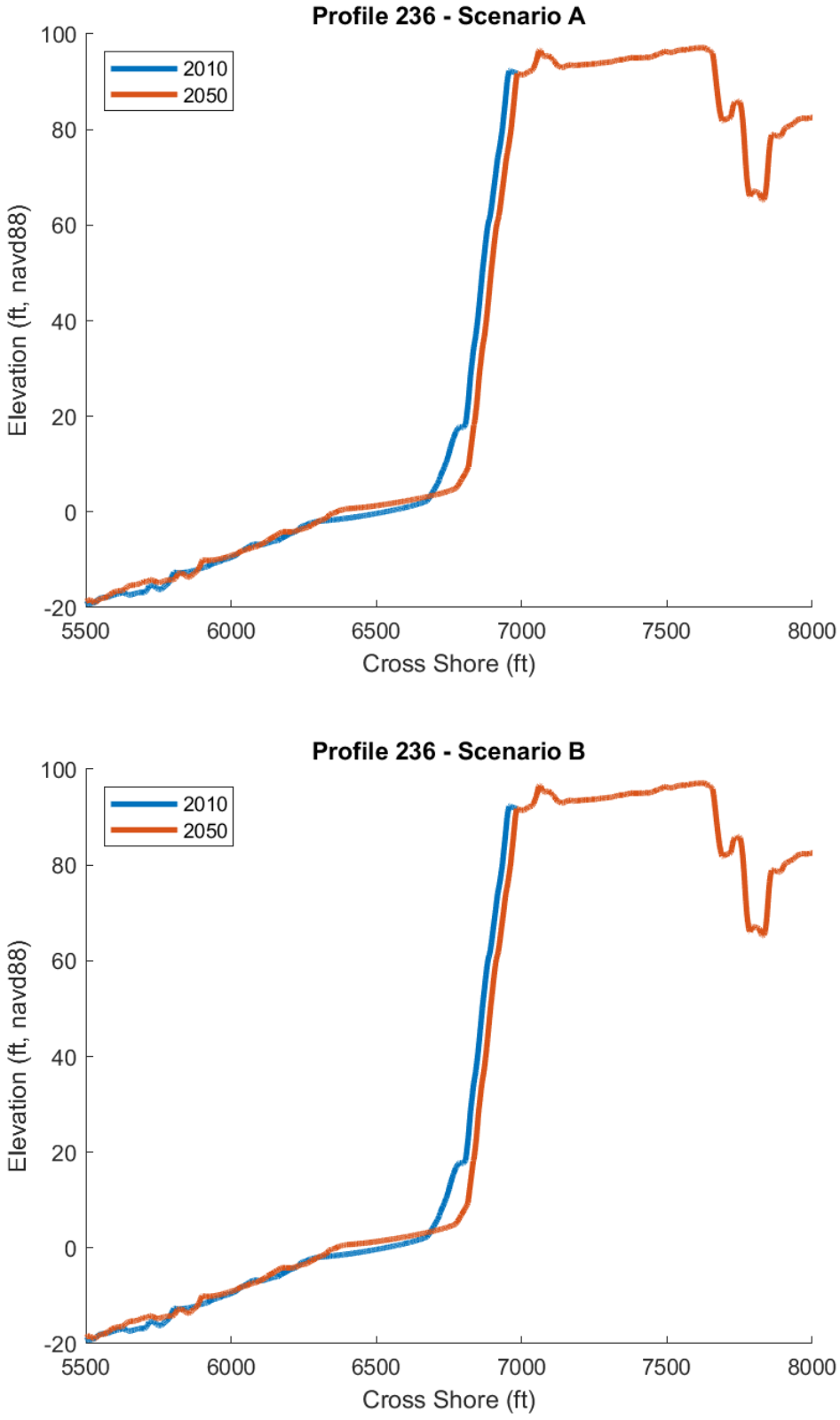


Figure A-27. Observed 2010 and modeled 2050 Profile 236.

APPENDIX B

DIGITAL ELEVATION MODELS (DEM) FROM 2020 AND 2021 REVETMENT SURVEYS



Figure B-1. Locations of 21 transects along the revetment, spaced 100 ft apart.

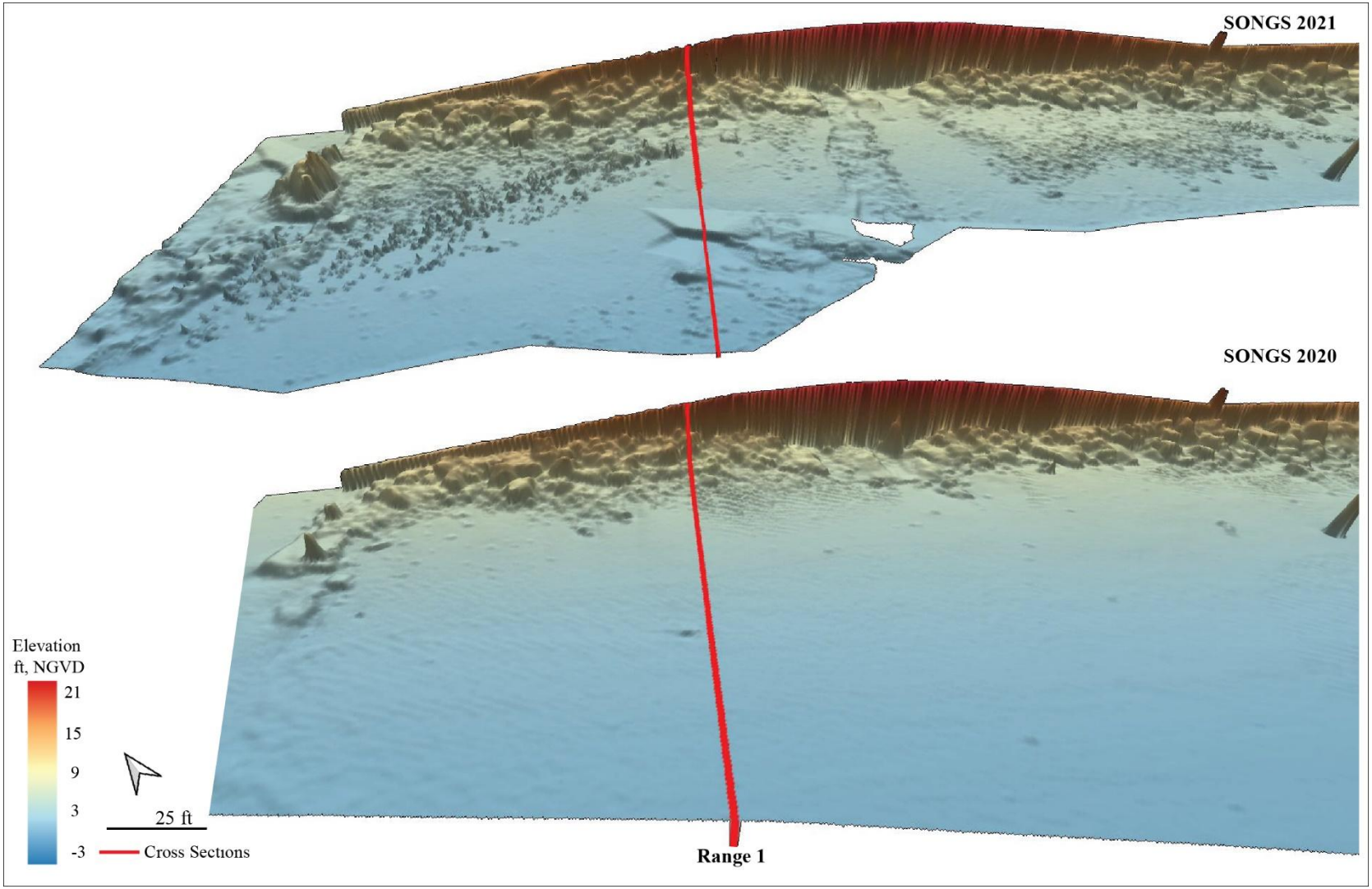


Figure B-2. DEM comparison between 2021 (top) and 2020 (bottom) showing Transect 1 along the SONGS revetment. Notice the increased presence of cobbles in 2021 on either side of Transect 1. There is no noticeable movement of the larger rocks against the wall of the walkway.

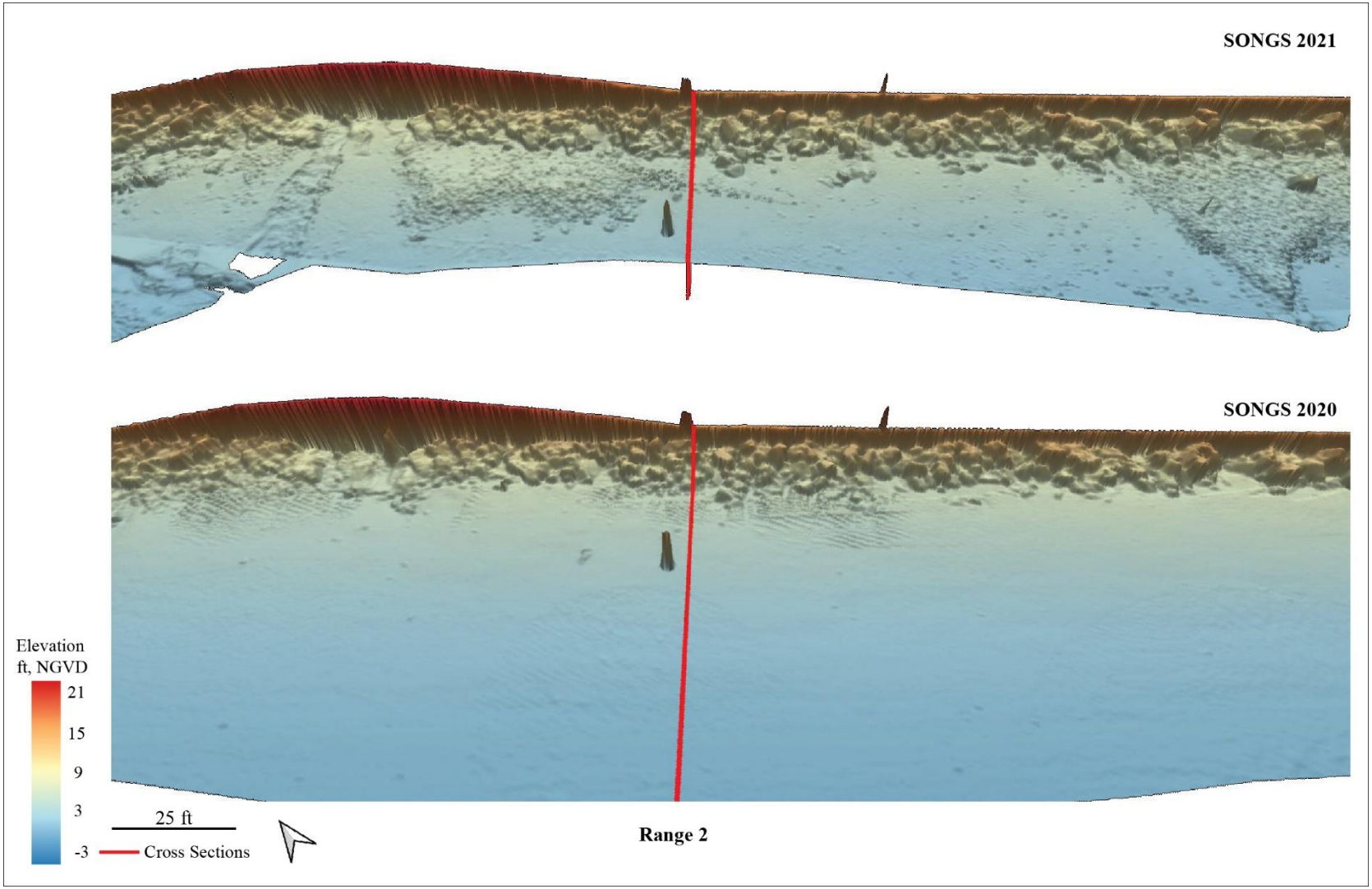


Figure B-3. DEM comparison between 2021 (top) and 2020 (bottom) showing Transect 2 along the SONGS revetment. Notice the increased presence of cobbles in 2021 just north of Transect 2. There is no noticeable movement of the larger rocks against the seawall.

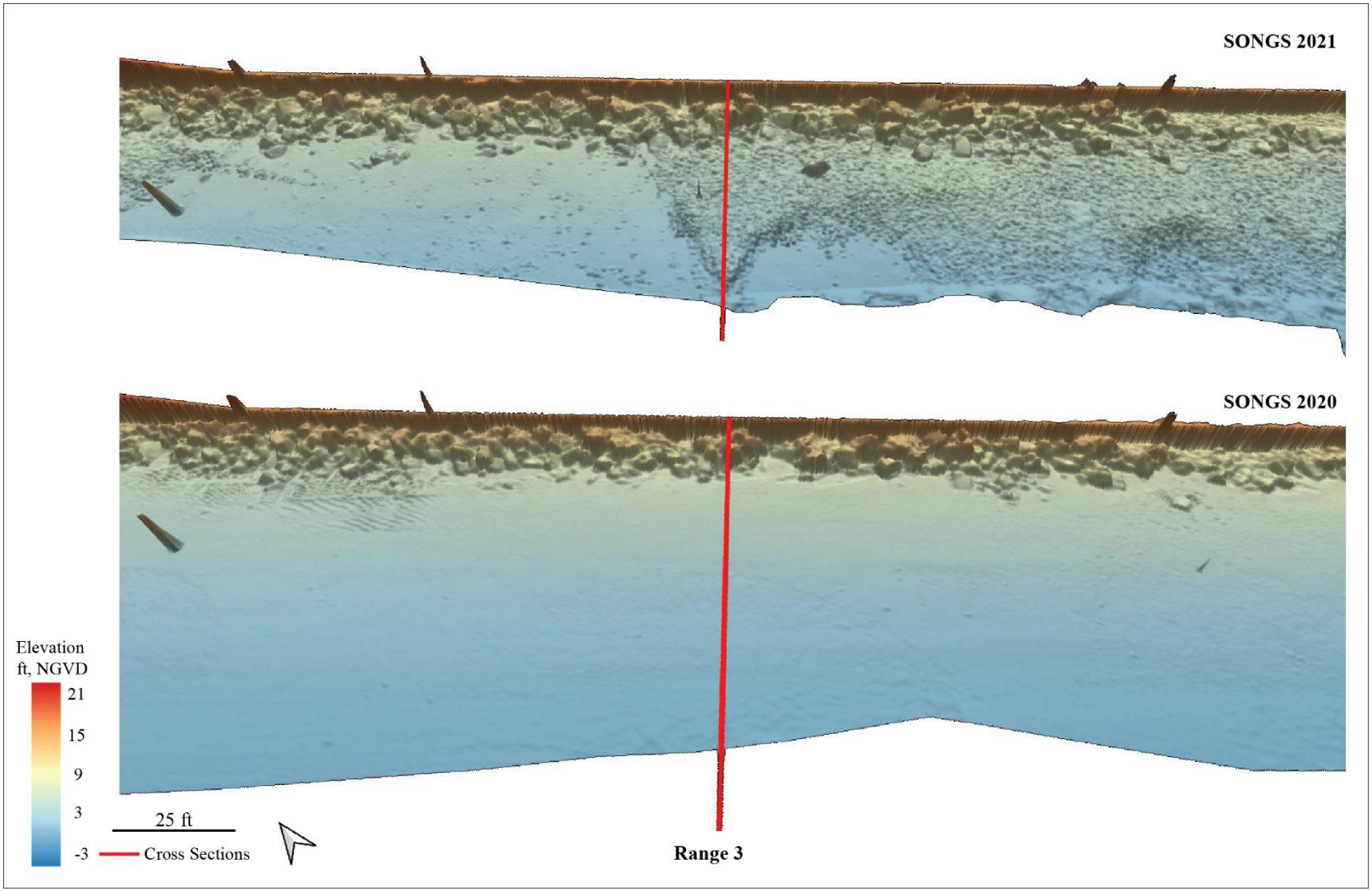


Figure B-4. DEM comparison between 2021 (top) and 2020 (bottom) showing Transect 3 along the SONGS revetment. Notice the increased presence of cobbles in the 2021 survey along and south of Transect 3. There is no noticeable movement of the larger rocks against the walkway wall.

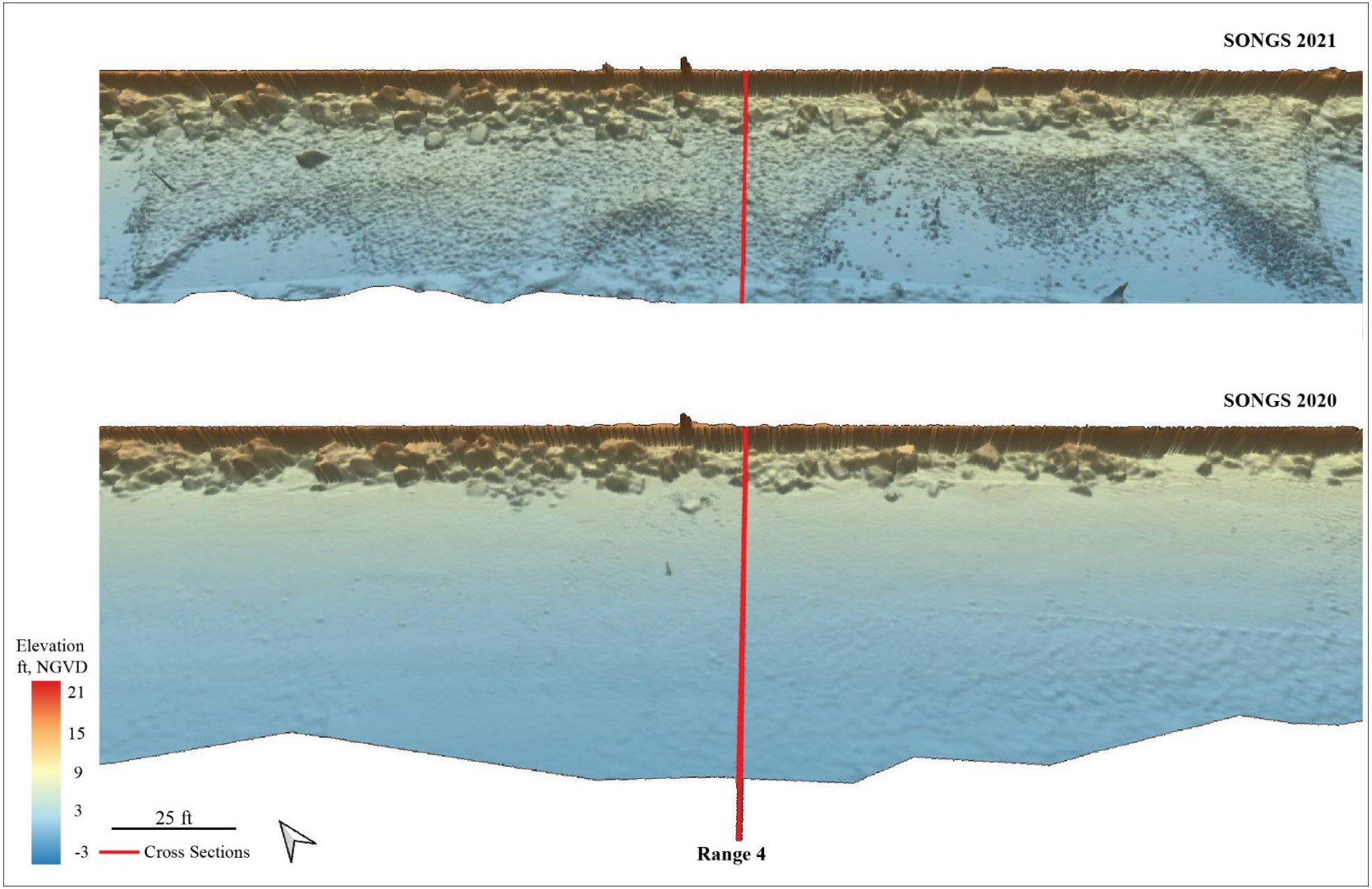


Figure B-5. DEM comparison between 2021 (top) and 2020 (bottom) showing Transect 4 along the SONGS revetment. Notice the increased presence of cobbles along the entire beach in 2021. There is no noticeable movement of the larger rocks against the walkway wall.

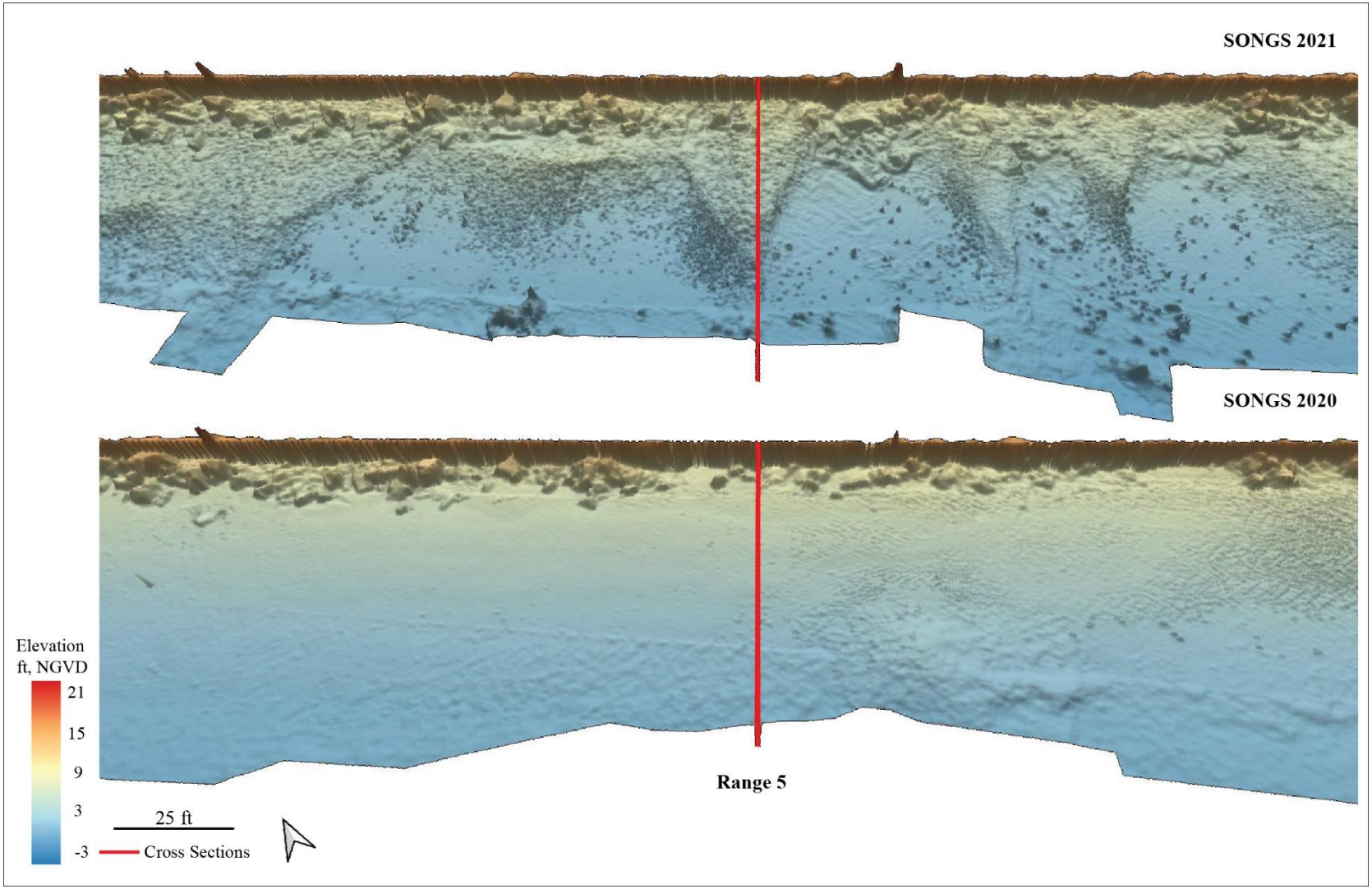


Figure B-6. DEM comparison between 2021 (top) and 2020 (bottom) showing Transect 5 along the SONGS revetment. Notice the increased exposure of cobbles along the beach and larger rocks against the walkway wall just south of Transect 5 in 2021 due to erosion.

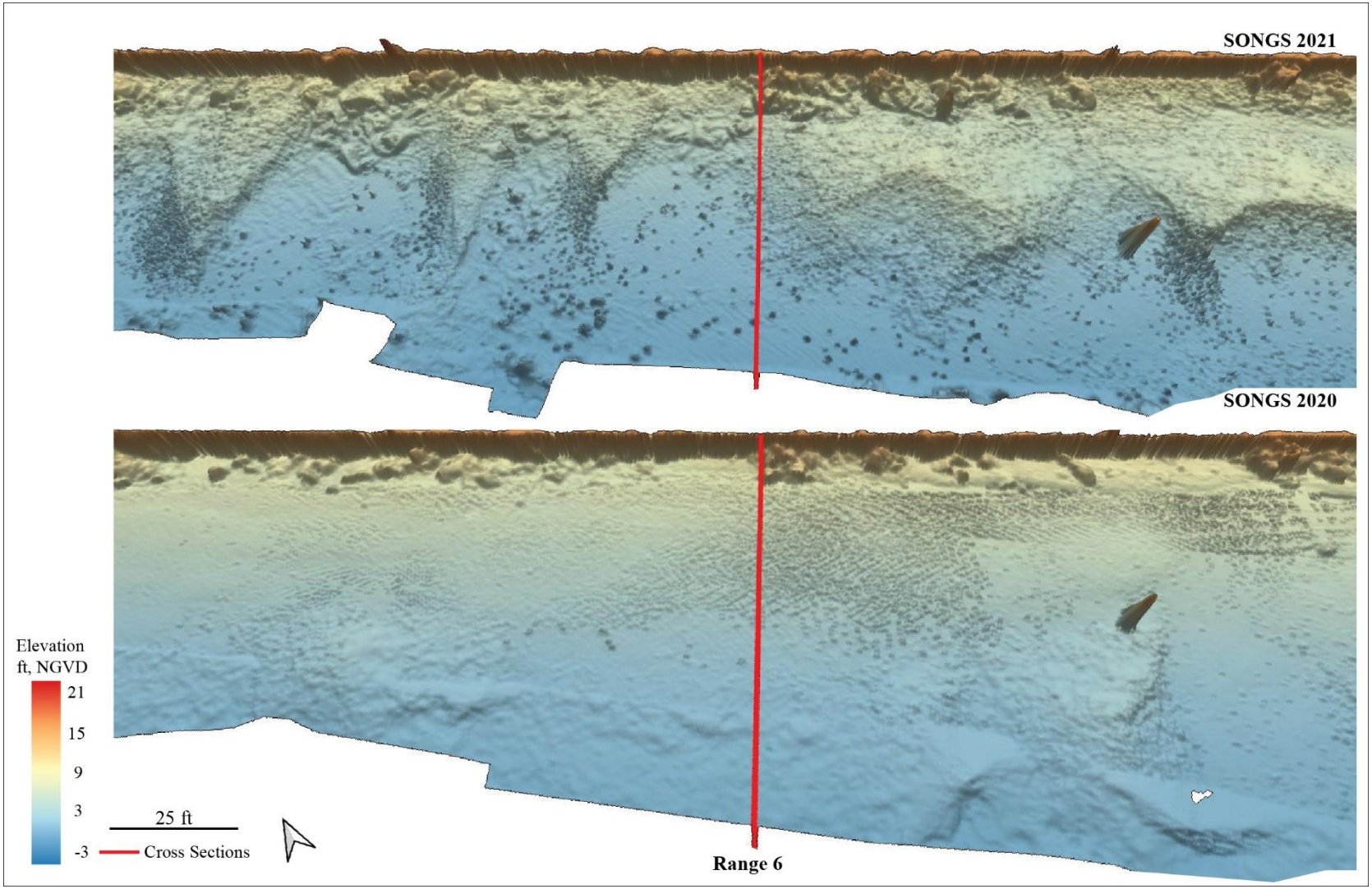


Figure B-7. DEM comparison between 2021 (top) and 2020 (bottom) showing Transect 6 along the SONGS revetment. Notice the increased exposure of cobbles along the beach and larger rocks against the walkway wall just south of Transect 6 in 2021 due to erosion.

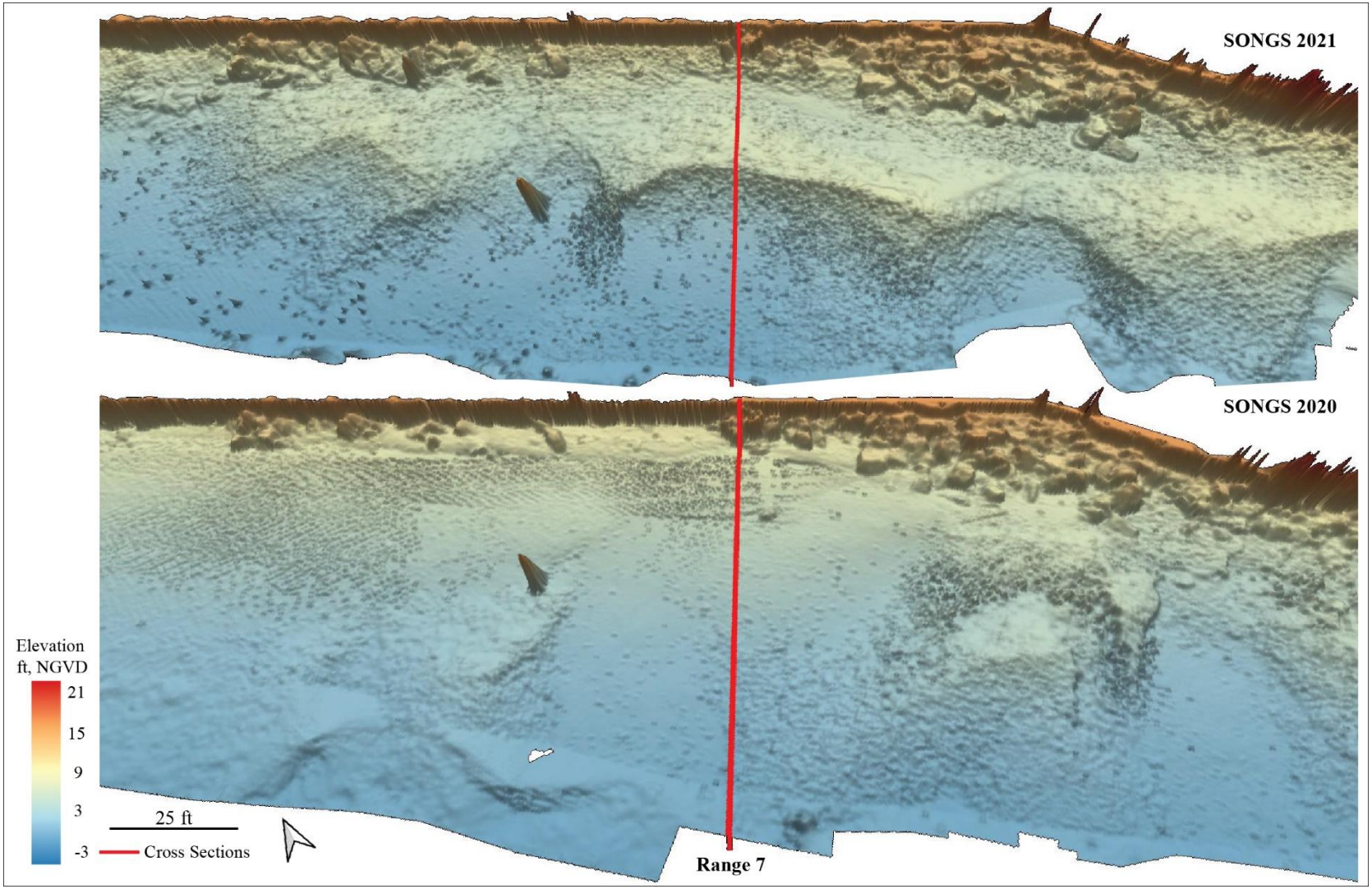


Figure B-8. DEM comparison between 2021 (top) and 2020 (bottom) showing Transect 7 along the SONGS revetment. Notice the presence of both an elevated berm and exposed cobbles along Transect 7 in 2021. There is no noticeable change in the larger rocks against the walkway wall along Transect 7.

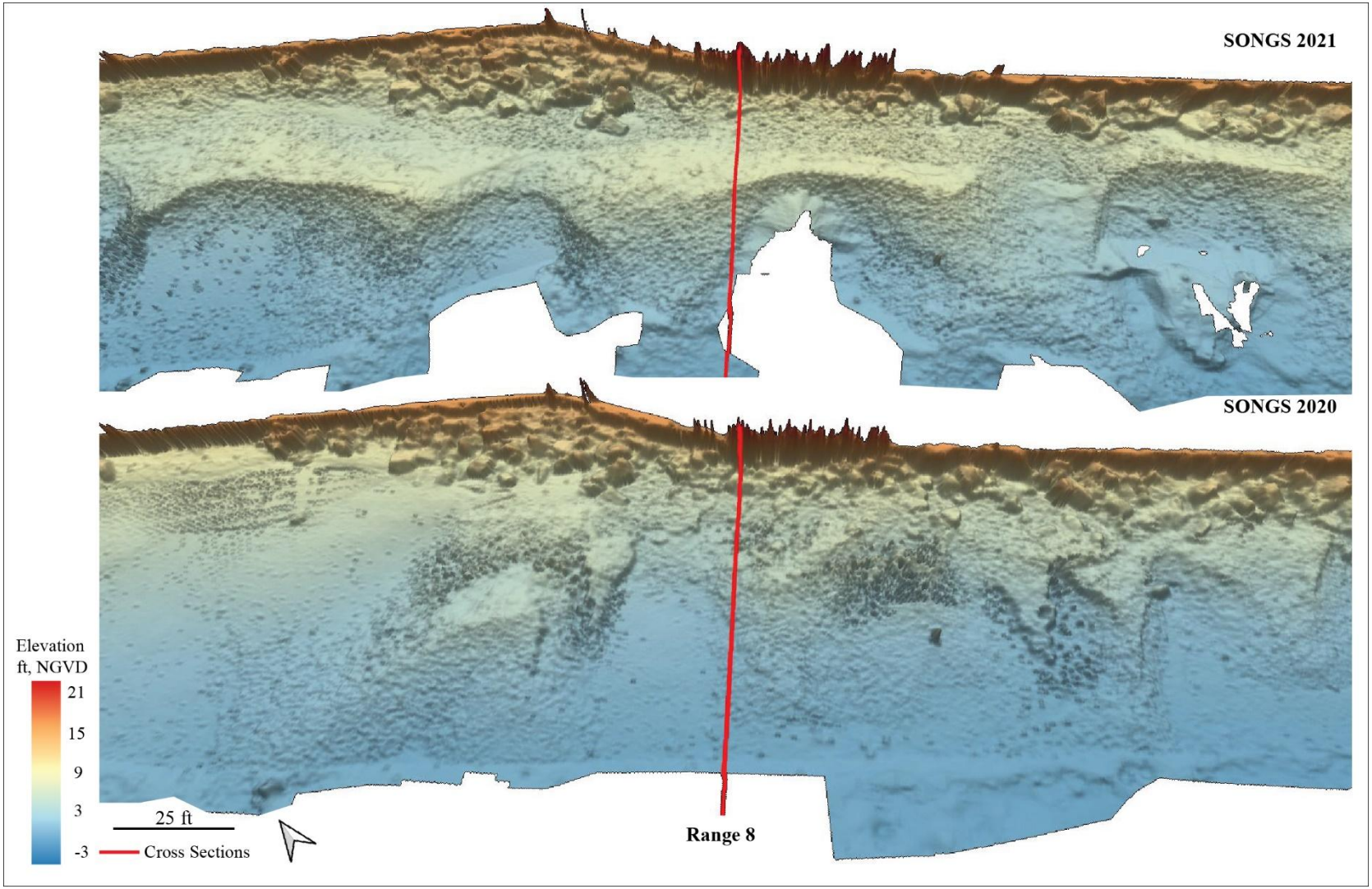


Figure B-9. DEM comparison between 2021 (top) and 2020 (bottom) showing Transect 8 along the SONGS revetment. Notice the elevated sand berm and partial coverage of larger rocks against the walkway wall due to accretion in 2021.

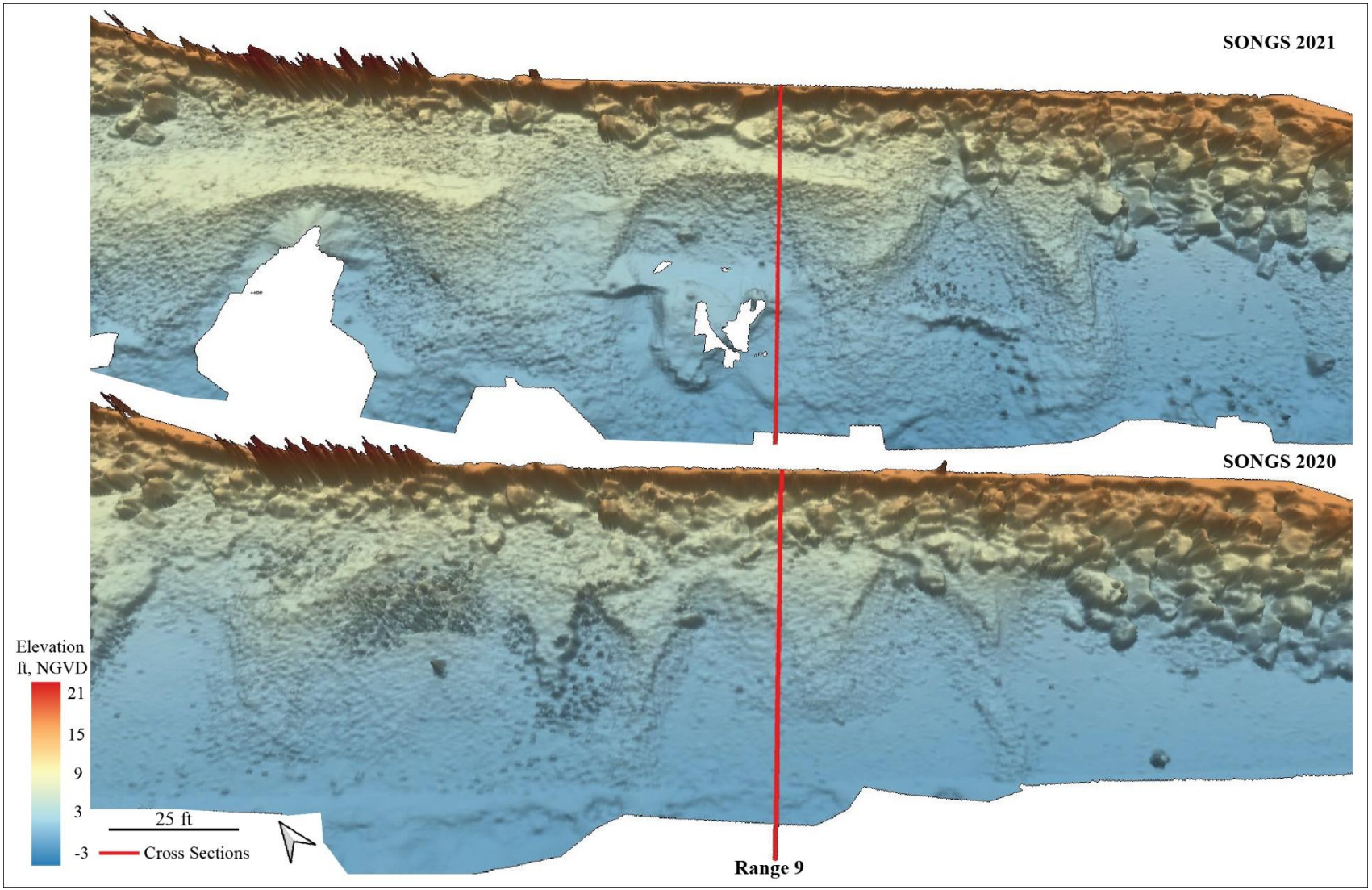


Figure B-10. DEM comparison between 2021 (top) and 2020 (bottom) showing Transect 9 along the SONGS revetment. Notice the elevated berm and partial coverage of larger rocks against the walkway wall due to accretion in 2021.

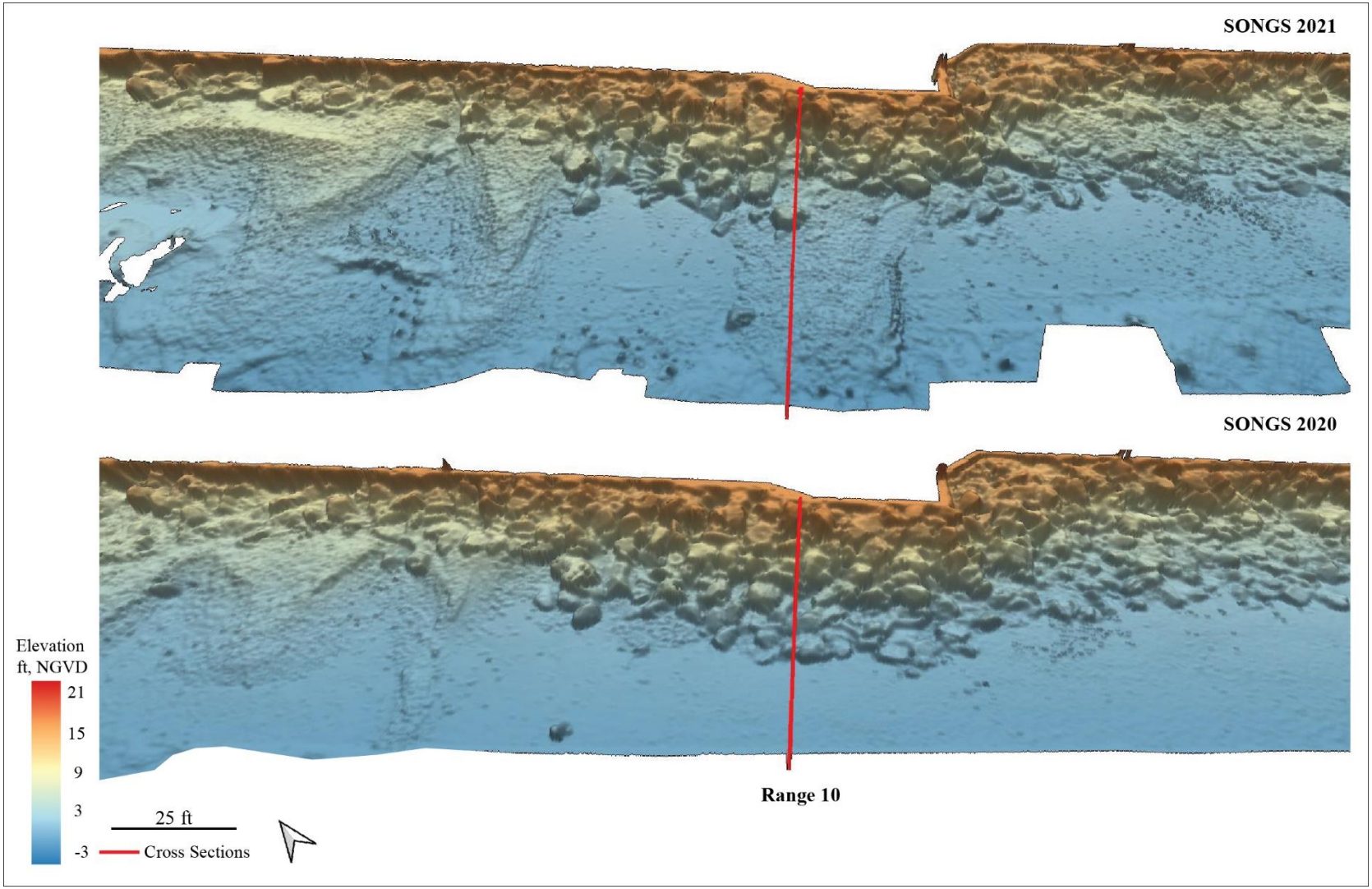


Figure B-11. DEM comparison between 2021 (top) and 2020 (bottom) showing Transect 10 along the SONGS revetment. Notice the movement of large rocks at the midpoint of the revetment along Transect 10 and increased presence of cobbles in 2021.

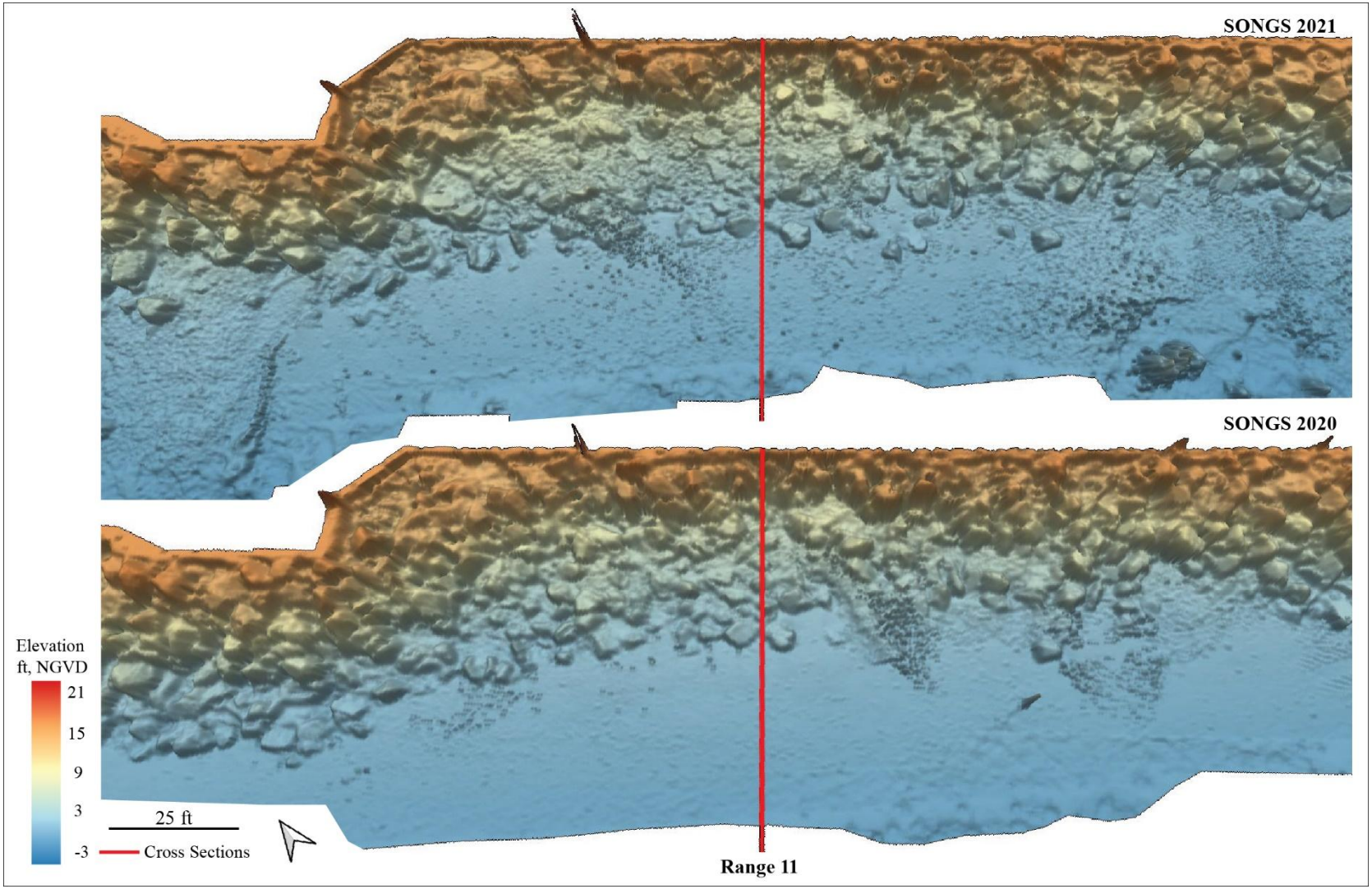


Figure B-12. DEM comparison between 2021 (top) and 2020 (bottom) showing Transect 11 along the SONGS revetment. Notice the partial burial of larger rocks in the middle of the revetment with sand and cobble in 2021.

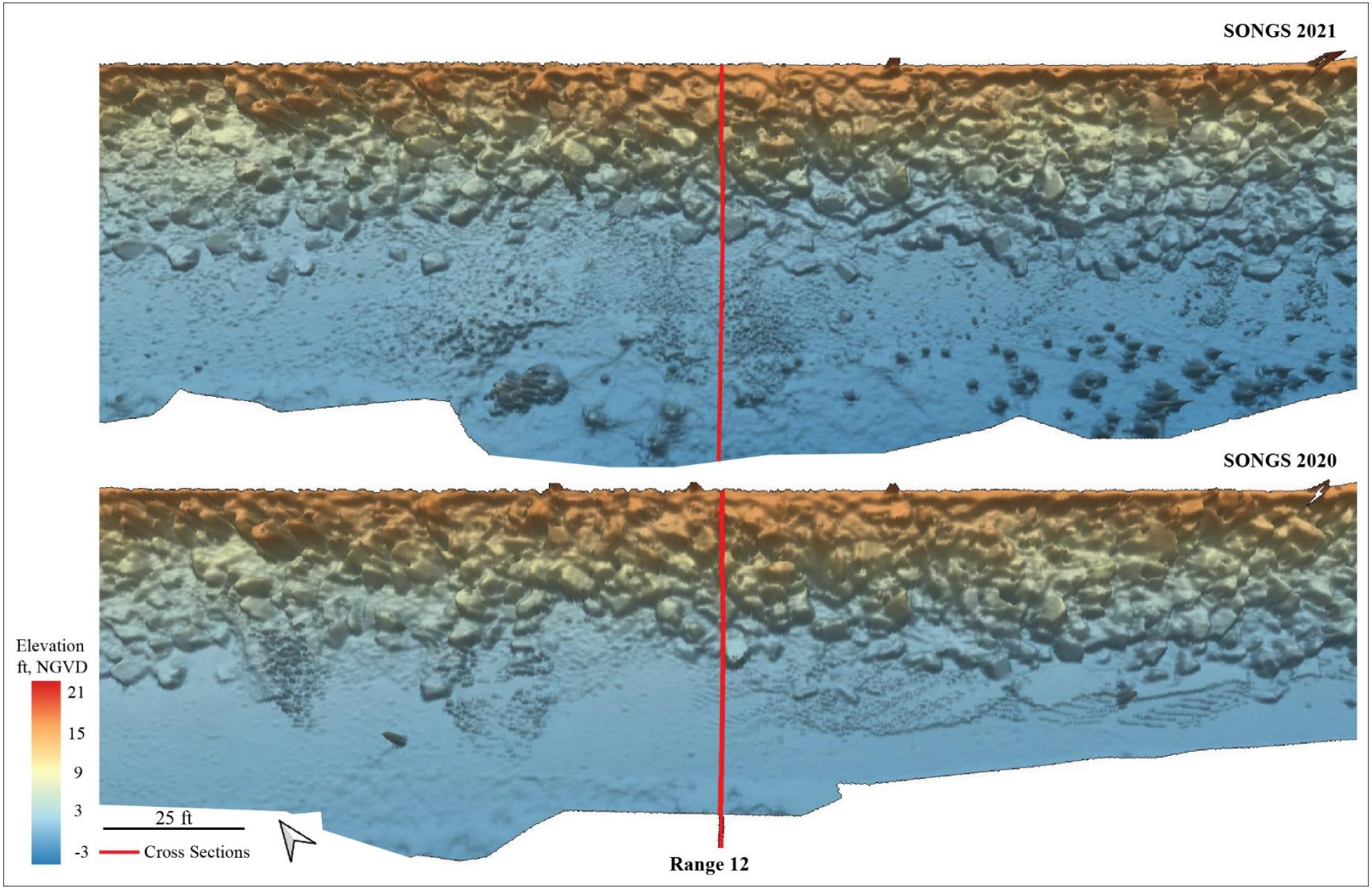


Figure B-13. DEM comparison between 2021 (top) and 2020 (bottom) showing Transect 12 along the SONGS revetment. Notice the increased presence of cobble on the beach along Transect 12 in 2021. There is no noticeable difference in the revetment rocks between the two years.

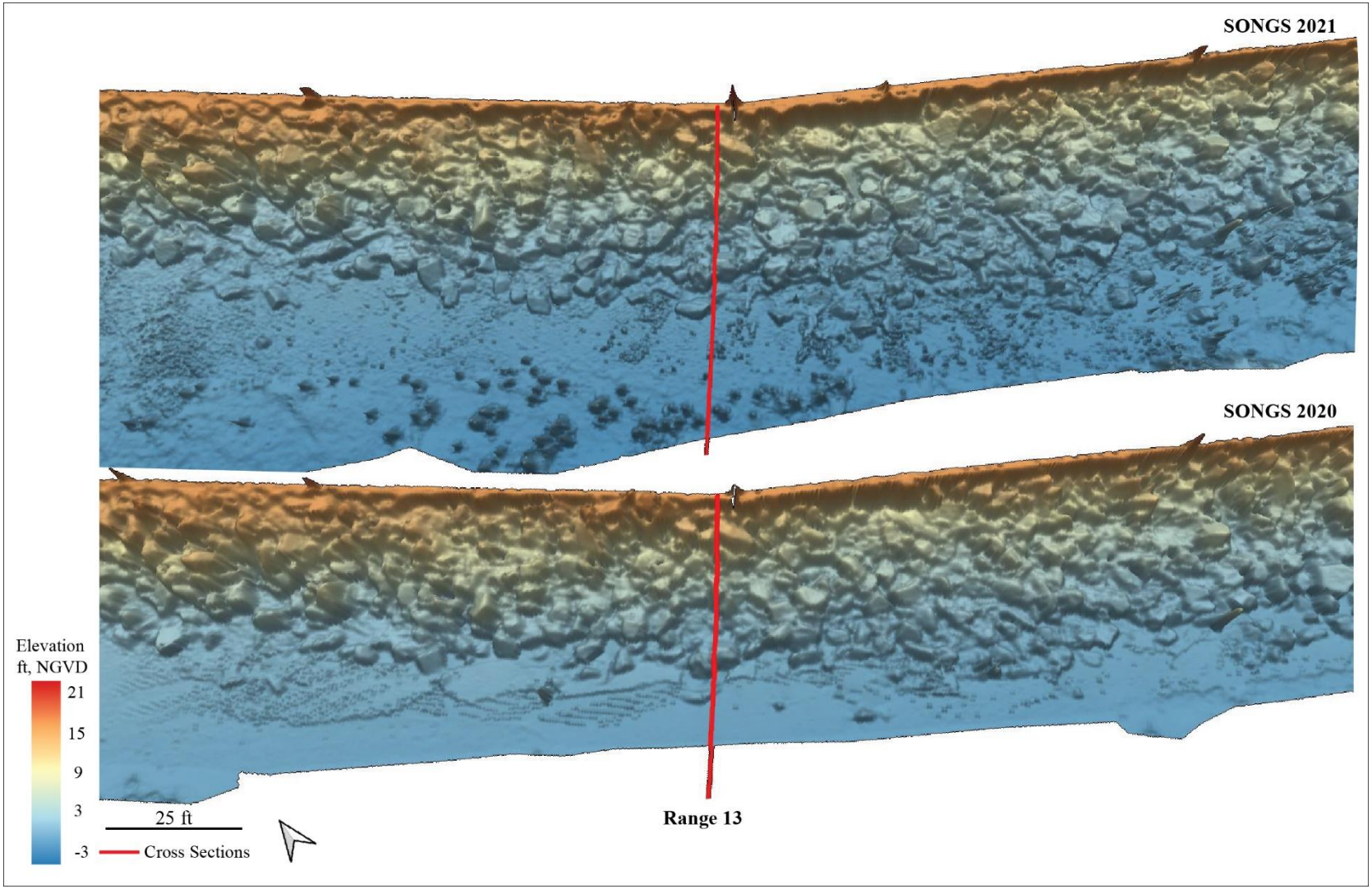


Figure B-14. DEM comparison between 2021 (top) and 2020 (bottom) showing Transect 13 along the SONGS revetment. Notice the slight erosion at the toe of the revetment in 2021. There is no noticeable difference in the revetment rocks between the two years.

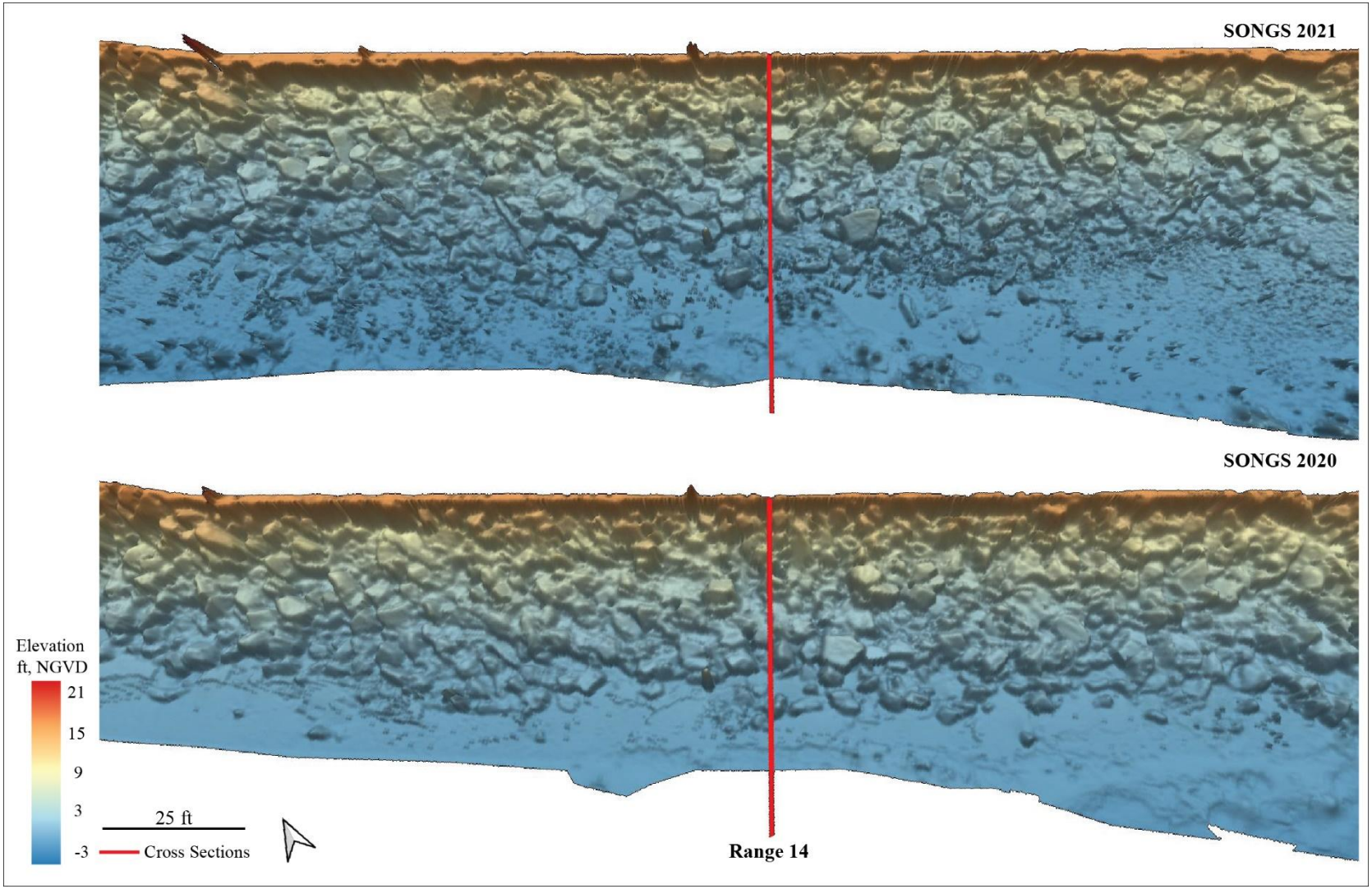


Figure B-15. DEM comparison between 2021 (top) and 2020 (bottom) showing Transect 14 along the SONGS revetment. Notice the increased cobbles, erosion, and movement of some larger rocks at the toe of the revetment in 2021.

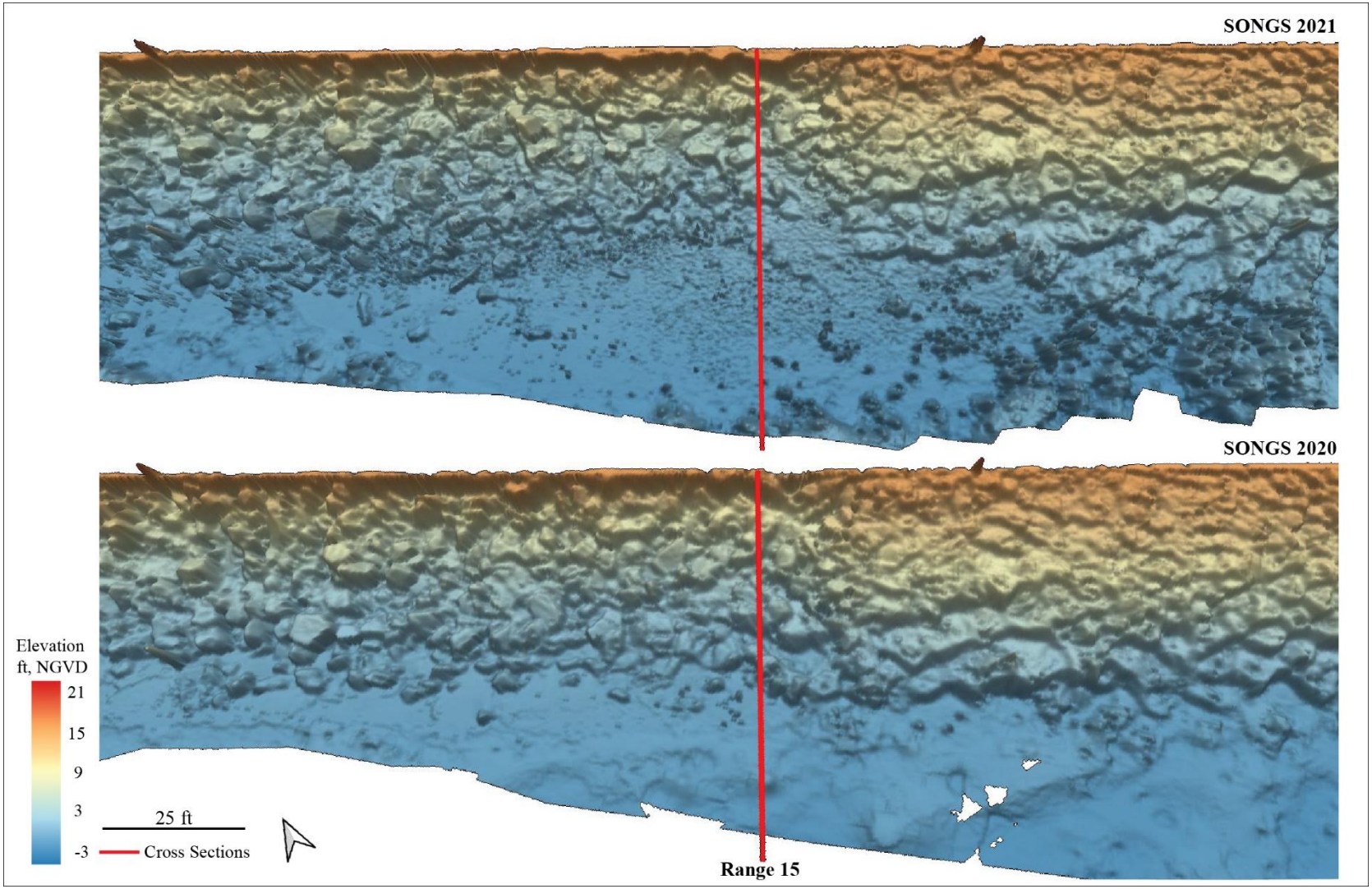


Figure B-16. DEM comparison between 2021 (top) and 2020 (bottom) showing Transect 15 along the SONGS revetment. Notice the increased cobbles and partial coverage of large rocks at the toe of the revetment due to accretion in 2021.

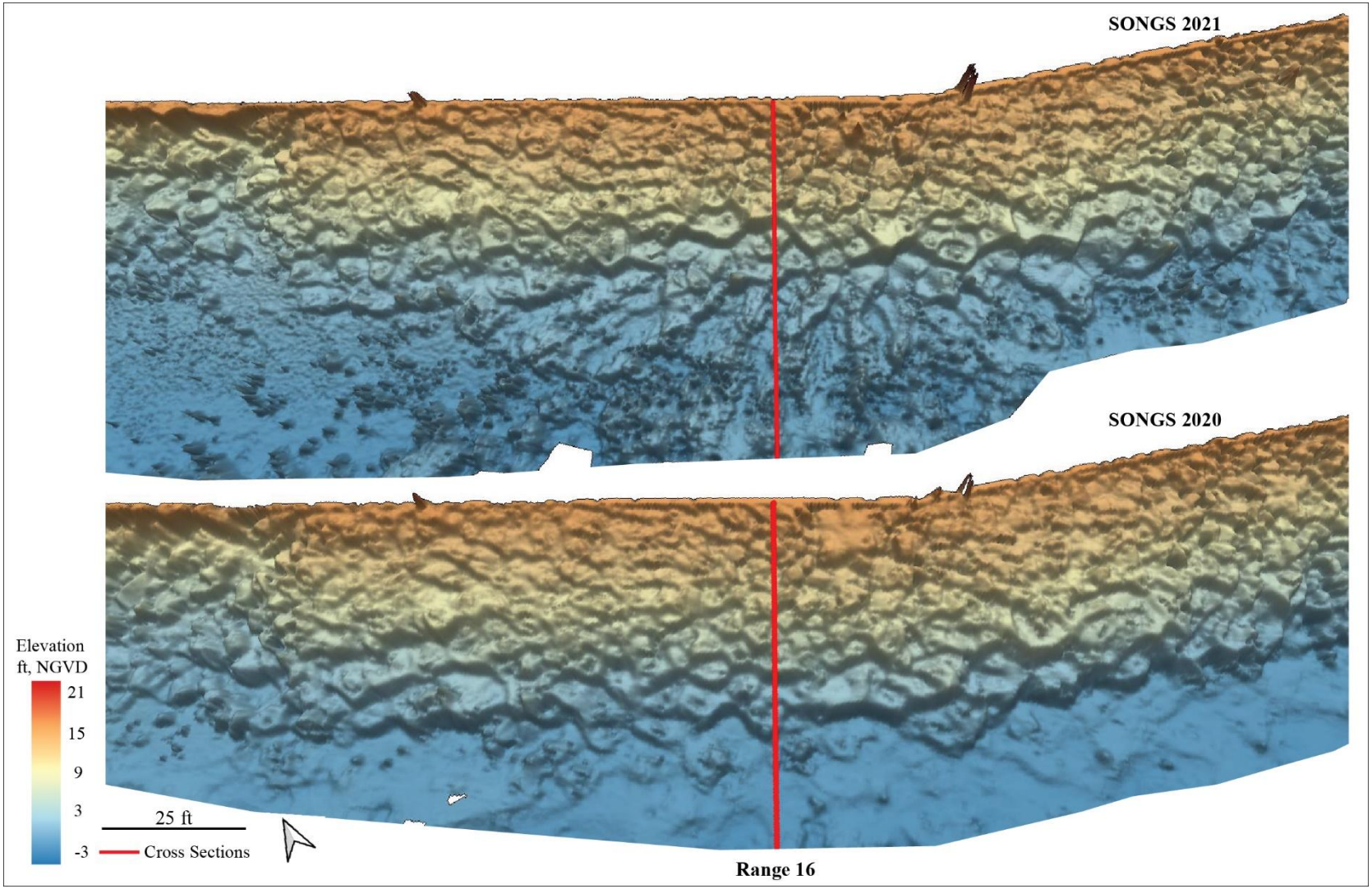


Figure B-17. DEM comparison between 2021 (top) and 2020 (bottom) showing Transect 16 along the SONGS revetment. Notice the increased amount of cobble at the toe of the revetment in 2021.

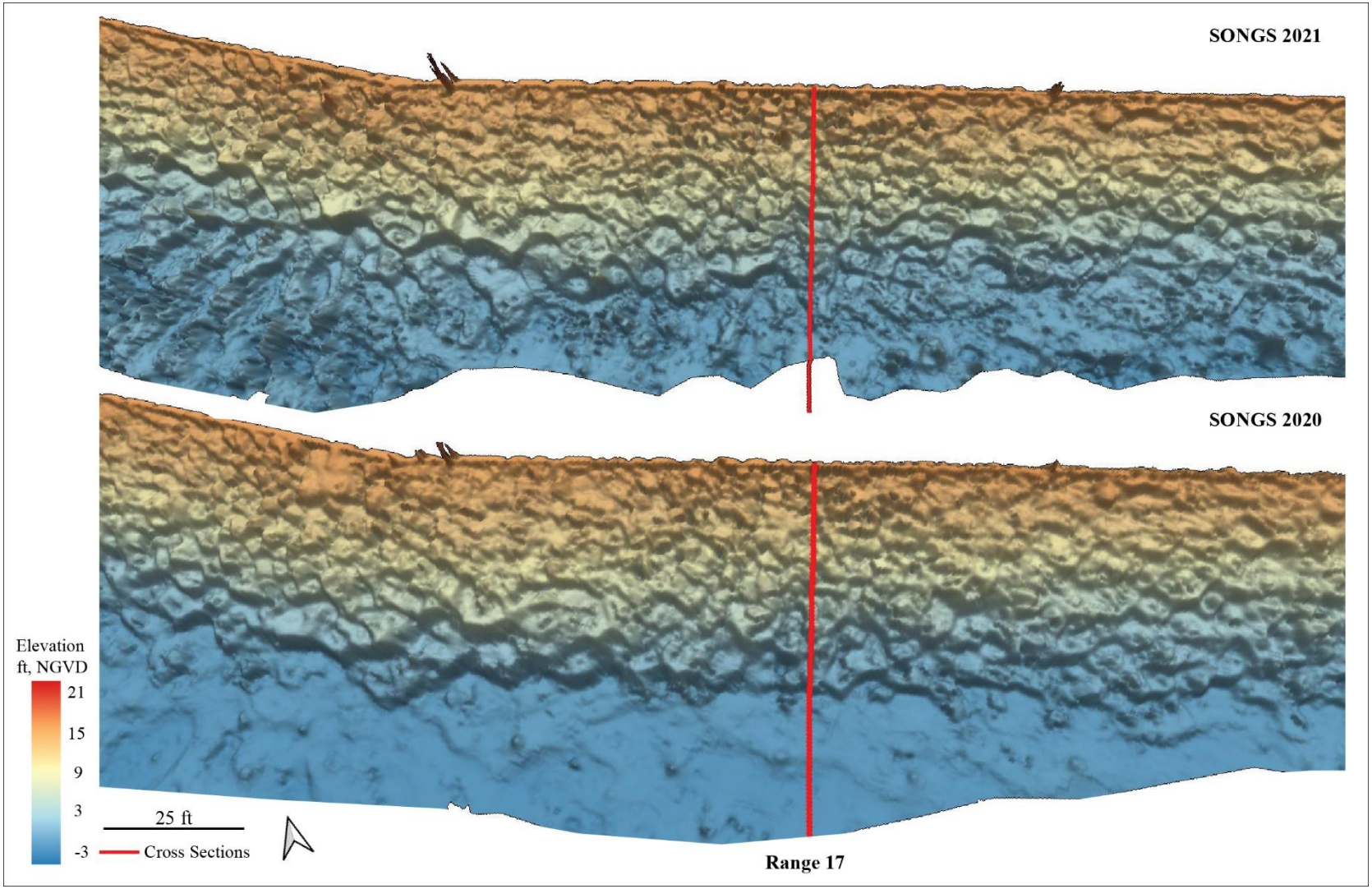


Figure B-18. DEM comparison between 2021 (top) and 2020 (bottom) showing Transect 17 along the SONGS revetment. Notice the increased amount of cobble at the toe of the revetment in 2021.

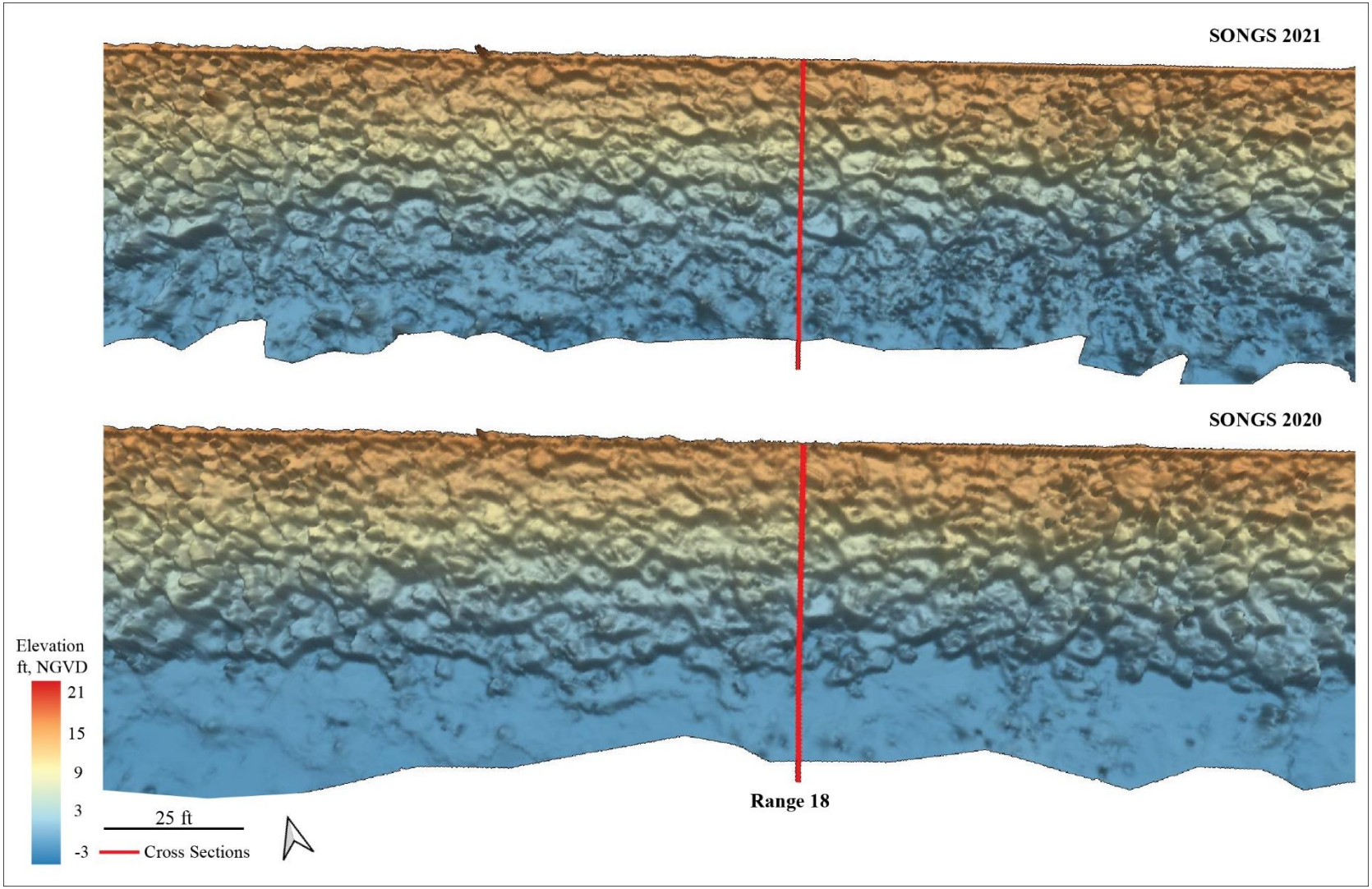


Figure B-19. DEM comparison between 2021 (top) and 2020 (bottom) showing Transect 18 along the SONGS revetment. Notice the increased amount of cobble at the toe of the revetment in 2021.

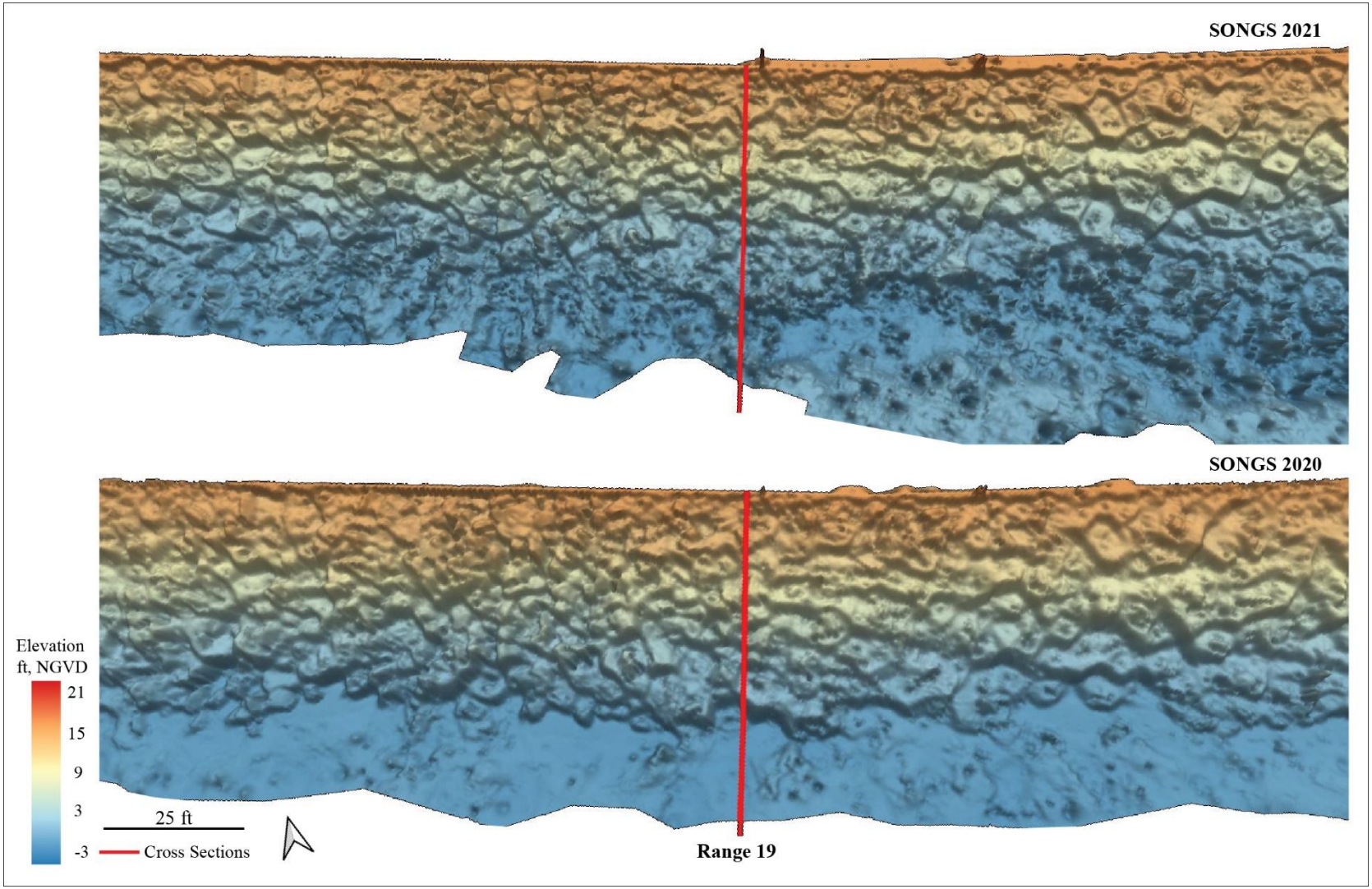


Figure B-20. DEM comparison between 2021 (top) and 2020 (bottom) showing Transect 19 along the SONGS revetment. Notice the increased amount of cobble at the toe of the revetment in 2021.

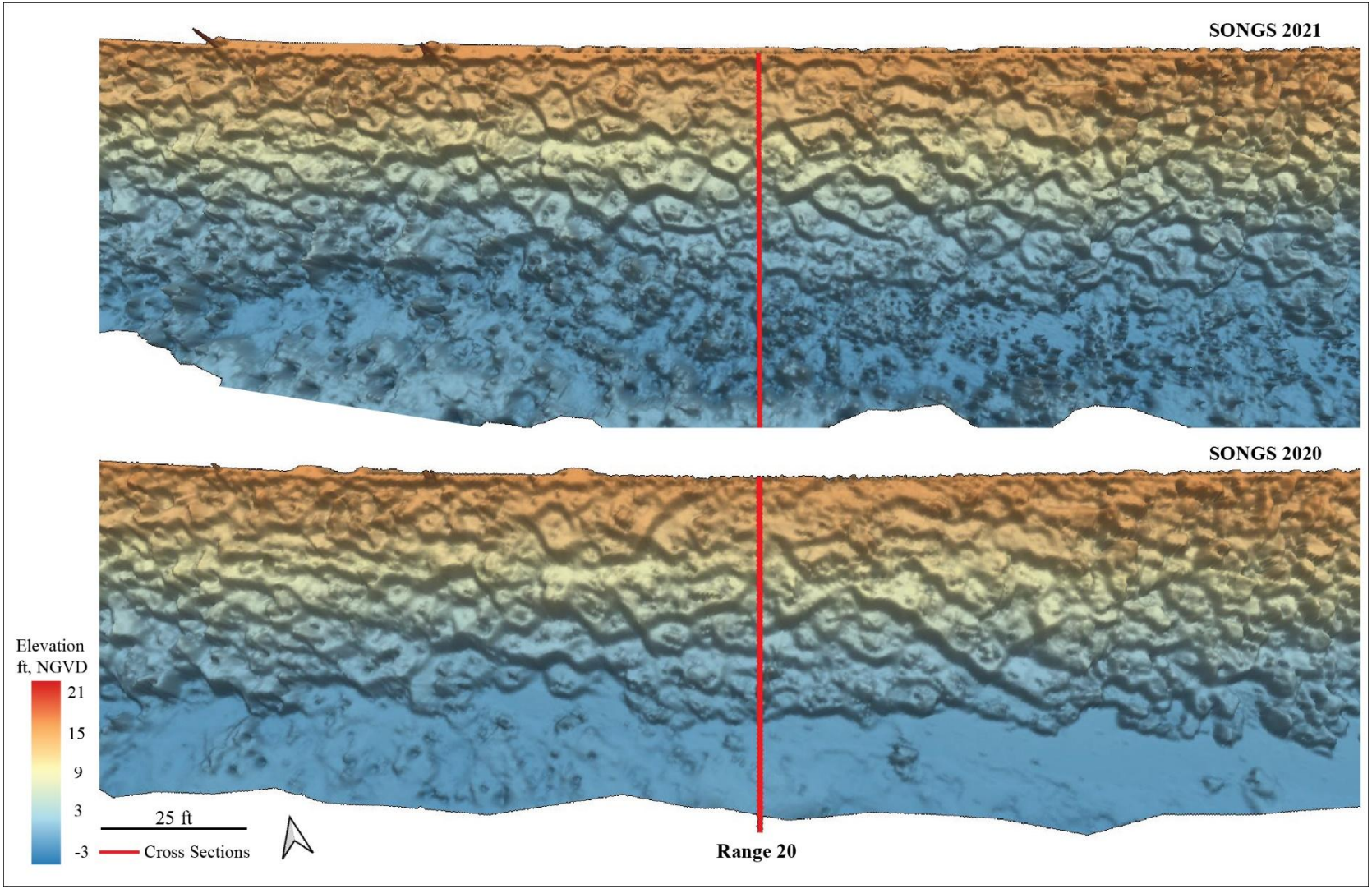


Figure B-21. DEM comparison between 2021 (top) and 2020 (bottom) showing Transect 20 along the SONGS revetment. Notice the increased amount of cobble at the toe of the revetment in 2021.

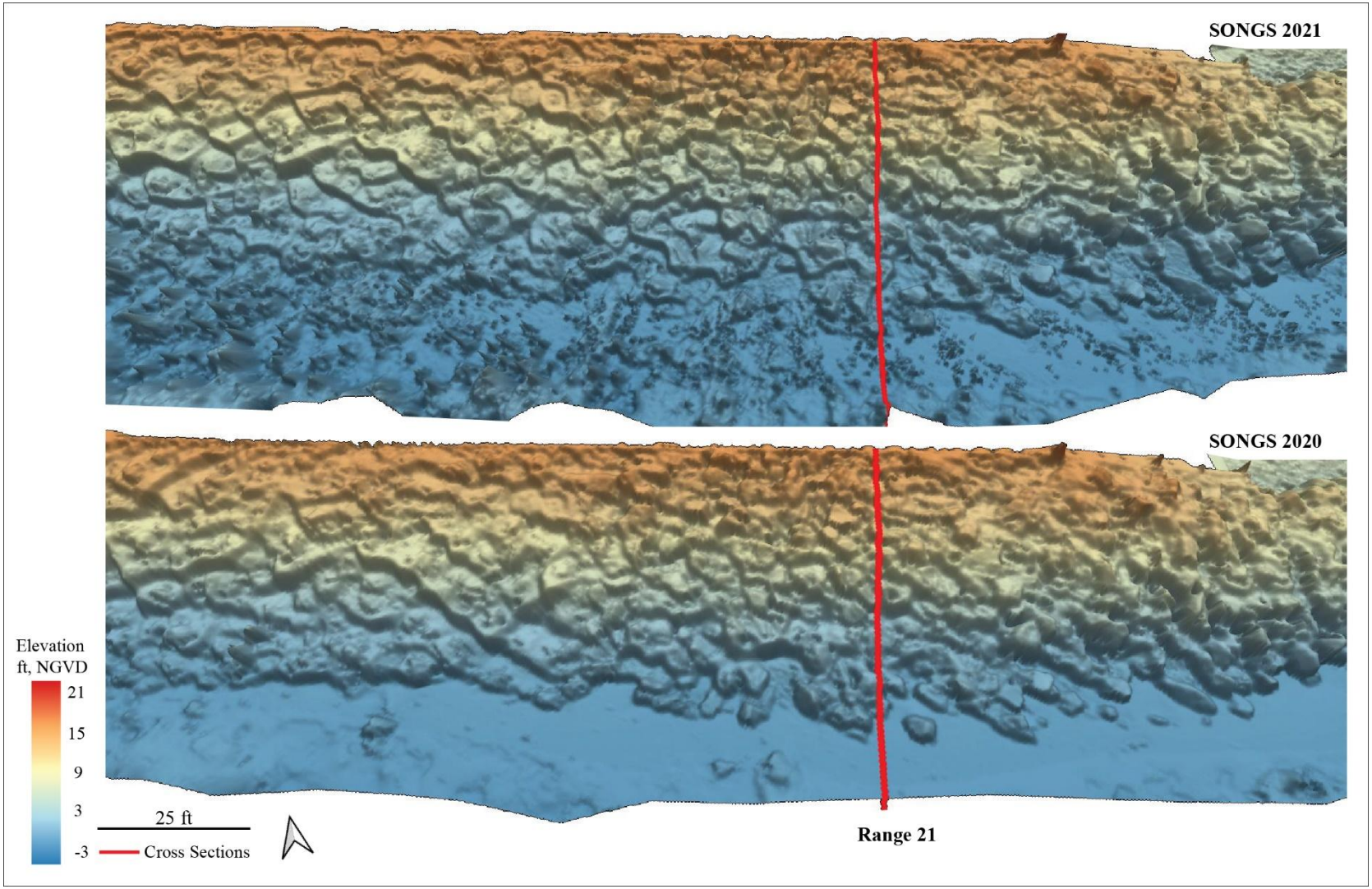


Figure B-22. DEM comparison between 2021 (top) and 2020 (bottom) showing Transect 21 along the SONGS revetment. Notice the increased amount of cobble at the toe of the revetment in 2021.

APPENDIX C

CROSS SECTION ELEVATIONS OF SONGS REVETMENT

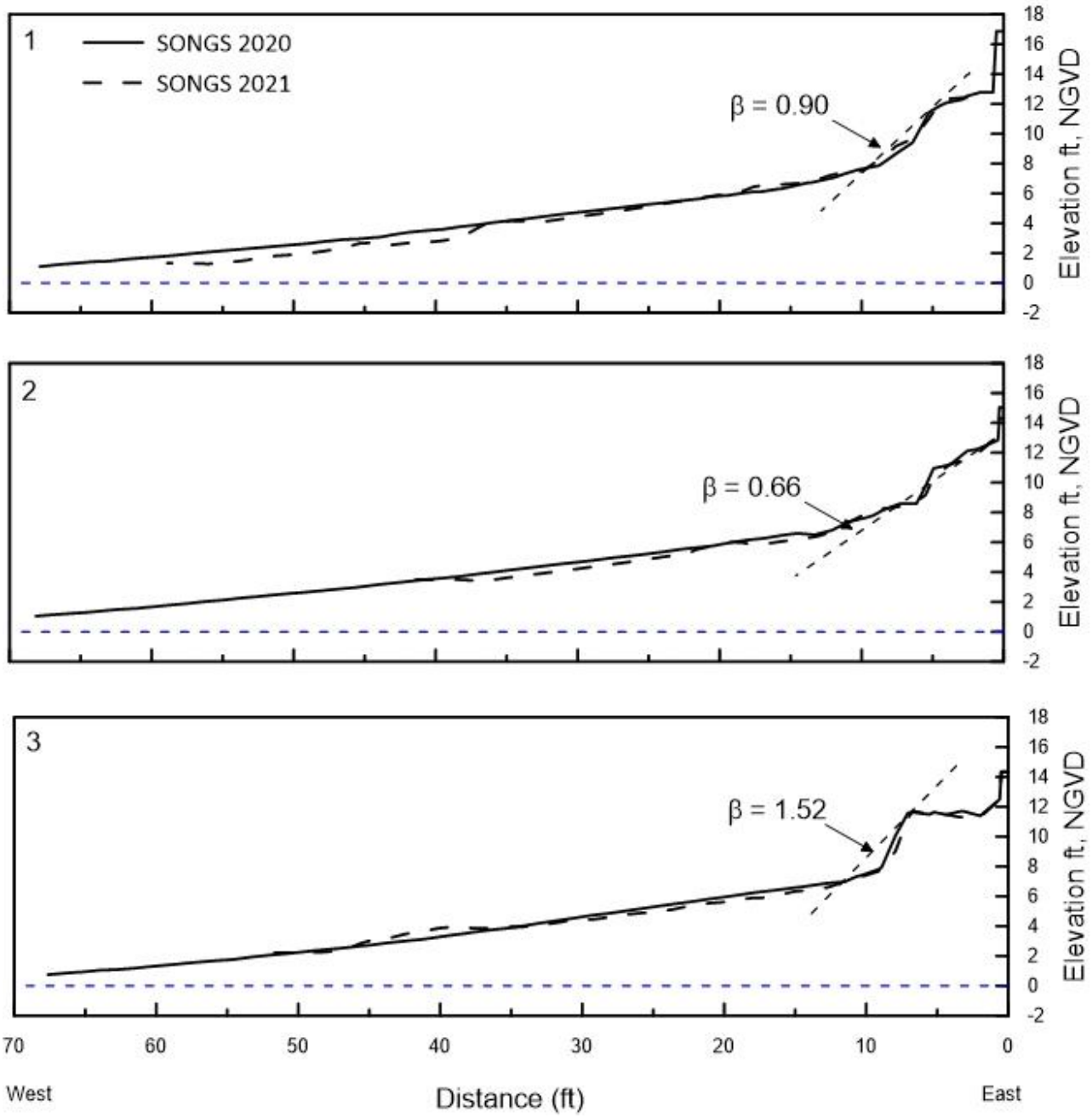


Figure C-1. Cross sections of SONGS revetment along transects 1-3, surveyed on 25 February 2021 and 5 March 2020. β represents the revetment slope.

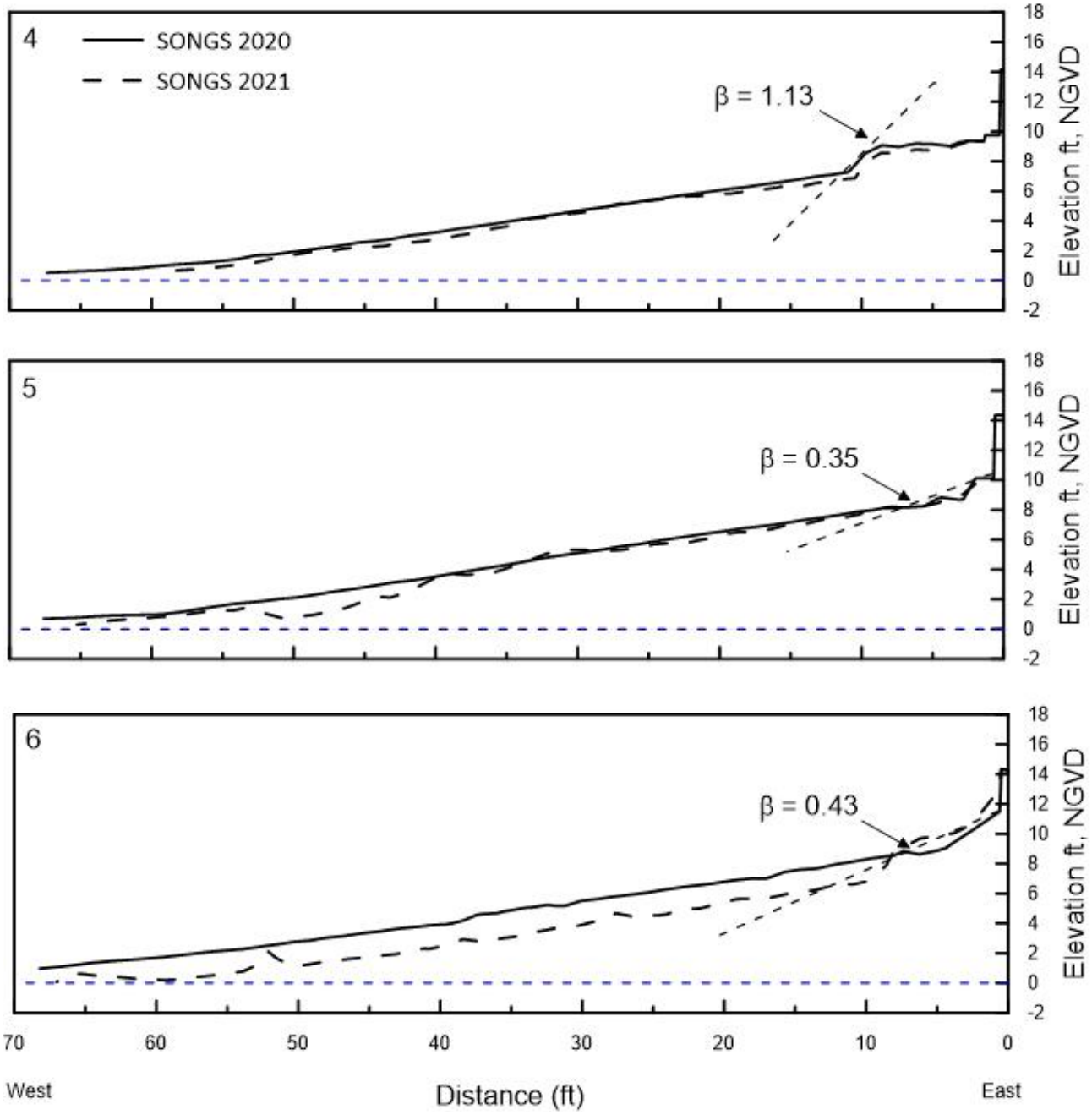


Figure C-2. Cross sections of SONGS revetment along transects 4-6, surveyed on 25 February 2021 and 5 March 2020. β represents the revetment slope.

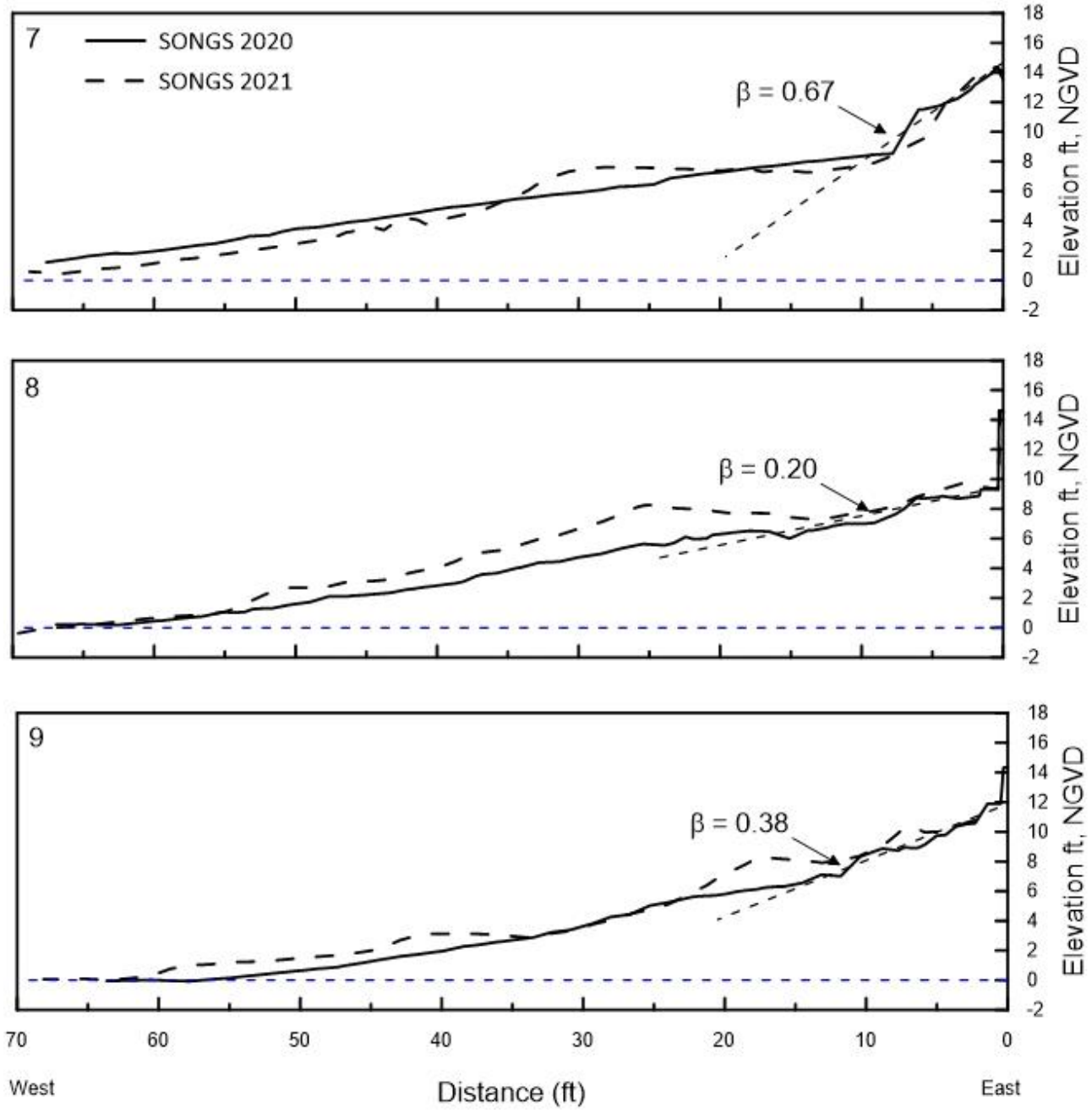


Figure C-3. Cross sections of SONGS revetment along transects 7-9, surveyed on 25 February 2021 and 5 March 2020. β represents the revetment slope.

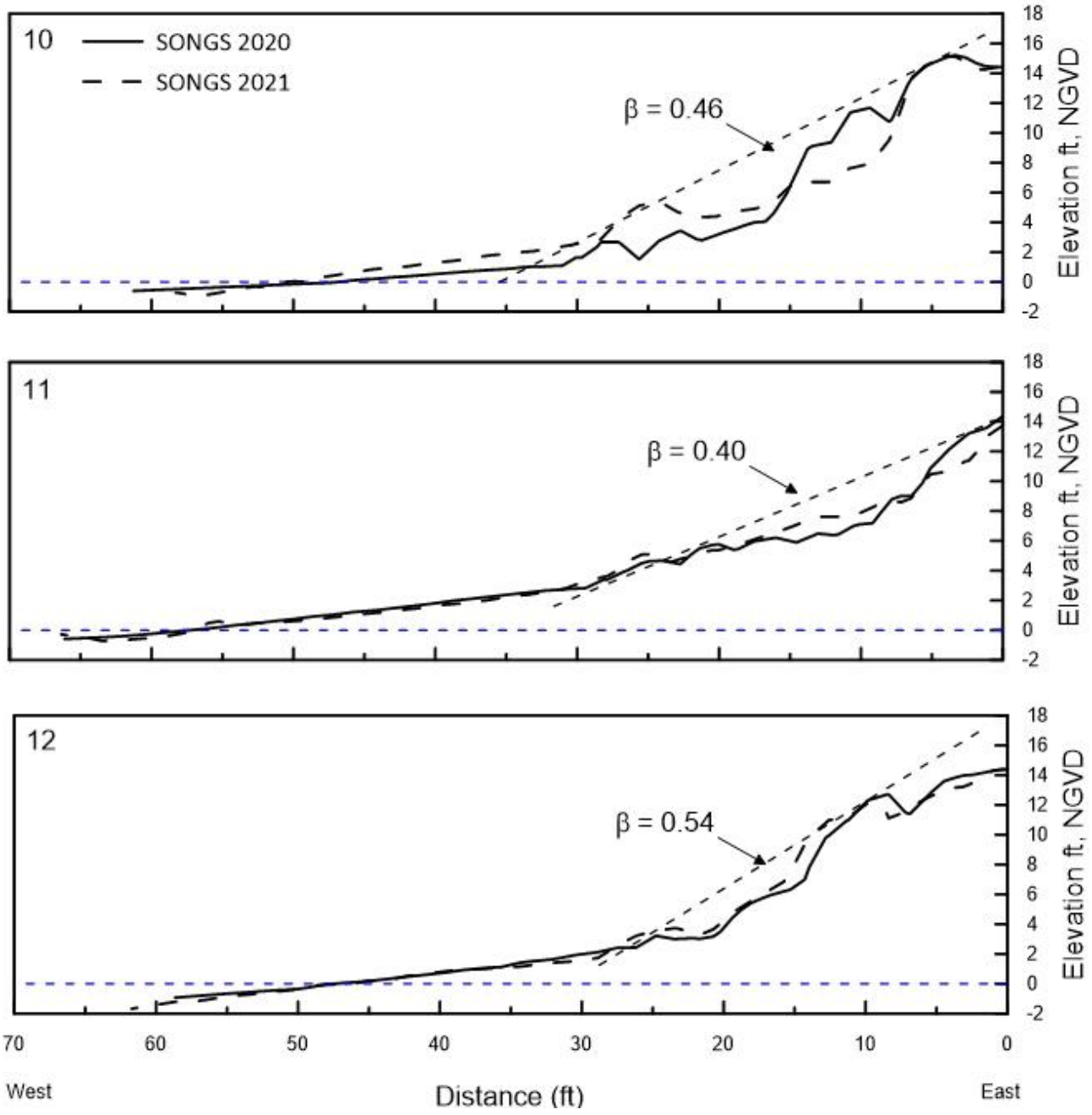


Figure C-4. Cross sections of SONGS revetment along transects 10-12, surveyed on 25 February 2021 and 5 March 2020. β represents the revetment slope.

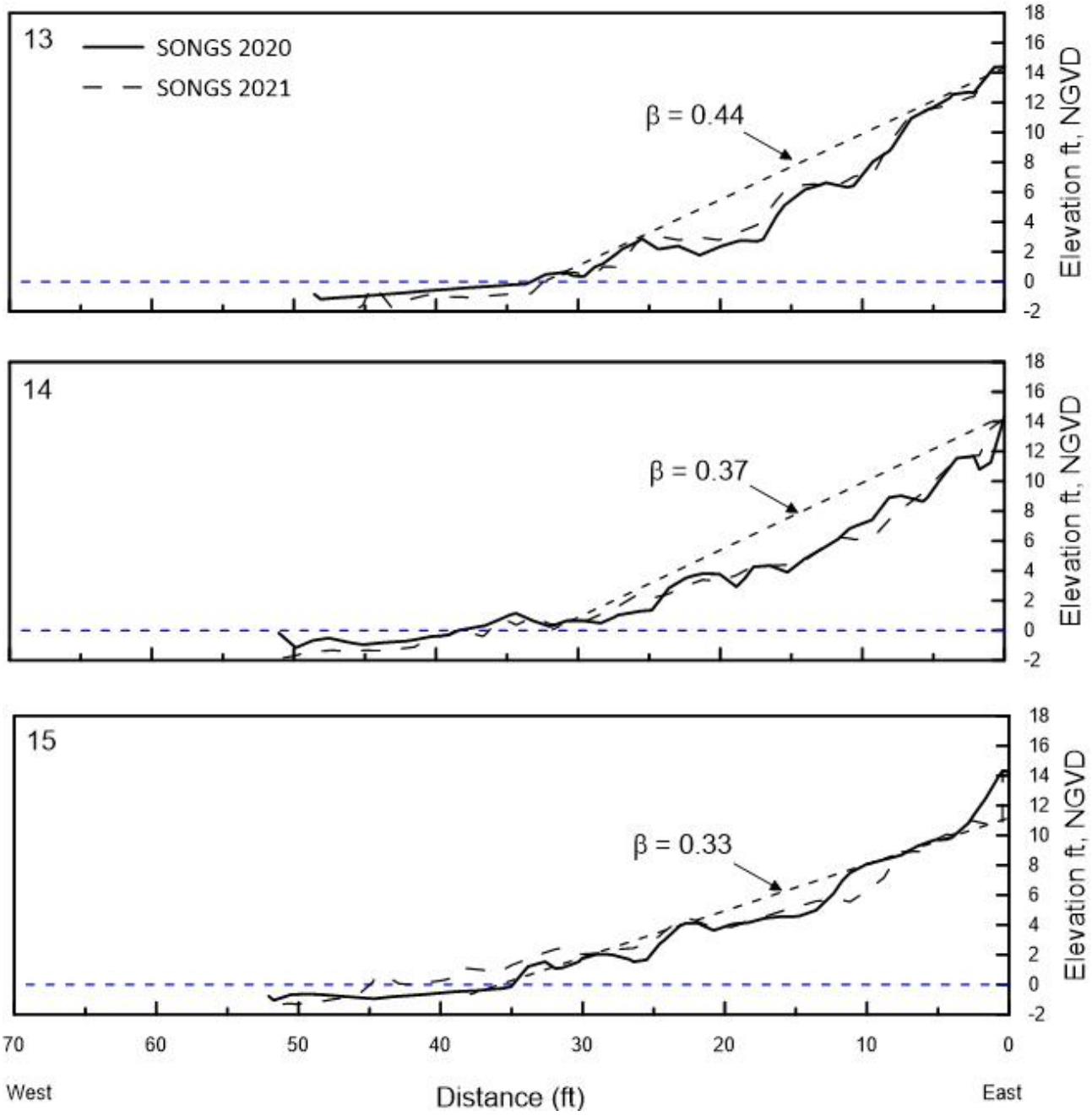


Figure C-5. Cross sections of SONGS revetment along transects 13-15, surveyed on 25 February 2021 and 5 March 2020. β represents the revetment slope.

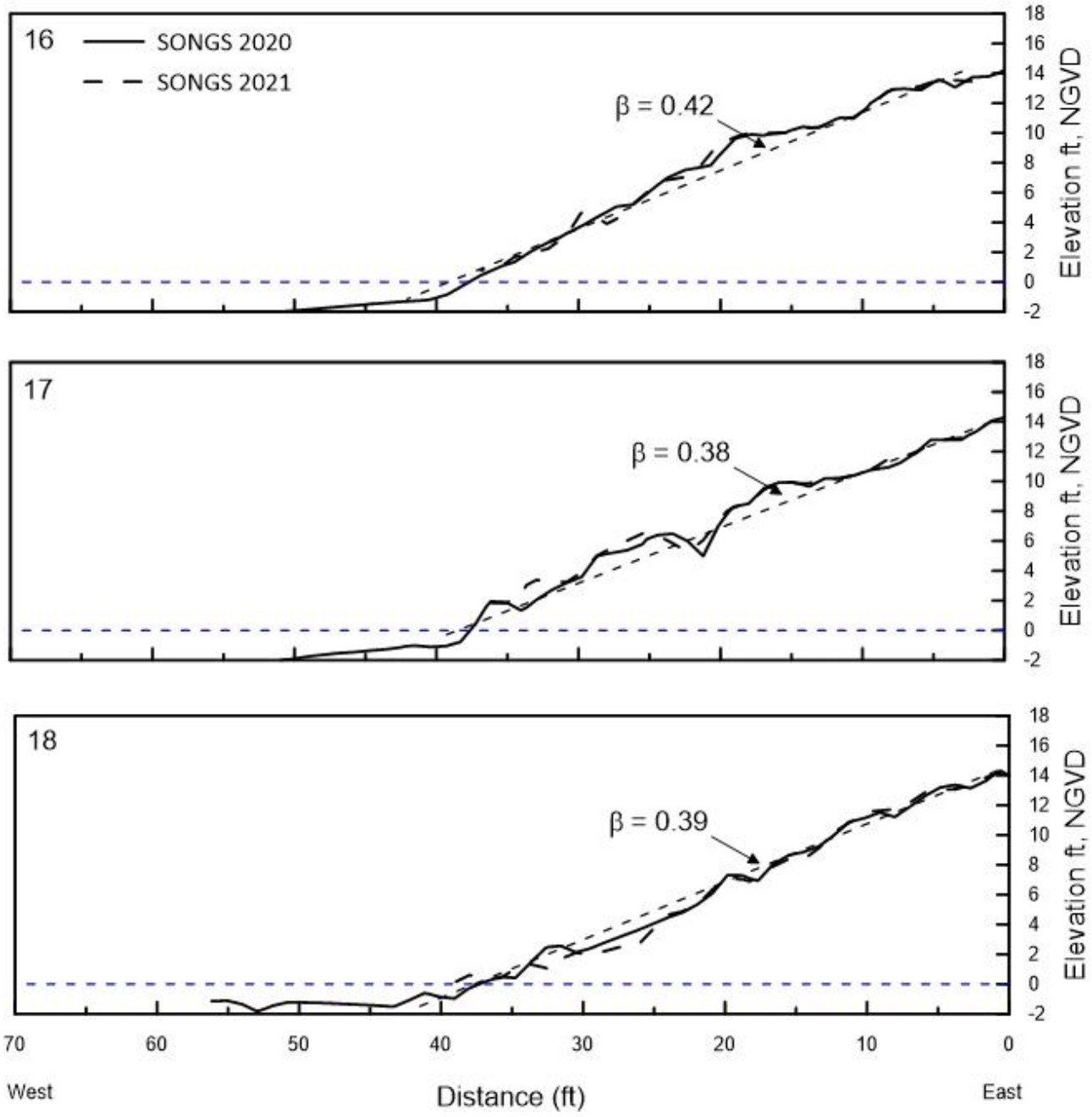


Figure C-6. Cross sections of SONGS revetment along transects 16-18, surveyed on 25 February 2021 and 5 March 2020. β represents the revetment slope.

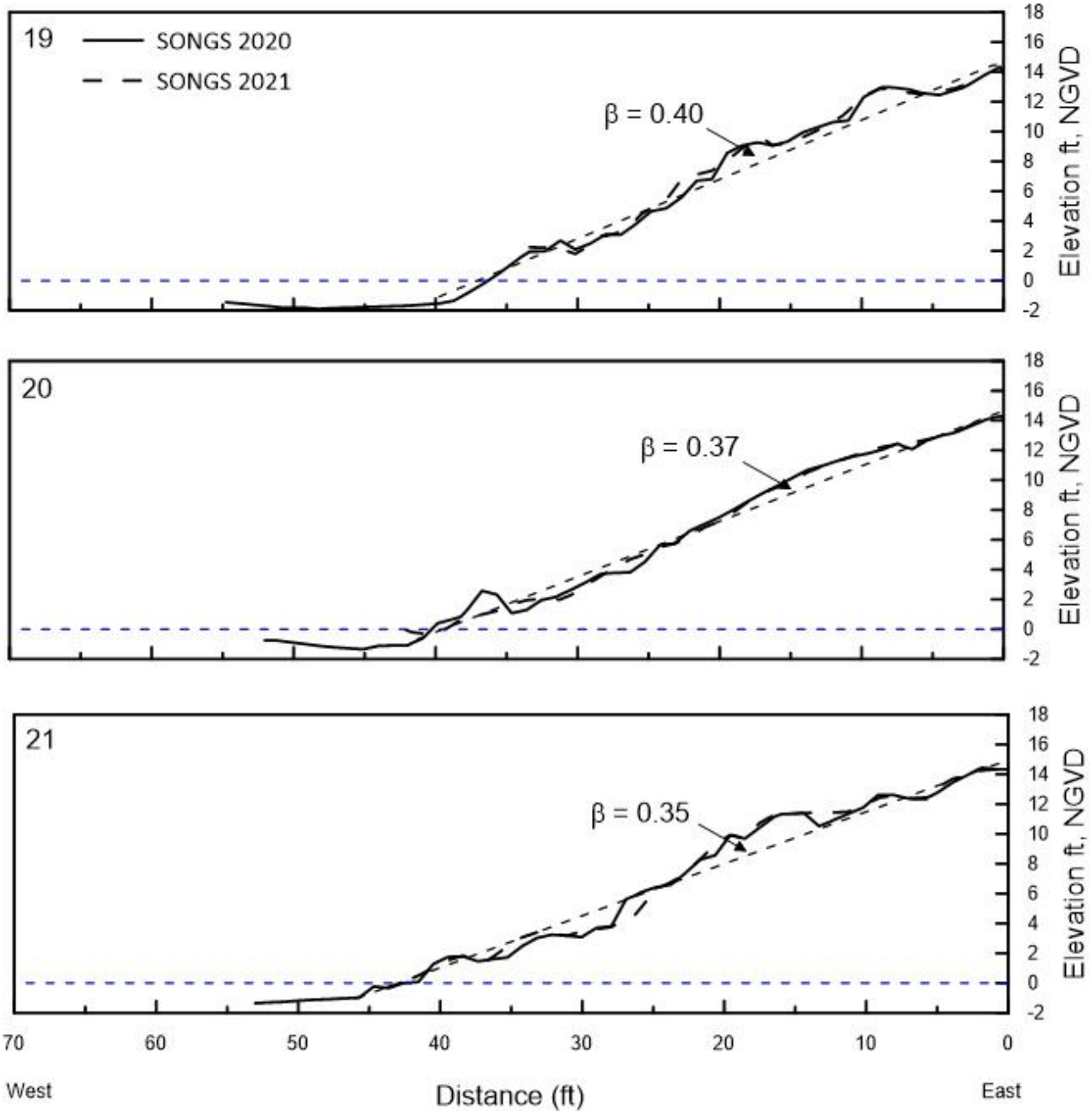


Figure C-7. Cross sections of SONGS revetment along transects 19-21, surveyed on 25 February 2021 and 5 March 2020. β represents the revetment slope.

APPENDIX D

AERIAL PHOTOGRAPHS
NORTH AND SOUTH SONGS, 2003-2020



Photo D-1. Photograph showing revetment covered by sand and fronted by a wide beach at the northern end of SONGS (10 March 2003).



Photo D-2. Photograph showing waves from north swell attacking SONGS revetment at the southern end of SONGS (10 March 2003).



Photo D-3. Photograph showing waves attacking the revetment and the presence of a sand beach at the northern end of SONGS (26 November 2003).



Photo D-4. Photograph showing waves attacking SONGS revetment at the southern end of SONGS (26 November 2003).



Photo D-5. Photograph showing revetment covered by sand and fronted by a wide beach at the northern end of SONGS (2 August 2006).

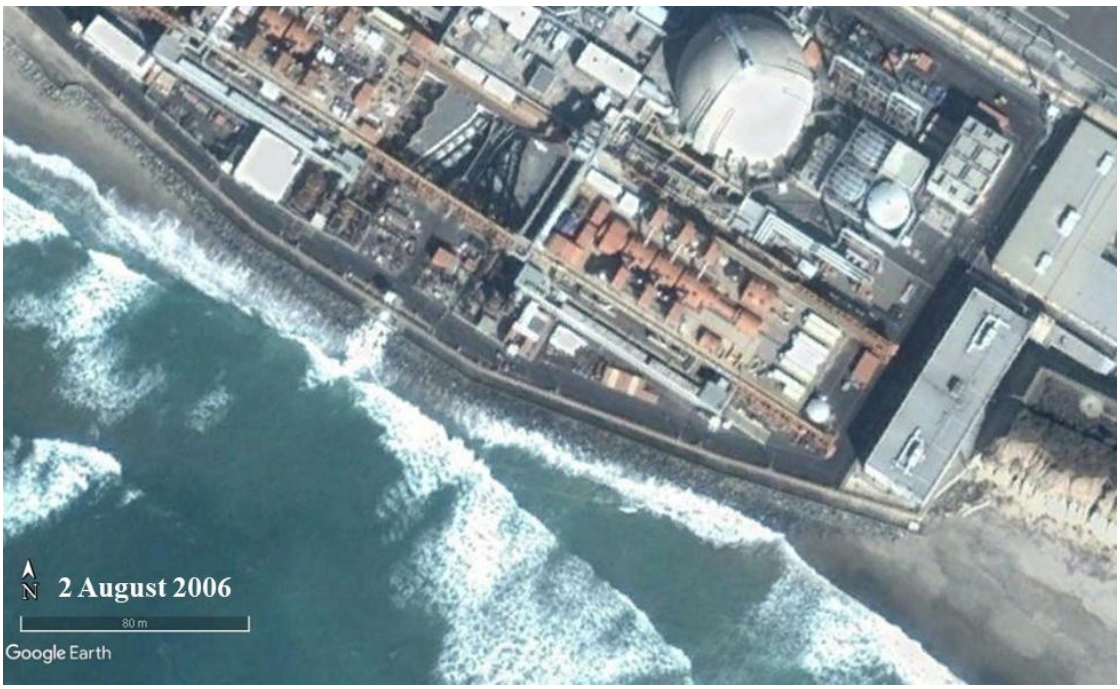


Photo D-6. Photograph showing waves from north swell attacking SONGS revetment at the southern end of SONGS (2 August 2006).

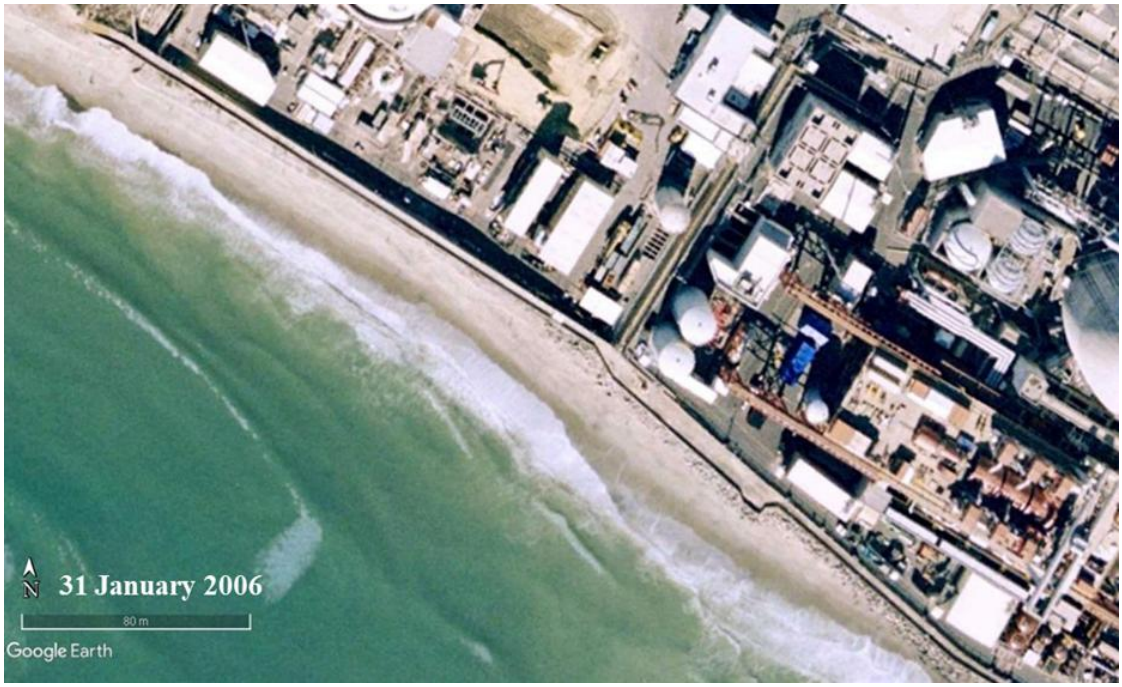


Photo D-7. Photograph showing revetment covered by sand and fronted by a wide beach at the northern end of SONGS (31 January 2006).



Photo D-8. Photograph showing waves from north swell attacking SONGS revetment and refracting towards south at the southern end of SONGS (31 January 2006).



Photo D-9. Photograph showing revetment covered by sand and fronted by a wide beach at the northern end of SONGS (31 January 2008).



Photo D-10. Photograph showing waves attacking SONGS revetment at the southern end of SONGS (31 January 2008).

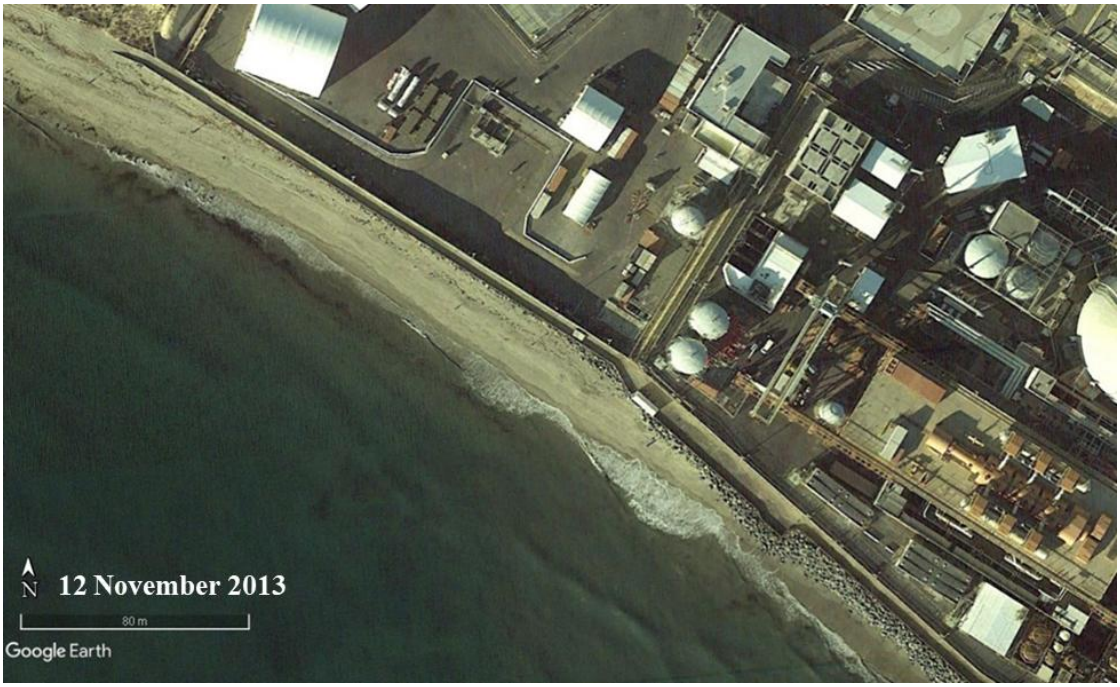


Photo D-11. Photograph showing revetment covered by sand and fronted by a wide beach at the northern end of SONGS (12 November 2013).



Photo D-12. Photograph showing waves attacking SONGS revetment and refracting towards south at the southern end of SONGS (12 November 2013).



Photo D-13. Photograph showing revetment exposed and fronted by a wide beach at the northern end of SONGS (27 April 2014).

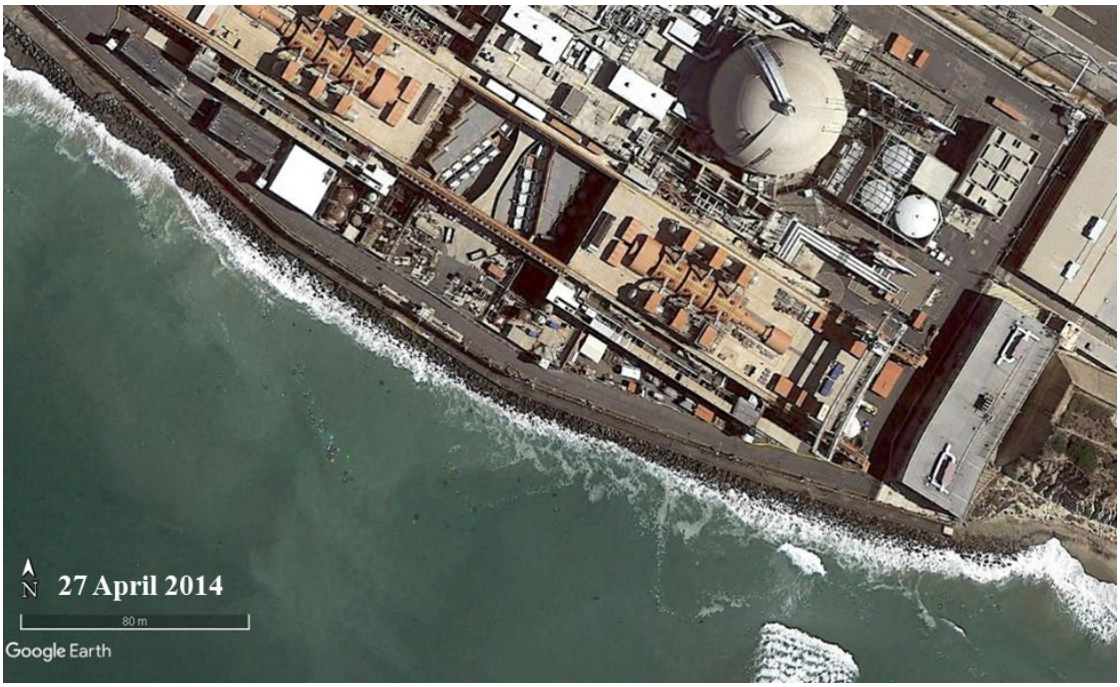


Photo D-14. Photograph showing waves attacking SONGS revetment and refracting towards south at the southern end of SONGS (27 April 2014).

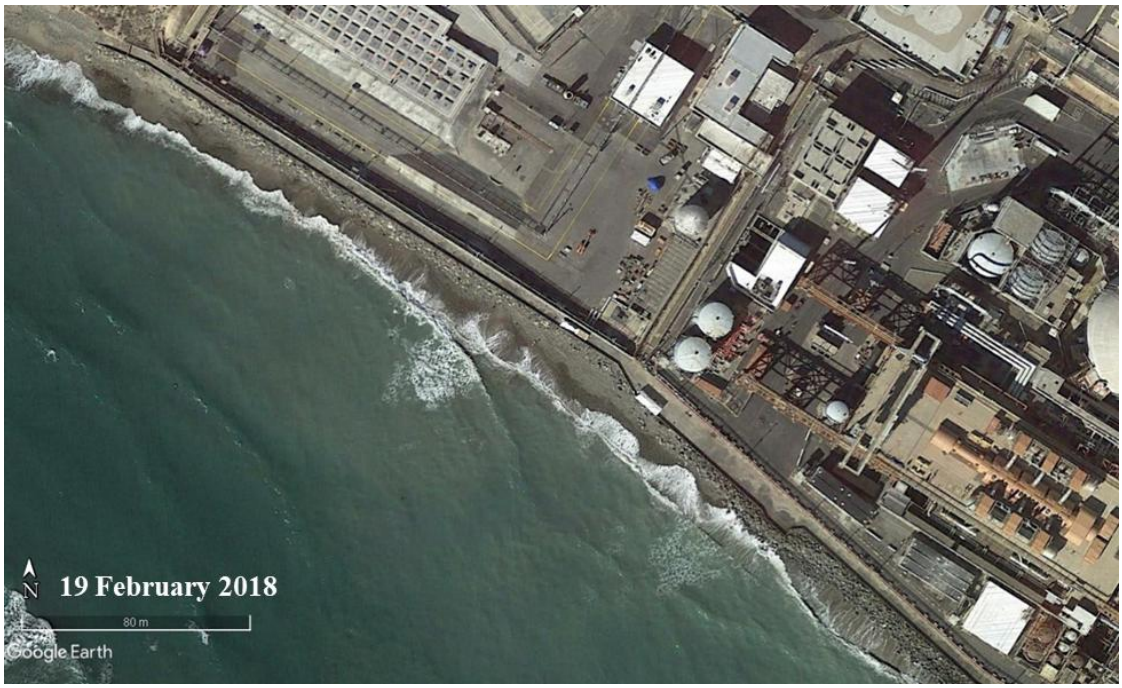


Photo D-15. Photograph showing revetment exposed and fronted by a sand beach at the northern end of SONGS (19 February 2018).



Photo D-16. Photograph showing waves from north swell attacking SONGS revetment and refracting towards south at the southern end of SONGS (19 February 2018).



Photo D-17. Photograph showing revetment exposed and fronted by a wide beach at the northern end of SONGS (24 August 2018).



Photo D-18. Photograph showing waves from north swell attacking SONGS revetment and refracting towards south at the southern end of SONGS (24 August 2018).

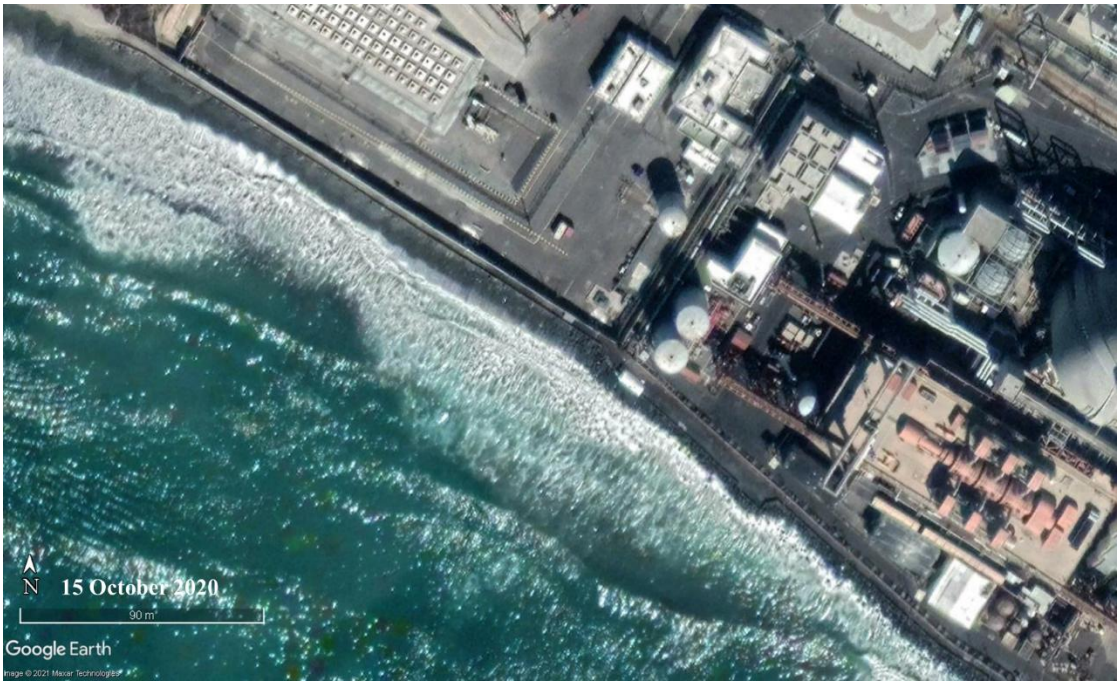


Photo D-19. Photograph showing revetment exposed and fronted by a wide beach at the northern end of SONGS (15 October 2020).

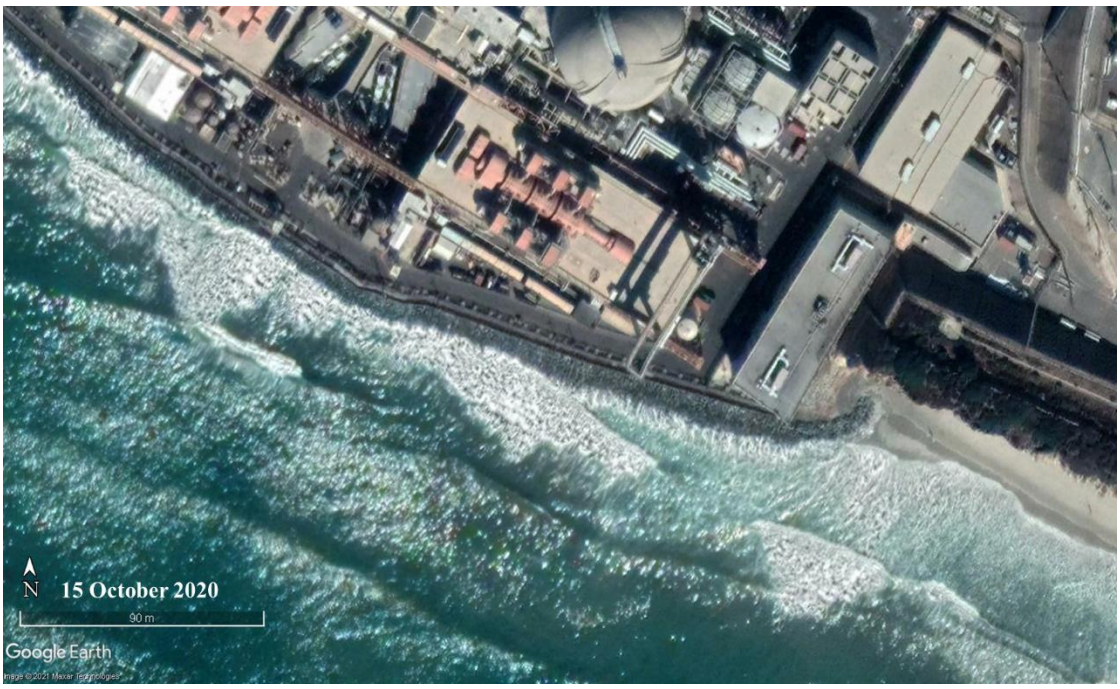


Photo D-20. Photograph showing waves attacking SONGS revetment and refracting towards south at the southern end of SONGS (15 October 2020).